Advances in Selectivity and Reactivity in Transition Metal Catalysis: Carbon–Silicon Bond Formation, Wacker Oxidation, and Olefin Metathesis

Thesis by

Crystal Kitying Chu

In Partial Fulfillment of the Requirements for

the degree of

Doctor of Philosophy

CALIFORNIA INSTITUTE OF TECHNOLOGY

Pasadena, California

2017

(Defended May 26, 2017)

ACKNOWLEDGEMENTS

There are so many people who helped me throughout grad school. First, I want to thank my advisor, Professor Robert Grubbs, for taking me on as a grad student and for the amount of trust that you have had in me. As a student in Bob's lab, I have met a lot of scientists at meetings and conferences who come up to me, excited to see his name on my poster, discuss chemistry going on in the group now and how it has developed over the years, and chat with me about stories they have experienced or heard. What I have noticed is this: when your name comes up in conversation, it is not solely in the context of your numerous accomplishments, but also, perhaps more importantly, your unparalleled kindness, support, and humility. Thank you for being the best role model I could ask for.

My grad school career began in the laboratory of Professor Gregory Fu. I want to thank Greg for taking a chance on me, as I did not come with a large amount of synthetic experience, and for teaching me to hold higher standards for myself than I could imagine. I will never forget pitching (bad) ideas to you in one of our first meetings; after saying that you would not discourage me from these projects, you proposed two more appropriate and promising options. I chose one, and when I returned to your office after doing some literature searches on the topic, you asked "are you confident that you are the world's expert on this topic now?" I learned faster in the first few months in your lab than I ever have; thank you for setting the bar high, your understanding, and your continued support over the last few years.

I need to thank my committee chair, Professor Brian Stoltz, for his guidance and advice through this process. I have learned a lot from running around Schlinger and observing your management and teaching style. I want to thank Professor Harry Gray for being on my committee and the time he has put in to providing me career advice and support. From you I have learned that science is about people, and that great science is done best in the presence of great company and with a sense of humor. My undergraduate advisors and mentors at Berkeley got me to Caltech. Professors Michelle Chang, Jean Fréchet, and Phillip Geissler have been excellent role models and teachers.

I have had the privilege to work with many extraordinary labmates in two groups at Caltech. In the Fu group, the silylation project was started by Dr. Alex Dudnik, who provided

a very promising project for me as a first year. I am grateful to postdocs Dr. Nathan Schley, Dr. Rylan Lundgren, Dr. Hien Do, and Dr. Huan Cong, who answered so many of my nickel related questions and provided first year me with much needed insight. Dr. Søren Kramer and Dr. Xin Mu helped bring balance to my life, and are great friends inside and outside of the lab. Dr. Susan Zultanski and Dr. Junwon Choi were senior graduate students when I began, and were important as both mentors and friends. If it weren't for Sue's sense of adventure (and your car), I would have never been able to see any part of LA for years. I spent a lot of late nights in the lab with Junwon – I am so thankful that you were there…every single night…otherwise no one would have been around to criticize the lack of purity of my NMRs. My project would not have been completed without the help of Dr. Yufan Liang. Your devotion to being a good friend is as strong as your work ethic; anyone who has seen you in the lab would know that means a lot. I need to give special thanks to those who shared an office with me. Dr. Junwon Choi, Dr. Daniel Ziegler, and Shoshana Bachman: you guys made the office a fun place to be and provided motivation every day. Dr. Sarah Lee and Trixia Buscagan were really supportive friends in the group. I was lucky to have Dr. Aga Bartoszewicz, Dr. Linglin Wu, Dr. Sue Zultanski, and Dr. Jose Muñoz-Molina as neighbors in the lab. Dr. Hendrik Wagner, Dr. Nicole Biber, Dr. Yu Shibata, Dr. Xingwen Sun, Gregory Harlow, and Joe Ahn were also great labmates in the group.

I have collaborated with a lot of wonderful people in the Grubbs group: Dr. Daniel Ziegler, Dr. Zach Wickens, Dr. Allegra Liberman-Martin, Dr. Tzu-Pin Lin, Brian Carr, and Jiaming Li have all been fun to work with and have taught me a lot about chemistry. Dan in particular has been a great friend to share stories with in both the Fu and Grubbs groups. I am super indebted to Zach, who guided me through Wacker and the paper writing process. I would not have been able to complete grad school without the friendships I have made here. Dr. Keary Engle, Jae Engle, Dr. Zach Wickens, Natalie Khuen, Dr. Rob Macfarlane, Dr. Hans Renata, Dr. Justin Lomont, and Alice Chang (around half of these friends were not technically in the group, but…eh basically) welcomed me when I joined and made the Grubbs group feel like home. Our adventures, whether centered around board games and/or fried chicken, are some of the best memories I have from grad school; I admire you all

tremendously as scientists and as friends. I intend to see more of all of you for years to come, even Hans.

Many friends from the Grubbs group share the belief that the second most important thing in life (after chemistry) is food. Carl Blumenfeld and Ilana Golbin have been great friends to both me and Yali. You guys have literally made a home for us, and I am so grateful for your friendship and your cooking. Dr. Noah Nathel deserves special recognition for his ultra-refined palate and unrefined sense of humor. Dr. Lauren Rosebrugh, Dr. Allegra Liberman-Martin, Alice Chang, and Zainab Al-Saihati have been the best of brunch and yoga buddies. Dr. Willie Wolf and Julian Edwards have been known to enjoy the occasional ramen egg. I had the privilege of mentoring Jacob Sertich, a visiting undergraduate student, for a summer. Thanks for taking on a tough project and working hard to get us a lead. Dr. Peter Dornan, Dr. John Hartung, Dr. Choon Woo Lee, Dr. Vanessa Marx, Dr. Shane Mangold, Dr. Brendan Quigley, Dr. Raymond Weitekamp, Dr. Karthish Manthiram, Dr. Chris Bates, Dr. Patrick Montgomery, Dr. Anton Toutov, Dr. Chris Marotta, Dr. Juneyoung Lee, Dr. Mike Haibach & Togo, Dr. Michael Schulz, Dr. Melanie Pribisko Yen, Tonia Ahmed, Brendon McNicholas, and Lennon Luo have all been great labmates. I need to thank Linda Syme for dealing with anything that comes her way; without you, the lab would not be able to function. I would like to thank all of the Fu and Grubbs group members I have overlapped with over the years. I also want to acknowledge our collaborators from the University of Pittsburgh, Huiling Shao and Professor Peng Liu, for their computational insights and hard work.

There are many individuals across the chemistry department who have helped me through grad school. Other than labmates, Dr. Dave VanderVelde has definitely helped me the most with research during my time at Caltech. Thank you for all the discussions and the time you put into the NMR facility. I also want to thank Dr. Mona Shahgholi and Naseem Torian for their help with mass spectrometry. Dr. Scott Virgil has been very helpful with the catalysis center over the years. I want to thank Agnes Tong for keeping things organized and coordinating events in the department. I am lucky to have received so much support and advice from Felicia Hunt during my time at Caltech.

I have also received a lot of help from and become friends with members of other groups at Caltech. Dr. Kangway Chuang, Dr. Madeleine Kieffer, Dr. Haoxuan Wang, Dr.

Geanna Min, Beau Pritchett, Kayla Busby, Matt Smarte, Lauren Chapman, Linhan Shen, and Matt Chalkley have given me scientific advice and have been great food buddies and friends. I had a lot of fun late night conversations with my roommates over the years: Amy McCarthy, Katerina Korch, and Sam Ho.

There are a couple of friends from my class whose support has kept my life balanced during grad school. Shoshana Bachman has been my partner in crime since day one. Thank you for having my back and being down to earth. I have no idea how much boba I have had with Elizabeth Lunny. Despite being "the worst," you are one of the best people I know.

Finally, I want to thank my family and friends. I have to acknowledge my dog Yali of course, for bringing me joy and greeting me when I come home. Saya, you have always been there for me; thank you for keeping me grounded. And thank you for being a second mom to Yali. Grace, whether we are shopping, eating, or having real talk, we are always having fun. Thank you for providing perspective and a world outside of grad school. Mark, no one has supported me in grad school more than you have. Thanks for everything. To my mom, Tiffany, Shawn, and Camden, thank you for putting up with me, your understanding, and your support all these years.

ABSTRACT

The development of reaction methodology and catalysts that promote challenging transformations with high yields and selectivities is presented in Chapters 2–4 of this thesis. The three projects discussed address challenges in cross-coupling, olefin oxidation, and olefin metathesis.

Chapter 2 describes a nickel-catalyzed cross-coupling strategy for the formation of C–Si bonds using unactivated alkyl halides as substrates. Reaction optimization, exploration of the substrate scope, and mechanistic studies are described. This method is unique in its compatibility with not only secondary alkyl bromides, but tertiary alkyl bromides as well. Low loadings of the nickel catalyst, the absence of an added ligand, and relative tolerance of air and moisture contribute to the efficiency and robustness of this reaction. Mechanistic studies suggest that oxidative addition proceeds through a radical intermediate, consistent with previous studies of C–C bond formation.

Chapter 3 describes the application of an aldehyde-selective Wacker oxidation to allylic fluoride substrates to produce β-fluorinated aldehydes with remarkably high regioselectivities. Efficient anti-Markovnikov oxidation of allylic fluorides bearing a variety of functional groups was possible with reduced loadings of palladium, copper, and nitrite catalysts. In order to highlight the utility of this methodology, further derivatization of the aldehyde products to diverse fluorinated products is described. Mechanistic studies demonstrate the role of inductive effects in enhancing the regioselectivity of oxidation.

Chapter 4 investigates the synthesis, characterization, and reactivity studies of a new class of second-generation ruthenium olefin metathesis catalysts bearing aminophosphine ligands. The incorporation of P–N bonds into the dissociating phosphine ligand results in trends in catalyst initiation rates and catalyst activity that reveal important considerations for ligand design. The results from kinetics experiments correlate well with computational studies, which indicate that there are significant effects derived from sterics, electronic induction, orbital overlap from the nitrogen (aminophosphine) lone pair, and ligand distortion energies that contribute to trends in phosphine dissociation.

PUBLISHED CONTENT AND CONTRIBUTIONS

Crystal K. Chu, Yufan Liang, and Gregory C. Fu. Silicon–Carbon Bond Formation via Nickel-Catalyzed Cross-Coupling of Silicon Nucleophiles with Unactivated Secondary and Tertiary Alkyl Electrophiles. *Journal of the American Chemical Society* **2016**, *138* (20), 6404–6407. DOI: 10.1021/jacs.6b03465.

C.K.C. participated in project design, developed the standard reaction conditions, evaluated the reaction scope, and participated in writing of the manuscript.

Crystal K. Chu, Daniel T. Ziegler, Brian Carr, Zachary K. Wickens, and Robert H. Grubbs. Direct Access to β-Fluorinated Aldehydes by Nitrite-Modified Wacker Oxidation. *Angewandte Chemie International Edition* **2016**, *55* (29), 8435–8439. DOI: 10.1002/anie.201603424.

C.K.C. participated in project design, evaluated the reaction scope and derivatizations of products, and participated in writing of the manuscript.

TABLE OF CONTENTS

Chapter 1

INTRODUCTION

Significant research efforts in the field of transition metal catalysis have led to the development of powerful methods for the formation of C–C and C–heteroatom bonds. Appropriate design of the catalyst and reaction conditions, along with careful choice of the substrate, can enable new and challenging transformations to proceed in high yield and selectivity. In this thesis, three categories of such transformations are presented: cross-coupling reactions to form carbon–silicon bonds, aldehyde-selective Wacker oxidations of fluorinated olefins, and olefin metathesis catalyzed by aminophosphine-ligated ruthenium complexes.

Nickel-catalyzed cross-coupling has proven to be a very effective strategy for the addition of organometallic reagents to unactivated alkyl electrophiles. In particular, secondary alkyl halides are useful coupling partners, despite previously being considered to exhibit poor reactivity in comparison to aryl and alkenyl electrophiles, due to challenging oxidative addition and competitive β-hydride elimination. While this class of reactions has predominantly been applied to the formation of C–C bonds, the extension of this strategy to the formation of C–B bonds presented by Fu and coworkers inspired the work presented in the second chapter of this thesis, which details the development of a nickel-catalyzed cross-coupling reaction of unactivated alkyl bromides and silylzinc nucleophiles, resulting in C–Si bond formation. A brief overview of established strategies to form C–Si bonds, as well as some of the current challenges, is discussed.

The palladium-catalyzed Wacker oxidation is a powerful tool for the oxidation of terminal olefins. However, controlling the regioselectivity of this process (i.e. whether C–O bond formation occurs at the internal position to produce a ketone or at the terminal position to produce an aldehyde) has been a longstanding challenge. Recent studies have led to new methods that promote Wacker oxidations that afford either ketones or aldehydes with good regioselectivity, and the investigation of new substrate classes has expanded the applications of this reaction to olefins bearing diverse functional groups. In the third chapter of this thesis, the nitrite-modified Wacker oxidation of allylic fluorides to selectively produce β-fluorinated

aldehydes is presented. Related methodologies developed for regioselective Wacker oxidation are discussed in this chapter.

The final chapter of this thesis describes kinetics and computational studies of new second-generation ruthenium olefin metathesis catalysts bearing aminophosphine ligands. Olefin metathesis has become an extremely important reaction in laboratory and industrial syntheses of substituted olefins and polymers. A comprehensive understanding of the effects of ligand composition and structure is valuable for the design of efficient and highly active catalysts. Background research related to the development of ruthenium olefin metathesis catalysts and examples of ligands that have been studied are described.

The research projects presented in this thesis, while diverse in nature, are aimed at improving catalyst selectivity and reactivity to open doors to new substrate classes and applications. These studies are expected to aide in the design of new coupling partners in challenging bond formations, reaction conditions to enhance catalyst selectivity, and ligands for controlling catalyst activity.

Strategies for Carbon–Silicon Bond Formation

Silicon-containing organic molecules have traditionally served as important intermediates in natural product total synthesis,[1] since C–Si bonds have the ability to be transformed into a variety of C–C and C–heteroatom bonds.[2] More recently, organosilicon molecules have been studied as analogs for their carbon-containing counterparts.[3] Silicon bioisosterism involves the incorporation of silicon atoms in place of carbon, with the potential to chemically affect drug targets by bestowing candidate molecules with specific chemical properties. There are several properties of silicon which make its replacement of carbon a powerful tool to tune the toxicity and activity of potential drugs: 1) larger covalent radius, 2) increased lipophilicity and, therefore, cellular uptake, and 3) enhanced hydrogen-bonding.[3] Additionally, silicon does not introduce any intrinsic toxicity, and cellular profiling studies of organosilicons[4] as well as the synthesis of silicon-containing drug analogs[5] and non-natural amino acids[6] have shown the potential of this synthetic strategy toward new drug targets (Figure 1.1).

The chemistry of allylsilanes has long been utilized in traditional organic synthesis.[7,8] For this reason, many methods have been established for the formation of allylsilanes. However, organic transformations of unactivated alkylsilanes remain far less explored. While reactions such as hydrosilylation and conjugate addition strategies have been extensively investigated, regioselective silylation reactions are limited to certain classes of substrates. Furthermore, sterically hindered starting materials are challenging substrates in current methodology, and alternate paths to synthesize tertiary alkylsilanes with broad substrate scope are rare.

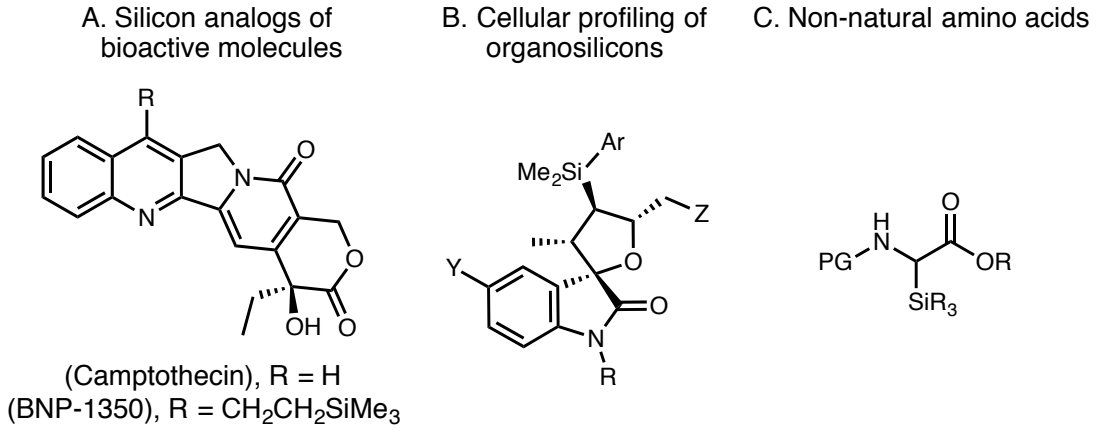

Figure 1.1. Biologically active compounds containing silicon.

The most established catalytic silylation reactions involve addition to unsaturated carbon–carbon bonds, via hydrosilylation[9-11] of olefins, conjugate addition[12-14] to α,β-unsaturated ketones, or silyl metalation and addition to olefins[15] (Figure 1.2). The field of hydrosilylation is well-developed and has important industrial use;[9] however, regioselectivity issues inherent to olefin addition remain. Furthermore, conjugate addition restricts substrate structure to α,β-unsaturated carbonyl compounds to form β-silyl products.

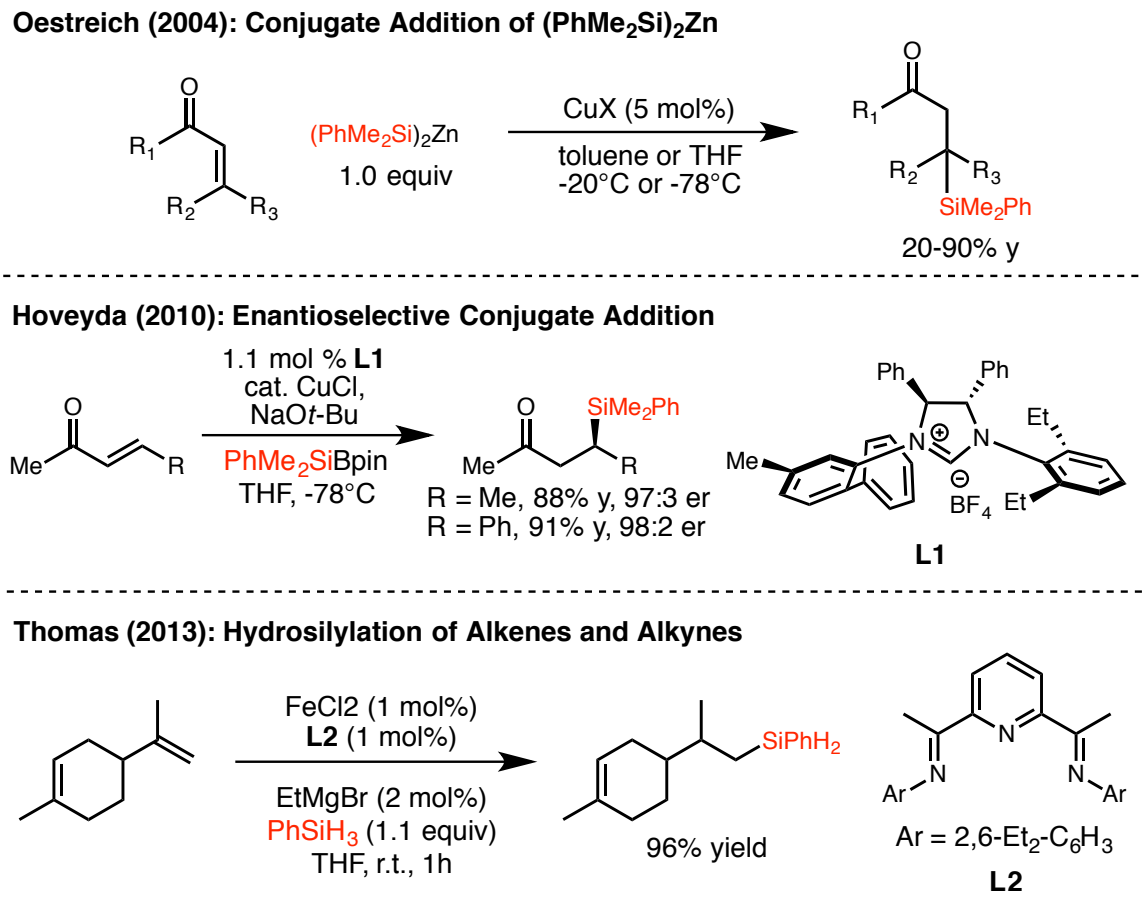

Figure 1.2. Established approaches for C–Si bond formation.

Copper, palladium, and nickel-catalyzed processes have been described for the silylative coupling of activated alkyl halides, including allylic, benzylic, and propargylic chlorides.[16-23] In 1980, Calas reported the cross-coupling of allylic and benzylic chlorides with disilanes catalyzed by $NiCp_2$.[17] Soon after, Nagai and coworkers published the Pd-catalyzed cross-coupling of benzylic chlorides to form dichloromethyl silanes.[18] The Oestreich group has worked extensively with silylative cross-coupling reactions,[16] employing both silylboron and disilylzinc nucleophiles to couple with allylic[19] and propargylic[20] alkyl chlorides. However, few cross-couplings of unactivated alkyl halides have been reported. The method described by Eaborn shown in Figure 1.3 is severely limited by sterics and does not display good functional group tolerance.[21] Thus, the cross-coupling of unactivated alkyl halides, especially of secondary and tertiary halides, to form C–Si bonds remains a challenging problem. The development of reaction conditions to address this challenge is presented in Chapter 2.

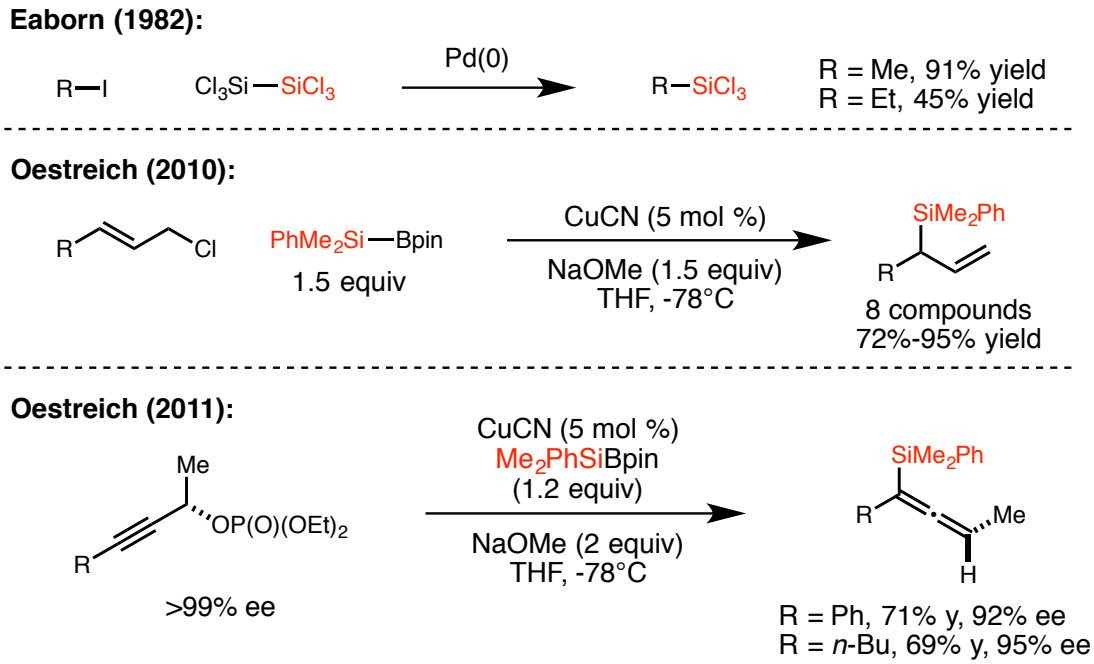

Figure 1.3. Cross-coupling strategies for C–Si bond formation.

Regioselectivity of the Wacker Oxidation

The Tsuji-Wacker oxidation is a widely-used reaction in the laboratory setting for the conversion of terminal olefins to methyl ketones.[24] However, although oxidation of terminal olefins is typically expected to proceed in accordance with Markovnikov's rule to form methyl ketones, the presence of proximal functional groups can lead to poor regioselectivity of oxidation. More recently, methods have been developed that promote selective oxidation of terminal olefins bearing substituents with a variety of electronic properties.

In 2009, Sigman and coworkers developed the ketone-selective peroxide-mediated oxidation of terminal olefins enabled by a palladium catalyst bearing a bidentate Quinox ligand (Scheme 1.1).[25]

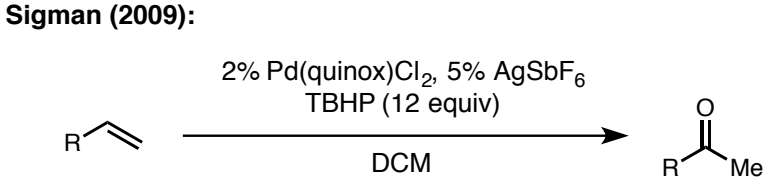

Scheme 1.1 Ketone-selective Wacker oxidation reported by Sigman.

This system provides high ketone yields for a broad scope of protected allylic alcohols and simple olefins.

In comparison to ketone-selective oxidations, the development of an aldehyde-selective Wacker oxidation has proven more elusive. Over the past few years, work by the Grubbs[26] and Feringa[27] groups has demonstrated aldehyde selectivity in the presence of a broad scope of functional groups. This work has been inspired by preliminary work reported by Feringa in the 1980s, in which a palladium nitrite catalyst provides modest aldehyde selectivity with the use of *tert*-butanol as the solvent (Scheme 1.2).[28] However, this reaction was limited by low oxidation yield.

Feringa (1986):

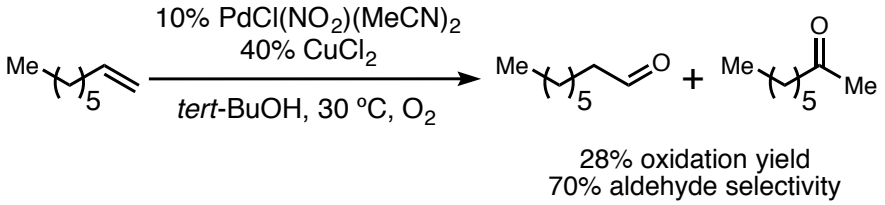

Scheme 1.2 Aldehyde-selective Wacker oxidation reported by Feringa.

Recently, the Grubbs group has significantly enhanced the aldehyde selectivity of this reaction through the use of a separate nitrite cocatalyst and a *tert*-butanol/nitromethane cosolvent system (Figure 1.4). These reaction conditions provide high yields and selectivity for both unbiased olefins as well as a variety of protected homoallylic alcohols.[26] Furthermore, isotope labeling experiments with ^{18}O-labeled nitrite, which show incorporation of ^{18}O from the nitrite salt in the carbonyl oxygen, have suggested that anti-Markovnikov addition of an NO_2 radical could be the cause of aldehyde selectivity under these reaction conditions.[26a] These mechanistic experiments provided insight into the origin of anti-Markovnikov addition in nitrite-modified Wacker oxidations, and are expected to guide future studies to expand the substrate scope of aldehyde-selective oxidations of diverse olefins. However, despite these advances, the reaction scope, particularly in relation to functional groups tolerated at the allylic position of the olefin,[29] remains limited. In a step toward overcoming this challenge, the development of reaction conditions for the anti-

Markonivkov oxidation of allylic fluorides to produce β-fluorinated aldehydes is presented in Chapter 3.

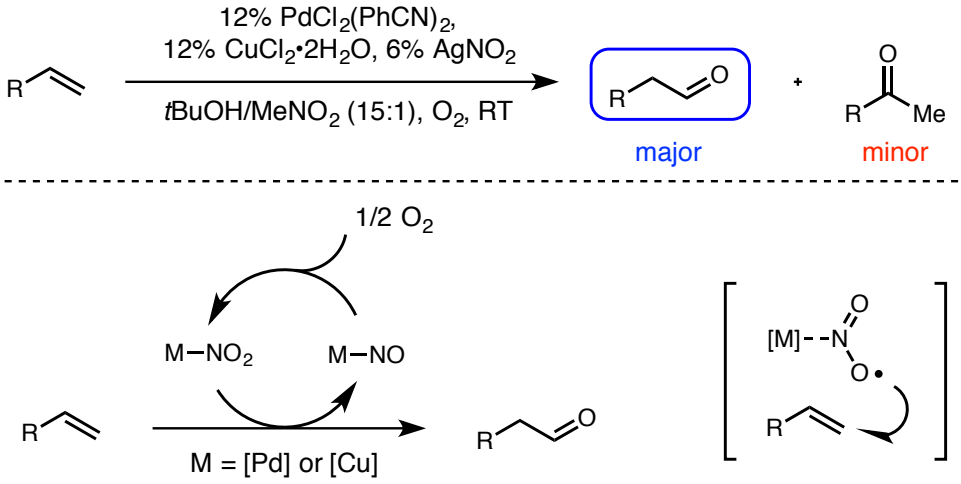

Figure 1.4. Proposed pathway leading to aldehyde selectivity in nitrite-modified Wacker oxidations reported by Grubbs and coworkers.

Ligand Effects on Ruthenium Olefin Metathesis Catalyst Activity

Ruthenium olefin metathesis catalysts have been widely used for their stability to air and moisture and high functional group tolerance. This strategy for the formation of carbon–carbon bonds has been applied extensively to the synthesis of small molecules and polymers in both laboratory and industrial settings. In the early 1990s, Grubbs reported the first well-defined ruthenium alkylidene catalysts (Figure 1.5).[30] This discovery soon led to the development of the ruthenium benzylidene complex referred to as the first-generation Grubbs catalyst (Figure 1.5).[31]

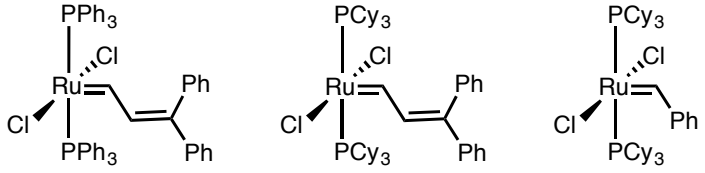

Figure 1.5. Early ruthenium olefin metathesis catalysts.

Despite the ease of use associated with ruthenium-based catalysts, the reactivities of the complexes shown in Figure 1.5 are low in comparison to early molybdenum olefin

metathesis catalysts. It was soon discovered that substitution of one of the phosphine ligands for an N-heterocyclic carbene (NHC) ligand dramatically increased ruthenium catalyst activity (Figure 1.6).[32] Examples of such catalysts include saturated and unsaturated NHC backbones. Furthermore, Hoveyda and coworkers reported ruthenium catalysts bearing chelating benzylidenes that exhibit increased stability.[33] Catalysts bearing two pyridine ligands have been shown to be particularly well suited for producing polymers by ring-opening metathesis polymerization (ROMP) with controlled molecular weights.[34]

Mechanistic studies of NHC-ligated ruthenium catalysts have revealed important information related to substituent effects of the phosphine ligand.[35] A number of arylphosphines containing phenyl substituents with varied electronic properties were compared in kinetics studies; these experiments showed that rates of phosphine dissociation (the catalyst initiation rates) correlate well with the donor strength of the phosphine ligand.[35b]

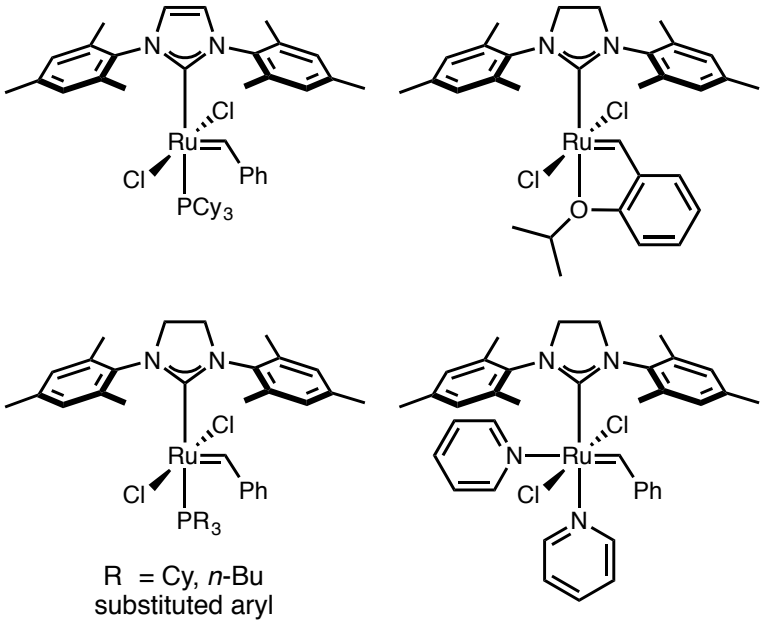

Figure 1.6. Examples of olefin metathesis catalysts bearing NHC ligands.

Phosphine ligands that have been used in second-generation ruthenium metathesis catalysts have predominantly contained three equivalent alkyl or aryl groups. Chapter 4 describes research involving ruthenium catalysts bearing phosphine ligands that contain incongruent substituents and P–X bonds, thereby expanding our understanding of ligand

effects on catalyst activity and potentially allowing access to new useful substrates for metathesis.

References

(1) For a review of silicon-containing intermediates in natural product synthesis: Langkopf, E.; Schinzer, D. *Chem. Rev.* **1995**, *95*, 1375-1408.

(2) For a review of C−Si bond transformations to C−C and C−Het: Oestreich, M.; Hartmann, E.; Mewald, M. *Chem. Rev.* **2013**, *113*, 402-441.

(3) For recent reviews on silicon isosterism: (a) Franz, A. K.; Wilson, S. O. *J. Med. Chem.* **2013**, *56*, 388-405. (b) Min, G. K.; Hernández, D.; Skrydstrup, T. *Acc. Chem. Res.* **2013**, *46*, 457-470.

(4) Cellular profiling of novel organosilicons: Franz, A. K.; Dreyfuss, P. D.; Schreiber, S. L. *J. Am. Chem. Soc.* **2007**, *129*, 1020-1021.

(5) For a study of silicon isosteres as drug analogs: Tacke, R.; Heinrich, T.; Bertermann, R.; Burschka, C.; Hamacher, A.; Kassack, M. U. *Organometallics* **2004**, *23*, 4468-4477.

(6) For a review on silicon-substituted amino acids: Mortensen, M.; Husmann, R.; Veri, E.; Bolm, C. *Chem. Soc. Rev.* **2009**, *38*, 1002-1010.

(7) For a review on allylsilanes in organic synthesis: Masse, C. E.; Panek, J. S. *Chem. Rev.* **1995**, *95*, 1293-1316.

(8) For selected transformations utilizing organosilanes: (a) Wu, J.; Chen, Y.; Panek, J. S. *Org. Lett.* **2010**, *12*, 2112-2115. (b) Lipomi, D. J.; Panek, J. S. *Org. Lett.* **2005**, *7*, 4701. (c) Su, Q.; Panek, J. S. *J. Am. Chem. Soc.* **2004**, *126*, 2425.

(9) For a review on industrial hydrosilylation processes: Troegel, D.; Stohrer, J. *Coord. Chem. Rev.* **2011**, *255*, 1440-1459.

(10) For selected hydrosilylation methods: (a) Tondreau, A. M. et al *Science* **2012**, *335*, 567-570. (b) Rooke, D. A.; Ferreira, E. M. *J. Am. Chem. Soc.* **2010**, *132*, 11926–11928. (c) Waymouth, R. M.; Kesti, M. R. *Organometallics* **1992**, *11*, 1095-1103. (d) Min, G. K.; Skrydstrup, T. *J. Org. Chem.* **2012**, *77*, 5894-5906.

(11) Iron-catalyzed hydrosilylation of alkenes and alkynes: Greenhalgh, M. D.; Frank, D. J.; Thomas, S. P. *Adv. Synth. Catal.* **2014**, *356*, 584-590.

(12) For selected silylative conjugate addition methods: (a) Lipshutz, B. H.; Sclafani, J. A.; Takanami, T. *J. Am. Chem. Soc.* **1998**, *120*, 4021-4022. (b) Tückmantel, W.; Oshima, K.; Nozaki, H. *Chem. Ber.* **1986**, *119*, 1581-1593. (c) Clark, C. T.; Lake, J. F.; Scheidt, K. A. *J. Am. Chem. Soc.* **2004**, *126*, 84-85.

(13) Cu-catalyzed conjugate addition of $(PhMe_2Si)_2Zn$: Oestreich, M.; Weiner, B. *Synlett* **2004**, *12*, 2139-2142.

(14) Cu/NHC-catalyzed enantioselective conjugate addition with $PhMe_2Si{-}Bpin$: Lee, K.; Hoveyda, A. H. *J. Am. Chem. Soc.* **2010**, *132*, 2898-2900.

(15) (a) Liepins, V.; Bäckvall, J.-E. *Org. Lett.* **2001**, *3*, 1861-1864. (b) Liepins, V.; Bäckvall, J.-E. *Chem. Commun.* **2001**, 265-266.

(16) For a review on Cu-catalyzed silylation chemistry: Weickgenannt A.; Oestreich, M. *Chem. Eur. J.* **2010**, *16*, 402-412.

(17) Lefort, M.; Simmonet, C.; Birot, M.; Deleris, G.; Dunogues, J.; Calas, R. *Tetrahedron Lett.* **1980**, *21*, 1857-1860.

(18) Matsumoto, H.; Kasahara, M.; Matsubara, I.; Takahashi, M.; Nakano, T.; Nagai, Y. *Chem. Lett.* **1982**, *11*, 399-400.

(19) Vyas, D. J.; Oestreich, M. *Angew. Chem., Int. Ed.* **2010**, *49*, 8513-8515.

(20) Vyas, D. J.; Hazra, C. K.; Oestreich, M. *Org. Lett.* **2011**, *13*, 4462-4465.

(21) Pd-catalyzed silylation of unactivated primary alkyl halides: Eaborn, C.; Griffiths, R. W.; Pidcock, A. *J. Organometallic Chem.* **1982**, *225*, 331-341.

(22) Laycock, B.; Kitching, W.; Wickham, G. *Tetrahedron Lett.* **1983**, *24*, 5785-5788.

(23) Vyas, D. J.; Oestreich, M. *Chem. Commun.* **2010**, 568-570.

(24) Tsuji, J. *Synthesis* **1984**, 369-384.

(25) Michel, B. W.; Camello, A. M.; Cornell, C. N.; Sigman, M. S. *J. Am. Chem. Soc.* **2009**, *131*, 6076-6077.

(26) (a) Wickens, Z. K.; Morandi, B. Grubbs, R. H. *Angew. Chem. Int. Ed.* **2013**, *52*, 11257-11260. (b) Wickens, Z. K.; Skakuj, K.; Morandi, B. Grubbs, R. H. *J. Am. Chem. Soc.* **2014**, *136*, 890-893.

(27) (a) Dong, J. J.; Fañanás-Mastral, M.; Alsters, P. L.; Browne, W. R.; Feringa, B. L. *Angew. Chem., Int. Ed.* **2013,** *52*, 5561-5565. (b) Dong, J. J.; Harvey, E. C.; Fañanás-Mastral, M.; Browne, W. R.; Feringa, B. L. *J. Am. Chem. Soc.* **2014,** *136*, 17302-17307.

(28) Feringa, B. L. *Chem. Commun*. **1986**, 909-910.

(29) Kim, K. E.; Li, J.; Grubbs, R. H.; Stoltz, B. M. *J. Am. Chem. Soc.* **2016**, *138*, 13179-13182.

(30) (a) Nguyen, S. T.; Johnson, L. K.; Grubbs, R. H.; Ziller, J. W. *J. Am. Chem. Soc.* **1992,** *114*, 3974-3975. (b) Nguyen, S. T.; Grubbs, R. H.; Ziller, J. W. *J. Am. Chem. Soc.* **1993,** *115*, 9858-9859.

(31) (a) Schwab, P.; France, M. B.; Ziller, J. W.; Grubbs, R. H. *Angew. Chem., Int. Ed. Engl.* **1995**, *34*, 2039-2041. (b) Schwab, P.; Grubbs, R. H.; Ziller, J. W. *J. Am. Chem. Soc.* **1996,** *118*, 100-110.

(32) (a) Scholl, M.; Trnka, T. M.; Morgan, J. P.; Grubbs, R. H. *Tetrahedron Lett.* **1999**, *40*, 2247-2250. (b) Scholl, M.; Ding, S.; Lee, C. W.; Grubbs, R. H. *Org. Lett.* **1999**, *1*, 953-956.

(33) (a) Kingsbury, J. S.; Harrity, J. P. A.; Bonitatebus, P. J.; Hoveyda, A. H. *J. Am. Chem. Soc.* **1999,** *121*, 791-799. (b) Garber, S. B.; Kingsbury, J. S.; Gray, B. L.; Hoveyda, A. H. *J. Am. Chem. Soc.* **2000,** *122*, 8168-8179.

(34) Choi, T.-L.; Grubbs, R. H. *Angew. Chem., Int. Ed.* **2003,** *42*, 1743-1746.

(35) (a) Sanford, M. S.; Love, J. A.; Grubbs, R. H. *J. Am. Chem. Soc.* **2001,** *123*, 6543-6554. (b) Love, J. A.; Sanford, M. S.; Day, M. W.; Grubbs, R. H. *J. Am. Chem. Soc.* **2003,** *125*, 10103-10109.

Chapter 2

NICKEL-CATALYZED CROSS-COUPLINGS OF UNACTIVATED SECONDARY AND TERTIARY ALKYL BROMIDES WITH SILICON NUCLEOPHILES

The text in this chapter was reproduced in part with permission from:
Chu, C. K.; Liang, Y.; Fu, G. C. *J. Am. Chem. Soc.* **2016**, *138*, 6404–6407.
The work described was performed in collaboration with Dr. Yufan Liang, who performed mechanistic studies and contributed to the writing of the manuscript.

Abstract

The formation of C–C bonds from unactivated alkyl electrophiles has been extensively investigated, but methods to form analogous C–heteroatom bonds are far less developed. The first cross-coupling reaction of unactivated secondary and tertiary alkyl electrophiles to form C–Si bonds is described. Using a commercially available nickel complex $NiBr_2$·diglyme, a variety of alkyl bromides efficiently undergo cross-coupling with silylzinc reagents at low temperature. This nickel-catalyzed silylation method represents a rare example of employing unactivated tertiary alkyl halides as electrophilic coupling partners. Additionally, the versatility of this reaction is demonstrated through compatibility with different classes of silicon nucleophiles. Stereochemical studies and relative reactivity experiments are consistent with the generation of a radical intermediate for C–X bond cleavage.

Introduction

Beyond their role as synthetic intermediates,[1] organosilicon compounds exhibit diverse applications in fields ranging from materials science[2] to agrochemistry[3] to medicinal chemistry.[4] Silicon-containing agrochemicals have reached broad commercial application due to their function as antifungals and insecticides. Furthermore, the introduction of silicon atoms as isosteres for carbon has become a strategy for tuning biological properties by

medicinal chemists. However, the synthesis of these compounds is limited by several factors. Tetraorganosilanes are typically prepared either through the hydrosilylation of olefins (Figure 2.1(a)), where issues of reactivity (e.g., hindered substrates) and regioselectivity (e.g., 1,2-disubstituted olefins) can present significant challenges,[5,6] or through the reaction of an organic nucleophile with a silicon electrophile (Figure 2.1(b)),[7] for which general methods are limited to primary alkyl nucleophiles.[8] In principle, the coupling of an alkyl electrophile with a silicon nucleophile (Figure 2.1(c)) could provide a general approach for the synthesis of tetraorganosilanes; however, progress in developing this reaction has been rather limited, especially with respect to catalyzed processes. Indeed, to the best of our knowledge, catalyzed methods have been restricted to couplings of activated alkyl electrophiles (e.g., allylic, benzylic, and propargylic),[9] with the exception of two reports of the cross-coupling of unactivated primary alkyl electrophiles.[10,11]

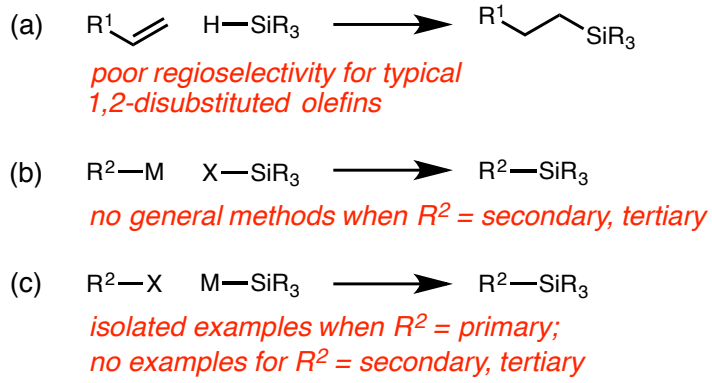

Figure 2.1. Three approaches to the synthesis of tetraorganosilanes.

Over the past decade, significant progress has been made toward developing catalytic cross-coupling reactions of alkyl electrophiles to generate C−C bonds.[12] However, similar transformations to generate bonds to heteroatoms are far less common. As part of an ongoing effort to broaden the scope of cross-couplings of alkyl electrophiles, we recently reported our first nickel-catalyzed C−X bond-forming process, the Miyaura borylation of primary, secondary, and tertiary alkyl halides.[13,14] Drawing inspiration from this transformation, we turned our attention to a related silylation reaction. Specifically, we establish that a commercially available nickel catalyst, without an added ligand, catalyzes the cross-coupling of unactivated secondary and tertiary alkyl bromides with silylzinc nucleophiles (Eq. 2.1).

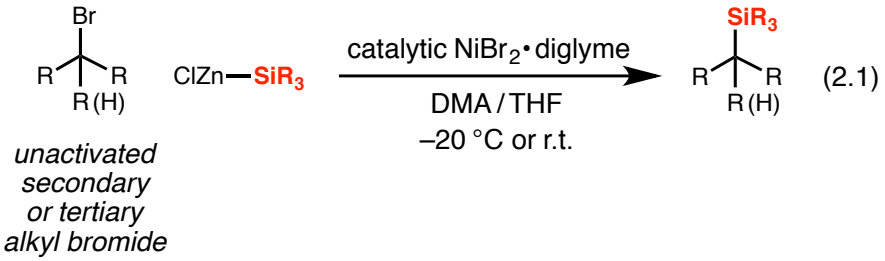

Reaction Optimization

During initial studies, we applied our previously discovered borylation reaction conditions to an analogous silylation reaction involving a silylboron reagent, hoping to achieve similar reactivity.[13] Unfortunately, only trace levels of C–Si bond formation were detected (Eq. 2.2),[15] and further attempts to increase product yields with this nucleophile failed.

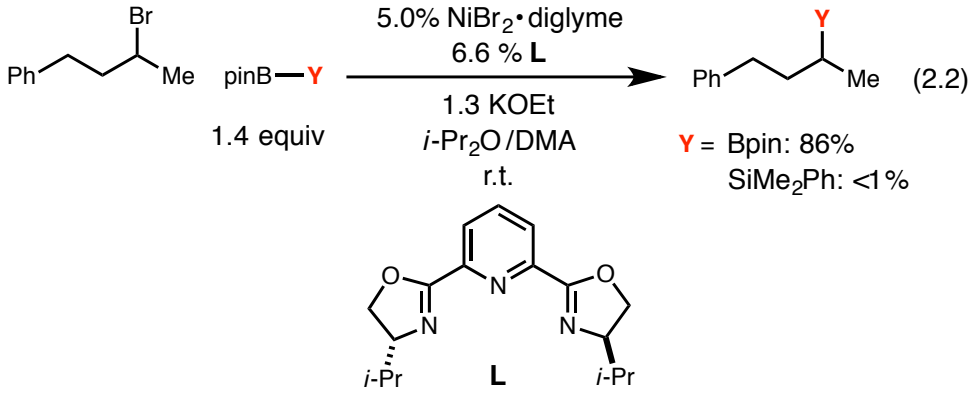

After exploring various reaction parameters with a monosilylzinc halide[16] serving as the nucleophile, we were delighted to find that $NiBr_2$·diglyme could catalyze the silylation reaction of a model unactivated secondary alkyl bromide with $PhMe_2Si$–ZnCl in good yield (Table 2.1, entry 1). As shown in Table 2.1, no C–Si bond formation is observed in the absence of $NiBr_2$·diglyme (entry 2). Under these conditions, other classes of silicon nucleophiles tested are not effective coupling partners (entries 3 and 4). Additionally, other selected transition metal complexes (Fe, Co, Cu, and Pd) are not able to facilitate the reaction (entries 5–8).[17] Without the use of DMA as a co-solvent, the reaction affords almost none of

the desired product (entry 9).[18] A reduction in yield occurs when the reaction is performed with lower catalyst loading, less nucleophile, and at room temperature (entries 10–12). Interestingly, the silylation is only moderately sensitive to air (entry 13) and very tolerant of water (entry 14). This is the first nickel-catalyzed cross-coupling reaction of alkyl electrophiles reported by the Fu laboratory that does not use an added ligand.

Table 2.1. Silylation of a Model Unactivated Secondary Bromide: Effect of Reaction Parameters

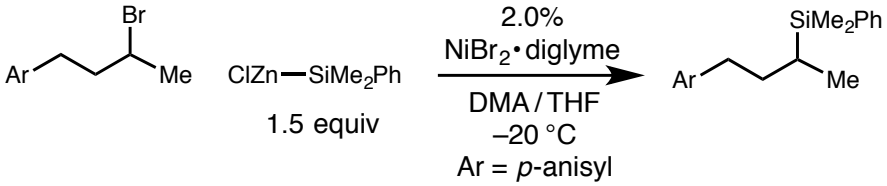

entry	variation from the "standard" conditions	yield (%)[a]
1	none	**84**
2	no $NiBr_2$•diglyme	<1
3	Li–$SiMe_2Ph$, instead of ClZn–$SiMe_2Ph$	2
4	ClMg–$SiMe_2Ph$, instead of ClZn–$SiMe_2Ph$	1
5	$FeCl_2$, instead of $NiBr_2$•diglyme	<1
6	$CoCl_2$, instead of $NiBr_2$•diglyme	2
7	CuBr•SMe_2, instead of $NiBr_2$•diglyme	<1
8	$Pd(MeCN)_2Cl_2$, instead of $NiBr_2$•diglyme	<1
9	no DMA	1
10	0.5 mol% $NiBr_2$•diglyme	60
11	1.1 equiv ClZn–$SiMe_2Ph$	78
12	r.t., instead of –20 °C	73
13	under air in a closed vial	69
14	added H_2O (2.0 equiv)	78

[a]Yields were deteremined by GC analysis with the aid of a calibrated standard (averages of two experiments).

Scope with Respect to the Electrophile

With the optimized conditions in hand, we next investigated the electrophile scope. The commercially available catalyst $NiBr_2$·diglyme can be used for the silylation of an array of unactivated secondary alkyl bromides at –20 ºC (Table 2.2). In addition to the model electrophile (entry 1) used for optimization, sterically hindered α-branched substrates such

Table 2.2. Silylation of Unactivated Secondary Alkyl Bromides: Scope

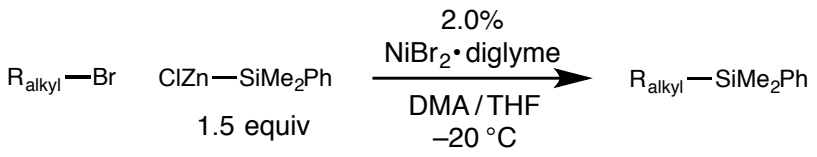

entry	substrate		yield (%)[a]
1	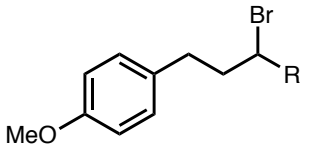	R= Me	79
2[b]		*i*-Pr	76
3[b]		*t*-Bu	68
4	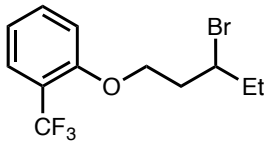		61
5	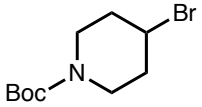		74
6	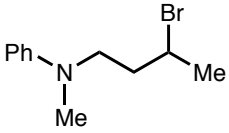		76
7	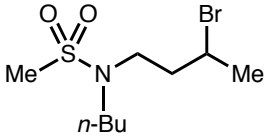		78
8	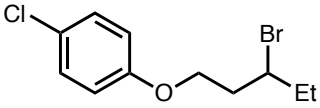		65
9	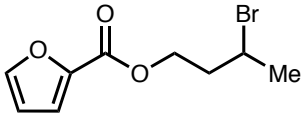		75
10[b]	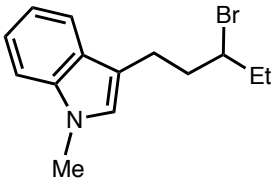		79

[a]Yields of purified products (averages of two experiments). [b]Catalyst loading: 5.0% $NiBr_2 \cdot$diglyme.

as an *iso*-propyl (entry 2) and even a *tert*-butyl (entry 3) substituted alkyl bromide are useful coupling partners. A variety of functional groups, including a trifluoromethyl group (entry 4), a carbamate (entry 5), a tertiary amine (entry 6), a sulfonamide (entry 7), and an aryl chloride (entry 8) are well suited for this reaction. Furthermore, heterocycles such as furan (entry 9) and indole (entry 10) enable efficient C–Si bond formation. These functionalized electrophiles include sensitive groups that are incompatible with the formation of alkyl nucleophiles used in the reaction shown in Figure 2.1(b).[19] Initial studies investigating an alkyl bromide containing thiophene, a secondary alkyl choride, and an alkyl tosylate showed that these are not useful coupling partners under the standard conditions.

While the standard reaction conditions did not facilitate C–Si bond formation with secondary alkyl chlorides, an unactivated secondary alkyl iodide was an effective electrophile (Eq. 2.3).[20] Additionally, this method is adaptable to scale-up, and the cross-coupling reaction shown in Table 2.2, entry 1 can be performed with reduced catalyst loading (1% Ni) in 81% yield.

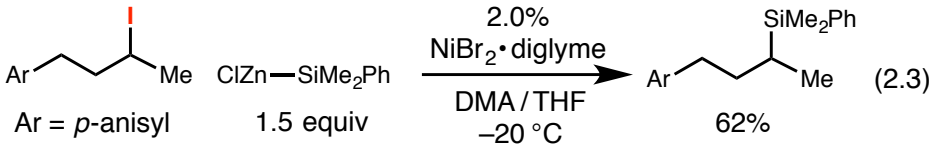

Tertiary alkyl electrophiles are known to be challenging substrates, and reports of unactivated tertiary alkyl electrophiles in cross-coupling reactions have been limited.[21] Thus, we were excited to find that the optimized conditions allow for the coupling of unactivated tertiary alkyl bromides (Table 2.3) in addition to secondary alkyl bromides. Both acyclic (entries 1–3) and cyclic (entries 4–6) substrates are compatible under the standard conditions. Furthermore, an alkyl bromide containing an olefin (entry 3) is demonstrated to be a suitable substrate.

Table 2.3. Silylation of Unactivated Tertiary Alkyl Bromides: Scope

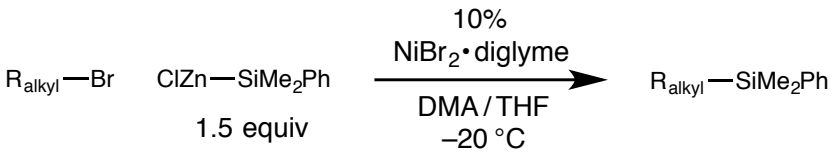

entry	substrate	yield (%)[a]
1	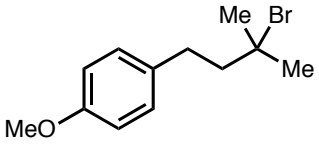	70
2	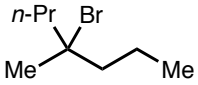	54
3	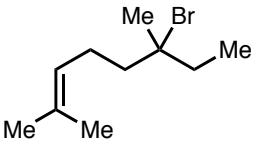	49
4	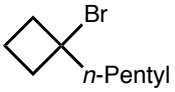	70
5	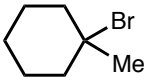	70
6[b]	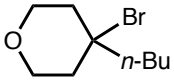	74

[a]Yields of purified products (averages of two experiments). [b]Catalyst loading: 2.0% $NiBr_2 \cdot$diglyme.

In addition to the tertiary alkyl bromides shown in Table 2.3, a preliminary attempt to silylate 3-iodoadamantane under the standard conditions provided a promising result toward the silylation of tertiary alkyl iodides (Eq. 2.4).

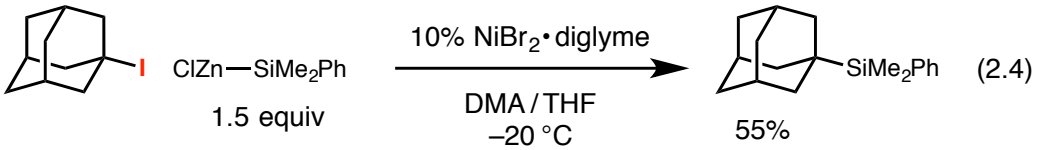

(2.4)

Scope with Respect to the Nucleophile

Following investigations demonstrating that the scope of this new silylation reaction is broad with respect to secondary and tertiary alkyl electrophiles, we next evaluated the compatibility of other silicon nucleophiles. The simple nickel catalyst facilitates C–Si bond formation with silylzinc reagents containing one, two, and three aryl substituents with high steric bulk in good yield (Eq. 2.5).[22]

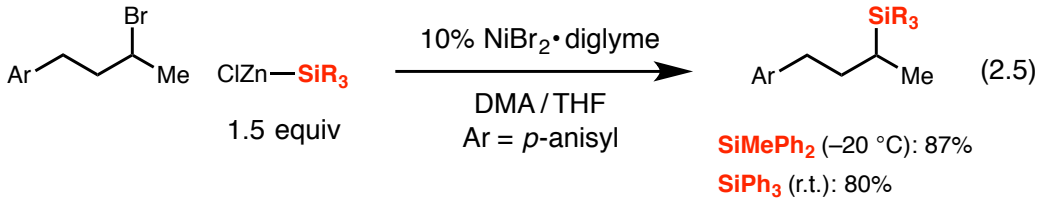

(2.5)

Mechanistic Insights

Previous studies of nickel-catalyzed cross-couplings of unactivated alkyl halides to generate C–C and C–B bonds from the Fu laboratory have suggested that alkyl electrophiles can undergo oxidative addition to form alkyl radical intermediates.[13,23] Our studies of this new C–Si bond forming reaction suggest that oxidative addition occurs by a similar radical mechanism. In the reactions of *exo*- and *endo*-2-bromonorbornane, the same diastereomeric mixture of products is formed (7:1 exo:endo; each alkyl bromide remains a single stereoisomer at partial conversion), consistent with the formation of a common intermediate

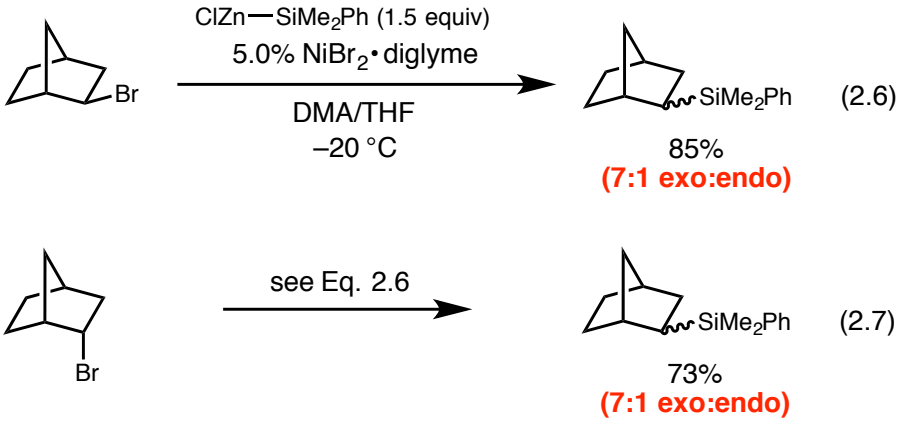

(2.6)

(2.7)

in the two reactions (Eqs. 2.6 and 2.7).[24] Furthermore, the addition of 2,2,6,6-tetramethylpiperidin-1-oxyl (TEMPO),[25] which rapidly traps alkyl radicals, inhibits C–Si bond formation under our standard conditions.

Inspired by the fact that unactivated *tertiary* alkyl electrophiles are effecting coupling partners under our standard conditions, we conducted competition experiments between a tertiary, a secondary, and a primary alkyl bromide (Eqs. 2.8 and 2.9). Electrophiles with higher degrees of substitution demonstrate higher levels of reactivity (tertiary > secondary > primary).[26] This result is consistent with the stability of the radical, rather than steric effects, being the dominant factor influencing relative reactivity, providing further evidence for the generation of a radical intermediate for the oxidative addition step.

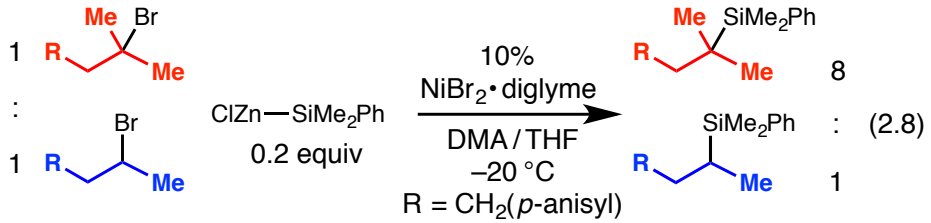

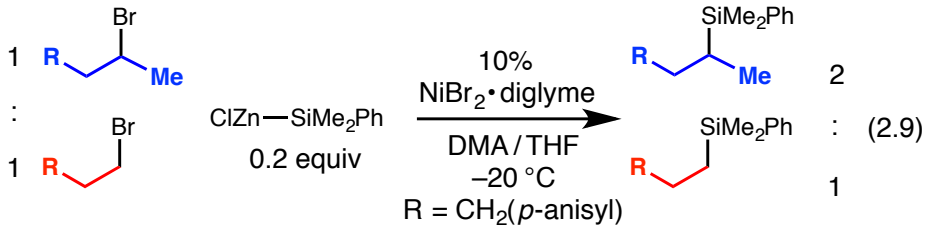

Conclusion

We have described the first cross-coupling reaction of unactivated secondary and tertiary alkyl electrophiles to form C−Si bonds. Using only a commercially available nickel catalyst, we have observed efficient cross-coupling of a variety of silylzinc nucleophiles with both secondary and tertiary alkyl bromides, demonstrating good tolerance of both steric bulk as well as diverse functional groups. Competition experiments suggest that tertiary alkyl bromides are more reactive than secondary or primary alkyl bromides. Preliminary mechanistic studies are consistent with a radical mechanism for oxidative addition.

Experimental Section

General Information

Anhydrous THF was purified and dried using a solvent-purification system that contained activated alumina. The following reagents and solvents were purchased and used as received: lithium metal (granular, 4-10 mesh particle size, 99%; Aldrich), zinc chloride (≥98%; Aldrich), dimethylphenylchlorosilane (TCI), chloro(methyl)diphenylsilane (Aldrich), chlorotriphenylsilane (Acros), $NiBr_2$·diglyme (Aldrich), dimethylacetamide (≥99%, over molecular sieves; Aldrich), triphenylphosphine (Aldrich), bromine (Aldrich), imidazole (Aldrich), LiBr (≥99%; Aldrich), and *N*-Boc-4-bromopiperidine (Aldrich). All other alkyl bromides were prepared from the corresponding alcohols according to General Procedure A or B.

^1H and ^{13}C NMR spectroscopic data were collected on a Varian 500 MHz spectrometer at ambient temperature. GC analyses were obtained on an Agilent 6890 Series GC system with a DB-1 column (length 30 m, internal diameter 0.25 mm).

Preparation of Electrophiles

General Procedure A: Bromination of Secondary Alcohols.[27] Triphenylphosphine (1.3 equiv) and imidazole (1.3 equiv) were dissolved in dry CH_2Cl_2 (0.2 M), and the resulting solution was stirred at 0 °C under a nitrogen atmosphere. Bromine (1.3 equiv) was added dropwise, and the reaction mixture was stirred at 0 °C for 5 min. The alcohol was then added dropwise over 3 min. The reaction mixture was allowed to warm to r.t., and then it was stirred for 6–12 h. A saturated aqueous solution of NH_4Cl was added to the reaction mixture, which was then extracted two times with Et_2O. The combined organic layers were dried over $MgSO_4$, filtered, and concentrated. The residue was purified by flash chromatography (Et_2O/hexane).

General Procedure B: Bromination of Tertiary Alcohols.[28] LiBr (2.0 equiv) was dissolved in 48 wt% aqueous HBr, and the resulting solution was cooled to 0 °C. The alcohol was added at 0 °C, and the reaction mixture was allowed to warm to r.t. and stirred for 3 h. The mixture was then diluted with Et_2O and washed once with each of the following: deionized water, saturated aqueous $NaHCO_3$ solution, and brine. The organic layer was dried

over Na_2SO_4, filtered, and concentrated. The residue was purified by distillation under reduced pressure.

The yields have not been optimized.

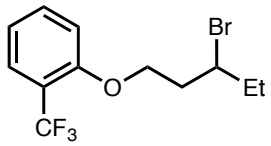

1-((3-Bromopentyl)oxy)-2-(trifluoromethyl)benzene. The bromide was prepared according to General Procedure A from the corresponding alcohol, 1-(2-(trifluoromethyl)phenoxy)pentan-3-ol. The product was purified by flash chromatography (0→2% Et_2O/hexane). Pale-yellow oil (1.42 g, 90%).

^{1}H NMR (500 MHz, $CDCl_3$) δ 7.59 – 7.54 (m, 1H), 7.52 – 7.46 (m, 1H), 7.05 – 6.98 (m, 2H), 4.33 – 4.19 (m, 3H), 2.37 (dddd, 1H, *J* = 15.0, 8.4, 5.8, 3.4 Hz), 2.23 (ddt, 1H, *J* = 14.7, 10.0, 4.5 Hz), 2.03 – 1.87 (m, 2H), 1.10 (t, 3H, *J* = 7.3 Hz).

^{13}C NMR (126 MHz, $CDCl_3$) δ 156.6, 133.3, 127.1 (q, *J* = 5.2 Hz), 123.7 (q, *J* = 272.3 Hz), 120.1, 118.8 (q, *J* = 30.6 Hz), 112.8, 66.4, 55.9, 38.1, 32.4, 12.0.

FT-IR (film) 2971, 1608, 1495, 1460, 1322, 1276, 1258, 1116, 1057, 1037, 754 cm^{-1}.

MS (EI) *m/z* (M^+) calcd for $C_{12}H_{14}{}^{79}BrF_3O$: 310, found: 310.

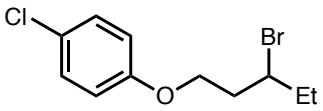

1-((3-Bromopentyl)oxy)-4-chlorobenzene. The bromide was prepared according to General Procedure A from the corresponding alcohol, 1-(4-chlorophenoxy)pentan-3-ol. The product was purified by flash chromatography (0→2% Et_2O/hexane). Pale-yellow oil (1.01 g, 92%).

^{1}H NMR (500 MHz, $CDCl_3$) δ 7.27 – 7.20 (m, 2H), 6.85 – 6.80 (m, 2H), 4.23 (ddt, 1H, *J* = 12.6, 8.1, 2.8), 4.17 – 4.08 (m, 2H), 2.35 – 2.25 (m, 1H), 2.25 – 2.15 (m, 1H), 2.01 – 1.85 (m, 2H), 1.10 (t, 3H, *J* = 7.3 Hz).

^{13}C NMR (126 MHz, $CDCl_3$) δ 157.3, 129.3, 125.7, 115.8, 66.1, 55.9, 38.1, 32.4, 12.0.

FT-IR (film) 2969, 2934, 2877, 1597, 1581, 1492, 1468, 1245, 823, 670 cm^{-1}.

MS (EI) *m/z* (M^+) calcd for $C_{11}H_{14}{}^{79}BrClO$: 276, found: 276.

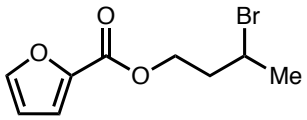

3-Bromobutyl furan-2-carboxylate. The bromide was prepared according to General Procedure A from the corresponding alcohol, 3-hydroxylbutyl furan-2-carboxylate. The product was purified by flash chromatography (10% EtOAc/hexane). Pale-yellow oil (1.34 g, 54%).

^{1}H NMR (500 MHz, $CDCl_3$) δ 7.57 (dd, 1H, *J* = 1.8, 0.9 Hz), 7.17 (dd, 1H, *J* = 3.5, 0.9 Hz), 6.51 (dd, 1H, *J* = 3.5, 1.7 Hz), 4.53 – 4.47 (m, 1H), 4.42 (ddd, 1H, *J* = 11.2, 7.9, 5.7 Hz), 4.27 (dqd, 1H, *J* = 9.0, 6.7, 4.5 Hz), 2.29 – 2.14 (m, 2H), 1.77 (d, 3H, *J* = 6.7 Hz).

^{13}C NMR (126 MHz, $CDCl_3$) δ 158.5, 146.4, 144.4, 118.1, 111.8, 62.9, 46.7, 39.7, 26.5.

FT-IR (film) 2969, 1724, 1473, 1296, 1179, 1116, 885, 761 cm^{-1}.

MS (EI) *m/z* (M^+) calcd for $C_9H_{11}{}^{79}BrO_3$: 246, found: 246.

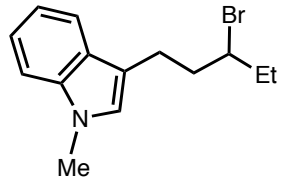

3-(3-Bromopentyl)-1-methyl-1*H*-indole. The bromide was prepared according to General Procedure A from the corresponding alcohol, 1-(1-methyl-1*H*-indol-3-yl)pentan-3-ol. The product was purified by flash chromatography (5→10% EtOAc/hexane). Pale-yellow oil (0.86 g, 34%).

^{1}H NMR (500 MHz, $CDCl_3$) δ 7.63 (dt, 1H, *J* = 7.9, 1.0 Hz), 7.33 – 7.30 (m, 1H), 7.27 – 7.23 (m, 1H), 7.15 – 7.10 (m, 1H), 6.91 (s, 1H), 4.03 (ddt, 1H, *J* = 8.6, 7.1, 5.2 Hz), 3.76 (s, 3H), 3.11 – 3.02 (m, 1H), 2.98 – 2.89 (m, 1H), 2.27 – 2.12 (m, 2H), 1.95 – 1.85 (m, 2H), 1.06 (t, 3H, *J* = 7.2 Hz).

^{13}C NMR (126 MHz, $CDCl_3$) δ 137.0, 127.7, 126.5, 121.5, 118.9, 118.6, 113.5, 109.2, 60.3, 39.3, 32.6, 32.3, 23.2, 12.0.

FT-IR (film) 2933, 1473, 1377, 1325, 1249, 802, 737 cm^{-1}.

MS (EI) *m/z* (M^+) calcd for $C_{14}H_{18}{}^{79}BrN$: 279, found: 281 (M^++2).

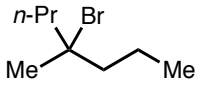

4-Bromo-4-methylheptane. The bromide was prepared according to General Procedure B from the corresponding alcohol, 4-methylheptan-4-ol. The product was distilled at 35 °C under reduced pressure (5 torr). Colorless oil (3.01 g, 81%).

^{1}H NMR (500 MHz, $CDCl_3$) δ 1.87 – 1.72 (m, 4H), 1.70 (s, 3H), 1.56 – 1.45 (m, 4H), 0.94 (t, 6H, *J* = 7.3 Hz).

^{13}C NMR (126 MHz, $CDCl_3$) δ 74.1, 47.7, 31.5, 19.1, 14.1.

FT-IR (film) 2960, 2873, 1465, 1380, 1142, 1125, 806, 745 cm^{-1}.

MS (EI) *m/z* (M^+–Br) calcd for C_8H_{17}: 113, found: 113.

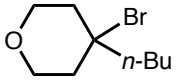

4-Bromo-4-butyltetrahydro-2*H*-pyran. The bromide was prepared according to General Procedure B from the corresponding alcohol, 4-butyltetrahydro-2*H*-pyran-4-ol. The product was distilled at 34 °C under reduced pressure (0.16 torr). Colorless oil (3.43 g, 88%).

^{1}H NMR (500 MHz, $CDCl_3$) δ 3.88 – 3.82 (m, 4H), 1.99 – 1.92 (m, 2H), 1.90 – 1.82 (m, 2H), 1.74 (ddd, 2H, *J* = 14.7, 9.2, 7.7 Hz), 1.59 – 1.51 (m, 2H), 1.41 – 1.31 (m, 2H), 0.94 (t, 3H, *J* = 7.3 Hz).

^{13}C NMR (126 MHz, $CDCl_3$) δ 72.6, 64.6, 46.8, 40.6, 26.6, 22.7, 14.0.

FT-IR (film) 2956, 2862, 1467, 1241, 1140, 1106, 1017, 857, 813, 637 cm^{-1}.

MS (EI) *m/z* (M^+–Br) calcd for $C_9H_{17}O$: 141, found: 141.

Nickel-Catalyzed Silylations of Unactivated Alkyl Halides

General procedure for the preparation of solutions of ClZn–SiMe$_2$Ph and ClZn–SiMePh$_2$.[29] An oven-dried 40-mL vial equipped with a magnetic stir bar was charged

with elemental lithium (174 mg, 25 mmol, 2.5 equiv), closed with a PTFE septum cap, and placed under vacuum. The vial was refilled with argon, and this evacuation-refill cycle was repeated three times. THF (10 mL) was then added via syringe, an argon-filled balloon was attached to the vial, and the suspension was cooled to 0 °C. The chlorosilane (10 mmol, 1.0 equiv) was added via syringe, and then the reaction mixture was sonicated in an ice/water bath for 1 h, allowing the final bath temperature to reach ~10 °C. The mixture was then stirred under argon at 0 °C for 12 h. Next, the vial was warmed to r.t., and the supernatant was removed from the residual lithium metal and transferred via syringe to an oven-dried, septum-capped 40-mL vial equipped with a stir bar under a nitrogen atmosphere; the silyllithium was titrated against diphenylacetic acid according to Kofron's method.[30] In air, $ZnCl_2$ (dried with a heat gun under high vacuum for 20 min prior to the reaction; 1.0 equiv with respect to titrated silyllithium) was quickly weighed into an oven-dried 8-mL vial and placed under vacuum. The vial was refilled with nitrogen, and this evacuation-refill cycle was repeated three times. Dry THF was then added to form an ~1.2 M solution of $ZnCl_2$. This solution was added via syringe into a 40-mL vial equipped with a nitrogen-filled balloon that contained the silyllithium at 0 °C, and the reaction mixture was stirred at 0 °C for 30 min. After warming to r.t., the mixture was filtered under a nitrogen atmosphere by injecting it through a syringe filter directly into a nitrogen-filled, 20-mL scintillation vial sealed with a septum cap. The silylzinc solution (routinely formed as an ~0.4 M solution) was titrated using Knochel's method (at r.t.).[31]

These solutions of silylzinc halide reagents can be stored for 1 month without deterioration under an inert atmosphere at −35 °C.

Procedure for the preparation of a solution of ClZn–SiPh$_3$. An oven-dried 40-mL vial equipped with a magnetic stir bar was charged with elemental lithium (87 mg, 12.5 mmol, 2.5 equiv) and chlorotriphenylsilane (1.47 g, 5.0 mmol, 1.0 equiv), closed with a PTFE septum cap, and placed under vacuum. The vial was refilled with argon, and this evacuation-refill cycle was repeated three times. THF (10 mL) was then added via syringe, an argon-filled balloon was attached to the vial, and the suspension was cooled to 0 °C and sonicated in an ice/water bath for 2 h, allowing the final bath temperature to reach r.t. and forming a brownish-green slurry. The mixture was then stirred under argon at 0 °C for 12 h. Next, the vial was warmed to r.t. and transferred into a nitrogen-filled glovebox. The

supernatant was removed from the residual lithium metal and filtered through a fritted funnel; the dark-green silyllithium was then titrated against diphenyl acetic acid. $ZnCl_2$ (dried with a heat gun under high vacuum for 20 min prior to the reaction; 1.0 equiv with respect to titrated silyllithium) was weighed in the glovebox into an oven-dried 8-mL vial, and dry THF was added to form an ~1.2 M solution of $ZnCl_2$. Outside of the glovebox, this solution was added via syringe into a 40-mL vial that contained the silyllithium at 0 °C, and the reaction mixture was stirred at this temperature for 30 min. After warming to r.t., the vial was transferred into the glovebox, and the reaction mixture was filtered by injecting it through a syringe filter. The silylzinc solution was titrated using Knochel's method for alkylzinc titration.[31]

General procedure for nickel-catalyzed silylations of unactivated alkyl halides. An oven-dried 20-mL vial equipped with a magnetic stir bar was charged with $NiBr_2$·diglyme (4.9 mg, 0.014 mmol) and sealed with a PTFE septum cap. The vial was placed under vacuum and refilled with nitrogen, and this evacuation-refill cycle was repeated three times. DMA (2.1 mL) was added via syringe, and the mixture was stirred vigorously at r.t. for 10 min. The alkyl bromide (0.7 mmol) was added via syringe, followed by stirring at r.t. for 5 min. A nitrogen-filled balloon was attached to the vial, which was then cooled to −20 °C. The mixture was stirred for 5 min, and then the solution of the silylzinc in THF (1.05 mmol, 1.5 equiv) was added, the balloon was removed, the puncture hole was covered with vacuum grease, and the reaction mixture was stirred at −20 °C for 6–24 h. The reaction was then quenched by the addition of ethanol (0.7 mL), followed by stirring for 1 min. The mixture was next allowed to warm to r.t., and then it was diluted with Et_2O (100 mL) and washed with deionized water (20 mL × 3). The organic layer was dried over Na_2SO_4, filtered, and concentrated. The residue was purified by flash chromatography.

For electrophiles that are solids or are viscous liquids: The alkyl bromide (0.70 mmol) was weighed into an oven-dried 20-mL vial charged with a magnetic stir bar, which was then placed under vacuum. The vial was refilled with nitrogen, and this evacuation-refill cycle was repeated three times. The solution of $NiBr_2$·diglyme in DMA prepared as described above was added to the alkyl bromide, and the mixture was stirred vigorously at r.t. for 5 min. The procedure was then completed as described above.

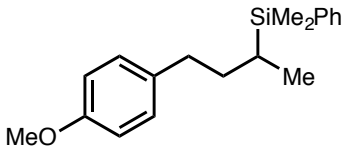

(4-(4-Methoxyphenyl)butan-2-yl)dimethyl(phenyl)silane (Table 2.2, Entry 1). The title compound was synthesized according to the General Procedure, using 2.0 mol% $NiBr_2$·diglyme, from 1-(3-bromobutyl)-4-methoxybenzene (170 mg, 0.70 mmol). Reaction time: 6 h. The product was purified by column chromatography on silica gel (10→15% CH_2Cl_2/hexane). Colorless oil.

First run: 167 mg (80% yield). Second run: 164 mg (78% yield).

This compound was also prepared on a 4.5 mmol scale, using (1-(3-bromobutyl)-4-methoxybenzene (1.09 g, 4.50 mmol), the silylzinc reagent (0.46 M; 14.7 mL, 6.8 mmol, 1.5 equiv), and $NiBr_2$·diglyme (15.9 mg, 0.045 mmol; 1.0 mol%). Reaction time: 12 h. The title compound was isolated in 81% yield (1.09 g).

^{1}H NMR (500 MHz, $CDCl_3$) δ 7.52 – 7.47 (m, 2H), 7.39 – 7.33 (m, 3H), 7.06 – 7.02 (m, 2H), 6.84 – 6.80 (m, 2H), 3.80 (s, 3H), 2.72 (ddd, 1H, J = 14.4, 10.1, 4.8 Hz), 2.43 (ddd, 1H, J = 13.7, 9.7, 6.8 Hz), 1.79 (dddd, 1H, J = 16.7, 9.7, 6.5, 3.2 Hz), 1.46 – 1.34 (m, 1H), 1.05 – 1.00 (m, 3H), 0.96 – 0.87 (m, 1H), 0.26 (d, 6H, J = 4.6 Hz).

^{13}C NMR (126 MHz, $CDCl_3$) δ 157.7, 138.6, 134.9, 133.9, 129.2, 128.8, 127.6, 113.7, 55.2, 33.91, 33.89, 18.7, 14.0, −4.7, −5.0.

FT-IR (film) 2952, 1512, 1246, 1112, 1038, 816, 701 cm^{-1}.

MS (EI) *m/z* (M^+) calcd for $C_{19}H_{26}OSi$: 298, found: 298.

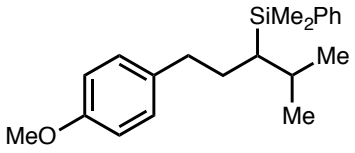

1-(4-Methoxyphenyl)-4-methylpentan-3-yl)dimethyl(phenyl)silane (Table 2.2, Entry 2). The title compound was synthesized according to the General Procedure, using 5.0 mol% $NiBr_2$·diglyme, from 1-(3-bromo-4-methylpentyl)-4-methoxybenzene (190 mg, 0.70 mmol). Reaction time: 24 h. The product was purified by column chromatography on silica gel (0→20% CH_2Cl_2/hexane). Colorless oil.

First run: 175 mg (76% yield). Second run: 173 mg (76% yield).

^{1}H NMR (500 MHz, $CDCl_3$) δ 7.54 – 7.50 (m, 2H), 7.37 – 7.33 (m, 3H), 6.98 – 6.93 (m, 2H), 6.81 – 6.77 (m, 2H), 3.79 (s, 3H), 2.53 – 2.36 (m, 2H), 1.99 (ddq, 1H, *J* = 10.7, 6.9, 3.5 Hz), 1.72 – 1.63 (m, 2H), 0.96 (d, 3H, *J* = 6.8 Hz), 0.92 – 0.87 (m, 4H), 0.34 (d, 6H, *J* = 3.7 Hz).

^{13}C NMR (126 MHz, $CDCl_3$) δ 157.6, 140.1, 135.0, 133.8, 129.2, 128.6, 127.6, 113.6, 55.2, 35.8, 32.6, 29.3, 28.6, 22.9, 21.3, −1.9, −2.7.

FT-IR (film) 2953, 1511, 1246, 1110, 1039, 820, 701 cm^{-1}.

MS (EI) *m/z* (M^+) calcd for $C_{21}H_{30}OSi$: 326, found: 326.

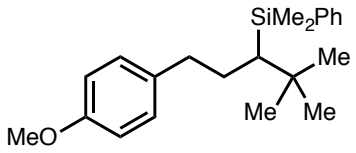

(1-(4-Methoxyphenyl)-4,4-dimethylpentan-3-yl)dimethyl(phenyl)silane (Table 2.2, Entry 3). The title compound was synthesized according to the General Procedure, using 5.0 mol% $NiBr_2$·diglyme, from 1-(3-bromo-4,4-dimethylpentyl)-4-methoxybenzene (200 mg, 0.70 mmol). Reaction time: 24 h. The product was purified by column chromatography on silica gel (0→20% CH_2Cl_2/hexane). Colorless oil.

First run: 161 mg (68% yield). Second run: 161 mg (68% yield).

^{1}H NMR (500 MHz, $CDCl_3$) δ 7.62 – 7.55 (m, 2H), 7.41 – 7.35 (m, 3H), 6.87 – 6.81 (m, 2H), 6.80 – 6.75 (m, 2H), 3.78 (s, 3H), 2.38 (ddd, 1H, *J* = 13.2, 11.5, 5.9 Hz), 2.09 (ddd, 1H, *J* = 13.2, 11.7, 5.6 Hz), 1.67 – 1.52 (m, 2H), 0.96 (s, 9H), 0.75 (dd, 1H, *J* = 4.9, 3.8 Hz), 0.43 (s, 3H), 0.38 (s, 3H).

^{13}C NMR (126 MHz, $CDCl_3$) δ 157.6, 141.0, 135.2, 134.0, 129.1, 128.5, 127.6, 113.6, 55.2, 38.76, 38.74, 34.8, 30.9, 30.6, 0.1, −2.0.

FT-IR (film) 2953, 1512, 1246, 816, 702 cm^{-1}.

MS (EI) *m/z* (M^+) calcd for $C_{22}H_{32}OSi$: 340, found: 325 (M^+-CH_3).

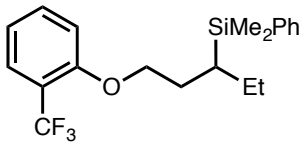

Dimethyl(phenyl)(1-(2-(trifluoromethyl)phenoxy)pentan-3-yl)silane (Table 2.2, Entry 4). The title compound was synthesized according to the General Procedure, using 2.0 mol% $NiBr_2$·diglyme, from 1-((3-bromopentyl)oxy)-2-(trifluoromethyl)benzene (218 mg, 0.70 mmol). Reaction time: 6 h. The product was purified by column chromatography on silica gel (hexane). Colorless oil.

First run: 145 mg (57% yield). Second run: 166 mg (65% yield).

^{1}H NMR (500 MHz, $CDCl_3$) δ 7.58 – 7.52 (m, 3H), 7.43 – 7.39 (m, 1H), 7.37 – 7.33 (m, 3H), 6.99 – 6.94 (m, 1H), 6.79 (d, 1H, *J* = 8.4 Hz), 3.97 – 3.92 (m, 2H), 1.99 (dtd, 1H, *J* = 14.3, 7.2, 5.1 Hz), 1.80 (ddt, 1H, *J* = 14.4, 8.3, 6.1 Hz), 1.61 (dqd, 1H, *J* = 14.0, 7.4, 5.1 Hz), 1.46 – 1.37 (m, 1H), 1.10 (ddt, 1H, *J* = 8.3, 7.1, 5.1 Hz), 0.93 (t, 3H, *J* = 7.4 Hz), 0.33 (d, 6H, *J* = 3.7 Hz).

^{13}C NMR (126 MHz, $CDCl_3$) δ 156.9 (d, *J* = 1.8 Hz), 138.8, 133.8, 133.1, 128.8, 127.7, 127.0 (q, *J* = 5.3 Hz), 127.8 (q, *J* = 272.3 Hz), 119.6, 118.7 (q, *J* = 30.5 Hz), 112.6, 67.9, 28.6, 22.9, 22.5, 13.8, −3.7, −4.2.

FT-IR (film) 2959, 1610, 1460, 1323, 1275, 1258, 1133, 1117, 1057, 1038, 830, 810, 755, 701 cm^{-1}.

MS (EI) *m/z* (M^+) calcd for $C_{20}H_{25}F_3OSi$: 366, found: 351 (M^+−CH_3).

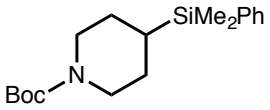

***tert*-Butyl 4-(dimethyl(phenyl)silyl)piperidine-1-carboxylate (Table 2.2, Entry 5).** The title compound was synthesized according to the General Procedure, using 2.0 mol% $NiBr_2$·diglyme, from *tert*-butyl 4-bromopiperidine-1-carboxylate (185 mg, 0.70 mmol). Reaction time: 6 h. The product was purified by column chromatography on silica gel (8:4:1 hexane/CH_2Cl_2/Et_2O). Colorless oil.

First run: 168 mg (75% yield). Second run: 162 mg (73% yield).

^{1}H NMR (500 MHz, $CDCl_3$) δ 7.50 – 7.45 (m, 2H), 7.38 – 7.33 (m, 3H), 4.20 – 4.00 (br, 2H), 2.64 – 2.54 (m, 2H), 1.61 – 1.52 (m, 2H), 1.44 (s, 9H), 1.36 – 1.21 (m, 2H), 0.95 – 0.84 (m, 1H), 0.26 (s, 6H).

^{13}C NMR (126 MHz, $CDCl_3$) δ 154.9, 137.5, 133.9, 129.0, 127.8, 79.1, 45.7, 28.5, 26.6, 23.9, −5.4.

FT-IR (film) 2928, 1693, 1427, 1248, 1167, 832, 809 cm^{-1}.

MS (EI) *m/z* (M^+) calcd for $C_{18}H_{29}NO_2Si$: 319, found: 218 (M^+−Boc).

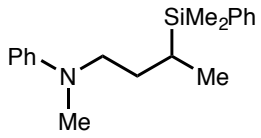

***N*-(3-(Dimethyl(phenyl)silyl)butyl)-*N*-methylaniline (Table 2.2, Entry 6)**. The title compound was synthesized according to the General Procedure, using 2.0 mol% $NiBr_2$·diglyme, from *N*-(3-bromobutyl)-*N*-methylaniline (170 mg, 0.70 mmol). Reaction time: 6 h. The product was purified by column chromatography on silica gel (10→20% CH_2Cl_2/hexane). Pale-yellow oil.

First run: 158 mg (76% yield). Second run: 160 mg (77% yield).

^{1}H NMR (500 MHz, $CDCl_3$) δ 7.54 – 7.49 (m, 2H), 7.40 – 7.33 (m, 3H), 7.23 – 7.17 (m, 2H), 6.70 – 6.60 (m, 3H), 3.41 (ddd, 1H, *J* = 14.9, 10.6, 4.6 Hz), 3.19 (ddd, 1H, *J* = 14.5, 10.3, 6.0 Hz), 2.86 (s, 3H), 1.81 (dddd, 1H, *J* = 13.8, 10.6, 6.1, 3.4 Hz), 1.37 – 1.26 (m, 1H), 1.06 (d, 3H, *J* = 7.3 Hz), 0.93 – 0.85 (m, 1H), 0.28 (d, 6H, *J* = 2.9 Hz).

^{13}C NMR (126 MHz, $CDCl_3$) δ 149.4, 138.3, 133.9, 129.1, 128.9, 127.7, 115.9, 112.1, 52.2, 37.9, 28.4, 17.1, 14.4, −4.7, −5.1.

FT-IR (film) 2953, 1600, 1506, 1248, 1112, 833, 814, 746, 701, 691 cm^{-1}.

MS (EI) *m/z* (M^+) calcd for $C_{19}H_{27}NSi$: 297, found: 297.

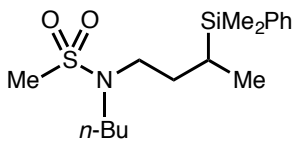

***N*-Butyl-*N*-(3-(dimethyl(phenyl)silyl)butyl)methanesulfonamide (Table 2.2, Entry 7)**. The title compound was synthesized according to the General Procedure, using

2.0 mol% $NiBr_2$·diglyme, from *N*-(3-bromobutyl)-*N*-butylmethanesulfonamide (200 mg, 0.70 mmol). Reaction time: 6 h. The product was purified by column chromatography on silica gel (25→35% Et_2O/hexane). Colorless oil.

First run: 192 mg (80% yield). Second run: 182 mg (76% yield).

^{1}H NMR (500 MHz, $CDCl_3$) δ 7.52 – 7.47 (m, 2H), 7.38 – 7.33 (m, 3H), 3.18 (ddd, 1H, *J* = 14.3, 9.9, 4.6 Hz), 3.13 – 2.96 (m, 3H), 2.74 (s, 3H), 1.75 (dddd, 1H, *J* = 13.4, 10.1, 6.8, 3.5 Hz), 1.52 – 1.40 (m, 2H), 1.33 – 1.20 (m, 3H), 0.99 (d, 3H, *J* = 7.3 Hz), 0.91 – 0.85 (m, 4H), 0.28 (d, 6H, *J* = 0.7 Hz).

^{13}C NMR (126 MHz, $CDCl_3$) δ 138.0, 133.9, 129.0, 127.8, 47.4, 47.0, 38.3, 30.8, 30.7, 19.9, 16.8, 14.0, 13.6, −4.7, −5.4.

FT-IR (film) 2956, 2869, 1334, 1249, 1146, 1112, 835, 816, 773, 702 cm^{-1}.

MS (EI) *m/z* (M^+) calcd for $C_{17}H_{31}NO_2SSi$: 341, found: 326 (M^+-CH_3).

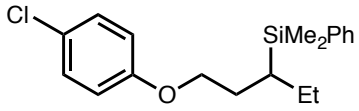

(1-(4-Chlorophenoxy)pentan-3-yl)dimethyl(phenyl)silane (Table 2.2, Entry 8). The title compound was synthesized according to the General Procedure, using 2.0 mol% $NiBr_2$·diglyme, from 1-((3-bromopentyl)oxy)-4-chlorobenzene (195 mg, 0.70 mmol). Reaction time: 6 h. The product was purified by column chromatography on silica gel (0→2% Et_2O/hexane). Colorless oil.

First run: 146 mg (63% yield). Second run: 156 mg (67% yield).

^{1}H NMR (500 MHz, $CDCl_3$) δ 7.55 – 7.50 (m, 2H), 7.39 – 7.32 (m, 3H), 7.21 – 7.16 (m, 2H), 6.73 – 6.67 (m, 2H), 3.88 – 3.75 (m, 2H), 1.93 (dddd, 1H, *J* = 13.6, 8.2, 6.6, 5.1 Hz), 1.77 (dtd, 1H, *J* = 13.8, 8.0, 5.7 Hz), 1.61 (dqd, 1H, *J* = 13.9, 7.5, 5.0 Hz), 1.44 – 1.36 (m, 1H), 1.00 – 0.90 (m, 4H), 0.32 (d, 6H, *J* = 4.1 Hz).

^{13}C NMR (126 MHz, $CDCl_3$) δ 157.6, 138.8, 133.8, 129.2, 128.9, 127.8, 125.3, 115.7, 67.9, 28.7, 23.7, 22.7, 13.9, −3.7, −4.2.

FT-IR (film) 2957, 1492, 1244, 823, 701 cm^{-1}.

MS (EI) *m/z* (M^+) calcd for $C_{19}H_{25}ClOSi$: 332, found: 332.

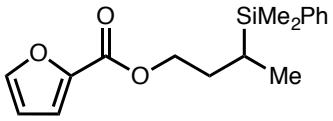

3-(Dimethyl(phenyl)silyl)butyl furan-2-carboxylate (Table 2.2, Entry 9). The title compound was synthesized according to the General Procedure, using 2.0 mol% $NiBr_2$·diglyme, from 3-bromobutyl furan-2-carboxylate (173 mg, 0.70 mmol). Reaction time: 6 h. The product was purified by column chromatography on silica gel (10→15% CH_2Cl_2/hexane). Colorless oil.

First run: 158 mg (75% yield). Second run: 158 mg (75% yield).

^{1}H NMR (500 MHz, $CDCl_3$) δ 7.58 – 7.56 (m, 1H), 7.53 – 7.48 (m, 2H), 7.38 – 7.33 (m, 3H), 7.14 (dd, 1H, J = 3.5, 0.9 Hz), 6.50 (dd, 1H, J = 3.5, 1.7 Hz), 4.40 – 4.22 (m, 2H), 2.01 – 1.91 (m, 1H), 1.54 – 1.41 (m, 1H), 1.09 – 1.00 (m, 4H), 0.29 (d, 6H, J = 4.2 Hz).

^{13}C NMR (126 MHz, $CDCl_3$) δ 158.7, 146.1, 145.0, 137.9, 133.9, 129.0, 127.7, 117.6, 111.7, 64.3, 30.6, 15.9, 13.9, −4.9, −5.2.

FT-IR (film) 2956, 1728, 1475, 1295, 1180, 1117, 833, 815, 764, 702 cm^{-1}.

MS (EI) *m/z* (M^+) calcd for $C_{17}H_{22}O_3Si$: 302, found: 302.

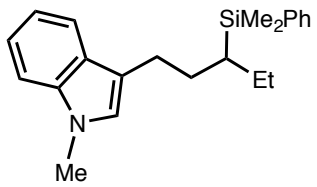

3-(3-(Dimethyl(phenyl)silyl)pentyl)-1-methyl-1*H*-indole (Table 2.2, Entry 10). The title compound was synthesized according to the General Procedure, using 5.0 mol% $NiBr_2$·diglyme, from 3-(3-bromopentyl)-1-methyl-1*H*-indole (196 mg, 0.70 mmol). Reaction time: 6 h. The product was purified by column chromatography on silica gel (10→15% CH_2Cl_2/hexane). Pale-yellow oil.

First run: 186 mg (79% yield). Second run: 185 mg (79% yield).

^{1}H NMR (500 MHz, $CDCl_3$) δ 7.57 – 7.53 (m, 2H), 7.47 (dt, 1H, J = 7.9, 0.9 Hz), 7.40 – 7.34 (m, 3H), 7.30 – 7.27 (m, 1H), 7.24 – 7.20 (m, 1H), 7.10 – 7.07 (m, 1H), 6.72 (s, 1H), 3.73 (s, 3H), 2.79 (dddd, 1H, J = 14.6, 10.8, 5.1, 0.9 Hz), 2.65 (dddd, 1H, J = 14.5, 10.9, 6.0, 0.9 Hz), 1.89 (dddd, 1H, J = 13.7, 10.7, 6.0, 4.7 Hz), 1.79 – 1.62 (m, 2H), 1.56 – 1.45 (m, 1H), 1.01 – 0.90 (m, 4H), 0.33 (d, 6H, J = 3.3 Hz).

^{13}C NMR (126 MHz, $CDCl_3$) δ 139.5, 137.1, 133.9, 128.7, 128.0, 127.7, 125.8, 121.3, 119.1, 118.4, 115.7, 109.0, 32.5, 30.2, 27.1, 24.8, 22.4, 13.8, −3.5, −3.7.

FT-IR (film) 2955, 2929, 1484, 1472, 1426, 1376, 1325, 1247, 1111, 830, 810, 736, 701 cm^{-1}.

MS (EI) *m/z* (M^+) calcd for $C_{22}H_{29}NSi$: 335, found: 335.

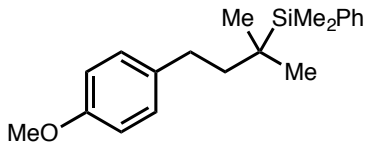

(4-(4-Methoxyphenyl)-2-methylbutan-2-yl)dimethyl(phenyl)silane (Table 2.3, Entry 1). The title compound was synthesized according to the General Procedure, using 10 mol% $NiBr_2$·diglyme, from 1-(3-bromo-3-methylbutyl)-4-methoxybenzene (180 mg, 0.70 mmol). Reaction time: 24 h. The product was purified by column chromatography on silica gel (10→20% CH_2Cl_2/hexane). Colorless oil.

First run: 154 mg (70% yield). Second run: 150 mg (69% yield). The isolated product includes a small amount of a non-polar impurity that co-elutes with the desired product during column chromatography.

^{1}H NMR (500 MHz, $CDCl_3$) δ 7.56 – 7.50 (m, 2H), 7.42 – 7.33 (m, 3H), 7.07 – 7.01 (m, 2H), 6.87 – 6.78 (m, 2H), 3.79 (s, 3H), 2.51 – 2.44 (m, 2H), 1.58 – 1.50 (m, 2H), 0.99 (s, 6H), 0.32 (s, 6H).

^{13}C NMR (126 MHz, $CDCl_3$) δ 157.5, 137.8, 135.6, 134.5, 129.1, 128.8, 127.5, 113.7, 55.2, 41.6, 29.2, 23.1, 20.1, −5.6.

FT-IR (film) 2953, 1512, 1246, 1039, 817, 770, 736, 701 cm^{-1}.

MS (EI) *m/z* (M^+) calcd for $C_{20}H_{28}OSi$: 312, found: 312.

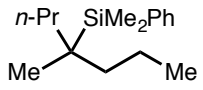

Dimethyl(4-methylheptan-4-yl)(phenyl)silane (Table 2.3, Entry 2). The title compound was synthesized according to the General Procedure, using 10 mol% $NiBr_2$·diglyme, from 4-bromo-4-methylheptane (135 mg, 0.70 mmol). Reaction time: 24 h. The product was purified by column chromatography on silica gel (hexane). Colorless oil.

First run: 94 mg (54% yield). Second run: 92 mg (53% yield).

^{1}H NMR (500 MHz, $CDCl_3$) δ 7.56 – 7.49 (m, 2H), 7.37 – 7.31 (m, 3H), 1.36 – 1.17 (m, 8H), 0.91 – 0.80 (m, 9H), 0.30 (s, 6H).

^{13}C NMR (126 MHz, $CDCl_3$) δ 139.0, 134.5, 128.5, 127.4, 39.3, 24.0, 22.2, 17.5, 15.2, –4.1.

FT-IR (film) 2956, 2871, 1467, 1427, 1248, 1112, 816, 767, 735, 700 cm^{-1}.

MS (EI) *m/z* (M^+) calcd for $C_{16}H_{28}Si$: 248, found: 248.

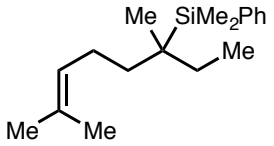

(3,7-Dimethyloct-6-en-3-yl)dimethyl(phenyl)silane (Table 2.3, Entry 3). The title compound was synthesized according to the General Procedure, using 10 mol% $NiBr_2$·diglyme, from 6-bromo-2,6-dimethyloct-2-ene (153 mg, 0.70 mmol). Reaction time: 24 h. The product was purified by column chromatography on silica gel (hexane). Colorless oil.

First run: 92 mg (48% yield). Second run: 95 mg (49% yield).

^{1}H NMR (500 MHz, $CDCl_3$) δ 7.56 – 7.49 (m, 2H), 7.38 – 7.30 (m, 3H), 5.08 – 5.03 (m, 1H), 1.92 – 1.84 (m, 2H), 1.71 – 1.65 (m, 3H), 1.58 – 1.56 (m, 3H), 1.41 – 1.24 (m, 4H), 0.89 (s, 3H), 0.81 (t, 3H, J = 7.5 Hz), 0.32 (s, 6H).

^{13}C NMR (126 MHz, $CDCl_3$) δ 138.9, 134.5, 130.8, 128.6, 127.4, 125.4, 36.0, 28.6, 25.7, 23.8, 23.0, 21.6, 17.6, 8.7, −4.1, −4.2.

FT-IR (film) 2960, 1460, 1427, 1377, 1248, 1110, 830, 811, 767, 735, 701 cm^{-1}.

MS (EI) *m/z* (M^+) calcd for $C_{18}H_{30}Si$: 274, found: 274.

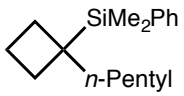

Dimethyl(1-pentylcyclobutyl)(phenyl)silane (Table 2.3, Entry 4). The title compound was synthesized according to the General Procedure, using 10 mol% $NiBr_2$·diglyme, from 1-bromo-1-pentylcyclobutane (144 mg, 0.70 mmol). Reaction time: 24

h. The product was purified by column chromatography on silica gel (hexane). Colorless oil.

First run: 121 mg (66% yield). Second run: 132 mg (73% yield).

^{1}H NMR (500 MHz, $CDCl_3$) δ 7.58 – 7.53 (m, 2H), 7.39 – 7.32 (m, 3H), 2.13 – 2.05 (m, 2H), 1.93 – 1.76 (m, 3H), 1.70 – 1.59 (m, 1H), 1.51 – 1.42 (m, 2H), 1.31 – 1.15 (m, 6H), 0.86 (t, 3H, J = 7.1 Hz), 0.33 (s, 6H).

^{13}C NMR (126 MHz, $CDCl_3$) δ 138.9, 134.1, 128.7, 127.5, 39.6, 32.9, 29.2, 28.3, 25.2, 22.6, 17.2, 14.1, −4.9.

FT-IR (film) 2924, 2853, 1247, 1112, 815, 699 cm^{-1}.

MS (EI) *m/z* (M^+) calcd for $C_{17}H_{28}Si$: 260, found: 260.

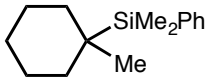

Dimethyl(1-methylcyclohexyl)(phenyl)silane (Table 2.3, Entry 5). The title compound was synthesized according to the General Procedure, using 10 mol% $NiBr_2$·diglyme, from 1-bromo-1-methylcyclohexane (124 mg, 0.70 mmol). Reaction time: 24 h. The product was purified by column chromatography on silica gel (hexane). Colorless oil.

First run: 113 mg (69% yield). Second run: 118 mg (72% yield). The isolated product includes a small amount of a non-polar impurity that co-elutes with the desired product during column chromatography.

^{1}H NMR (500 MHz, $CDCl_3$) δ 7.54 – 7.48 (m, 2H), 7.38 – 7.32 (m, 3H), 1.65 – 1.56 (m, 1H), 1.55 – 1.40 (m, 4H), 1.40 – 1.26 (m, 4H), 1.17 – 1.05 (m, 1H), 0.95 (s, 3H), 0.27 (s, 6H).

^{13}C NMR (126 MHz, $CDCl_3$) δ 137.7, 134.7, 128.6, 127.3, 31.9, 26.7, 20.3, 20.0, 17.9, −6.5.

FT-IR (film) 2916, 1426, 1246, 1106, 815, 766, 734, 699 cm^{-1}.

MS (EI) *m/z* (M^+) calcd for $C_{15}H_{24}Si$: 232, found: 232.

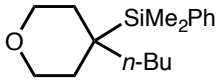

(4-Butyltetrahydro-2*H*-pyran-4-yl)dimethyl(phenyl)silane (Table 2.3, Entry 6). The title compound was synthesized according to the General Procedure, using 2.0 mol% $NiBr_2$·diglyme, from 4-bromo-4-butyltetrahydro-2*H*-pyran (155 mg, 0.70 mmol). Reaction time: 24 h. The product was purified by column chromatography on silica gel (5→10% Et_2O/hexane). Colorless oil.

First run: 145 mg (75% yield). Second run: 142 mg (73% yield).

^{1}H NMR (500 MHz, $CDCl_3$) δ 7.52 – 7.47 (m, 2H), 7.38 – 7.32 (m, 3H), 3.71 – 3.56 (m, 4H), 1.90 – 1.79 (m, 2H), 1.61 – 1.54 (m, 2H), 1.37 – 1.30 (m, 2H), 1.28 – 1.20 (m, 2H), 1.17 – 1.09 (m, 2H), 0.85 (t, 3H, J = 7.3 Hz), 0.32 (s, 6H).

^{13}C NMR (126 MHz, $CDCl_3$) δ 137.9, 134.5, 128.9, 127.6, 62.6, 31.5, 30.6, 27.6, 23.8, 21.8, 14.0, −4.7.

FT-IR (film) 2953, 2931, 2858, 1427, 1249, 1105, 866, 826, 809, 767, 736, 701 cm^{-1}.

MS (EI) *m/z* (M^+) calcd for $C_{17}H_{28}OSi$: 276, found: 261 (M^+-CH_3).

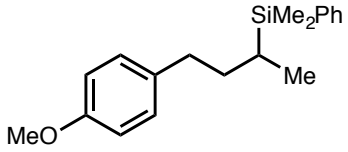

(4-(4-Methoxyphenyl)butan-2-yl)dimethyl(phenyl)silane (Eq. 2.3). The title compound was synthesized according to the General Procedure, using 2.0 mol% $NiBr_2$·diglyme, from 1-(3-iodobutyl)-4-methoxybenzene (203 mg, 0.70 mmol). Reaction time: 6 h. The product was purified by column chromatography on silica gel (10→25% CH_2Cl_2/hexane). Colorless oil.

First run: 130 mg (62% yield). Second run: 130 mg (62% yield).

For the characterization data, see Table 2, Entry 1 (above).

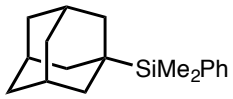

(Adamantan-1-yl)dimethyl(phenyl)silane (Eq. 2.4). The title compound was synthesized according to the General Procedure, using 10 mol% $NiBr_2$·diglyme, from 1-iodoadamantane (183 mg, 0.70 mmol). Reaction time: 24 h. The product was purified by column chromatography on silica gel (hexane). Colorless oil.

First run: 102 mg (54% yield). Second run: 105 mg (56% yield).

^{1}H NMR (500 MHz, $CDCl_3$) δ 7.51 – 7.46 (m, 2H), 7.39 – 7.33 (m, 3H), 1.84 – 1.81 (m, 3H), 1.77 – 1.63 (m, 12H), 0.23 (s, 6H).

^{13}C NMR (126 MHz, $CDCl_3$) δ 137.2, 134.6, 128.6, 127.3, 37.5, 37.1, 27.6, 21.5, −7.3.

FT-IR (film) 2896, 2843, 1426, 1252, 1115, 852, 827, 799, 764, 733, 699 cm^{-1}.

MS (ESI) *m/z* (M^+) calcd for $C_{18}H_{26}Si$: 270, found: 270.

The spectral data are in agreement with literature data.[32]

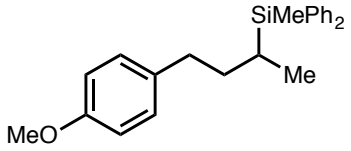

(4-(4-Methoxyphenyl)butan-2-yl)(methyl)diphenylsilane (Eq. 2.5). The title compound was synthesized according to the General Procedure, using 10 mol% $NiBr_2$·diglyme, from 1-(3-bromobutyl)-4-methoxybenzene (170 mg, 0.70 mmol) and a silylzinc reagent prepared from chloro(methyl)diphenylsilane. Reaction time: 24 h. The product was purified by column chromatography on silica gel (10→20% CH_2Cl_2/hexane). Colorless oil.

First run: 224 mg (89% yield). Second run: 216 mg (85% yield).

^{1}H NMR (500 MHz, $CDCl_3$) δ 7.52 – 7.48 (m, 4H), 7.41 – 7.32 (m, 6H), 7.05 – 7.00 (m, 2H), 6.85 – 6.80 (m, 2H), 3.81 (s, 3H), 2.76 (ddd, 1H, J = 14.0, 9.6, 4.7 Hz), 2.47 (ddd, 1H, J = 13.7, 9.2, 7.4 Hz), 1.94 – 1.84 (m, 1H), 1.46 (dddd, 1H, J = 13.6, 10.8, 9.2, 4.7 Hz), 1.39 – 1.30 (m, 1H), 1.10 (d, 3H, J = 7.3 Hz), 0.54 (s, 3H).

^{13}C NMR (126 MHz, $CDCl_3$) δ 157.6, 136.5, 136.3, 134.81, 134.78, 134.6, 129.4, 129.03, 128.99, 127.71, 127.69, 113.6, 55.2, 33.77, 33.71, 16.8, 14.0, −6.4.

FT-IR (film) 3068, 2952, 2852, 1611, 1511, 1427, 1244, 1110, 1037, 785, 699 cm^{-1}.

MS (EI) *m/z* (M^+) calcd for $C_{24}H_{28}OSi$: 360, found: 360.

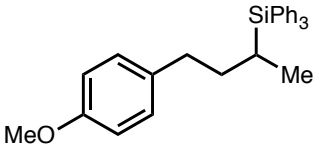

(4-(4-Methoxyphenyl)butan-2-yl)triphenylsilane (Eq. 2.5). The title compound was synthesized according to the General Procedure, using 10 mol% $NiBr_2$·diglyme, from 1-(3-bromobutyl)-4-methoxybenzene (170 mg, 0.70 mmol) and a silylzinc reagent prepared from chlorotriphenylsilane. Reaction time: 24 h; reaction temperature: r.t. The product was purified by column chromatography on silica gel (10→20% CH_2Cl_2/hexane). Colorless, viscous oil.

First run: 234 mg (79% yield). Second run: 236 mg (80% yield).

^{1}H NMR (500 MHz, $CDCl_3$) δ 7.56 – 7.53 (m, 6H), 7.44 – 7.40 (m, 3H), 7.39 – 7.34 (m, 6H), 7.09 – 7.05 (m, 2H), 6.88 – 6.84 (m, 2H), 3.82 (s, 3H), 2.83 (ddd, 1H, *J* = 13.6, 9.0, 4.6 Hz), 2.56 (dt, 1H, *J* = 13.6, 8.3 Hz), 2.10 (dddd, 1H, *J* = 13.7, 9.0, 8.0, 2.3 Hz), 1.75 – 1.66 (m, 1H), 1.58 – 1.48 (m, 1H), 1.25 (d, 3H, *J* = 7.3 Hz).

^{13}C NMR (126 MHz, $CDCl_3$) δ 157.6, 136.0, 134.5, 134.3, 129.5, 129.2, 127.7, 113.6, 55.2, 34.0, 33.6, 15.8, 14.3.

FT-IR (film) 3067, 2931, 1511, 1428, 1246, 1109, 741, 700 cm^{-1}.

MS (ESI) *m/z* (M^+) calcd for $C_{29}H_{30}OSi$: 422, found: 345 ($M^+-C_6H_5$).

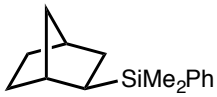

(*exo*-Bicyclo[2.2.1]heptan-2-yl)dimethyl(phenyl)silane (Eq. 2.6) [65118-96-9]. The title compound was synthesized according to the General Procedure, using 5.0 mol% $NiBr_2$·diglyme, from *exo*-2-bromobicyclo[2.2.1]heptane (123 mg, 0.70 mmol). Reaction time: 24 h. The product was purified by column chromatography on silica gel (hexane). Colorless oil. The diastereoselectivity was determined by GC analysis of the unpurified cross-coupling product.

The major diastereomer was determined to be the exo isomer by comparing the ^{1}H NMR data with the data reported in the literature.[33] Additionally, after converting the product mixture to the corresponding bicyclo[2.2.1]heptan-2-ol via a Fleming oxidation,[34] the major alcohol product was confirmed to be the exo isomer by comparing with commercially available *exo*-bicyclo[2.2.1]heptan-2-ol.

First run: 136 mg (84% yield, exo/endo = 7:1). Second run: 137 mg (85% yield, exo/endo = 7:1).

^{1}H NMR (500 MHz, $CDCl_3$) δ (major, exo) 7.57 – 7.52 (m, 2H), 7.38 – 7.35 (m, 3H), 2.25 – 2.23 (m, 2H), 1.56 – 1.39 (m, 4H), 1.29 – 1.20 (m, 2H), 1.08 (m, 2H), 0.86 – 0.82 (m, 1H), 0.27 (s, 3H), 0.25 (s, 3H).

^{13}C NMR (126 MHz, $CDCl_3$) δ (major, exo) 139.4, 133.9, 128.7, 127.6, 37.9, 37.8, 36.9, 34.3, 32.7, 28.9, 28.5, –4.06, –4.10.

FT-IR (film) 2947, 2865, 1427, 1246, 1113, 698 cm^{-1}.

MS (ESI) *m/z* (M^+) calcd for $C_{15}H_{22}Si$: 230, found: 230.

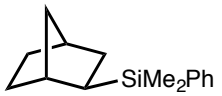

(*exo*-Bicyclo[2.2.1]heptan-2-yl)dimethyl(phenyl)silane (Eq. 2.7) [65118-96-9]. The title compound was synthesized according to the General Procedure, using 5.0 mol% catalyst loading, from *endo*-2-bromobicyclo[2.2.1]heptane (123 mg, 0.70 mmol). Reaction time: 24 h. The product was purified by column chromatography on silica gel (hexane). Colorless oil. The diastereoselectivity was determined by GC analysis of the unpurified cross-coupling product.

First run: 121 mg (75% yield, exo/endo = 7:1). Second run: 114 mg (71% yield, exo/endo = 7:1).

^{1}H NMR (500 MHz, $CDCl_3$) δ (major, exo) 7.56 – 7.52 (m, 2H), 7.38 – 7.35 (m, 3H), 2.25 – 2.23 (m, 2H), 1.57 – 1.39 (m, 4H), 1.29 – 1.20 (m, 2H), 1.08 (m, 2H), 0.86 – 0.81 (m, 1H), 0.27 (s, 3H), 0.25 (s, 3H).

^{13}C NMR (126 MHz, $CDCl_3$) δ (major, exo) 139.3, 133.9, 128.7, 127.6, 37.9, 37.8, 36.9, 34.3, 32.7, 28.9, 28.5, –4.06, –4.10.

FT-IR (film) 2946, 2864, 1426, 1246, 1113, 698 cm^{-1}.

MS (ESI) *m/z* (M^+) calcd for $C_{15}H_{22}Si$: 230, found: 230.

Competition Experiments (Eqs. 2.8 and 2.9). In a nitrogen-filled glovebox, $NiBr_2$·diglyme (3.5 mg, 0.010 mmol) was added to an oven-dried 4-mL vial equipped with a stir bar. DMA (0.3 mL) was added to the vial, and then the vial was closed with a PTFE septum cap and removed from the glovebox. The mixture was vigorously stirred at r.t. for 10 min, and then the two alkyl bromides (0.10 mmol each) were added to the vial via syringe, and the mixture was stirred at r.t. for 5 min. Next, the vial was cooled to –20 °C, and the reaction mixture was stirred for 5 min. Then, a solution of the silylzinc reagent (0.060 M; 0.33 mL, 0.020 mmol, 0.20 equiv) was added in one portion. The reaction mixture was stirred at −20 °C for 4 h, and then the reaction was quenched with ethanol (0.1 mL). *n*-Tetradecane (26 μL) was added to the vial as an internal standard, and the reaction mixture was analyzed via GC.

Effect of TEMPO

Entry 1 (no TEMPO): In a nitrogen-filled glovebox, $NiBr_2$·diglyme (7.0 mg, 0.020 mmol) was added to an oven-dried 4-mL vial equipped with a stir bar. DMA (3.0 mL) was added to the vial, and then the vial was closed with a PTFE septum cap. The mixture was vigorously stirred at r.t. for 10 min. Then, the stock solution of the catalyst (0.30 mL; 0.0020 mmol) was added to a 4-mL vial that contained the alkyl bromide (0.10 mmol) and a stir bar. The vial was closed with a PTFE septum cap and removed from the glovebox. The reaction mixture was stirred at r.t. for 5 min, and then the vial was cooled to –20 °C and the reaction mixture was stirred for an additional 5 min. A nitrogen-filled balloon was affixed to the vial. Next, a solution of the silylzinc reagent in THF (0.15 mmol, 1.5 equiv) was added, and the balloon was removed. The reaction mixture was stirred at –20 °C for 2 h, and then the reaction was quenched by the addition of ethanol (0.1 mL). The mixture was allowed to warm to r.t., *n*-tetradecane (26 μL) was added to the vial, and the reaction mixture was analyzed by GC.

Entries 2 and 3 (with TEMPO): In a nitrogen-filled glovebox, $NiBr_2$·diglyme (7.0 mg, 0.020 mmol) was added to an oven-dried 4-mL vial equipped with a stir bar. DMA (3.0 mL) was added to the vial, and then the vial was closed with a PTFE septum cap. The

mixture was vigorously stirred at r.t. for 10 min. Then, the stock solution of the catalyst (0.30 mL; 0.0020 mmol) was added to a 4-mL vial that contained the alkyl bromide (0.10 mmol), TEMPO (1.6 mg, 0.010 mmol; or, 16 mg, 0.10 mmol), and a stir bar. The vial was closed with a PTFE septum cap and removed from the glovebox. The reaction mixture was stirred at r.t. for 5 min, and then the vial was cooled to –20 °C and the reaction mixture was stirred for an additional 5 min. A nitrogen-filled balloon was affixed to the vial. Next, a solution of the silylzinc reagent in THF (0.15 mmol, 1.5 equiv) was added, and the balloon was removed. The reaction mixture was stirred at –20 °C for 2 h, and then the reaction was quenched by the addition of ethanol (0.1 mL). The mixture was allowed to warm to r.t., *n*-tetradecane (26 μL) was added to the vial, and the reaction mixture was analyzed by GC.

Table 2.4 Effect of TEMPO

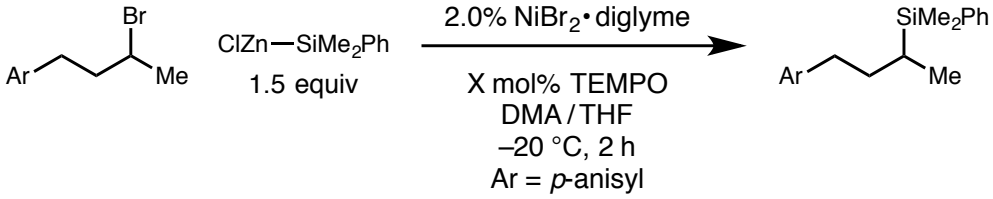

entry	X mol% TEMPO	yield (%)[a]
1	0	86
2	10	24
3	100	<2

[a]Yields were determined by GC analysis with the aid of a calibrated internal standard (average of two experiments).

^{1}H and ^{13}C NMR Spectra

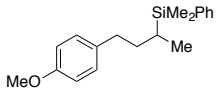

Table 2, Entry 1
^{1}H NMR
($CDCl_3$, 500 MHz)

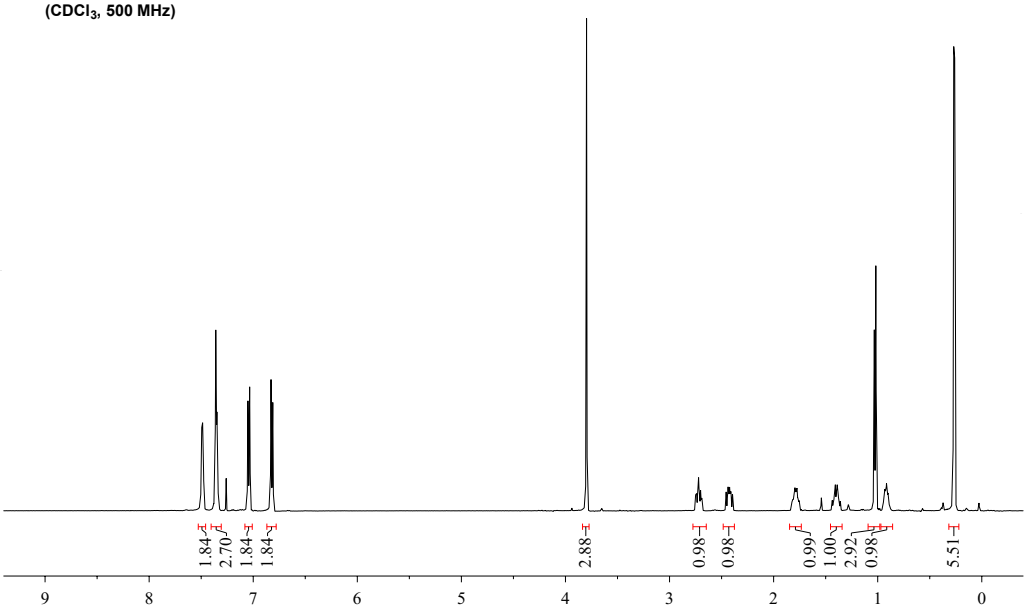

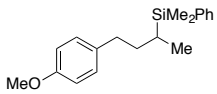

Table 2, Entry 1
^{13}C NMR
($CDCl_3$, 126 MHz)

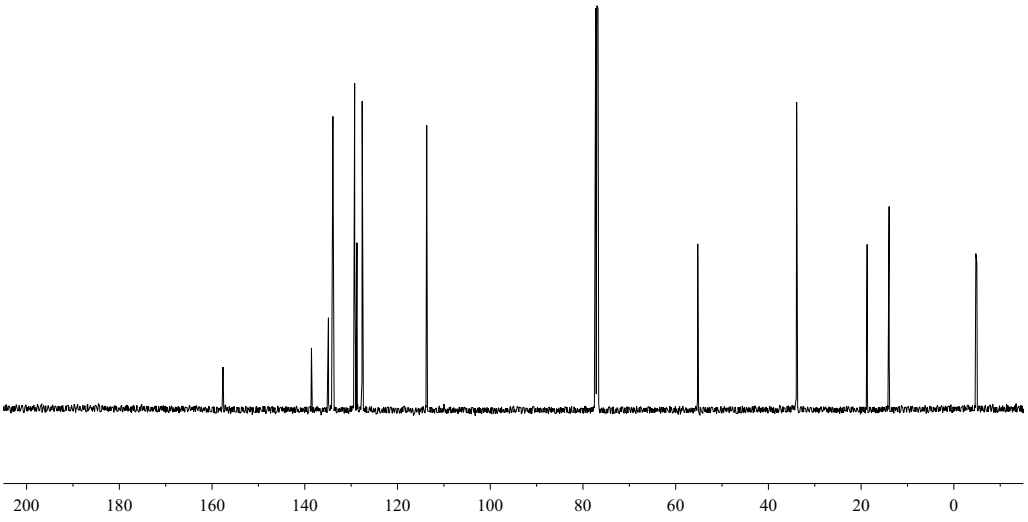

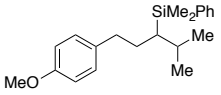

Table 2, Entry 2
^{1}H NMR
($CDCl_3$, 500 MHz)

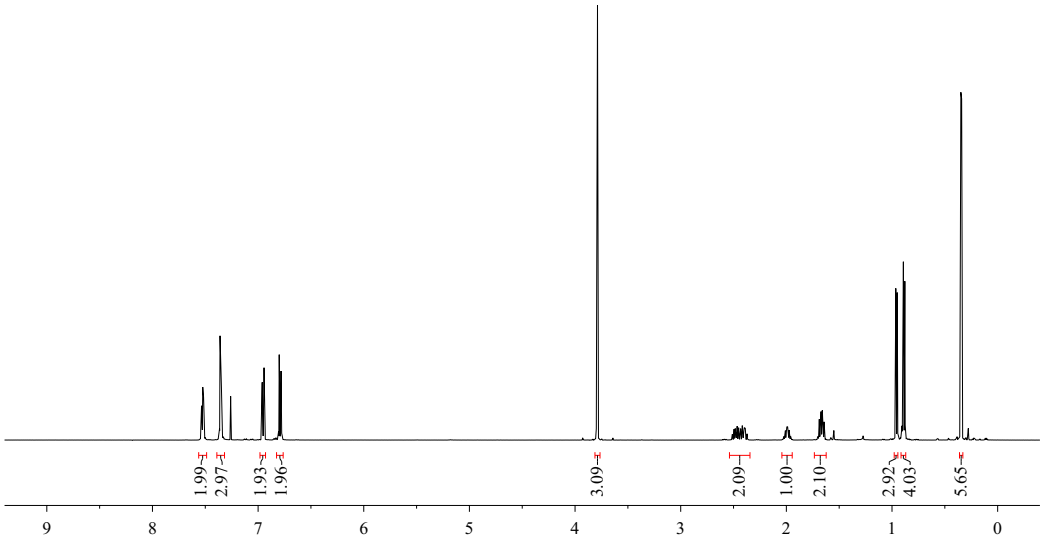

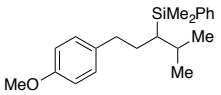

Table 2, Entry 2
^{13}C NMR
($CDCl_3$, 126 MHz)

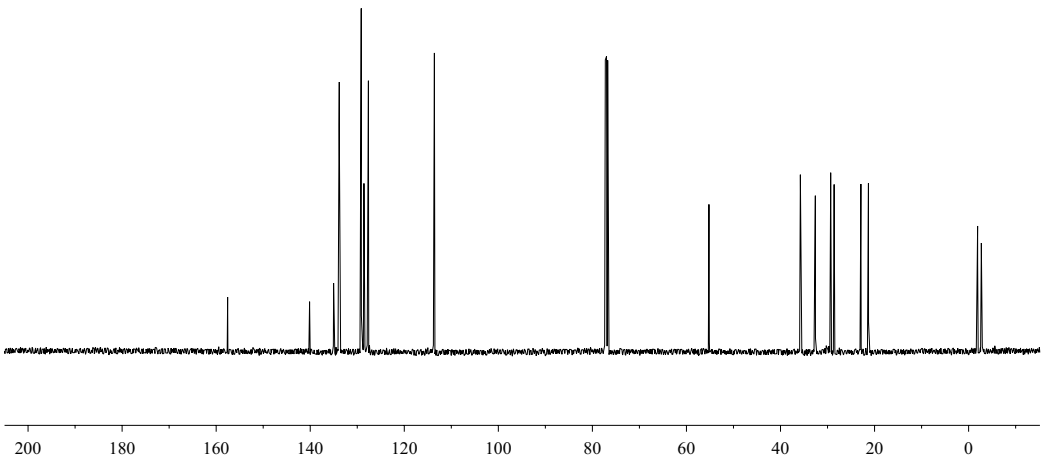

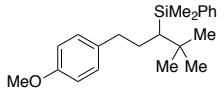

Table 2, Entry 3
^{1}H NMR
($CDCl_3$, 500 MHz)

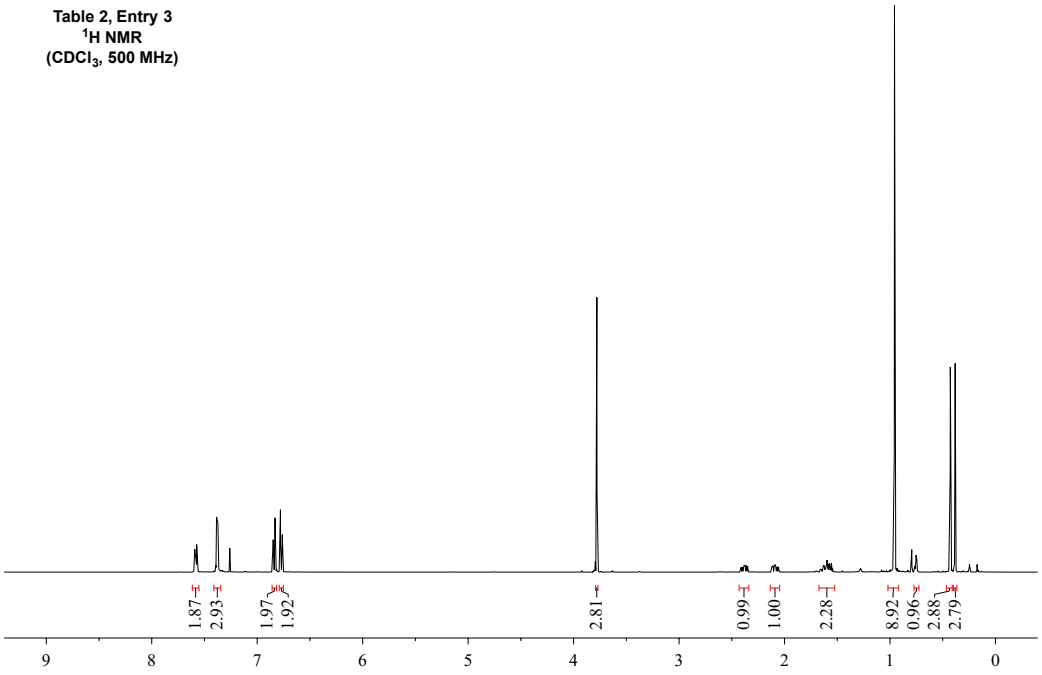

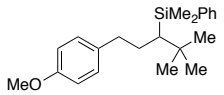

Table 2, Entry 3
^{13}C NMR
($CDCl_3$, 126 MHz)

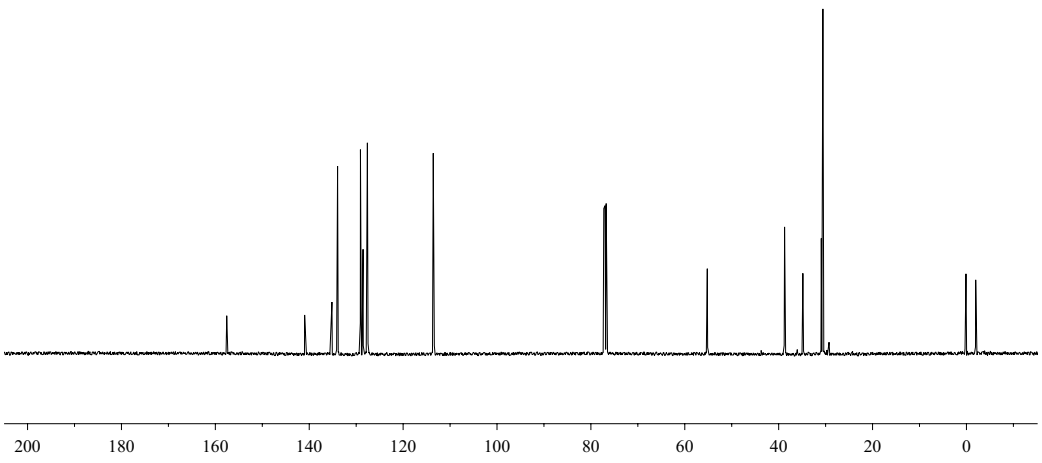

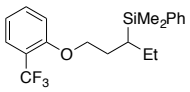

Table 2, Entry 4
^{1}H NMR
($CDCl_3$, 500 MHz)

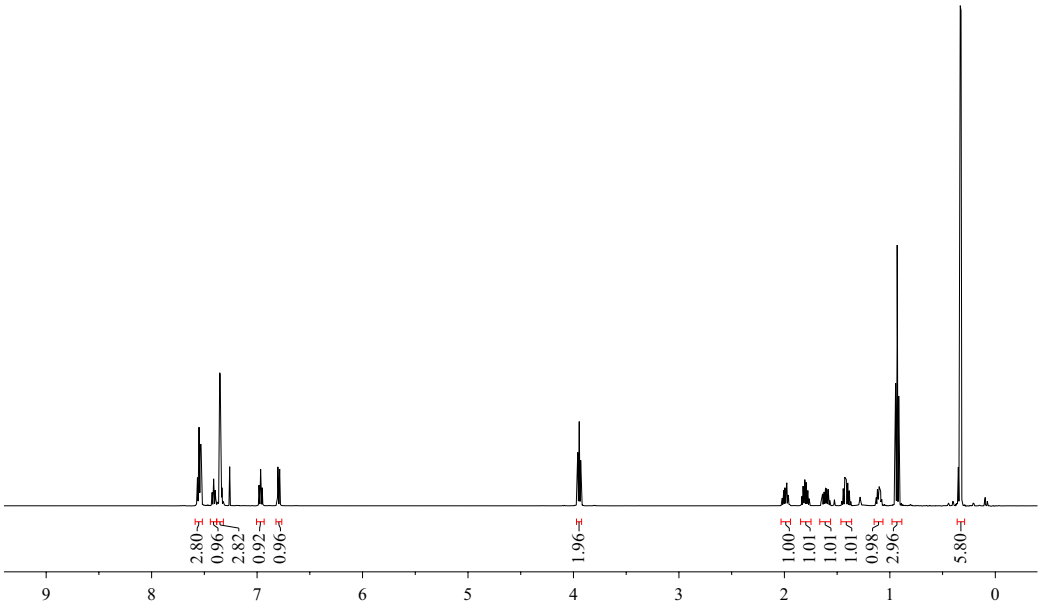

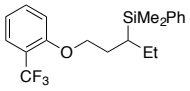

Table 2, Entry 4
^{13}C NMR
($CDCl_3$, 126 MHz)

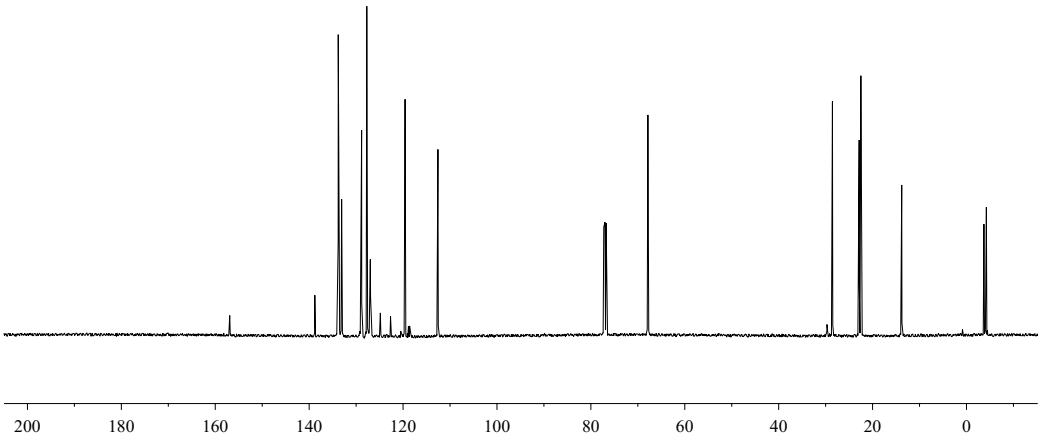

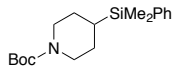

Table 2, Entry 5
^{1}H NMR
($CDCl_3$, 500 MHz)

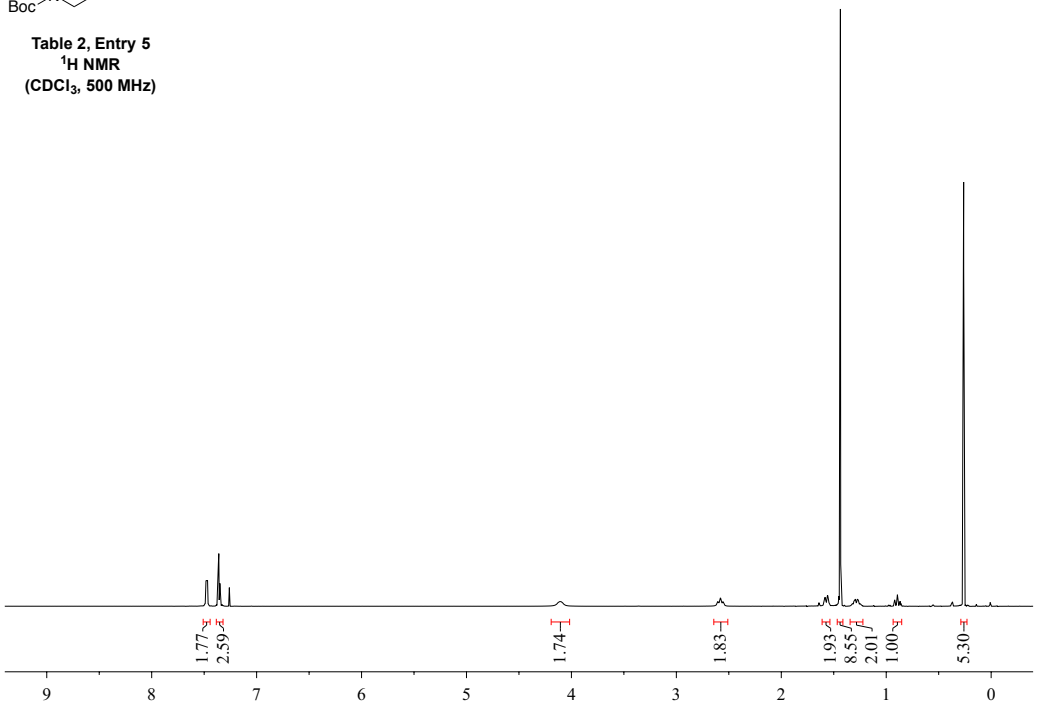

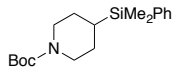

Table 2, Entry 5
^{13}C NMR
($CDCl_3$, 126 MHz)

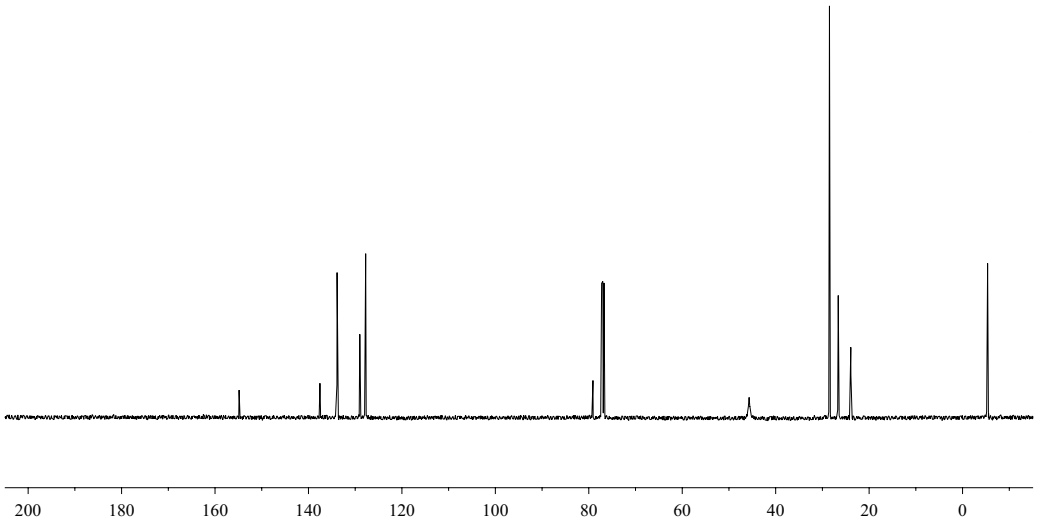

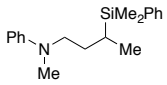

Table 2, Entry 6
^{1}H NMR
($CDCl_3$, 500 MHz)

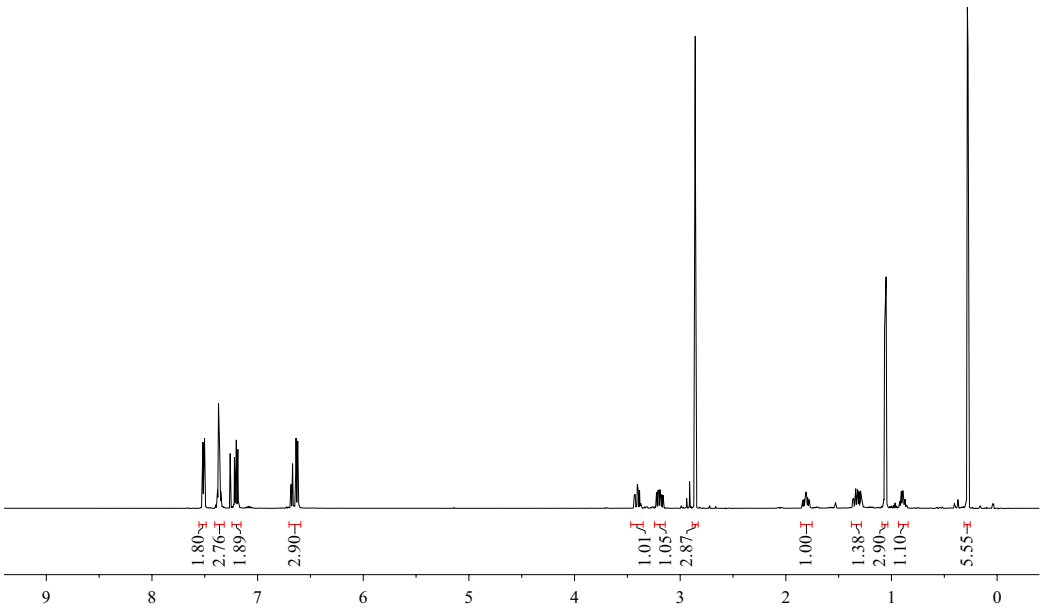

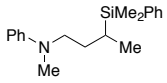

Table 2, Entry 6
^{13}C NMR
($CDCl_3$, 126 MHz)

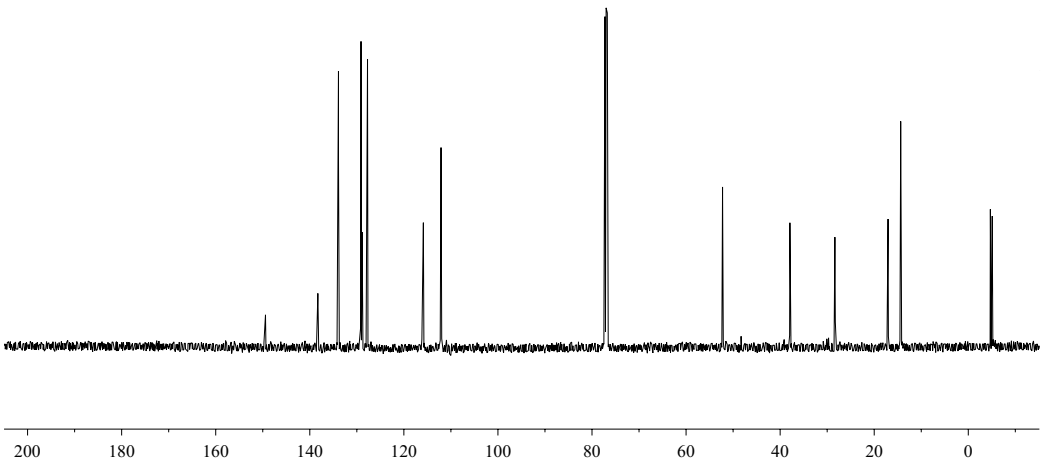

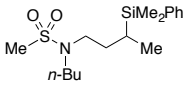

Table 2, Entry 7
^{1}H NMR
($CDCl_3$, 500 MHz)

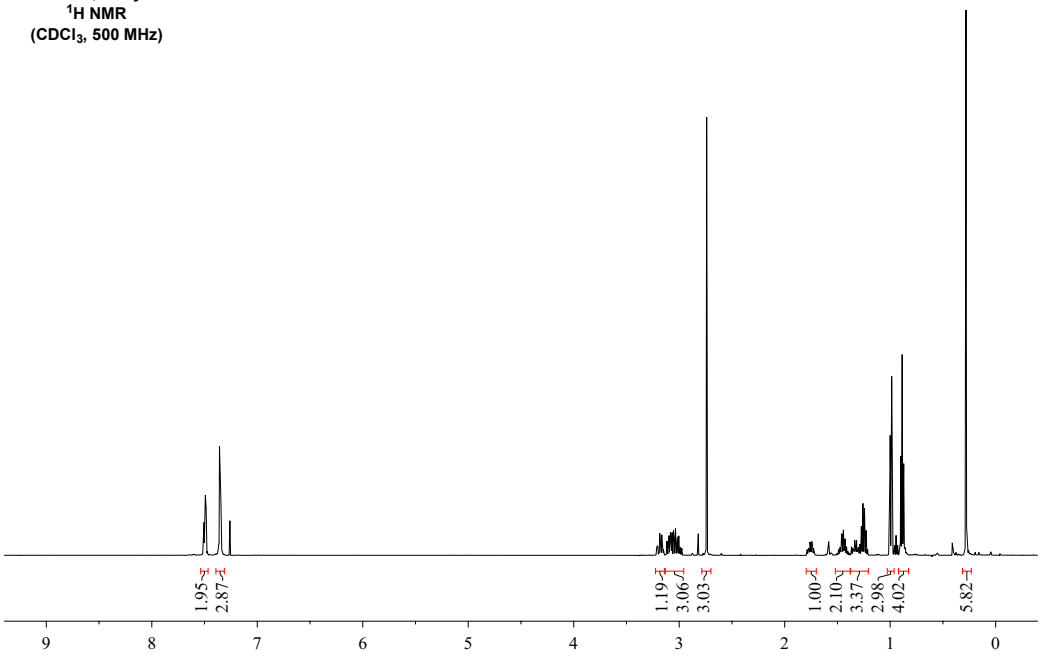

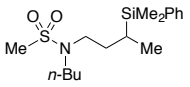

Table 2, Entry 7
^{13}C NMR
($CDCl_3$, 126 MHz)

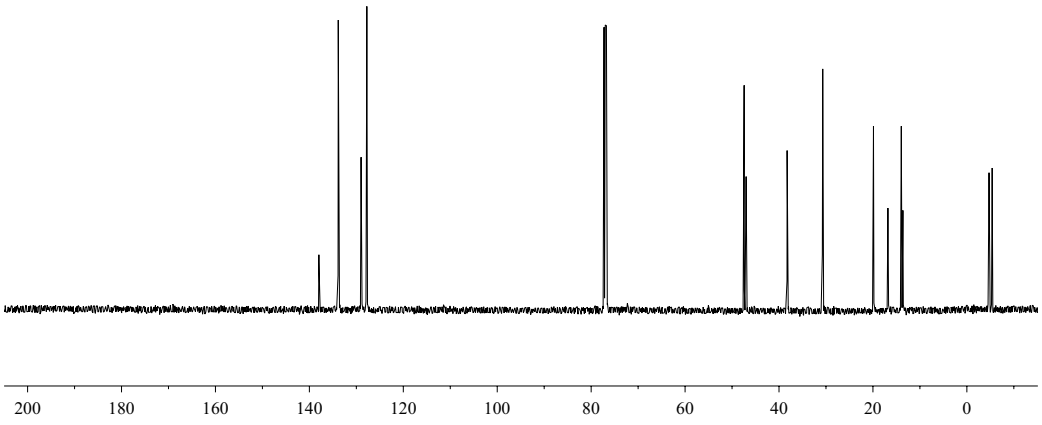

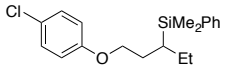

Table 2, Entry 8
^{1}H NMR
($CDCl_3$, 500 MHz)

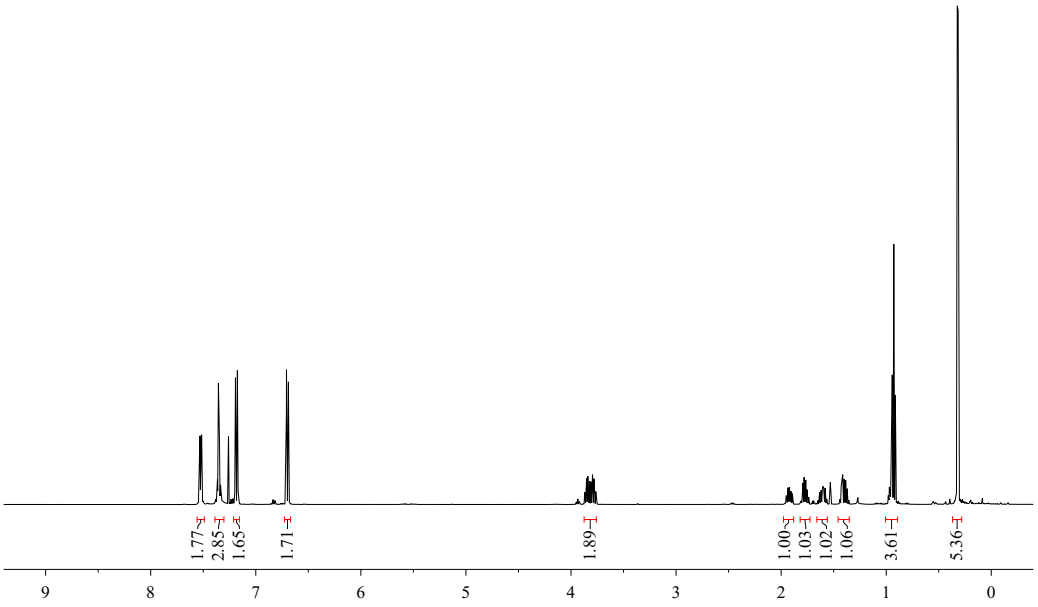

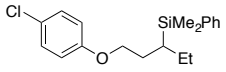

Table 2, Entry 8
^{13}C NMR
($CDCl_3$, 126 MHz)

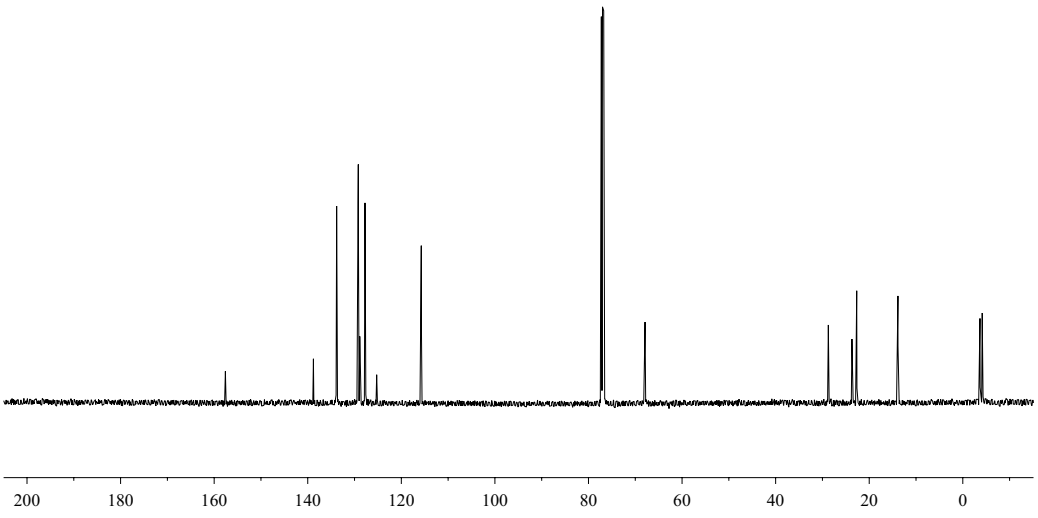

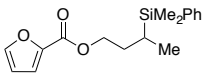

Table 2, Entry 9
^{1}H NMR
($CDCl_3$, 500 MHz)

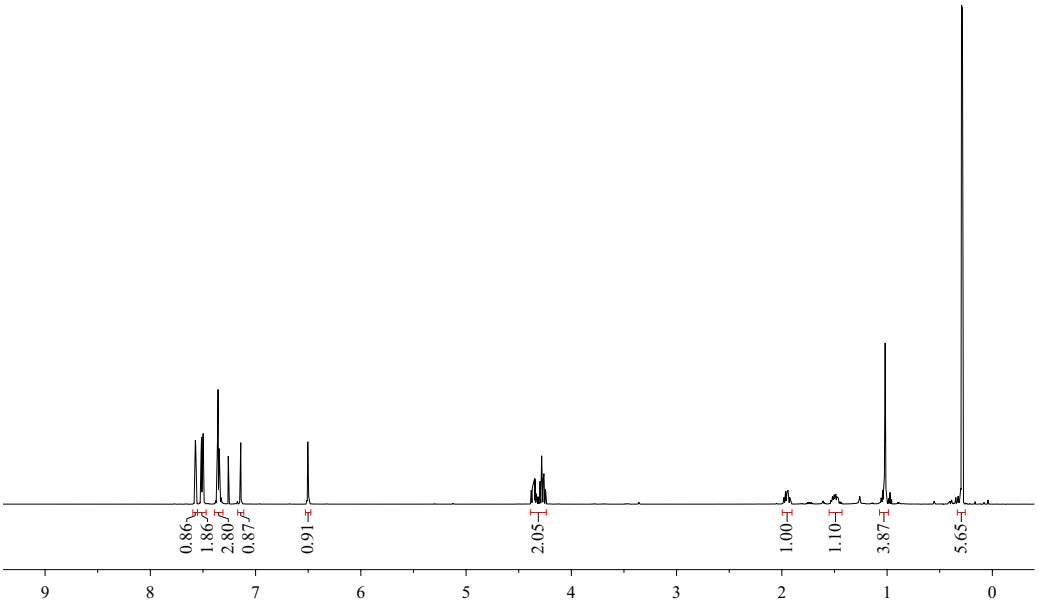

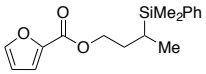

Table 2, Entry 9
^{13}C NMR
($CDCl_3$, 126 MHz)

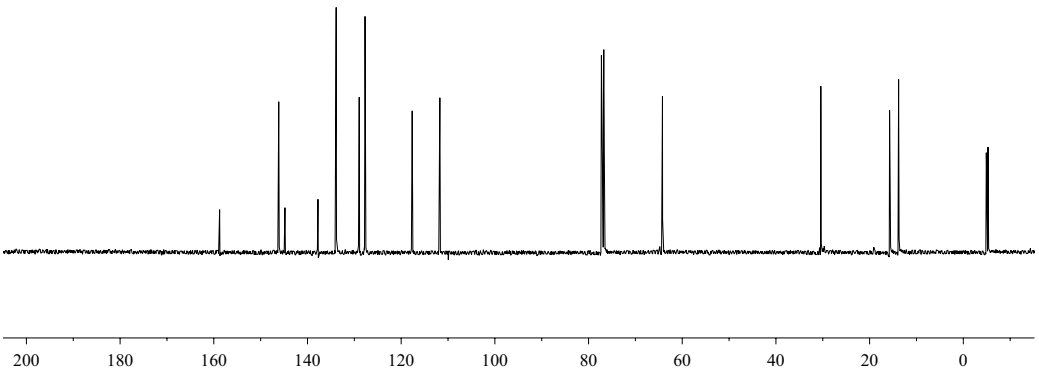

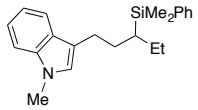

Table 2, Entry 10
^{1}H NMR
($CDCl_3$, 500 MHz)

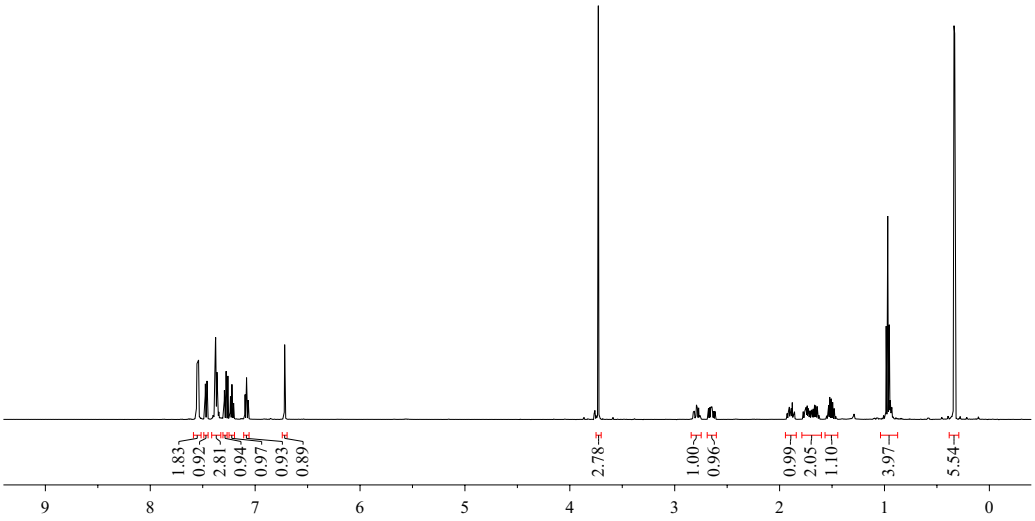

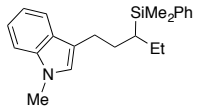

Table 2, Entry 10
^{13}C NMR
($CDCl_3$, 126 MHz)

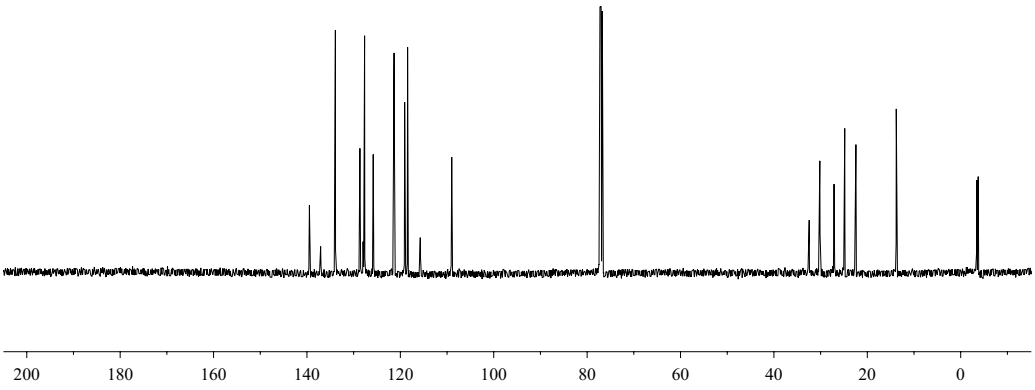

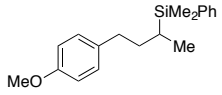

Eq 3
^{1}H NMR
($CDCl_3$, 500 MHz)

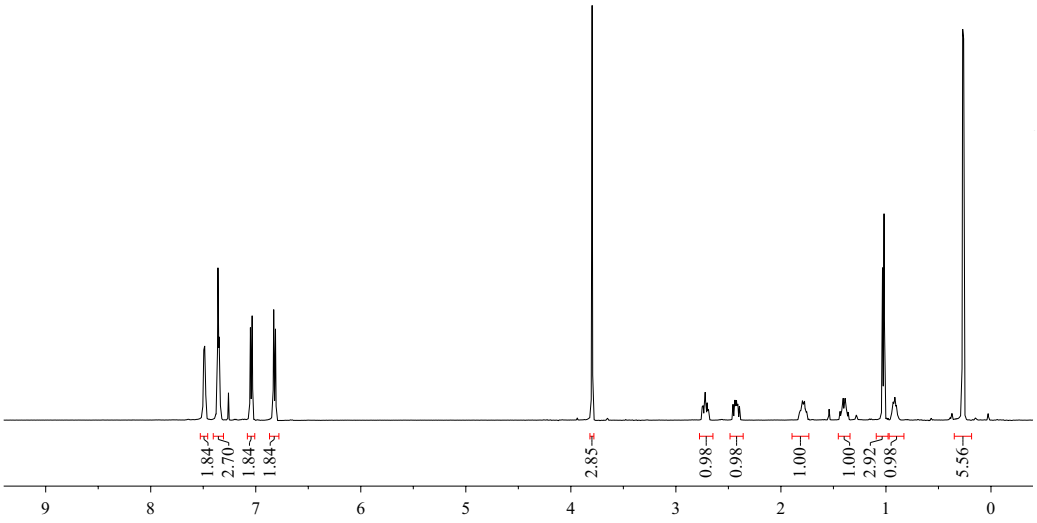

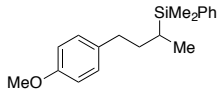

Eq 3
^{13}C NMR
($CDCl_3$, 126 MHz)

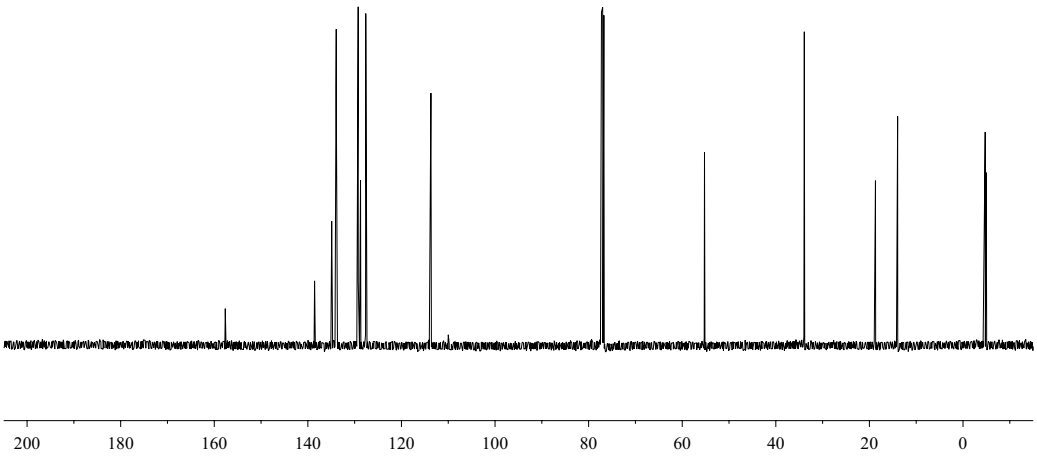

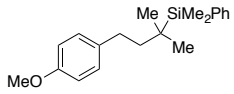

Table 3, Entry 1
^{1}H NMR
($CDCl_3$, 500 MHz)

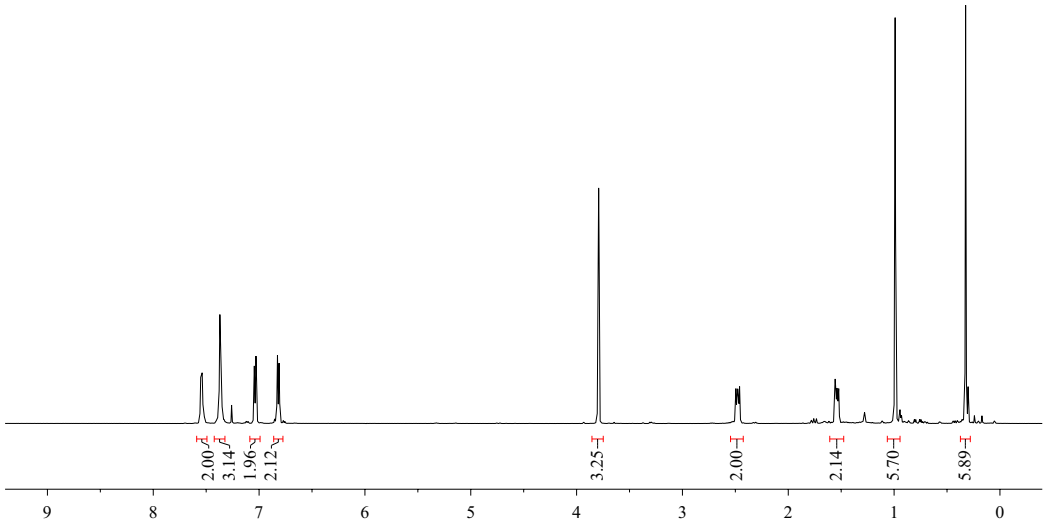

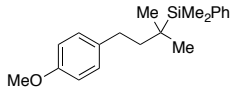

Table 3, Entry 1
^{13}C NMR
($CDCl_3$, 126 MHz)

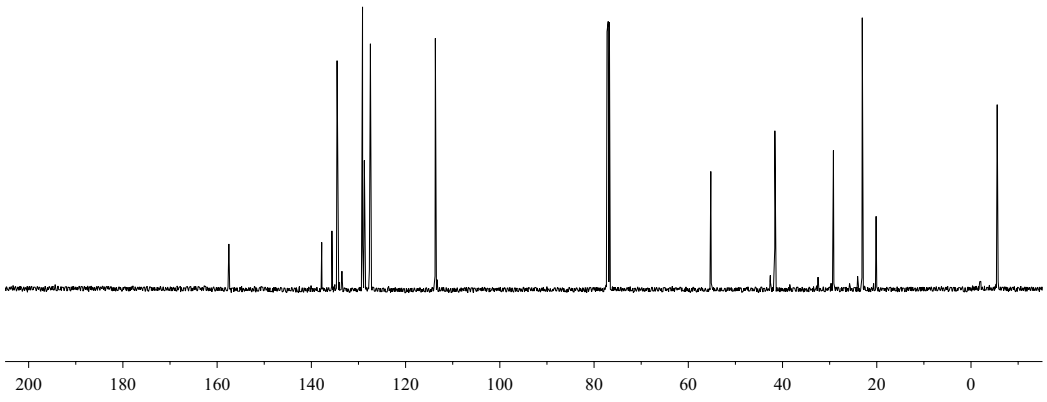

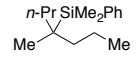

Table 3, Entry 2
^{1}H NMR
($CDCl_3$, 500 MHz)

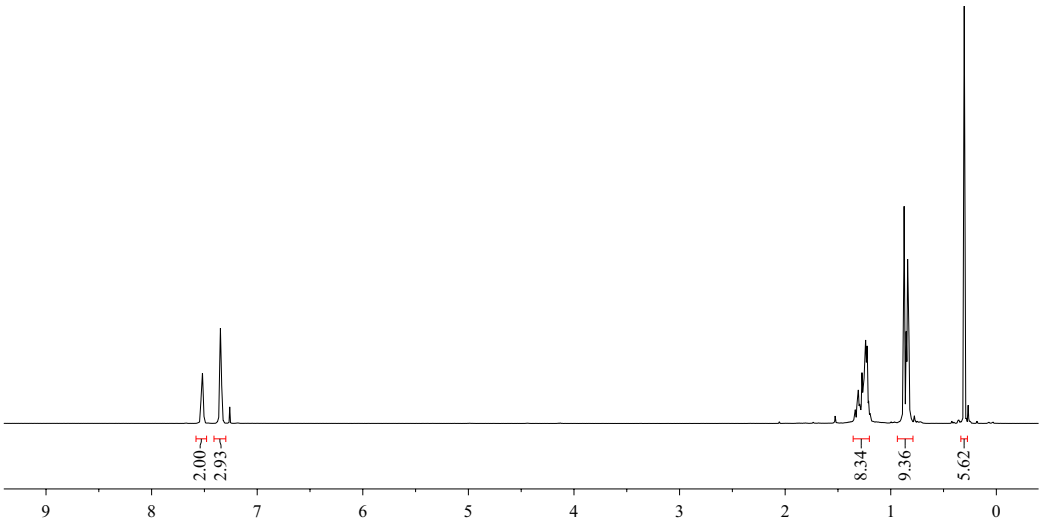

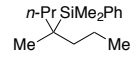

Table 3, Entry 2
^{13}C NMR
($CDCl_3$, 126 MHz)

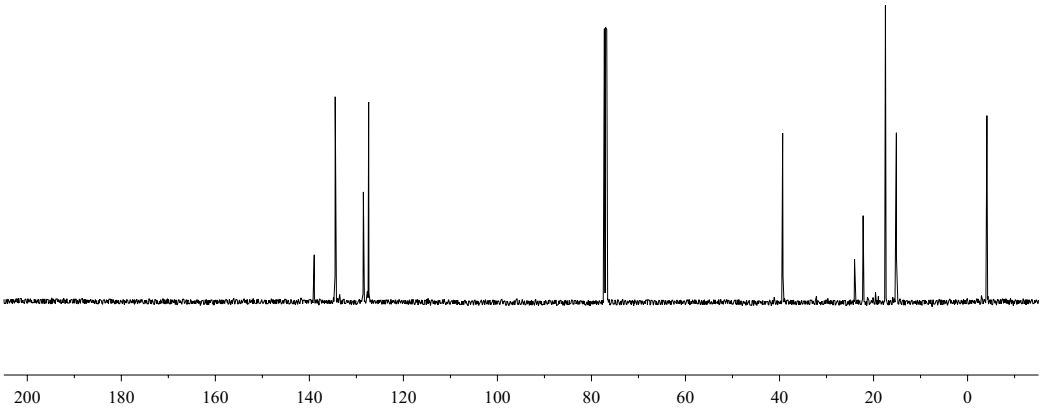

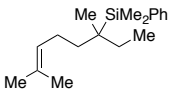

Table 3, Entry 3
^{1}H NMR
($CDCl_3$, 500 MHz)

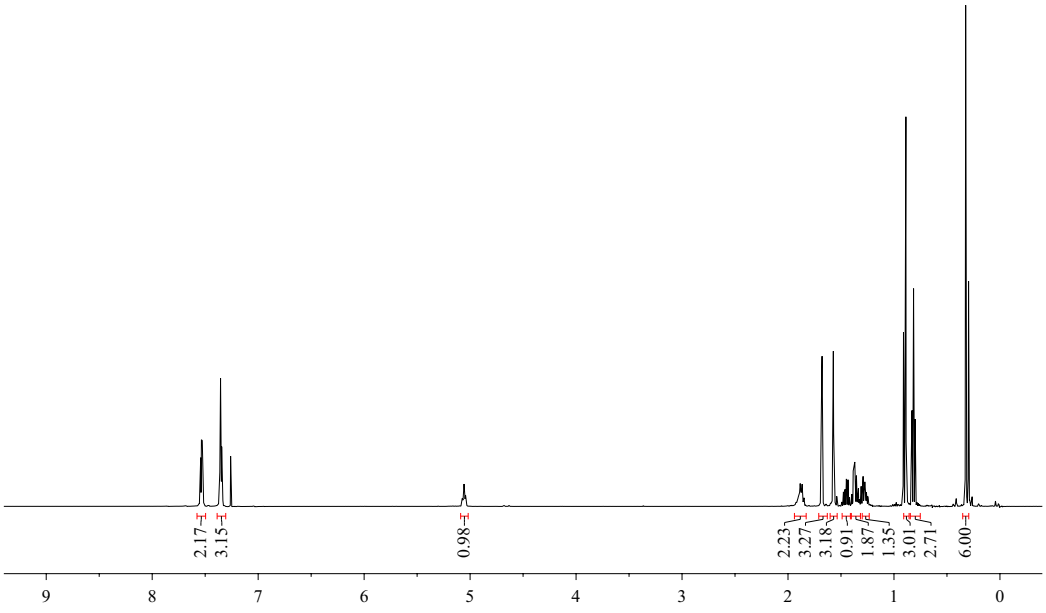

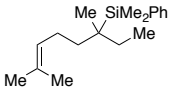

Table 3, Entry 3
^{13}C NMR
($CDCl_3$, 126 MHz)

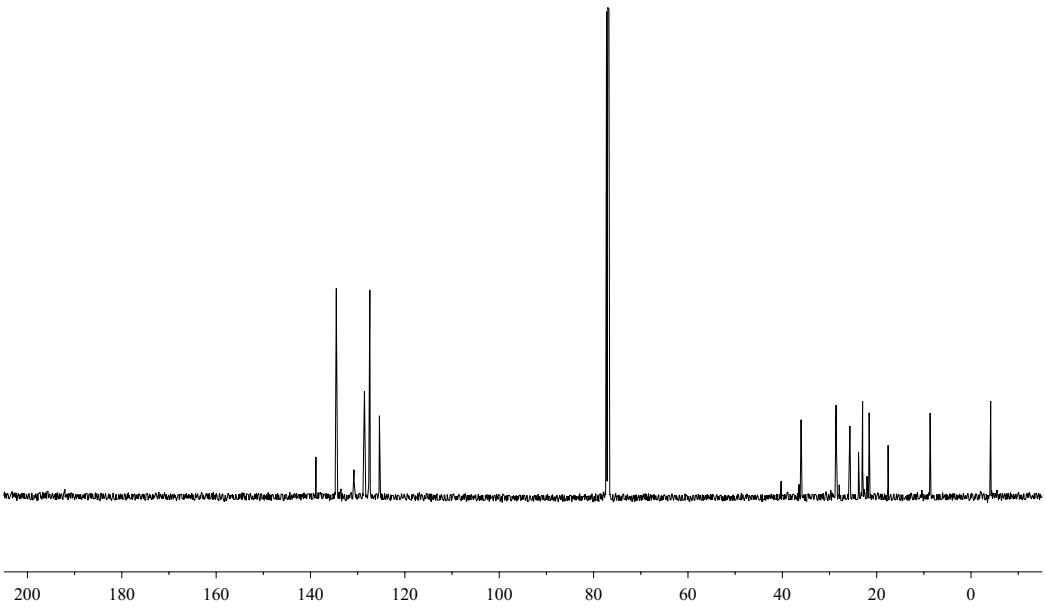

Table 3, Entry 4
^{1}H NMR
($CDCl_3$, 500 MHz)

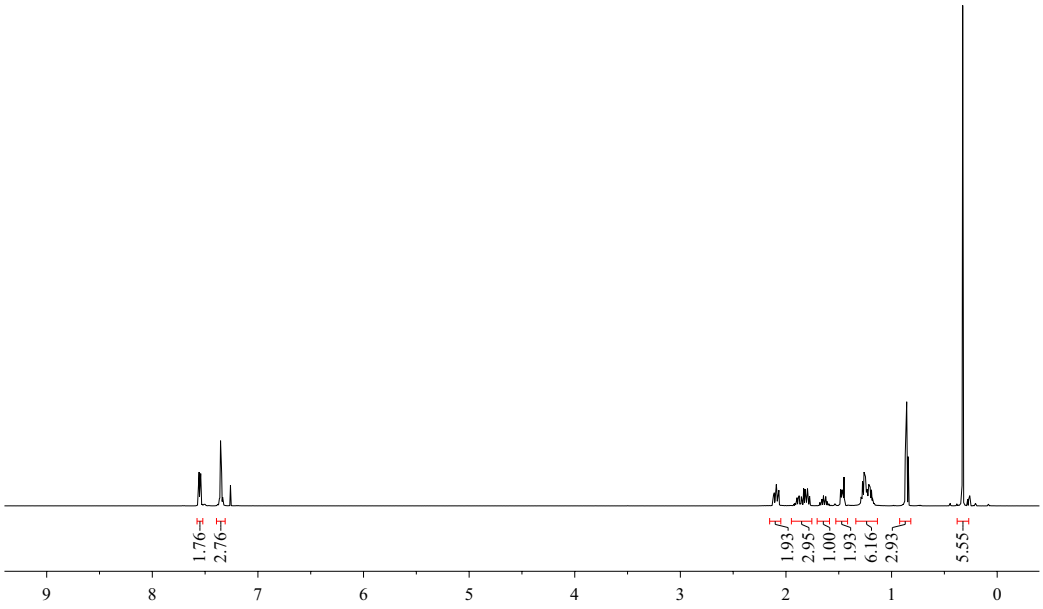

Table 3, Entry 4
^{13}C NMR
($CDCl_3$, 126 MHz)

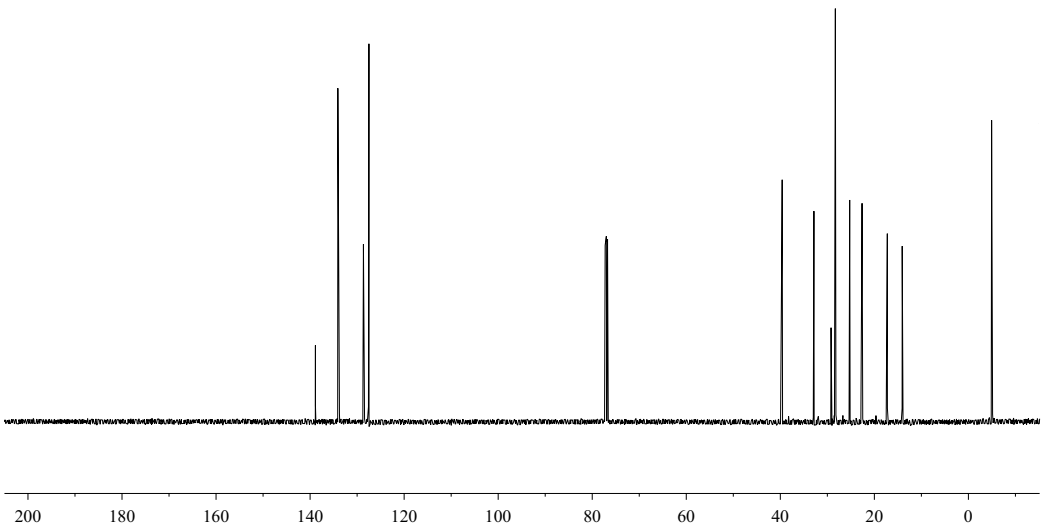

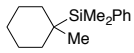

Table 3, Entry 5
^{1}H NMR
($CDCl_3$, 500 MHz)

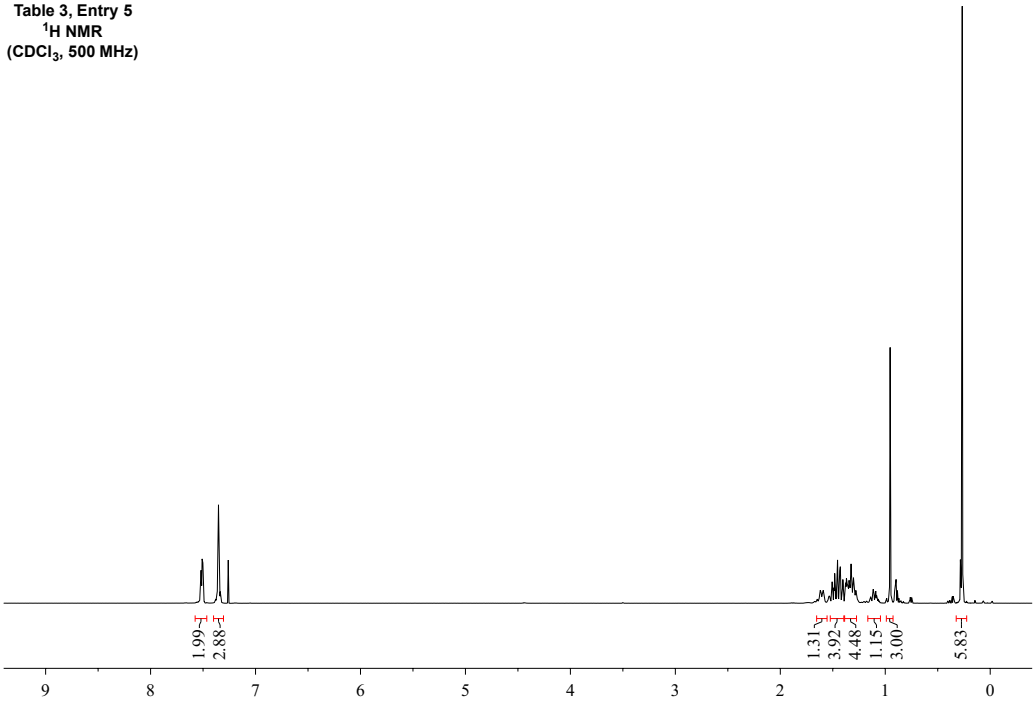

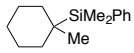

Table 3, Entry 5
^{13}C NMR
($CDCl_3$, 126 MHz)

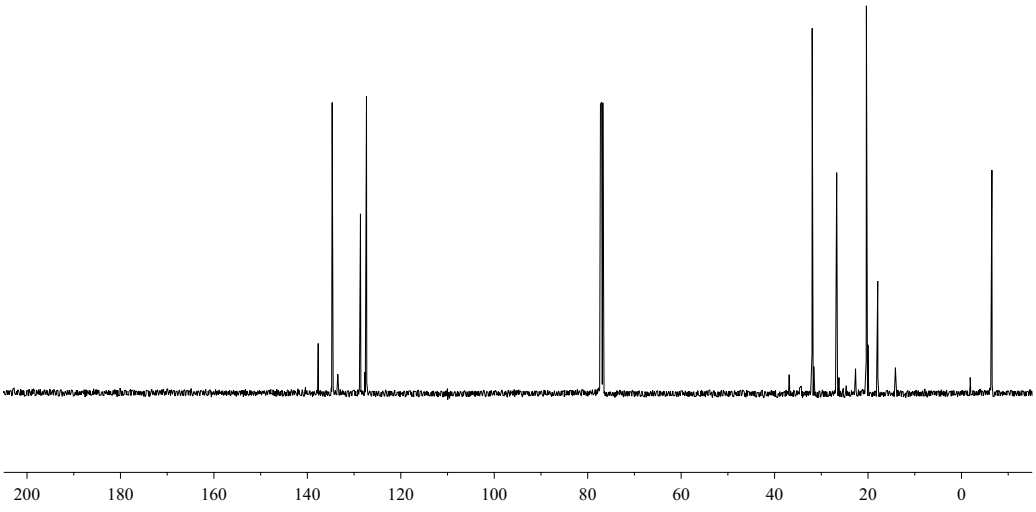

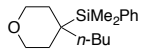

Table 3, Entry 6
^{1}H NMR
($CDCl_3$, 500 MHz)

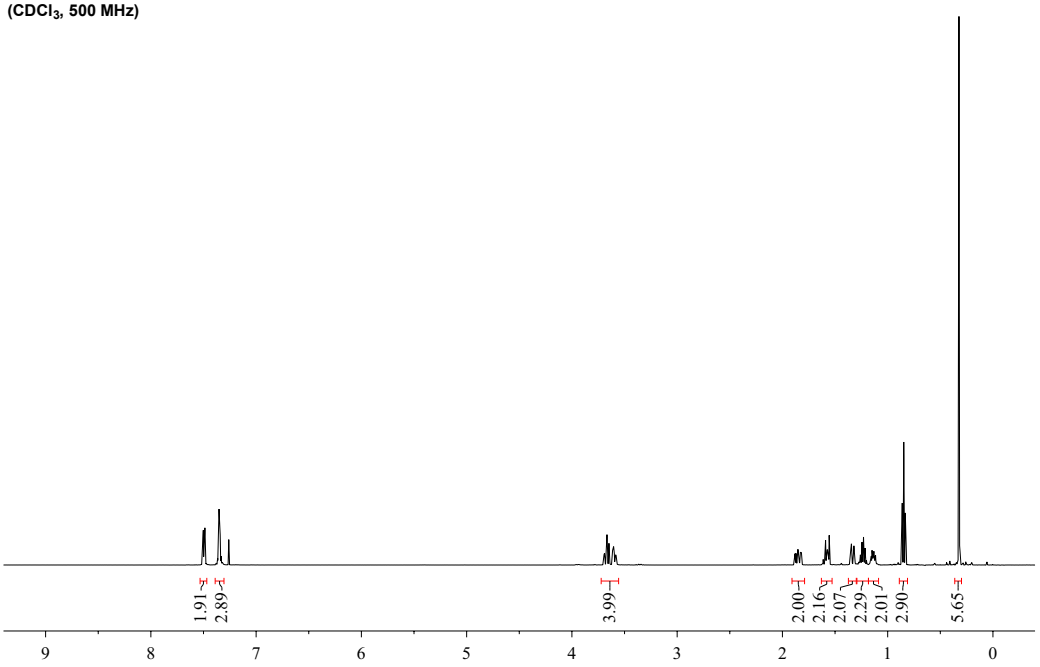

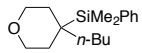

Table 3, Entry 6
^{13}C NMR
($CDCl_3$, 126 MHz)

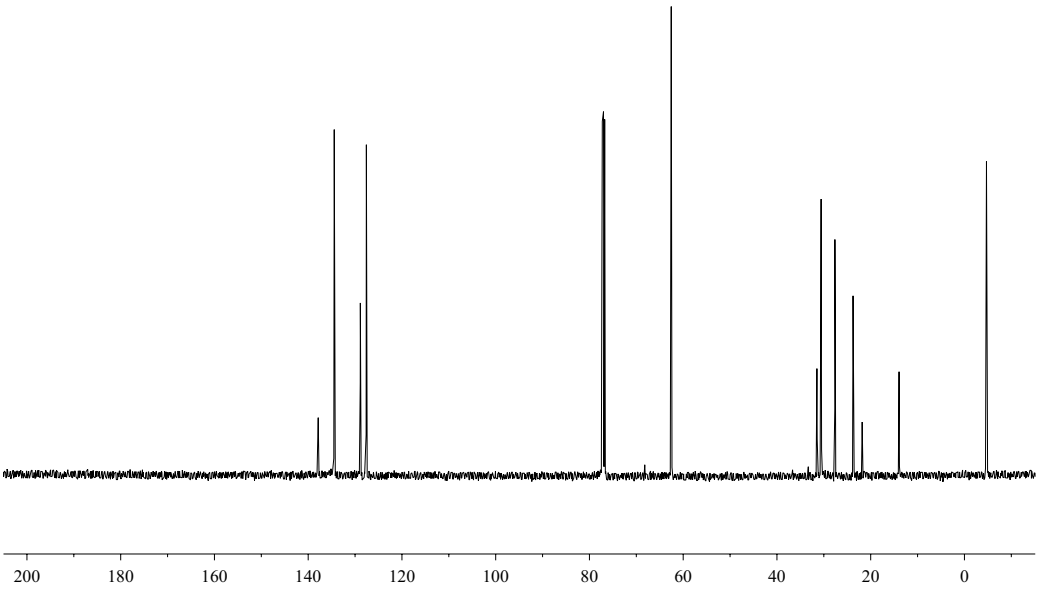

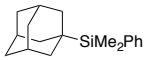

Eq 4
^{1}H NMR
($CDCl_3$, 500 MHz)

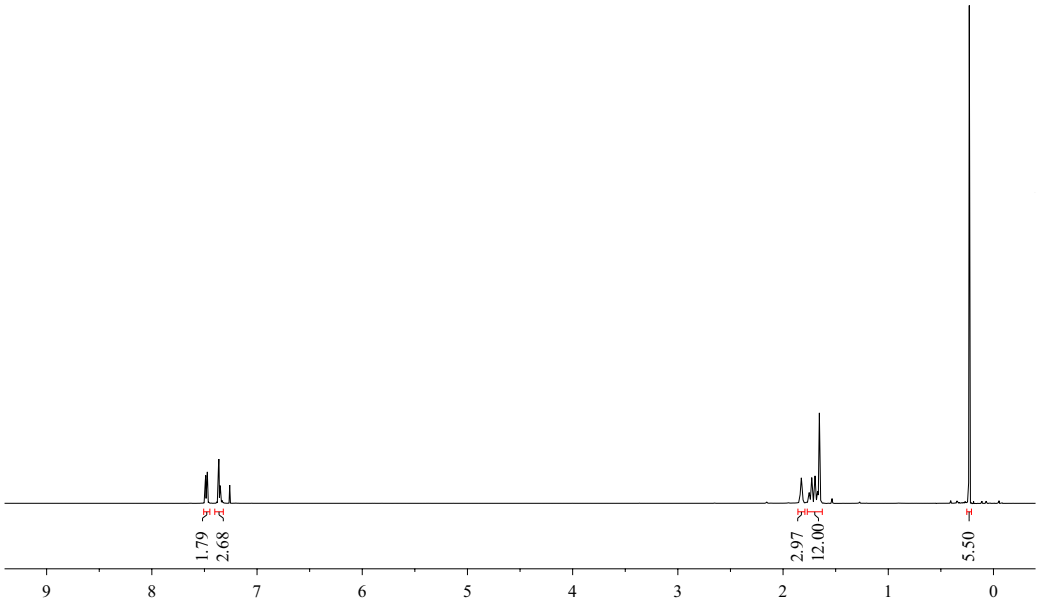

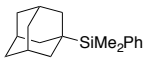

Eq 4
^{13}C NMR
($CDCl_3$, 126 MHz)

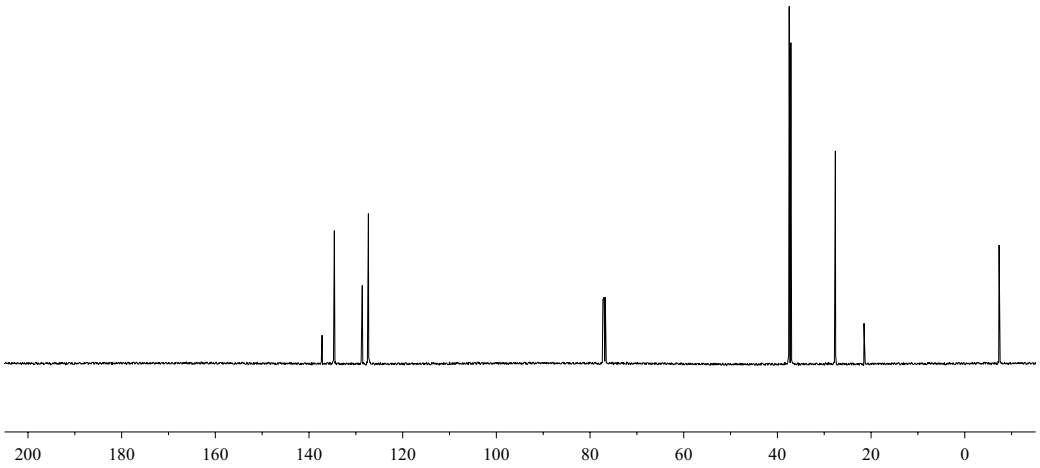

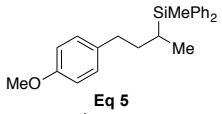

Eq 5
^{1}H NMR
($CDCl_3$, 500 MHz)

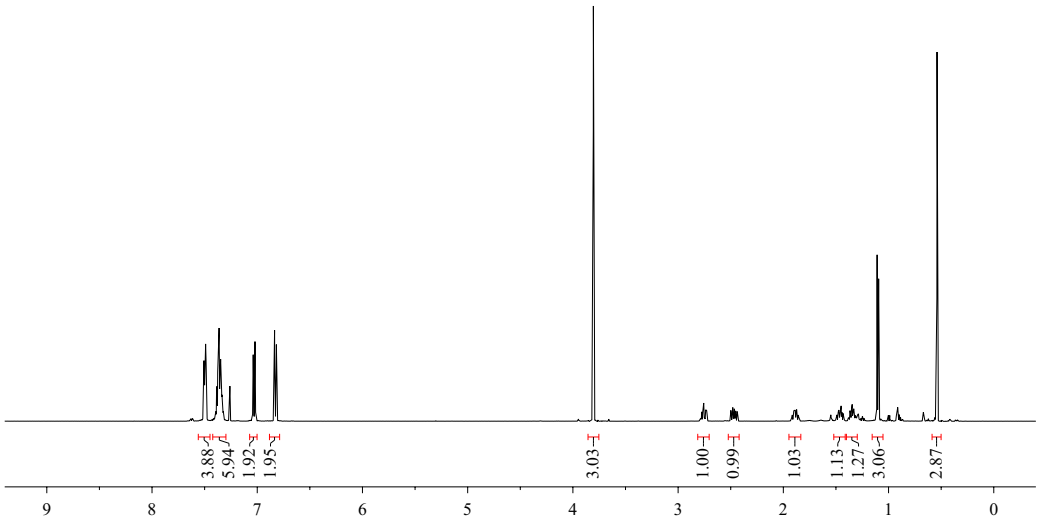

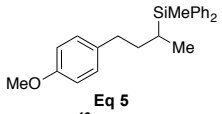

Eq 5
^{13}C NMR
($CDCl_3$, 126 MHz)

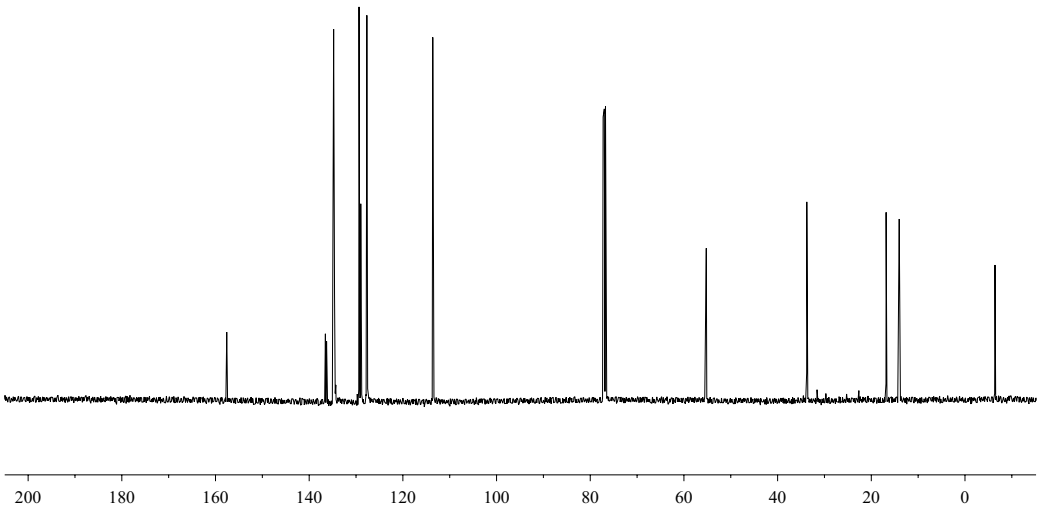

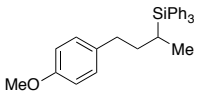

Eq 5
^{1}H NMR
($CDCl_3$, 500 MHz)

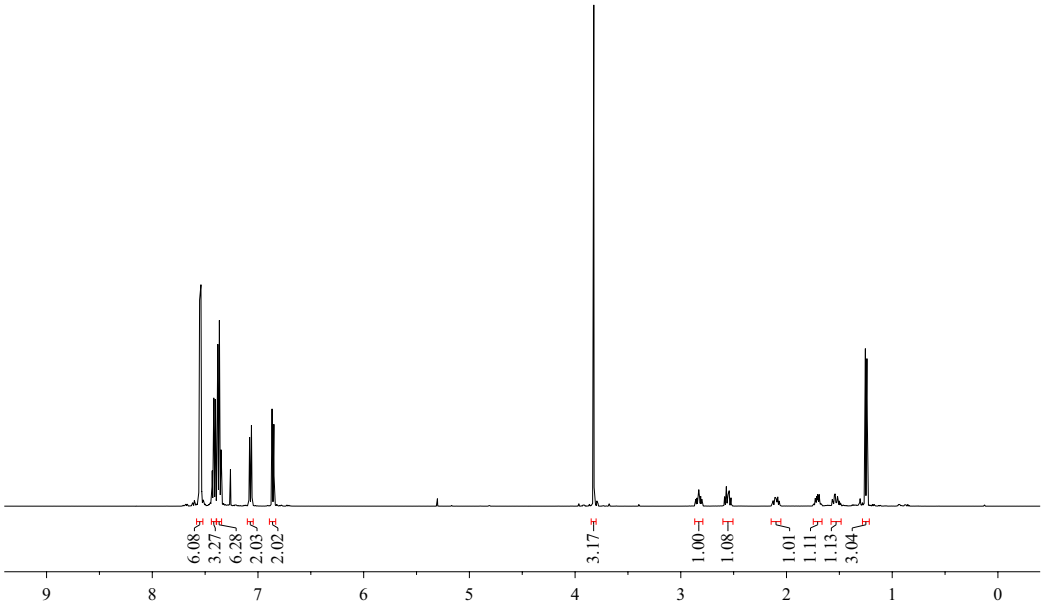

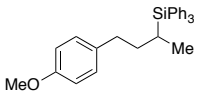

Eq 5
^{13}C NMR
($CDCl_3$, 126 MHz)

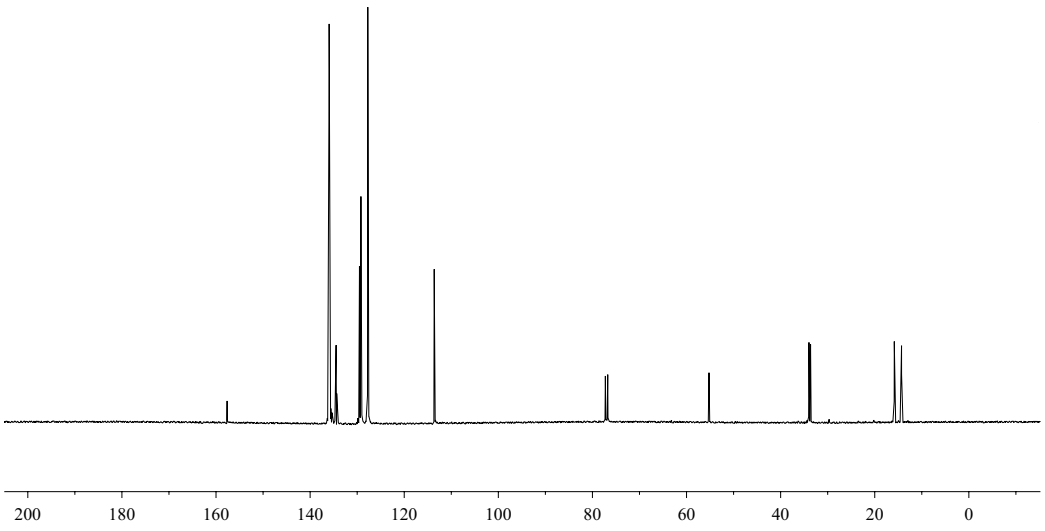

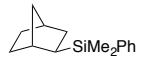

Eq 6
7:1 exo/endo
^{1}H NMR
($CDCl_3$, 500 MHz)

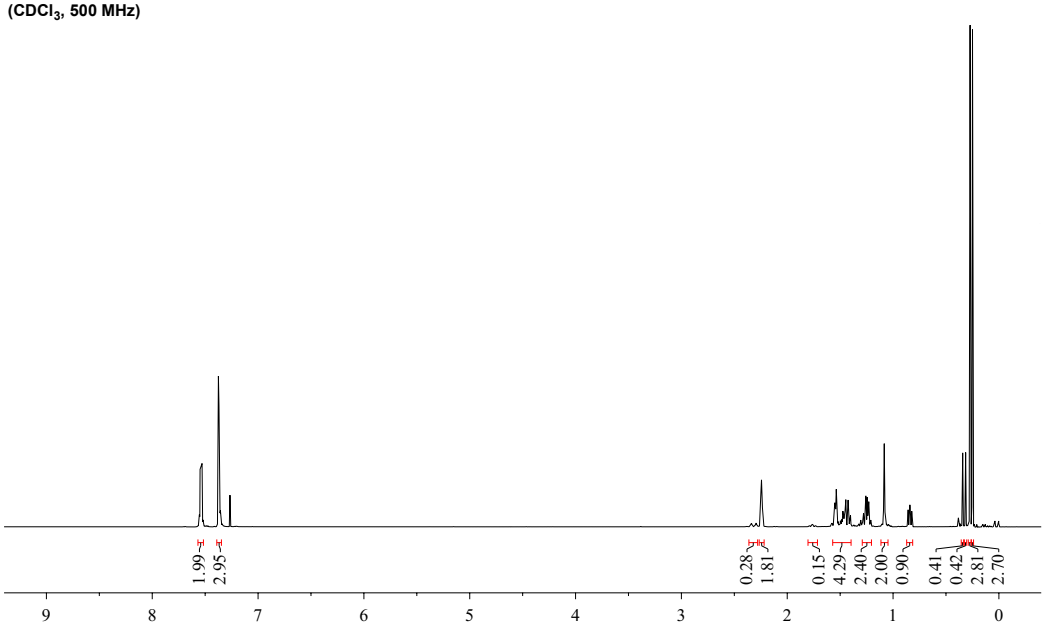

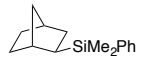

Eq 6
7:1 exo/endo
^{13}C NMR
($CDCl_3$, 126 MHz)

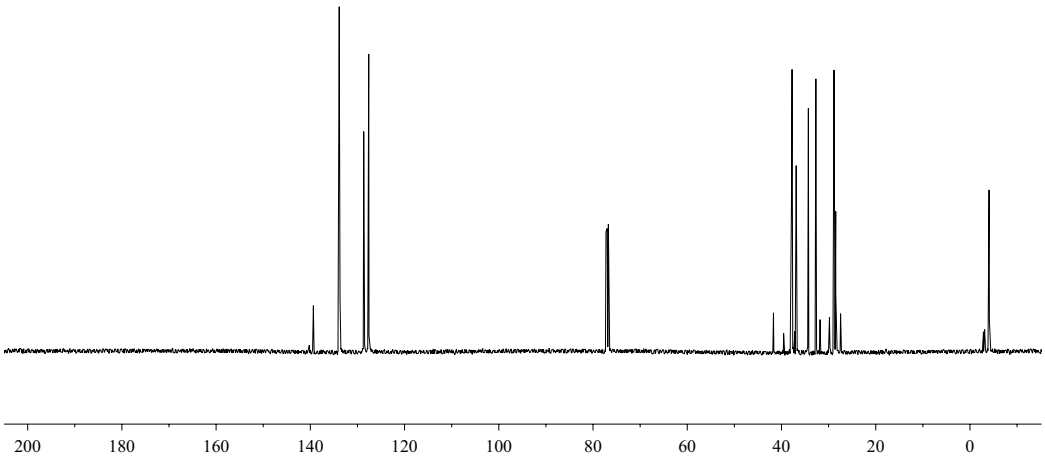

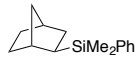

Eq 7
7:1 exo/endo
^{1}H NMR
($CDCl_3$, 500 MHz)

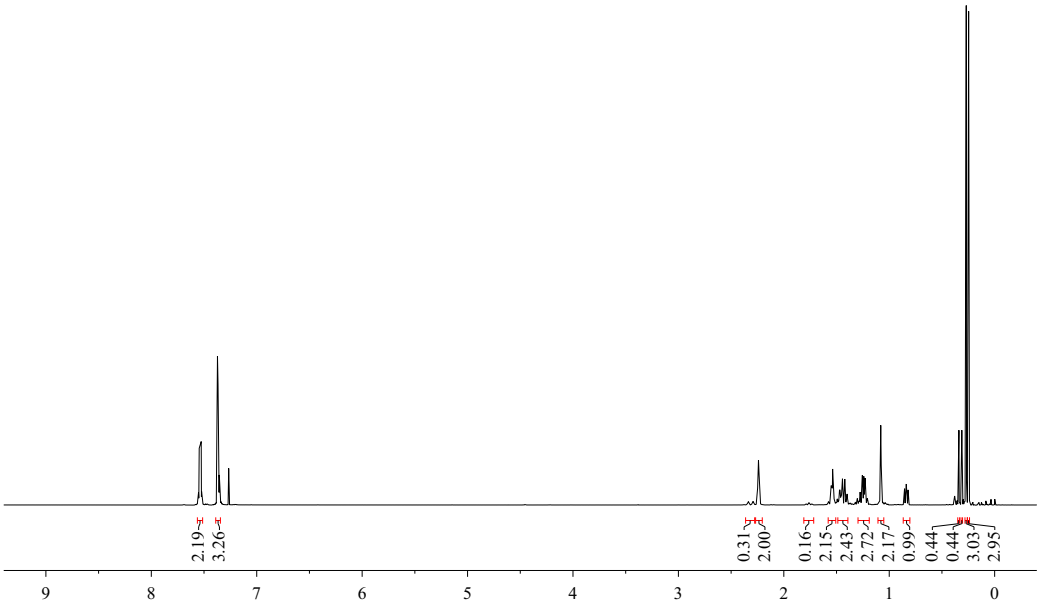

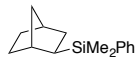

Eq 7
7:1 exo/endo
^{13}C NMR
($CDCl_3$, 126 MHz)

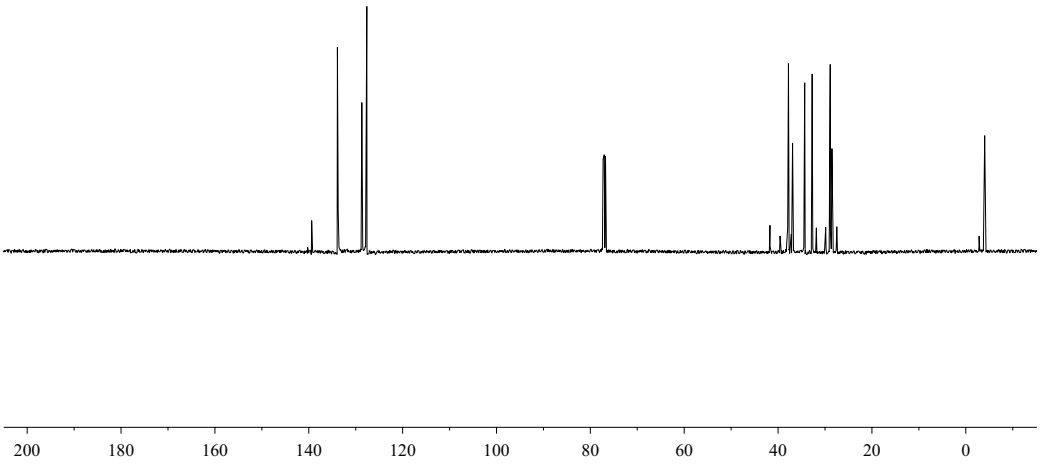

References

(1) *Handbook of Reagents for Organic Synthesis: Reagents for Silicon-Mediated Organic Synthesis*; Fuchs, P. L., Ed.; John Wiley & Sons: Chichester, UK, 2011.

(2) *Organosilicon Chemistry V: From Molecules to Materials*; Auner, N., Weis, J., Eds.; Wiley–VCH: Weinhiem, Germany, 2004.

(3) Meanwell, N. A. *J. Med. Chem.* **2011**, *54*, 2529–2591.

(4) (a) Min, G. K.; Hernández, D.; Skrydstrup, T. *Acc. Chem. Res.* **2013**, *46*, 457–470. (b) Franz, A. K.; Wilson, S. O. *J. Med. Chem.* **2013**, *56*, 388–405.

(5) For overviews of recent advances, as well as leading references, see: (a) Nakajima, Y.; Shamada, S. *RSC Advances* **2015**, *26*, 20603–20616. (b) Troegel, D.; Stohrer, J. *Coord. Chem. Rev.* **2011**, *255*, 1440–1459.

(6) For an example of silyl-Heck reactions to generate allylsilanes, see: McAtee, J. R.; Martin, S. E. S.; Ahneman, D. T.; Johnson, K. A.; Watson, D. A. *Angew. Chem. Int. Ed.* **2012**, *51*, 3663–3667.

(7) For leading references, see: In *Science of Synthesis*; Georg Theime Verlag: Stuttgart, Germany, 2002; Vol. 4, Chapter 4.4.

(8) For reactions of primary alkyl nucleophiles with silicon nucleophiles, see: (a) Morita, E.; Murakami, K.; Iwasaki, M.; Hirano, K.; Yorimitsu, H.; Oshima, K. *Bull. Chem. Soc. Jpn.* **2009**, *82*, 1012–1014. (b) Murakami, K.; Yorimitsu, H.; Oshima, K. *J. Org. Chem.* **2009**, *74*, 1415–1417. For isolated examples with unactivated secondary and tertiary alkyl nucleophiles, see: (c) Lennon, P. J.; Mack, D. P.; Thompson, Q. E. *Organometallics* **1989**, *8*, 1121–1122. (d) Bréfort, J.-L.; Corriu, R. J. P.; Guérin, C.; Henner, B. J. L.; Man, W. W. C. W. C. *Organometallics* **1990**, *9*, 2080–2085. (e) Itami, K.; Terakawa, K.; Yoshida, J.-i.; Kajimoto, O. *J. Am. Chem. Soc.* **2003**, *125*, 6058–6059.

(9) For selected examples, see: (a) Lefort, M.; Simmonet, C.; Birot, M.; Deleris, G.; Dunogues, J.; Calas, R. *Tetrahedron Lett.* **1980**, *21*, 1857–1860. (b) Tobisu, M.; Kita, Y.; Ano, Y.; Chatani, N. *J. Am. Chem. Soc.* **2008**, *130*, 15982–15989. (c) Vyas, D. J.; Oestreich, M. *Angew. Chem. Int. Ed.* **2010**, *49*, 8513–8515. (d) Hazra, C. K.; Oestreich,

M. *Org. Lett.* **2012**, *14*, 4010–4013. (e) Zarate, C.; Martin, R. *J. Am. Chem. Soc.* **2014**, *136*, 2236–2239.

(10) (a) Eaborn, C.; Griffiths, R. W.; Pidcock, A. *J. Organomet. Chem.* **1982**, *225*, 331–341. (b) Scharfbier, J.; Oestreich, M. *Synlett* **2016**, *27*, doi: 10.1055/s-0035-1561407.

(11) (a) For copper-catalyzed couplings that proceed in low (<40%) yield, see: Okuda, Y.; Morizawa, Y.; Oshima, K.; Nozaki, H. *Tetrahedron Lett.* **1984**, *25*, 2483–2486. (b) For a rhodium-catalyzed substitution of a cyano group with a silyl group (48% yield), see Ref 9b.

(12) (a) For an early report, see: Netherton, M. R.; Dai, C.; Neuschütz, K.; Fu, G. C. *J. Am. Chem. Soc.* **2001**, *123*, 10099–10100. (b) For a recent report and leading references, see: Liang, Y.; Fu, G. C. *J. Am. Chem. Soc.* **2015**, *137*, 9523–9526.

(13) Dudnik, A. S.; Fu, G. C. *J. Am. Chem. Soc.* **2012**, *134*, 10693–10697 (nickel catalyst; primary, secondary, and tertiary electrophiles).

(14) For contemporaneous work by others, see: (a) Yang, C.-T.; Zhang, Z.-Q.; Tajuddin, H.; Wu, C.-C.; Liang, J.; Liu, J.-H.; Fu, Y.; Czyzewska, M.; Steel, P. G.; Marder, T. B.; Liu, L. *Angew. Chem. Int. Ed.* **2012**, *51*, 528–532 (copper catalyst; primary and secondary electrophiles). (b) Ito, H.; Kubota, K. *Org. Lett.* **2012**, *14*, 890–893 (copper catalyst; primary and secondary electrophiles). (c) Yi, J.; Liu, J.-H.; Liang, J.; Dai, J.-J.; Yang, C.-T.; Fu, Y.; Liu, L. *Adv. Synth. Catal.* **2012**, *354*, 1685–1691 (palladium and nickel catalysts; primary and secondary electrophiles). (d) Joshi-Pangu, A.; Ma, X.; Diane, M.; Iqbal, S.; Kribs, R. J.; Huang, R.; Wang, C.-Y.; Biscoe, M. R. *J. Org. Chem.* **2012**, *77*, 6629–6633 (palladium catalyst; primary electrophiles).

(15) Under our previously reported borylation conditions, reaction with the silylborane nucleophile resulted in low electrophile conversion and no C–B bond formation.

(16) Hemeon, I.; Singer, R. D. In *Science of Synthesis*; Georg Theime Verlag: Stuttgart, Germany, 2002; Vol. 4, Chapter 4.4.9.

(17) Rudolph, A.; Lautens, M. *Angew. Chem. Int. Ed.* **2009**, *48*, 2656–2670.

(18) At least 20 equiv of DMA are required to maintain high yield. Almost no product formation is observed in the case of stoichiometric DMA (1 equiv), suggesting a more significant role than that of a ligand.

(19) Functionalized alkyl magnesium reagents are rare coupling partners: Knochel, P.; Dohle, W.; Gommermann, N; Kneisel, F. F.; Kopp, F.; Korn, T.; Sapountzis, I.; Vu, V. A. *Angew. Chem. Int. Ed.* **2003**, *42*, 4302–4320.

(20) Notes: (a) We have not yet attempted to separately optimize the yield for this family of electrophiles. (b) Under the same conditions, an unactivated secondary alkyl chloride and tosylate were not useful cross-coupling partners (<1% yield).

(21) For selected examples of cross-couplings of unactivated tertiary alkyl halides, see: (a) Tsuji, T.; Yorimitsu, H.; Oshima, K. *Angew. Chem. Int. Ed.* **2002**, *41*, 4137–4139. (b) Mitamura, Y.; Asada, Y.; Murakami, K.; Someya, H.; Yorimitsu, H.; Oshima, K. *Chem. Asian J.* **2010**, *5*, 1487–1493. (c) Reference 10. (d) Zultanski, S. L.; Fu, G. C. *J. Am. Chem. Soc.* **2013**, *135*, 624–627. (e) Wu, X.; See, J. W. T.; Xu, K.; Hirao, H.; Roger, J.; Hierso, J.-C.; Zhou, J. *Angew. Chem. Int. Ed.* **2014**, *53*, 13573–13577. (f) Wang, X.; Wang, S.; Xue, W.; Gong, H. *J. Am. Chem. Soc.* **2015**, *137*, 11562–11565.

(22) At least one aryl substituent on silicon is required for lithiation during nucleophile synthesis. For a thorough study of the phenyldimethylsilyllithium reagent, see: Fleming, I.; Roberts, R. S.; Smith, S. C. *J. Chem. Soc., Perkin Trans. 1* **1998**, 1209–1214.

(23) For recent discussions and leading references, see: (a) Liang, Y.; Fu, G. C. *Angew. Chem. Int. Ed.* **2015**, *54*, 9047–9051. (b) Schley, N. D.; Fu, G. C. *J. Am. Chem. Soc.* **2014**, *136*, 16588–16593.

(24) No stereochemical scrambling of the bromonorbornanes was observed at low conversion.

(25) Henry-Riyad, H.; Montanari, F.; Quici, S.; Studer, A.; Tidwell, T. T.; Vogler T. In *Handbook of Reagents for Organic Synthesis*; Fuchs, P. L., Ed.; Wiley: Chichester, UK, 2013; pp 620–626.

(26) We have observed similar trends in nickel-catalyzed borylations of unactivated alkyl bromides: Reference 13.

(27) Do, H.-Q.; Bachman, S.; Bissember, A. C.; Peters, J. C.; Fu, G. C. *J. Am. Chem. Soc*. **2014**, *136*, 2162–2167.

(28) Dudnik, A. S.; Fu, G. C. *J. Am. Chem. Soc*. **2012**, *134*, 10693–10697.

(29) Procedure adapted from: Vyas, D. J.; Oestreich, M. *Chem. Commun.* **2010**, *46*, 568–570.

(30) Kofron, W. G.; Baclawski, L. M. *J. Org. Chem.* **1976**, *41*, 1879–1880.

(31) Krasovskiy, A.; Knochel, P. *Synthesis* **2006**, 890−891.

(32) Pai, Y.-M.; Wanek, E.; Weber, W. P. *J. Organomet. Chem.* **1984**, *270*, 271–275.

(33) Nakamura, S.; Uchiyama, M. *J. Am. Chem. Soc.* **2007**, *129*, 28–29.

(34) For a representative procedure, see Reference 33.

Chapter 3

SYNTHESIS OF β-FLUORINATED CARBONYL COMPOUNDS BY NITRITE-MODIFIED WACKER OXIDATION

The text in this chapter was reproduced in part with permission from:
Chu, C. K.; Ziegler, D. T.; Carr, B.; Wickens, Z. K.; Grubbs, R. H. *Angew. Chem. Int. Ed.* **2016**, *55*, 8435–8439.
The work described was conducted in collaboration with Dr. Daniel Ziegler, who performed mechanistic experiments, as well as with Brian Carr and Dr. Zachary Wickens, who conceived the project and developed reaction conditions.

Abstract

An aldehyde-selective Wacker-type oxidation of allylic fluorides employing a nitrite catalyst is described. The method represents a direct route to prepare β-fluorinated aldehydes. Allylic fluorides bearing a variety of functional groups are transformed in high yield and very high regioselectivity. Additionally, crude aldehyde products serve as versatile intermediates, enabling access to a diverse array of fluorinated building blocks. Preliminary mechanistic investigations suggest that inductive effects have a strong influence on the rate and regioselectivity of oxidation.

Introduction

The demand for organofluorine compounds is rapidly growing as a result of their prevalence in the pharmaceutical,[1] agrochemical,[2] and materials[3] industries. Due to a low abundance of fluorinated chemical feedstocks,[4] the development of efficient routes toward organofluorine building blocks has been recognized as an important challenge in the synthetic community.[5] Traditional fluorination protocols typically employ harsh reagents such as diethylaminosulfur trifluoride (DAST), restricting their tolerance of functional groups. Consequently, careful selection of an appropriate fluorinating agent must often be performed on a case-by-case basis.[6]

Significant progress has been made toward mild, catalytic alkyl fluorination, with much of this work dedicated to installing fluorine atoms adjacent to π systems (Scheme 3.1A).[7] α-Fluorination of carbonyl compounds is achieved efficiently via organo- and transition-metal catalysis.[8] Allylic fluorides can also be readily prepared by regio- and enantioselective methods.[7a-d,f,h] For example, Ir-catalyzed allylic substitution[7d,h] and Pd-catalyzed C–H fluorination[7f] methods can serve as convenient approaches to allylic fluorides.

Despite the depth of research dedicated to α-fluorination of activated π systems, catalytic installation of fluorine β to functional groups remains a major challenge.[9] One promising strategy enables the syntheses of β- and γ- fluorinated ketones via catalytic ring opening of strained cyclopropanols and cyclobutanols, respectively.[10] Alternative methods amenable to producing β-fluorinated carbonyl compounds have been reported,[11] but a general solution employing simple starting materials has yet to be developed. Herein, we report a catalytic approach to directly access β-fluorinated aldehydes from readily accessible allylic fluorides (Scheme 3.1B).

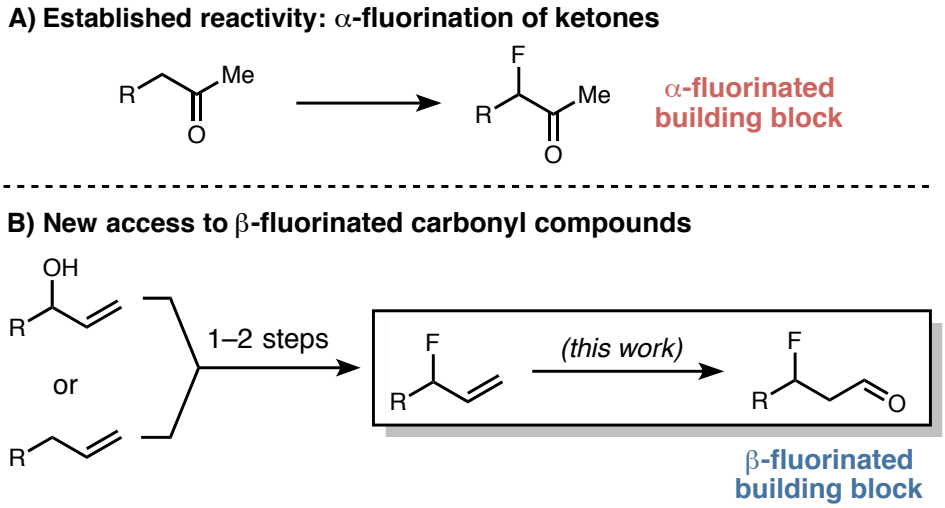

Scheme 3.1. Strategies toward alkylfluorine compounds.

The Wacker reaction is a powerful method[12] for the oxidation of olefins that typically favors Markovnikov selectivity.[13] However, in the presence of proximal functional groups, regioselectivity of oxidation can be difficult to rationally predict.[14] In our recent study of a dicationic Pd-catalyzed Wacker-type oxidation of internal olefins,[15]

inductively withdrawing trifluoromethyl groups were found to substantially enhance selectivity for distal oxidation.[16] In fact, even the oxidation of a terminal olefin, 4,4,4-trifluoro-1-butene, occurred with modest anti-Markovnikov selectivity (3:1 aldehyde/ketone). We therefore reasoned that modified Wacker conditions, combined with the inductive influence of allylic fluorides, could be employed as a general strategy for the synthesis of β-fluorinated aldehydes under mild conditions.

Development of Reaction Conditions

The model allylic fluoride **A** was initially subjected to a range of Wacker-type oxidation conditions toward optimization of aldehyde selectivity.[17] Traditional Tsuji-Wacker conditions proved poorly suited for oxidation of the electron deficient allylic fluoride, resulting in defluorination and no aldehyde selectivity (Figure 3.1a). When subjected to our previously reported dicationic palladium system, this substrate was oxidized in moderate yield with preference for the aldehyde (3:1 aldehyde/ketone; Figure 3.1b), revealing some innate aldehyde selectivity of the substrate.

To emphasize this effect, we next explored nitrite ligands[18] and exogenous nitrite co-catalysts, utilized by Feringa and our own group, respectively, for the catalyst-controlled oxidation of terminal olefins to aldehydes. When **A** was subjected to Feringa's conditions, catalyzed by $[PdNO_2Cl(MeCN)_2]$,[19] high aldehyde selectivity was observed (18:1 aldehyde/ketone), albeit in poor yield (Figure 3.1c). Our group recently developed a Wacker system that employs an exogenous nitrite catalyst in a tBuOH/$MeNO_2$ solvent system, which oxidizes unbiased terminal olefins with anti-Markovnikov selectivity.[20] This nitrite co-catalyzed system oxidized allylic fluoride **A** in moderate yield and high selectivity (26:1 aldehyde/ketone; Figure 3.1d). Further optimization, involving exclusion of water from the reaction system, increased nitromethane concentration, and even a reduction in catalyst loading, resulted in very high selectivity for aldehyde formation (36:1 aldehyde/ketone) in high yield (77%; Figure 3.1e). Since the use of tBuOH has been established as a strategy to enhance aldehyde selectivity in Wacker-type oxidations,[21,22] the importance of the nitrite catalyst and nitromethane as a cosolvent was assessed. Elimination

of these components from the optimized conditions led to diminished aldehyde selectivity (8:1 aldehyde/ketone) and formation of defluorination products (Figure 3.1f).[23]

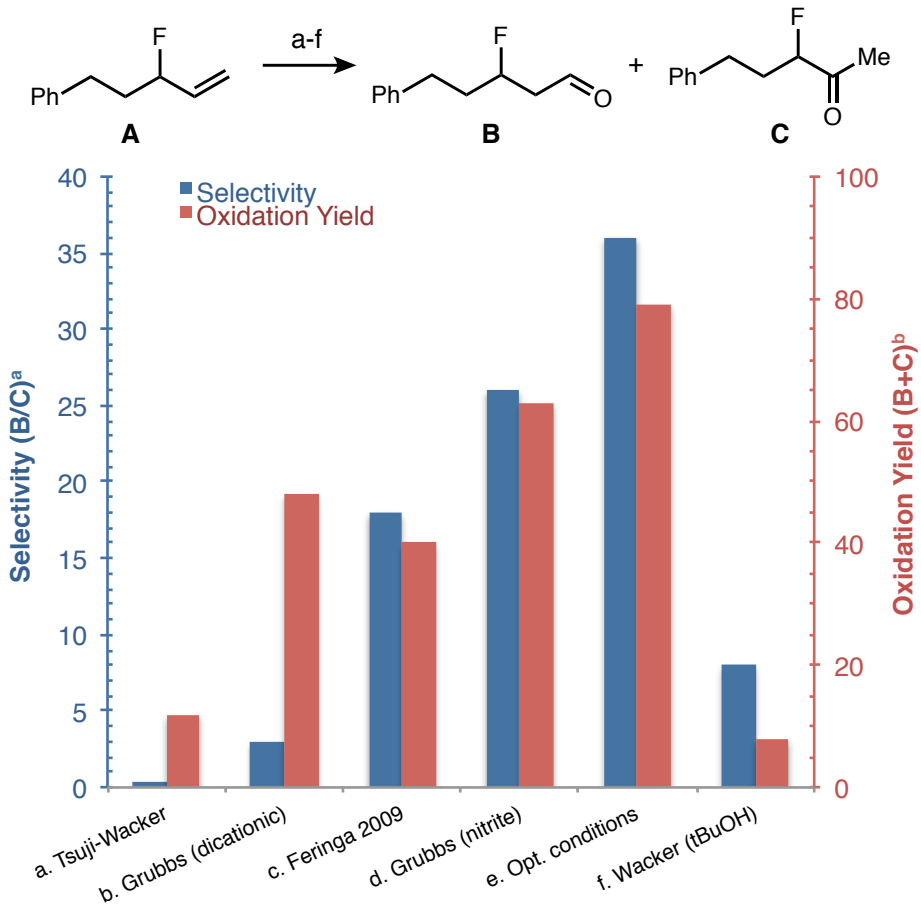

Figure 3.1. Comparison of oxidation conditions with a model substrate. (a) Selectivity (aldehyde/ketone) determined by ^{1}H NMR analysis. (b) Oxidation yield (aldehyde + ketone) determined by ^{1}H NMR analysis versus an internal standard. Only fluorinated products are included. (See Table 3.1 for standard conditions).

Reaction Scope

With optimized conditions in hand, we next explored the reaction scope, and found the method to be well suited for regioselective oxidation of allylic fluorides bearing a variety of functional groups.[24] Branched allylic fluorides without added bias were oxidized to the corresponding β-fluorinated aldehydes in high yield and ≥20:1 selectivity, with an ester and alkyl chloride being well tolerated (Table 3.1, entries 1, 2, 6, and 7). High

Table 3.1. Nitrite-Modified Wacker Oxidations of Allylic Fluorides: Substrate Scope

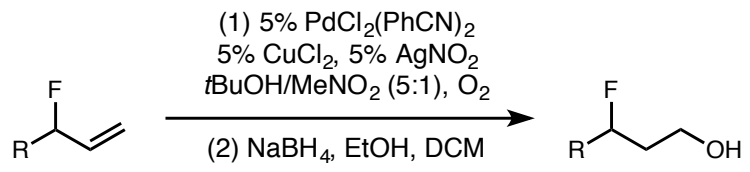

entry	substrate	yield[a]	selectivity[b]
1	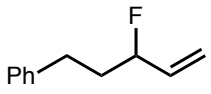	82	≥20:1
2	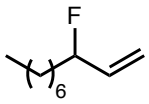	87	≥20:1
3	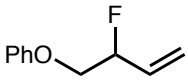	94	≥20:1
4	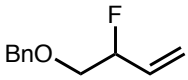	93	≥20:1
5	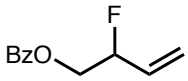	93	≥20:1
6	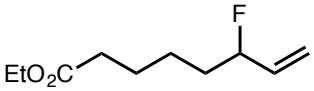	72	≥20:1
7	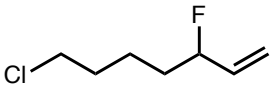	81[c]	≥20:1
8	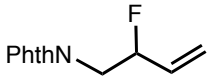	77	≥20:1

[a]Yield of purified product following $NaBH_4$ reduction. [b]Selectivity (aldehyde:ketone) determined by ^1H NMR analysis of crude reaction mixture prior to reduction. [c]Yield of aldehyde determined by ^1H NMR analysis versus an internal standard.

aldehyde selectivities were maintained for allylic fluorides bearing an additional directing group. Olefins with phenyl and benzyl ethers, benzoate, and phthalimide branches were oxidized to the corresponding aldehydes with only trace levels of ketone detected (entries

3, 4, 5, and 8, respectively). When comparing previous nitrite-modified Wacker oxidations of functionalized olefins, fluoride has shown to be an exceptionally potent directing group.

Derivatization of Products

Despite the relative instability of β-fluorinated aldehydes, the high purity of the crude products allows for direct transformation to a variety of organofluorine compounds. Reaction with Oxone furnished the β-fluorinated carboxylic acid **3-1** in excellent yield (Scheme 3.2a). Wittig olefination and protection of the carbonyl were achieved in synthetically useful yields in spite of potential base or acid lability of the fluoride (Scheme 3.2b, d). The aldehyde was reduced nearly quantitatively to γ-fluorinated alcohol **3-3** (Scheme 3.2c). Furthermore, nucleophilic addition to aldehydes provides access to a range of new fluorinated building blocks, demonstrated by the addition of allylB(pin) to produce

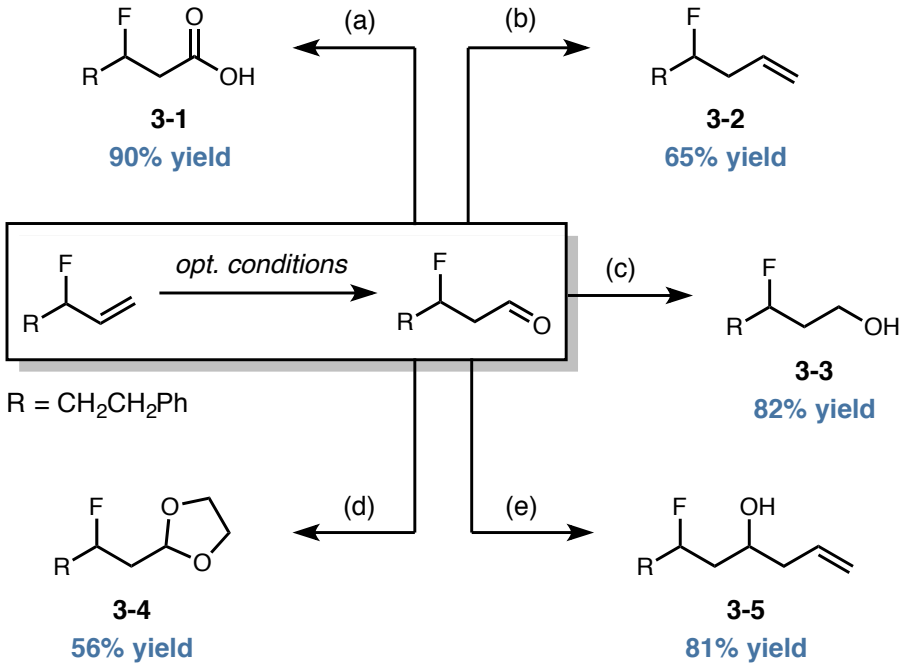

Scheme 3.2. Derivatization of a β-fluorinated aldehyde crude product. All derivatizations performed using crude Wacker oxidation product. Yields reported over 2 steps. (a) Oxone, DMF. (b) $MePPh_3Br$, *n*BuLi, THF. (c) $NaBH_4$, DCM/EtOH. (d) *p*TsOH, ethylene glycol, mol. sieves. (e) AllylB(pin), DCM.

homoallylic alcohol **3-5** (Scheme 3.2e). Overall, the efficient preparation of β-fluorinated aldehydes via Wacker-type oxidation serves as a unique synthetic handle to produce diverse fluorinated molecules.

In order to investigate how our method may be used to generate stereodefined organofluorines, we were interested in the aldehyde-selective oxidation of enantioenriched allylic fluoride **3-6**.[7h] Under the optimal reaction conditions, oxidation occurred without erosion of enantiopurity,[25] allowing for the isolation of enantioenriched fluorinated product **3-7** in good yield and ee (Eq. 3.1). This result suggests that Pd-catalyzed olefin isomerization does not occur on the time scale of oxidation to the aldehyde product.

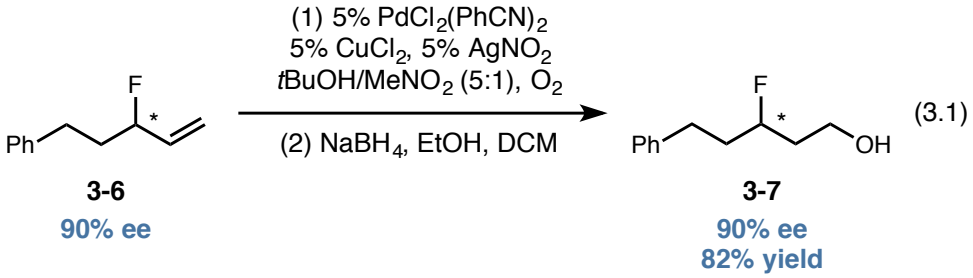

(3.1)

Mechanistic Insights

Having demonstrated the synthetic utility of the transformation, we sought to gain insight into the role of the fluoride in influencing regioselectivity and reactivity. To this end, a study of the distance dependence of regioselectivity on fluoride proximity was conducted. Three alkyl fluoride isomers were synthesized with systematic variation of the distance between fluoride and olefin. The oxidations of these compounds under our standard conditions were then compared along with that of 1-decene (Figure 3.2). The high aldehyde selectivity (96%) in the case of the allylic fluoride (n = 0) depreciates as n increases. A strong preference for oxidation to the aldehyde is maintained in the reaction of a homoallylic fluoride (n = 1), suggesting that this method can provide a convenient route to γ-fluorinated aldehydes. However, aldehyde selectivity diminishes for the analogue fluorinated in a more distal position (n = 2), and poor regioselectivity is observed in the oxidation of the unbiased olefin 1-decene (58%).[26] The gradual loss in selectivity as

fluoride substitution is placed further from the olefin is consistent with a key inductive effect that enhances regioselectivity under these nitrite-modified Wacker conditions.

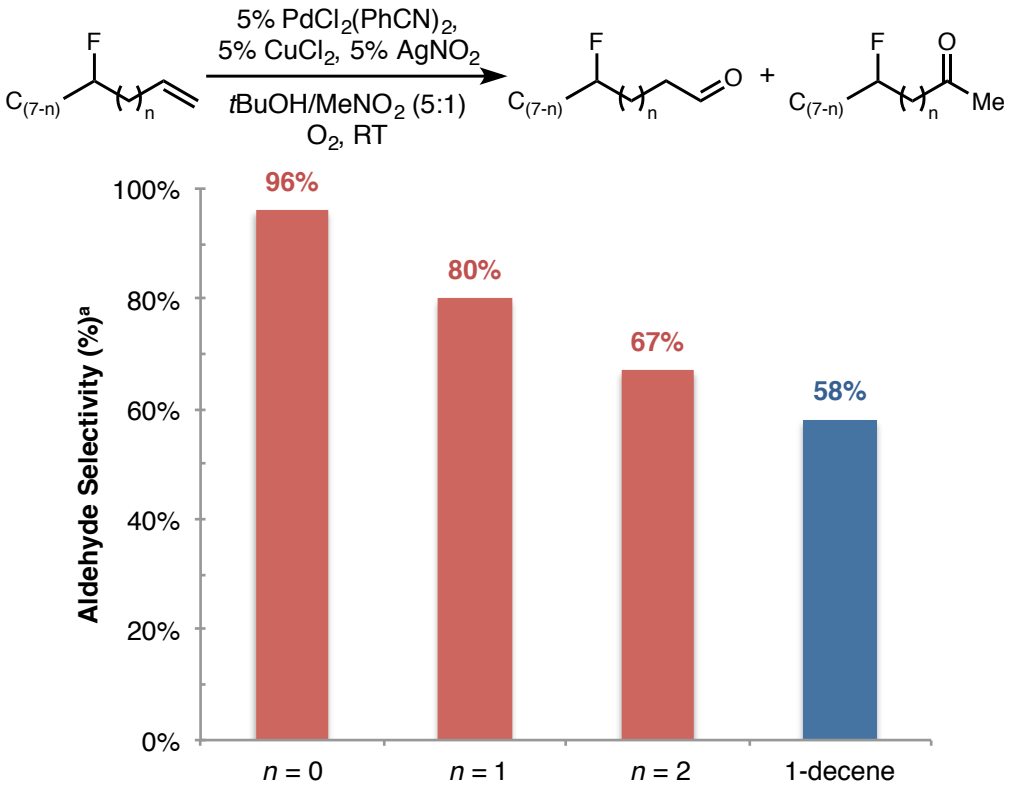

Figure 3.2. Influence of fluoride proximity on regioselectivity of oxidation. [a]Selectivity (aldehyde/total oxidation yield) determined by ^{1}H NMR analysis.

The relative rates of conversion of a fluorinated and non-fluorinated olefin were studied in order to further elucidate the effect of fluoride substitution (Figure 3.3). Individual rate comparisons of the two compounds show that the more electron deficient fluorinated olefin reacts at an accelerated rate relative to the unfunctionalized olefin (Figure 3.3A). However, when the two olefins were oxidized in competition in a 1:1 ratio, the non-fluorinated olefin was consumed 2.3 times faster than the allylic fluoride, potentially due to saturation of the catalyst with non-fluorinated olefin (Figure 3.3B). This inversion of relative reactivity, which results from a decrease in the rate of conversion of the fluorinated olefin rather than an increase in the rate of conversion of the non-fluorinated olefin,

suggests that stronger olefin coordination does not inherently lead to accelerated rate of oxidation.

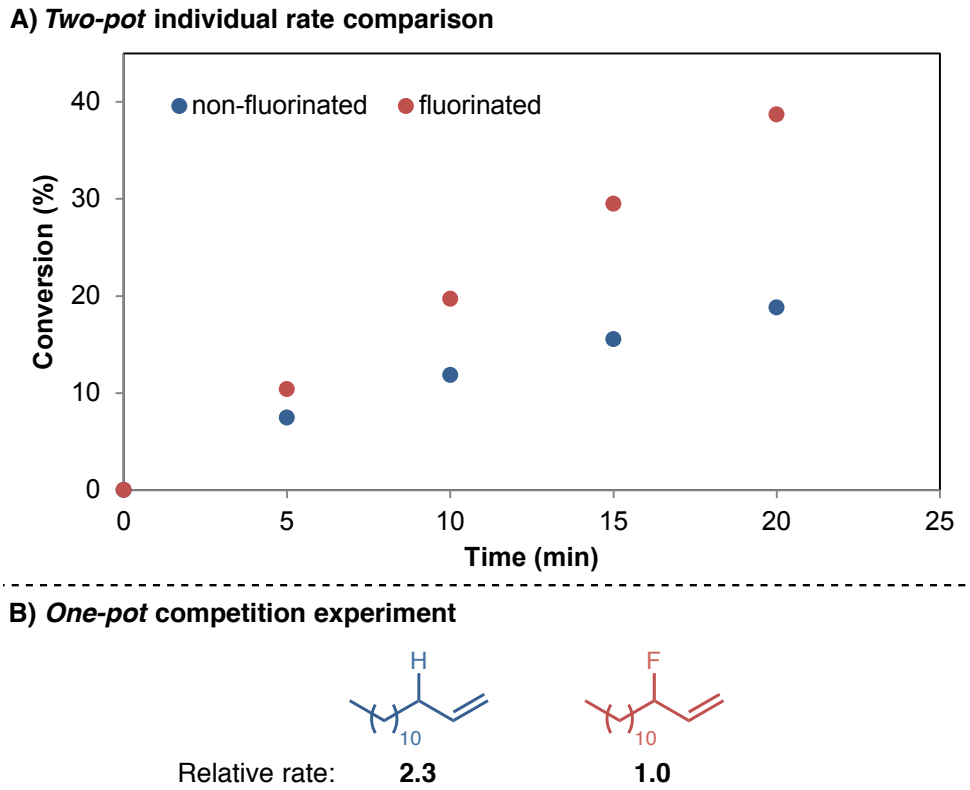

Figure 3.3. Individual rate and competition experiments performed to measure relative rates of conversion.

Conclusion

In summary, we have developed a practical synthesis of β-fluorinated aldehydes from readily accessible allylic fluorides. This method represents a rare example of catalysis to produce β-fluorinated carbonyl compounds under procedurally simple conditions. Direct transformation of crude aldehyde products demonstrates the versatility of β-fluorinated aldehyde building blocks. Preliminary mechanistic studies are consistent with inductive effects having a significant influence on both the regioselectivity and rate of oxidation and will facilitate further study of this new catalytic system.

Experimental Section

General Information

Anhydrous ether and dichloromethane used for substrate syntheses were purified and dried using a solvent-purification system containing activated alumina. All other solvents were purchased anhydrous with Sure/Seal^{TM} septa from Sigma Aldrich and used without further purification. All reagents and standards were purchased from Sigma Aldrich and used without further purification. All metal salts were purchased from Sigma Aldrich or Strem and used without further purification. NMR analysis was performed on the following instruments at ambient temperature: Varian 300 MHz, Varian 400 MHz, Varian 500 MHz, Bruker 400 MHz spectrometers. High-resolution mass spectra were provided by the California Institute of Technology Mass Spectrometry Facility using a JEOL JMS- 600H High Resolution Mass Spectrometer.

Optimization of Reaction Conditions (Figure 3.1)

For all reactions in Figure 1: Following work up procedure, nitrobenzene (0.1 mmol, 10.3 μL) was added as a standard, and ^{1}H NMR analysis of the crude product was performed to determine yield and selectivity.

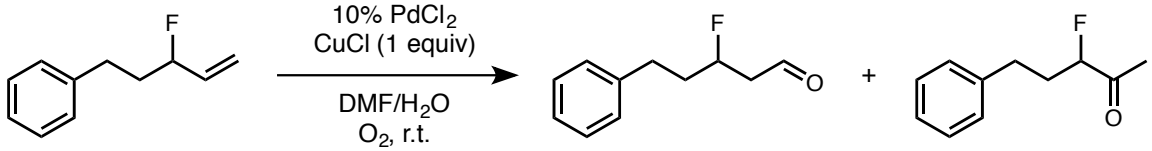

Figure 1a: Tsuji-Wacker conditions. The model substrate (0.1 mmol, 16.4 mg) was reacted using the "Procedure for Tsuji-Wacker oxidations" reported by Grubbs.[20b] Oxidation yield: 12%. Selectivity: 0.3:1 (aldehyde/ketone).

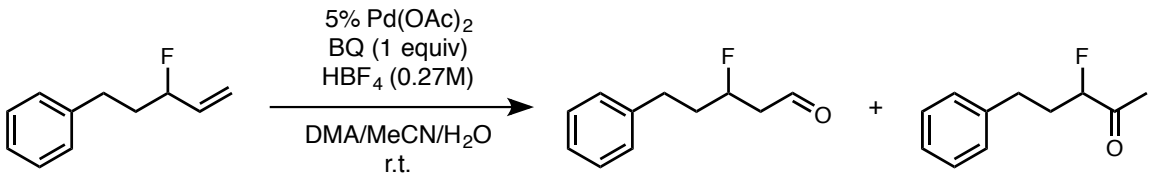

Figure 1b: Grubbs (dicationic) conditions.[15a] The model substrate (0.1 mmol, 16.4 mg) was reacted using "General Procedure 2" reported by Grubbs. Following overnight reaction in a 1-dram vial, the work up procedure was followed. Oxidation yield: 48%. Selectivity: 3:1 (aldehyde/ketone).

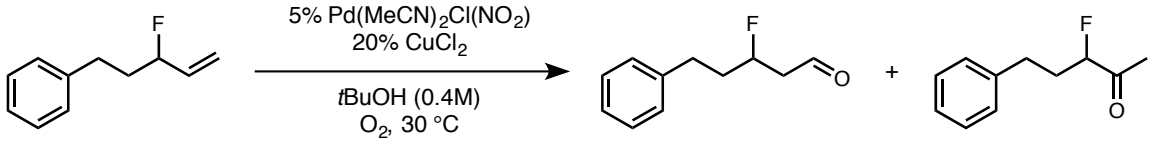

Figure 1c: Feringa conditions.[19] The model substrate (0.1 mmol, 16.4 mg) was reacted using the "General procedure for oxidation reactions with $Pd(MeCN)_2Cl(NO_2)/CuCl_2$" reported by Feringa. Following overnight reaction in a 1-dram vial, the work up procedure was followed. Oxidation yield: 40%. Selectivity: 18:1 (aldehyde/ketone).

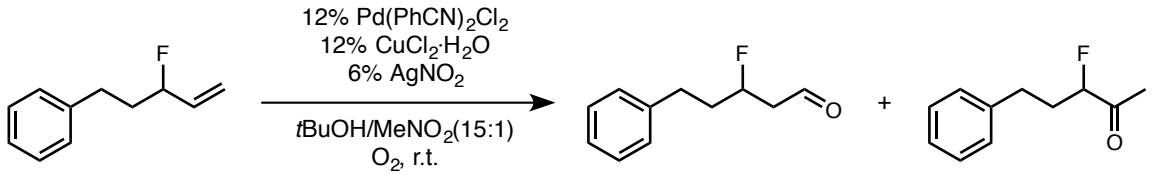

Figure 1d: Grubbs (nitrite) conditions.[20a] The model substrate (0.1 mmol, 16.4 mg) was reacted using the "Procedure (C) for small-scale oxidation of alkenes (NMR analysis)" reported by Grubbs. A 1-dram vial was used for the reaction, and, following sparging, the oxygen balloon was removed for the course of the reaction. Oxidation yield: 63%. Selectivity: 26:1 (aldehyde/ketone).

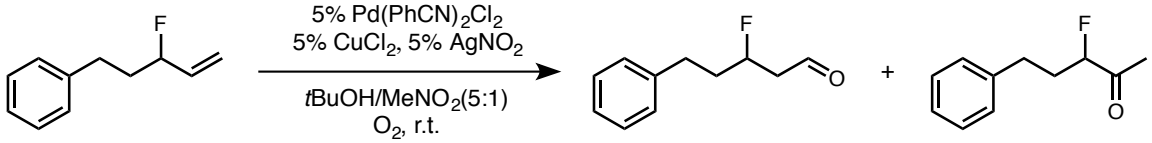

Figure 1e: Optimized conditions. A 1-dram vial equipped with a septum cap and magnetic stir bar was charged with $CuCl_2$ (0.7 mg, 0.005 mmol, 0.05 equiv), $AgNO_2$ (0.8 mg, 0.005 mmol, 0.05 equiv), and $Pd(PhCN)_2Cl_2$ (1.9 mg, 0.005 mmol, 0.05 equiv). The atmosphere was then purged using an oxygen-filled balloon for ~30 seconds. *Tert*-butanol (0.88 mL) was then added via syringe, followed by nitromethane (0.18 mL). This mixture

was sparged using an oxygen-filled balloon for ~60 seconds. (3-fluoropent-4-en-1-yl)benzene (0.1 mmol, 16.4 mg) was injected via glass syringe, the balloon was removed, and the septum cap was greased. The reaction mixture was stirred for 4 hours at room temperature. Upon completion, the solvent was removed via rotary evaporation. The reaction crude was resuspended in dichloromethane and filtered through a glass pipet containing celite, which was washed with dichloromethane. Dichloromethane was removed via rotary evaporation. Oxidation yield: 79%. Selectivity: 36:1 (aldehyde/ketone).

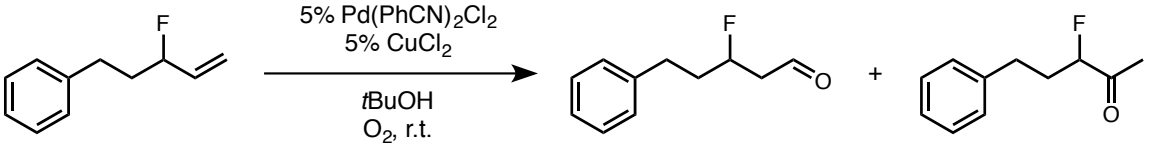

Figure 1f: Wacker conditions in *t*BuOH. A 1-dram vial equipped with a septum cap and magnetic stir bar was charged with $CuCl_2$ (0.7 mg, 0.005 mmol, 0.05 equiv) and $Pd(PhCN)_2Cl_2$ (1.9 mg, 0.005 mmol, 0.05 equiv). The atmosphere was then purged using an oxygen-filled balloon for ~30 seconds. *Tert*-butanol (1.06 mL) was then added via syringe. This mixture was sparged using an oxygen-filled balloon for ~60 seconds. (3-fluoropent-4-en-1-yl)benzene (0.1 mmol, 16.4 mg) was injected via glass syringe, the balloon was removed, and the septum cap was greased. The reaction mixture was stirred overnight at room temperature. Upon completion, the solvent was removed via rotary evaporation. The reaction crude was resuspended in dichloromethane and filtered through a glass pipet containing celite, which was washed with dichloromethane. Dichloromethane was removed via rotary evaporation. Oxidation yield: 8%. Selectivity: 8:1 (aldehyde/ketone).

Preparation of Allylic Fluorides

General Procedure A: Synthesis of Allylic Fluorides.[7d] $[IrClCOD]_2$ (0.025 equiv) was weighed into a 50 mL polypropylene centrifuge tube equipped with a large stir bar. A first portion of anhydrous ether (30% of the total solvent volume, 0.83 M relative to trichloroacetimidate) was added to the tube, followed by TEA·3HF (3 equiv). The trichloroacetimidate (1.0 equiv) was then dissolved in a second portion of anhydrous ether and added to the reaction vessel, bringing the final concentration of trichloroacetimidate to

0.25 M. The polypropylene tube was closed tightly, and the reaction was stirred vigorously at room temperature for 2 hours. Upon completion, the crude mixture was allowed to separate into two layers. A glass pipette was used to transfer the organic layer to a separatory funnel containing a saturated solution of $NaHCO_3$. Ether was added to the polypropylene tube followed by 2 minutes of vigorous stirring. The organic layer was again transferred to the separatory funnel, and this step was repeated once more. The combined organic layers were separated, and the remaining bicarb solution extracted once with ether. After drying over Na_2SO_4, the solvent was removed by rotary evaporation. The residue was purified by flash chromatography (ether/pentane).

General Procedure B: Fluorinaton of Alcohols. A three-neck round bottom flask was equipped with an addition funnel and two septa. The system was purged with argon, and DAST (0.85 mL, 6.40 mmol, 1 equiv) and anhydrous DCM (6 mL) were added to the flask via syringe. The round-bottom flask was cooled to -78 °C and stirred. The alcohol (1.0 g, 1 equiv) was dissolved in 6 mL anhydrous DCM, transferred to the addition funnel, and added dropwise over 30 minutes. The reaction was allowed to slowly warm to room temperature and stirred overnight. Following reaction completion, the crude mixture was cooled to 0 °C for quenching. One neck previously closed with a septum was opened and saturated $NaHCO_3$ solution was slowly added via addition funnel to bring the mixture to basic pH. The mixture was then stirred for 1 hour at room temperature. The layers were separated, and the organic layer washed with brine. The solvent was removed by rotary evaporation, and the residue was purified by column chromatography.

The yields have not been optimized.

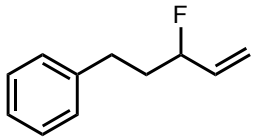

(3-fluoropent-4-en-1-yl)benzene. The fluoride was prepared according to General Procedure A from the corresponding trichloroacetimidate, 5-phenylpent-1-en-3-yl 2,2,2-trichloroacetimidate. The product was purified by flash chromatography (1% ether/pentane). Colorless oil (1.84 g, 68% yield).

^{1}H NMR (500 MHz, $CDCl_3$) δ 7.35–7.29 (m, 2H), 7.25–7.19 (m, 3H), 6.00–5.86 (m, 1H), 5.40–5.31 (m, 1H), 5.26 (dt, 1H, *J* = 10.7, 1.3 Hz), 4.99–4.82 (m, 1H), 2.86–2.69 (m, 2H), 2.14–1.86 (m, 2H).

^{13}C NMR (126 MHz, $CDCl_3$) δ 141.5, 136.7 (d, *J* = 20.2 Hz), 128.8, 126.4, 117.4 (d, *J* = 12.6 Hz), 93.0 (d, *J* = 167.6 Hz), 37.2 (d, *J* = 21.4 Hz), 31.3 (d, *J* = 5.0 Hz).

^{19}F NMR (376 MHz, $CDCl_3$) δ -178.86 (ddddd, *J* = 48.5, 28.0, 17.3, 14.2, 3.5 Hz).

MS (EI) *m/z* (M^+) calcd for $C_{11}H_{13}F$: 164.1001, found: 164.0982.

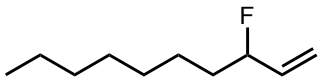

3-fluorodec-1-ene. The fluoride was prepared according to General Procedure A from the corresponding trichloroacetimidate, dec-1-en-3-yl 2,2,2-trichloroacetimidate. The product was purified by flash chromatography (pentane). Colorless oil (250 mg, 32% yield).

^{1}H NMR (500 MHz, $CDCl_3$) δ 5.88 (dddd, 1H, *J* = 16.9, 14.0, 10.6, 6.1 Hz), 5.30 (ddt, 1H, *J* = 17.3, 3.6, 1.4 Hz), 5.21 (dt, 1H, *J* = 10.6, 1.3 Hz), 4.94–4.78 (m, 1H), 1.79–1.52 (m, 2H), 1.49–1.21 (m, 10H), 0.92–0.81 (m, 3H).

^{13}C NMR (126 MHz, $CDCl_3$) δ 137.2 (d, *J* = 20.2 Hz), 117.1 (d, *J* = 11.3 Hz), 94.1 (d, *J* = 167.6 Hz), 35.6 (d, *J* = 21.4 Hz), 32.1, 29.7, 29.5, 25.0 (d, *J* = 5.0 Hz), 23.0, 14.4.

^{19}F NMR (376 MHz, $CDCl_3$) δ -176.74 (ddddd, *J* = 48.1, 26.2, 17.7, 13.9, 3.6 Hz).

MS (EI) *m/z* (M^+–HF) calcd for $C_{10}H_{18}$: 138.1408, found: 138.1430.

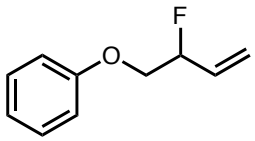

((2-fluorobut-3-en-1-yl)oxy)benzene. The fluoride was prepared according to General Procedure A from the corresponding trichloroacetimidate, 1-phenoxybut-3-en-2-yl 2,2,2-trichloroacetimidate. The product was purified by flash chromatography (5% ether/pentane). Colorless oil (1.20 g, 77% yield).

^{1}H NMR (500 MHz, $CDCl_3$) δ 7.33–7.27 (m, 2H), 7.02–6.97 (m, 1H), 6.96–6.91 (m, 2H), 6.08–5.96 (m, 1H), 5.53 (ddt, 1H, *J* = 17.3, 3.0, 1.3 Hz), 5.40 (dt, 1H, *J* = 10.8, 1.3 Hz), 5.35–5.18 (m, 1H), 4.20–4.04 (m, 2H).

^{13}C NMR (126 MHz, $CDCl_3$) δ 158.7, 132.8 (d, *J* = 20.2 Hz), 129.9, 121.6, 119.5 (d, *J* = 11.3 Hz), 115.0, 91.5 (d, *J* = 173.9 Hz), 70.0 (d, *J* = 23.9 Hz).

^{19}F NMR (376 MHz, $CDCl_3$) δ -185.41 (ddddd, *J* = 48.7, 24.7, 19.8, 14.8, 3.1 Hz).

MS (EI) *m/z* (M^+) calcd for $C_{10}H_{11}FO$: 166.0794, found: 166.0788.

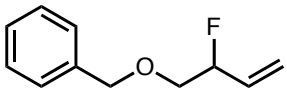

(((2-fluorobut-3-en-1-yl)oxy)methyl)benzene. The fluoride was prepared according to General Procedure A from the corresponding trichloroacetimidate, 1-(benzyloxy)but-3-en-2-yl 2,2,2-trichloroacetimidate. The product was purified by flash chromatography (5% ether/pentane). Colorless oil (144 mg, 52% yield).

^{1}H NMR (500 MHz, $CDCl_3$) δ 7.41–7.25 (m, 5H), 5.90 (dddd, 1H, *J* = 17.3, 15.1, 10.8, 5.7 Hz), 5.43 (ddt, 1H, *J* = 17.3, 2.9, 1.4 Hz), 5.31 (dt, 1H, *J* = 10.8, 1.3 Hz), 5.18–5.01 (m, 1H), 4.68–4.54 (m, 2H), 3.68–3.54 (m, 2H).

^{13}C NMR (126 MHz, $CDCl_3$) δ 138.1, 133.3 (d, *J* = 20.2 Hz), 128.8, 128.10, 128.06, 118.8 (d, *J* = 11.3 Hz), 92.6 (d, *J* = 171.4 Hz), 73.8, 72.3 (d, *J* = 22.7 Hz).

^{19}F NMR (376 MHz, $CDCl_3$) δ -184.63 – -185.09 (m).

MS (EI) *m/z* (M^+) calcd for $C_{11}H_{13}FO$: 180.0950, found: 180.0952.

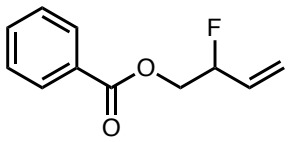

2-fluorobut-3-en-1-yl benzoate. The fluoride was prepared according to General Procedure A from the corresponding trichloroacetimidate, 2-(2,2,2-trichloro-1-iminoethoxy)but-3-en-1-yl benzoate. The product was purified by flash chromatography (10% ether/pentane). Colorless oil (344 mg, 60% yield).

^{1}H NMR (500 MHz, $CDCl_3$) δ 8.11–8.04 (m, 2H), 7.62–7.54 (m, 1H), 7.49–7.42 (m, 2H), 5.96 (dddd, 1H, *J* = 17.4, 15.1, 10.8, 5.7 Hz), 5.52 (ddt, 1H, *J* = 17.3, 2.8, 1.3 Hz), 5.40 (dt, 1H, *J* = 10.8, 1.2 Hz), 5.32–5.17 (m, 1H), 4.52 (ddd, 1H, *J* = 26.6, 12.4, 3.0 Hz), 4.42 (ddd, 1H, *J* = 20.4, 12.4, 7.0 Hz).

^{13}C NMR (126 MHz, $CDCl_3$) δ 166.5, 133.6, 132.3 (d, J = 20.2 Hz), 130.1, 130.0, 128.8, 119.8 (d, J = 11.3 Hz), 91.0 (d, J = 173.9 Hz), 66.1 (d, J = 22.7 Hz).

^{19}F NMR (376 MHz, $CDCl_3$) δ -186.05 (ddddd, J = 48.7, 26.5, 20.4, 15.0, 3.0 Hz).

MS (EI) *m/z* (M^+) calcd for $C_{11}H_{11}FO_2$: 194.0743, found: 194.0721.

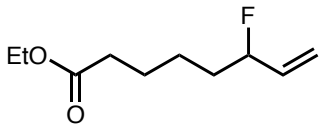

ethyl 6-fluorooct-7-enoate. The fluoride was prepared according to General Procedure A from the corresponding trichloroacetimidate, ethyl 6-(2,2,2-trichloro-1-iminoethoxy)oct-7-enoate. The product was purified by flash chromatography (10% ether/pentane). Colorless oil (124 mg, 55% yield).

^{1}H NMR (400 MHz, $CDCl_3$) δ 5.86 (dddd, 1H, J = 17.3, 14.0, 10.6, 6.1 Hz), 5.30 (ddt, 1H, J = 17.3, 3.6, 1.4 Hz), 5.21 (dt, 1H, J = 10.6, 1.3 Hz), 4.98–4.73 (m, 1H), 4.12 (q, 2H, J = 7.1 Hz), 2.31 (t, 2H, J = 7.5 Hz), 1.82–1.33 (m, 6H), 1.25 (t, 3H, J = 7.1 Hz).

^{13}C NMR (101 MHz, $CDCl_3$) δ 173.9, 136.8 (d, J = 20.2 Hz), 117.3 (d, J = 12.1 Hz), 93.7 (d, J = 167.7 Hz), 60.6, 35.2 (d, J = 22.2 Hz), 34.5, 25.0, 24.6 (d, J = 5.0 Hz), 14.6.

^{19}F NMR (376 MHz, $CDCl_3$) δ -177.17 – -177.57 (m).

MS (EI) *m/z* (M^+) calcd for $C_{10}H_{17}FO_2$: 188.1201, found: 188.1185.

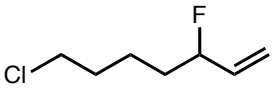

7-chloro-3-fluorohept-1-ene. The fluoride was prepared according to General Procedure A from the corresponding trichloroacetimidate, 7-chlorohept-1-en-3-yl 2,2,2-trichloroacetimidate. The product was purified by flash chromatography (1% ether/pentane). Colorless oil (583 mg, 57% yield).

^{1}H NMR (300 MHz, $CDCl_3$) δ 5.88 (dddd, 1H, J = 17.3, 14.1, 10.6, 6.0 Hz), 5.32 (ddt, 1H, J = 17.3, 3.5, 1.4 Hz), 5.23 (dt, 1H, J = 10.6, 1.3 Hz), 5.03–4.72 (m, 1H), 3.55 (t, 2H, J = 6.6 Hz), 1.93–1.43 (m, 6H).

^{13}C NMR (126 MHz, $CDCl_3$) δ 136.7 (d, J = 18.9 Hz), 117.4 (d, J = 12.6 Hz), 93.7 (d, J = 167.6 Hz), 45.1, 34.7 (d, J = 22.7 Hz), 32.6, 22.4 (d, J = 5.0 Hz).

^{19}F NMR (376 MHz, $CDCl_3$) δ -177.21 – -177.68 (m).

MS (EI) *m/z* (M^+) calcd for $C_7H_{12}ClF$: 150.0612, found: 150.0659.

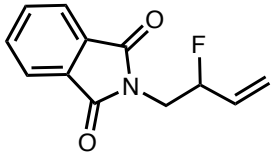

2-(2-fluorobut-3-en-1-yl)isoindoline-1,3-dione. The fluoride was prepared according to General Procedure A from the corresponding trichloroacetimidate, 1-(1,3-dioxoisoindolin-2-yl)but-3-en-2-yl 2,2,2-trichloroacetimidate. The product was purified by flash chromatography (20% Et_2O/pentane). White solid (173 mg, 65% yield).

^{1}H NMR (500 MHz, $CDCl_3$) δ 7.91–7.80 (m, 2H), 7.78–7.67 (m, 2H), 5.93 (dddd, 1H, *J* = 17.3, 14.5, 10.7, 6.0 Hz), 5.46 (ddt, 1H, *J* = 17.2, 3.3, 1.2 Hz), 5.34 (dt, 1H, *J* = 10.7, 1.2 Hz), 5.29–5.11 (m, 1H), 4.03 (ddd, 1H, *J* = 14.4, 13.7, 8.2 Hz), 3.82 (ddd, 1H, *J* = 26.4, 14.4, 4.0 Hz).

^{13}C NMR (126 MHz, $CDCl_3$) δ 168.3, 134.5, 133.3 (d, *J* = 17.6 Hz), 132.2, 123.8, 120.0 (d, *J* = 11.3 Hz), 90.4 (d, *J* = 173.9 Hz), 41.8 (d, *J* = 26.5 Hz).

^{19}F NMR (376 MHz, $CDCl_3$) δ -184.20 – -184.59 (m).

MS (FAB) *m/z* (M^++H) calcd for $C_{12}H_{11}FNO_2$: 220.0774, found: 220.0771.

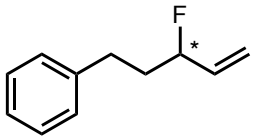

(3-fluoropent-4-en-1-yl)benzene. The fluoride was prepared according to literature procedure[7h] from the corresponding trichloroacetimidate, 5-phenylpent-1-en-3-yl 2,2,2-trichloroacetimidate. The commercially available Lin diene ligand investigated by Nguyen (CAS# 940280-80-8, (*S*,*S*)-enantiomer) was used. The product was purified by flash chromatography (1% ether/pentane) followed by purification by preparative HPLC (Daicel CHIRALPAK® IC column, 2.0 cm X 25.0 cm, 0.5% 2-PrOH/hexanes). Colorless oil (37 mg, 30% yield, 90% ee).

HPLC analysis: Daicel CHIRALCEL® OD column; 0.5% 2-PrOH/hexanes; 0.8 mL/min; retention times: 8.5 min (minor), 9.1 min (major).

^{1}H NMR (500 MHz, $CDCl_3$) δ 7.34–7.27 (m, 2H), 7.25–7.18 (m, 3H), 5.92 (dddd, 1H, *J* = 17.3, 14.2, 10.7, 6.0 Hz), 5.34 (ddt, 1H, *J* = 17.2, 3.6, 1.4 Hz), 5.25 (dt, 1H, *J* = 10.6, 1.3 Hz), 5.03–4.77 (m, 1H), 2.88–2.64 (m, 2H), 2.15–1.84 (m, 2H).

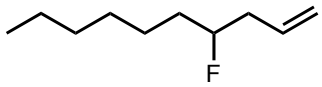

4-fluorodec-1-ene. The fluoride was prepared according to General Procedure B from the corresponding alcohol, dec-1-en-4-ol. The product was purified by flash chromatography (pentane). Colorless oil (374 mg, 37% yield).

^{1}H NMR (500 MHz, $CDCl_3$) δ 5.83 (ddt, 1H, *J* = 17.2, 10.2, 7.0 Hz), 5.18–5.05 (m, 2H), 4.61–4.43 (m, 1H), 2.46–2.22 (m, 2H), 1.71–1.21 (m, 10H), 0.93–0.85 (m, 3H).

^{13}C NMR (126 MHz, $CDCl_3$) δ 133.8 (d, *J* = 5.0 Hz), 118.0, 93.9 (d, *J* = 168.8 Hz), 39.9 (d, *J* = 21.4 Hz), 35.0 (d, *J* = 21.4 Hz), 32.1, 29.5, 25.3 (d, *J* = 5.0 Hz), 22.9, 14.4.

^{19}F NMR (376 MHz, $CDCl_3$) δ -179.49 – -180.17 (m).

MS (EI) *m/z* (M^+) calcd for $C_{10}H_{19}F$: 158.1471, found: 158.1478.

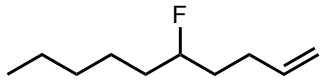

5-fluorodec-1-ene. The fluoride was prepared according to General Procedure B from the corresponding alcohol, dec-1-en-5-ol. The product was purified by flash chromatography (pentane). Colorless oil (495 mg, 49% yield).

^{1}H NMR (300 MHz, $CDCl_3$) δ 5.82 (ddt, 1H, *J* = 16.9, 10.2, 6.6 Hz), 5.12–4.90 (m, 2H), 4.63–4.34 (m, 1H), 2.33–2.03 (m, 2H), 1.83–1.17 (m, 10H), 0.94–0.83 (m, 3H).

^{13}C NMR (126 MHz, $CDCl_3$) δ 138.2, 115.3, 94.1 (d, *J* = 167.6 Hz), 35.5 (d, *J* = 20.2 Hz), 34.7 (d, *J* = 20.2 Hz), 32.04, 29.7 (d, *J* = 5.0 Hz), 25.1 (d, *J* = 5.0 Hz), 22.9, 14.4.

^{19}F NMR (376 MHz, $CDCl_3$) δ -180.92 – -181.52 (m).

MS (EI) *m/z* (M^+) calcd for $C_{10}H_{19}F$: 158.1471, found: 158.1497.

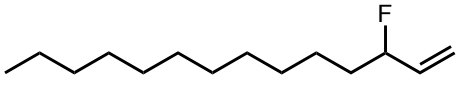

3-fluorotetradec-1-ene. The fluoride was prepared according to General Procedure A from the corresponding trichloroacetimidate, tetradec-1-en-3-yl 2,2,2-

trichloroacetimidate. The product was purified by flash chromatography (pentane). Colorless oil (693 mg, 65% yield).

^{1}H NMR (500 MHz, $CDCl_3$) δ 5.96–5.82 (m, 1H), 5.32 (ddt, 1H, *J* = 17.3, 3.6, 1.4 Hz), 5.22 (dt, 1H, *J* = 10.7, 1.3 Hz), 4.97–4.78 (m, 1H), 1.81–1.52 (m, 2H), 1.50–1.18 (m, 18H), 0.97–0.82 (m, 3H).

^{13}C NMR (126 MHz, $CDCl_3$) δ 137.1 (d, *J* = 20.2 Hz), 117.1 (d, *J* = 12.6 Hz), 94.1 (d, *J* = 167.6 Hz), 35.6 (d, *J* = 22.7 Hz), 32.3, 30.00, 29.98, 29.91, 29.86, 29.74, 29.70, 25.0 (d, *J* = 5.0 Hz), 23.0, 14.5.

^{19}F NMR (376 MHz, $CDCl_3$) δ -176.52 – -177.01 (m).

MS (EI) *m/z* (M^+) calcd for $C_{14}H_{27}F$: 214.2097, found: 214.2095.

Wacker Oxidations of Allylic Fluorides (Table 3.1)

General Procedure C: Nitrite-Modified Wacker Oxidations of Allylic Fluorides. A 2-dram vial equipped with a septum cap and magnetic stir bar was charged with $CuCl_2$ (2.7 mg, 0.02 mmol, 0.05 equiv), $AgNO_2$ (3.1 mg, 0.02 mmol, 0.05 equiv), and $Pd(PhCN)_2Cl_2$ (7.7 mg, 0.02 mmol, 0.05 equiv). The atmosphere was then purged using an oxygen-filled balloon for ~30 seconds. *Tert*-butanol (3.5 mL) was then added via syringe, followed by nitromethane (0.7 mL). This mixture was sparged using an oxygen-filled balloon for ~60 seconds, and the balloon was left attached to the vial for the remainder of the reaction. The allylic fluoride (0.4 mmol) was injected via glass syringe, and the reaction mixture was stirred for 4 hours. Upon completion, the solvent was removed via rotary evaporation. The reaction crude was resuspended in ~2 mL dichloromethane and filtered through a glass pipet containing celite washed with dichloromethane into a round-bottom flask. Dichloromethane was removed via rotary evaporation. The crude aldehyde product was subjected to ^{1}H NMR analysis to determine regioselectivity of oxidation prior to reduction.

For solid substrates: The reaction set up was completed as described above, but the allylic fluoride was added as a solution in nitromethane, followed by final sparging with oxygen.

General Procedure D: Reduction of Aldehyde Products and Isolation. The flask containing crude aldehyde product was equipped with a large stir bar, closed with a septum, and purged using an argon-filled balloon, left attached for the course of the

reduction. Dichloromethane (14 mL) and ethanol (10 mL) were added via syringe, and the mixture was stirred and cooled to 0 °C. Sodium borohydride (22.7 mg, 0.6 mmol, 1.5 equiv) was then added and the atmosphere purged again using an argon-filled balloon. This mixture was allowed to warm to room temperature and stirred for 30 minutes. Following reduction of the aldehyde, the reaction mixture was cooled to 0 °C. Saturated NH_4Cl solution (~70 mL) was added slowly (over 5-10 minutes) through the septum via syringe with the argon-filled balloon left intact, followed by vigorous stirring for 30 minutes at 0 °C. The reaction mixture was then transferred to a separatory funnel and extracted 4 times with ether, without further dilution with water. The combined organic layers were washed twice with saturated sodium bicarbonate solution and once with brine, and then dried over Na_2SO_4. The solvent was removed by rotary evaporation and the residue purified by column chromatography (ether/pentane).

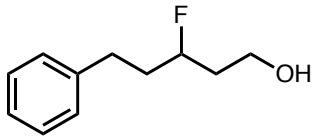

3-fluoro-5-phenylpentan-1-ol (Table 3.1, Entry 1). The title compound was synthesized according to General Procedures C and D from (3-fluoropent-4-en-1-yl)benzene (65.7 mg, 0.40 mmol). ^{1}H NMR analysis displayed 33:1 aldehyde selectivity. The product was purified by column chromatography on silica gel (40% ether/pentane). Pale yellow oil (60 mg, 82% yield).

^{1}H NMR (500 MHz, $CDCl_3$) δ 7.34–7.27 (m, 2H), 7.24–7.16 (m, 3H), 4.72 (dtt, 1H, J = 49.7, 8.9, 3.4 Hz), 3.88–3.75 (m, 2H), 2.84 (ddd, 1H, J = 14.6, 9.9, 5.2 Hz), 2.72 (ddd, 1H, J = 13.8, 9.5, 7.0 Hz), 2.12–1.73 (m, 4H), 1.66 (br s, 1H).

^{13}C NMR (126 MHz, $CDCl_3$) δ 141.6, 128.80, 128.77, 126.3, 91.9 (d, J = 166.3 Hz), 59.6 (d, J = 3.8 Hz), 38.2 (d, J = 20.2 Hz), 37.5 (d, J = 21.4 Hz), 31.6 (d, J = 5.0 Hz).

^{19}F NMR (376 MHz, $CDCl_3$) δ -184.22 (dtd, J = 65.9, 33.0, 16.1 Hz).

MS (FAB) *m/z* (M^++H) calcd for $C_{11}H_{16}FO$: 183.1185, found: 183.1204.

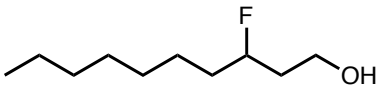

3-fluorodecan-1-ol (Table 3.1, Entry 2). The title compound was synthesized according to General Procedures C and D from 3-fluorodec-1-ene (63.3 mg, 0.40 mmol). ^{1}H NMR analysis displayed 29:1 aldehyde selectivity. The product was purified by column chromatography on silica gel (40% ether/pentane). Pale yellow solid (62 mg, 87% yield).

^{1}H NMR (500 MHz, $CDCl_3$) δ 4.80–4.59 (m, 1H), 3.87–3.75 (m, 2H), 1.94–1.19 (m, 15H), 0.96–0.81 (m, 3H).

^{13}C NMR (126 MHz, $CDCl_3$) δ 93.1 (d, J = 166.3 Hz), 59.9 (d, J = 3.8 Hz), 38.2 (d, J = 20.2 Hz), 35.7 (d, J = 21.4 Hz), 32.1, 29.7, 29.5, 25.4 (d, J = 3.8 Hz), 22.3, 14.4.

^{19}F NMR (376 MHz, $CDCl_3$) δ -182.30 (dddt, J = 50.6, 34.2, 29.6, 17.1 Hz).

MS (FAB) *m/z* (M^+–F) calcd for $C_{10}H_{21}O$: 157.1592, found: 157.1594.

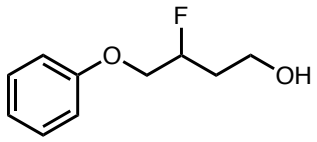

3-fluoro-4-phenoxybutan-1-ol (Table 3.1, Entry 3). The title compound was synthesized according to General Procedures C and D from ((2-fluorobut-3-en-1-yl)oxy)benzene (66.5 mg, 0.40 mmol). ^{1}H NMR analysis displayed ≥99:1 aldehyde selectivity. The product was purified by column chromatography on silica gel (50% ether/pentane). Pale yellow solid (69 mg, 94% yield).

^{1}H NMR (500 MHz, $CDCl_3$) δ 7.34–7.27 (m, 2H), 6.98 (t, 1H, J = 7.4 Hz), 6.93 (d, 2H, J = 8.0 Hz), 5.17–4.95 (m, 1H), 4.19–4.09 (m, 2H), 3.92–3.82 (m, 2H), 2.16–1.85 (m, 2H), 1.76 (br s, 1H).

^{13}C NMR (126 MHz, $CDCl_3$) δ 158.7, 129.9, 121.6, 114.9, 90.1 (d, J = 172.6 Hz), 69.9 (d, J = 23.9 Hz), 59.0 (d, J = 5.0 Hz), 34.6 (d, J = 20.2 Hz).

^{19}F NMR (376 MHz, $CDCl_3$) δ -189.32 (ddtd, J = 48.3, 31.6, 22.3, 16.3 Hz).

MS (EI) *m/z* (M^+) calcd for $C_{10}H_{13}FO_2$: 184.0900, found: 184.0912.

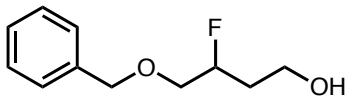

4-(benzyloxy)-3-fluorobutan-1-ol (Table 3.1, Entry 4). The title compound was synthesized according to General Procedures C and D from (((2-fluorobut-3-en-1-

yl)oxy)methyl)benzene (72.1 mg, 0.40 mmol). ^{1}H NMR analysis displayed ≥99:1 aldehyde selectivity. The product was purified by column chromatography on silica gel (50% ether/pentane). Pale yellow oil (74 mg, 93% yield).

^{1}H NMR (500 MHz, $CDCl_3$) δ 7.39–7.27 (m, 5H), 4.98–4.78 (m, 1H), 4.63–4.57 (m, 2H), 3.84–3.76 (m, 2H), 3.70–3.64 (m, 1H), 3.64–3.58 (m, 1H), 2.05–1.81 (m, 2H), 1.68 (br s, 1H).

^{13}C NMR (126 MHz, $CDCl_3$) δ 138.0, 128.8, 128.2, 128.1, 91.2 (d, J = 171.4 Hz), 73.8, 72.1 (d, J = 22.7 Hz), 59.0 (d, J = 5.0 Hz), 34.8 (d, J = 21.4 Hz).

^{19}F NMR (376 MHz, $CDCl_3$) δ -188.08 – -188.66 (m).

MS (EI) *m/z* (M^+) calcd for $C_{11}H_{15}FO_2$: 198.1056, found: 198.1084.

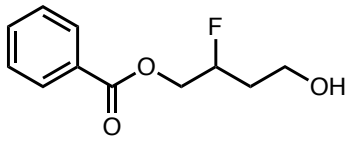

2-fluoro-4-hydroxybutyl benzoate (Table 3.1, Entry 5). The title compound was synthesized according to General Procedures C and D from 2-fluorobut-3-en-1-yl benzoate (77.7 mg, 0.40 mmol). ^{1}H NMR analysis displayed ≥99:1 aldehyde selectivity. The product was purified by column chromatography on silica gel (60% ether/pentane). White solid (79 mg, 93% yield).

^{1}H NMR (500 MHz, $CDCl_3$) δ 8.10–8.06 (m, 2H), 7.61–7.55 (m, 1H), 7.49–7.42 (m, 2H), 5.06 (ddddd, 1H, J = 49.2, 9.0, 6.4, 3.9, 2.7 Hz), 4.60–4.41 (m, 2H), 3.91–3.86 (m, 2H), 2.14–1.83 (m, 2H), 1.55 (br s, 1H).

^{13}C NMR (126 MHz, $CDCl_3$) δ 166.7, 133.6, 130.1, 129.9, 128.8, 89.6 (d, J = 172.6 Hz), 66.6 (d, J = 21.4 Hz), 58.8 (d, J = 5.0 Hz), 34.4 (d, J = 21.4 Hz).

^{19}F NMR (376 MHz, $CDCl_3$) δ -189.14 – -189.79 (m).

MS (FAB) *m/z* (M^++H) calcd for $C_{11}H_{14}FO_3$: 213.0927, found: 213.0938.

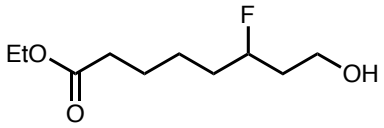

ethyl 6-fluoro-8-hydroxyoctanoate (Table 3.1, Entry 6). The title compound was synthesized according to General Procedures C and D from ethyl 6-fluorooct-7-enoate

(75.3 mg, 0.40 mmol). ^{1}H NMR analysis displayed 29:1 aldehyde selectivity. The product was purified by column chromatography on silica gel (60% ether/pentane). Colorless oil (59 mg, 72% yield).

^{1}H NMR (400 MHz, $CDCl_3$) δ 4.79–4.59 (m, 1H), 4.11 (q, 2H, J = 7.2 Hz), 3.83–3.74 (m, 2H), 2.30 (t, 2H, J = 7.4 Hz), 1.93–1.29 (m, 9H), 1.24 (t, 3H, J = 7.1 Hz).

^{13}C NMR (101 MHz, $CDCl_3$) δ 173.9, 92.5 (d, J = 166.3 Hz), 60.6, 59.6 (d, J = 3.8 Hz), 38.1 (d, J = 20.2 Hz), 35.3 (d, J = 21.4 Hz), 34.5, 25.0, 24.9 (d, J = 3.8 Hz), 14.6.

^{19}F NMR (376 MHz, $CDCl_3$) δ -182.90 (dddt, J = 50.2, 33.8, 29.7, 16.9 Hz).

MS (FAB) *m/z* (M^++H) calcd for $C_{10}H_{20}FO_3$: 207.1396, found: 207.1401.

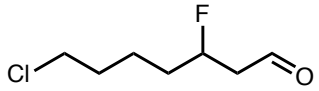

7-chloro-3-fluoroheptanal (Table 3.1, Entry 7). The title compound was synthesized according to General Procedure C from 7-chloro-3-fluorohept-1-ene (60.4 mg, 0.40 mmol). Upon completion, nitrobenzene (0.40 mmol) was added as an NMR standard. ^{1}H NMR analysis of an aliquot of the crude reaction mixture (without any rotary evaporation step) displayed 42:1 aldehyde selectivity and 81% yield.

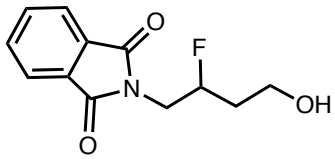

2-(2-fluoro-4-hydroxybutyl)isoindoline-1,3-dione (Table 1, Entry 8). The title compound was synthesized according to General Procedures C and D from 2-(2-fluorobut-3-en-1-yl)isoindoline-1,3-dione (87.7 mg, 0.40 mmol). ^{1}H NMR analysis displayed ≥99:1 aldehyde selectivity. The product was purified by column chromatography on silica gel (1:1:1 ether/DCM/pentane). Light yellow solid (73 mg, 77% yield).

^{1}H NMR (500 MHz, $CDCl_3$) δ 7.90–7.83 (m, 2H), 7.77–7.70 (m, 2H), 5.10–4.90 (m, 1H), 4.05 (ddd, 1H, J = 16.1, 14.5, 7.8 Hz), 3.92–3.78 (m, 3H), 2.02–1.86 (m, 2H).

^{13}C NMR (126 MHz, $CDCl_3$) δ 168.5, 134.5, 132.2, 123.8, 89.5 (d, J = 173.9 Hz), 59.0 (d, J = 5.0 Hz), 42.1 (d, J = 23.9 Hz), 35.7 (d, J = 20.2 Hz).

^{19}F NMR (376 MHz, $CDCl_3$) δ -188.23 – -188.74 (m).

MS (EI) *m/z* (M^+) calcd for $C_{12}H_{12}FNO_3$: 237.0801, found: 237.0797.

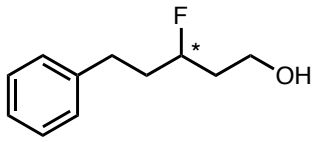

3-fluoro-5-phenylpentan-1-ol (Eq. 3.1). The title compound was synthesized according to General Procedures C and D from (3-fluoropent-4-en-1-yl)benzene (33 mg, 0.20 mmol). ^{1}H NMR analysis displayed 30:1 aldehyde selectivity. The product was purified by column chromatography on silica gel (25→75% ether/pentane). Colorless oil (30 mg, 82% yield, 90% ee).

HPLC analysis: Daicel CHIRALCEL® OD column; 15% 2-PrOH/hexanes; 0.9 mL/min; retention times: 7.3 min (minor), 8.7 min (major).

^{1}H NMR (500 MHz, $CDCl_3$) δ 7.34–7.27 (m, 2H), 7.24–7.16 (m, 3H), 4.72 (dtt, 1H, *J* = 49.7, 8.9, 3.4 Hz), 3.87–3.76 (m, 2H), 2.84 (ddd, 1H, *J* = 14.7, 9.9, 5.2 Hz, 1H), 2.72 (ddd, 1H, *J* = 13.8, 9.5, 7.0 Hz), 2.09–1.74 (m, 4H), 1.55 (br s, 1H).

Derivatizations of β-Fluorinated Aldehydes (Scheme 3.2)

All derivatizations were performed on crude aldehydes produced from (3-fluoropent-4-en-1-yl)benzene using General Procedure C. All yields reported over two steps.

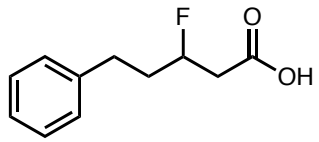

3-fluoro-5-phenylpentanoic acid (Scheme 3.2a). The title compound was synthesized from 3-fluoro-5-phenylpentanal (produced from 0.40 mmol (3-fluoropent-4-en-1-yl)benzene) using the "General Procedure for Oxidation of Aldehyde to Carboxylic Acid" reported by Borhan.[27] The product was purified by column chromatography on silica gel (5% MeOH/pentane). Clear crystals (71 mg, 90% yield).

^{1}H NMR (400 MHz, $CDCl_3$) δ 8.77 (br s, 1H), 7.35–7.27 (m, 2H), 7.24–7.15 (m, 3H), 4.95 (dtt, 1H, *J* = 48.1, 8.3, 4.0 Hz), 2.92–2.50 (m, 4H), 2.17–1.81 (m, 2H).

^{13}C NMR (101 MHz, $CDCl_3$) δ 176.2 (d, *J* = 6.1 Hz), 141.1, 128.9, 128.8, 126.5, 89.5 (d, *J* = 170.7 Hz), 40.4 (d, *J* = 24.2 Hz), 36.9 (d, *J* = 21.2 Hz), 31.4 (d, *J* = 4.0 Hz).

^{19}F NMR (376 MHz, $CDCl_3$) δ -181.38 – -181.83 (m).

MS (FAB) *m/z* (M^++H) calcd for $C_{11}H_{14}O_2F$: 197.0978, found: 197.0980.

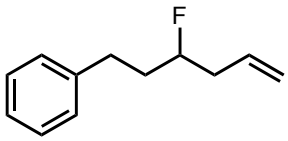

(3-fluorohex-5-en-1-yl)benzene (Scheme 3.2b). A 1-dram vial equipped with a septum cap and stir bar was charged with $MePPh_3Br$ (54 mg, 1.5 equiv, 0.15 mmol). The atmosphere was purged using an argon-filled balloon, and anhydrous THF was added via syringe (0.5 mL). The mixture was cooled to 0 °C with stirring, and *n*BuLi (2.5 M in hexanes, 1.4 equiv) was added via glass syringe. The mixture was allowed to stir for 30 minutes at 0 °C. 3-fluoro-5-phenylpentanal (produced from 0.10 mmol (3-fluoropent-4-en-1-yl)benzene) was dissolved in THF (0.2 mL) under argon atmosphere, and the solution was added via microsyringe to the reaction mixture. The reaction was allowed to warm to room temperature and stirred overnight. Saturated NH_4Cl solution was added to the crude mixture and extracted 3 times with ether. Following drying over Na_2SO_4, the solvent was removed by rotary evaporation. The residue was purified by preparative thin-layer chromatography on silica gel (2% ether/pentane). Pale yellow oil (12 mg, 65% yield).

^{1}H NMR (300 MHz, $CDCl_3$) δ 7.35–7.24 (m, 2H), 7.24–7.15 (m, 3H), 5.91–5.73 (m, 1H), 5.18–5.05 (m, 2H), 4.69–4.39 (m, 1H), 2.83 (ddd, 1H, *J* = 14.9, 9.8, 5.3 Hz), 2.69 (ddd, 1H, *J* = 13.8, 9.4, 7.1 Hz), 2.54–2.24 (m, 2H), 2.08–1.71 (m, 2H).

^{13}C NMR (126 MHz, $CDCl_3$) δ 141.7, 133.4 (d, *J* = 6.3 Hz), 128.80, 128.79, 126.3, 118.3, 92.8 (d, *J* = 170.1 Hz), 39.9 (d, *J* = 22.7 Hz), 36.8 (d, *J* = 21.4 Hz), 31.6 (d, *J* = 3.8 Hz).

^{19}F NMR (376 MHz, $CDCl_3$) δ -181.34 – -181.99 (m).

MS (EI) *m/z* (M^+) calcd for $C_{12}H_{15}F$: 178.1158, found: 178.1158.

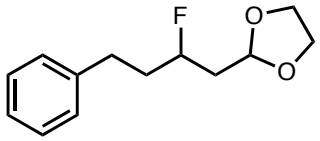

2-(2-fluoro-4-phenylbutyl)-1,3-dioxolane (Scheme 3.2d). 3-fluoro-5-phenylpentanal (produced from 0.40 mmol (3-fluoropent-4-en-1-yl)benzene) was dissolved in 2 mL ethylene glycol (0.2 M). Molecular sieves (4Å, 130 mg) were then added. *P*-toluenesulfonic acid (76.1 mg, 1 equiv, 0.40 mmol) was added, and the reaction was stirred for 6 hours at room temperature. The reaction was quenched with saturated $NaHCO_3$ solution, and extracted three times with ether. After drying over Na_2SO_4, the solvent was removed by rotary evaporation. The residue was purified by column chromatography on silica gel (20% Et_2O/pentane). Colorless oil (50 mg, 56% yield).

^{1}H NMR (500 MHz, $CDCl_3$) δ 7.33–7.27 (m, 2H), 7.23–7.17 (m, 3H), 5.03 (dd, 1H, *J* = 6.4, 3.6 Hz), 4.75 (dtt, 1H, *J* = 49.4, 8.7, 3.6 Hz), 4.03–3.92 (m, 2H), 3.92–3.82 (m, 2H), 2.84 (ddd, 1H, *J* = 13.8, 10.1, 5.2 Hz), 2.71 (ddd, 1H, *J* = 13.9, 9.7, 6.8 Hz), 2.14 (dddd, 1H, *J* = 16.4, 14.5, 8.7, 3.6 Hz), 2.08–1.77 (m, 3H).

^{13}C NMR (126 MHz, $CDCl_3$) δ 141.6, 128.8, 126.3, 101.9 (d, *J* = 5.0 Hz), 90.5 (d, *J* = 167.6 Hz), 65.3, 65.1, 40.0 (d, *J* = 20.2 Hz), 37.7 (d, *J* = 20.2 Hz), 31.5 (d, *J* = 3.8 Hz).

^{19}F NMR (376 MHz, $CDCl_3$) δ -183.15 (dtt, *J* = 48.9, 32.5, 16.4 Hz).

MS (FAB) *m/z* (M^++H) calcd for $C_{13}H_{18}FO_2$: 225.1291, found: 225.1281.

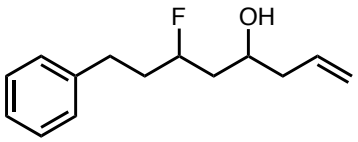

6-fluoro-8-phenyloct-1-en-4-ol (Scheme 3.2e). A 20 mL vial containing 3-fluoro-5-phenylpentanal (produced from 0.40 mmol (3-fluoropent-4-en-1-yl)benzene) was purged using an argon-filled balloon. The aldehyde was dissolved in 3.3 mL anhydrous DCM (0.12 M) and the mixture cooled to -78 °C. Allylboronic acid pinacol ester (75 μL, 0.4 mmol, 1.0 equiv) was then added via glass syringe. The reaction mixture was then allowed to warm to room temperature and stirred overnight. Water was added to the crude mixture and extracted three times with ether. After drying over Na_2SO_4, the solvent was removed by rotary evaporation. The residue was purified by column chromatography on silica gel (30% Et_2O/pentane). ^{1}H NMR analysis displayed ~1:1 dr. Colorless oil (72 mg, 81% yield).

^{1}H NMR (500 MHz, $CDCl_3$) δ 7.34–7.26 (m, 2H), 7.24–7.15 (m, 3H), 5.90–5.72 (m, 1H), 5.20–5.08 (m, 2H), 4.96–4.59 (m, 1H), 4.00–3.83 (m, 1H), 2.90–2.77 (m, 1H), 2.76–2.63 (m, 1H), 2.39–2.12 (m, 2H), 2.11–1.46 (m, 5H).

^{13}C NMR (126 MHz, $CDCl_3$) δ 141.7, 141.6, 134.65, 134.61, 128.80, 128.77, 128.76, 128.75, 126.4, 126.3, 118.9, 118.7, 93.3 (d, J = 166.3 Hz), 91.1 (d, J = 166.3 Hz), 69.1 (d, J = 3.8 Hz), 67.1 (d, J = 2.5 Hz), 42.8, 42.4 (d, J = 20.2 Hz), 42.1, 41.9 (d, J = 18.9 Hz), 37.7 (d, J = 21.4 Hz), 37.5 (d, J = 20.2 Hz), 31.7 (d, J = 5.0 Hz), 31.5 (d, J = 5.0 Hz).

^{19}F NMR (376 MHz, $CDCl_3$) δ -181.75 (dtt, J = 49.0, 32.5, 15.6 Hz), -183.91 – -184.74 (m).

MS (FAB) *m/z* (M^++H) calcd for $C_{14}H_{20}FO$: 223.1498, found: 223.1491.

Mechanistic Studies

General Procedure for Figure 3.2. A 1-dram vial equipped with a septum cap and magnetic stir bar was charged with $CuCl_2$ (0.7 mg, 0.005 mmol, 0.05 equiv), $AgNO_2$ (0.8 mg, 0.005 mmol, 0.05 equiv), and $Pd(PhCN)_2Cl_2$ (1.9 mg, 0.005 mmol, 0.05 equiv). The atmosphere was then purged using an oxygen-filled balloon for ~30 seconds. *Tert*-butanol (0.88 mL) was then added via syringe, followed by nitromethane (0.18 mL). This mixture was sparged using an oxygen-filled balloon for ~60 seconds. The olefin (0.1 mmol) was injected via glass syringe, the balloon was removed, and the septum cap was greased. The reaction mixture was stirred for 4 hours at room temperature. Upon completion, the solvent was removed via rotary evaporation. The reaction crude was resuspended in dichloromethane and filtered through a glass pipet containing celite, which was washed with dichloromethane. Dichloromethane was removed via rotary evaporation. Nitrobenzene (0.1 mmol, 10.3 μL) was added as a standard, and ^{1}H NMR analysis of the crude product was performed to determine yield and selectivity.

	Selectivity (%)		Oxidation Yield (%)	
	run 1	**run 2**	**run 1**	**run 2**
n=0	95	96	55	49
n=1	79	80	68	59
n=2	64	69	53	59
1-decene	54	61	54	51

General Procedure for Figure 3.3a: Individual rate comparison. A 4 mL vial with a stir bar was charged with $CuCl_2$ (2.7 mg, 0.020 mmol), $AgNO_2$ (3.1 mg, 0.020 mmol), and $Pd(PhCN)_2Cl_2$ (7.7 mg, 0.020 mmol). The vial was capped with a septum cap and purged with O_2 using an oxygen-filled balloon. Next, *tert*-BuOH (1.32 mL, anhydrous) and nitromethane (0.36 mL, anhydrous) were added via syringe, and the reaction mixture was stirred. In a separate vial, a solution of olefin (0.20 mmol) and diphenylmethane (16.7 μL, 0.10 mmol; internal standard) in *t*-BuOH (0.44 mL) was prepared. The olefin solution was added to the catalyst mixture via syringe, and an aliquot (0.3 mL) was immediately collected for a time = 0 data point. The aliquot was quenched with a solution of pyridine (6.0 μL) in DCM (0.2 mL). After quenching, the aliquot was concentrated, diluted with hexanes, and filtered through a plug of celite with hexanes. The filtrate was concentrated and analyzed by ^1H NMR. Aliquots were taken at time = 5, 10, 15, and 20 minutes following the same quenching procedure, and conversions were determined by ^1H NMR relative to the time = 0 data point.

Tetradecene

Time (min) Conversion (%)

	run 1	run 2	run 3	Average
0	0	0	0	0
5	7.7	6.7	8	7.5
10	12.1	11.9	11.6	11.9
15	17.2	13.7	15.7	15.5
20	19.9	16.9	19.6	18.8

Allylic Fluoride

Time (min) Conversion (%)

	run 1	run 2	Average
0	0	0	0
5	9.6	11.2	10.4
10	18.5	20.9	19.7
15	28.4	30.6	29.5
20	36.9	40.5	38.7

General Procedure for Figure 3.3b: Competition experiment. A 4 mL vial with a stir bar was charged with $CuCl_2$ (2.7 mg, 0.020 mmol), $AgNO_2$ (3.1 mg, 0.020 mmol), and $Pd(PhCN)_2Cl_2$ (7.7 mg, 0.020 mmol). The vial was capped with a septum cap and

purged with O_2 using an oxygen-filled balloon. Next, *tert*-BuOH (1.32 mL, anhydrous) and nitromethane (0.36 mL, anhydrous) were added via syringe, and the reaction mixture was stirred. In a separate vial, a solution of tetradecene (19.6 mg, 0.10 mmol), 3-fluorotetradec-1-ene (21.4 mg, 0.10 mmol), and diphenylmethane (16.7 μL, 0.10 mmol; internal standard) in *t*-BuOH (0.44 mL) was prepared. The olefin solution was added to the catalyst mixture via syringe, and an aliquot (0.3 mL) was immediately collected for a time = 0 data point. The aliquot was quenched with a solution of pyridine (6.0 μL) in DCM (0.2 mL). After quenching, the aliquot was concentrated, diluted with hexanes, and filtered through a plug of celite with hexanes. The filtrate was concentrated and analyzed by ^{1}H NMR. A second aliquot was collected at time = 10 minutes following the same quenching procedure, and the conversion of each olefin was determined by ^{1}H NMR relative to the time = 0 data point.

Conversion (%)

	Tetradecene	**Allylic Fluoride**	**Selectivity**
run 1	11.2	5.0	2.2:1
run 2	11.1	4.6	2.4:1

^{1}H, ^{13}C, and ^{19}F NMR Spectra

293PROTON01
bc-I-28-C13_1H

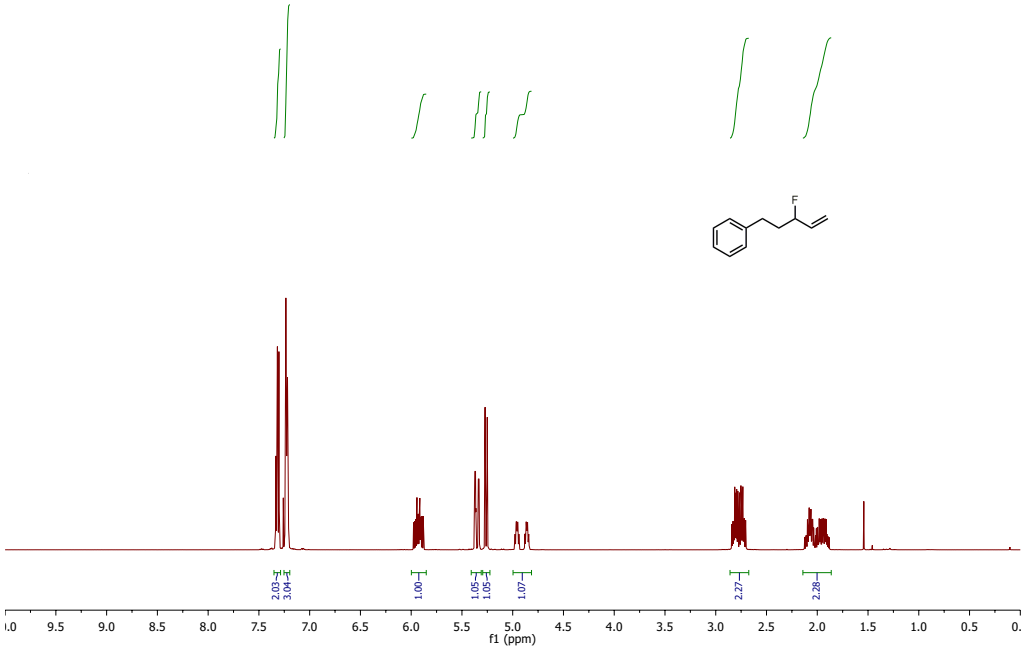

293CARBON01
bc-I-28-C13_1H

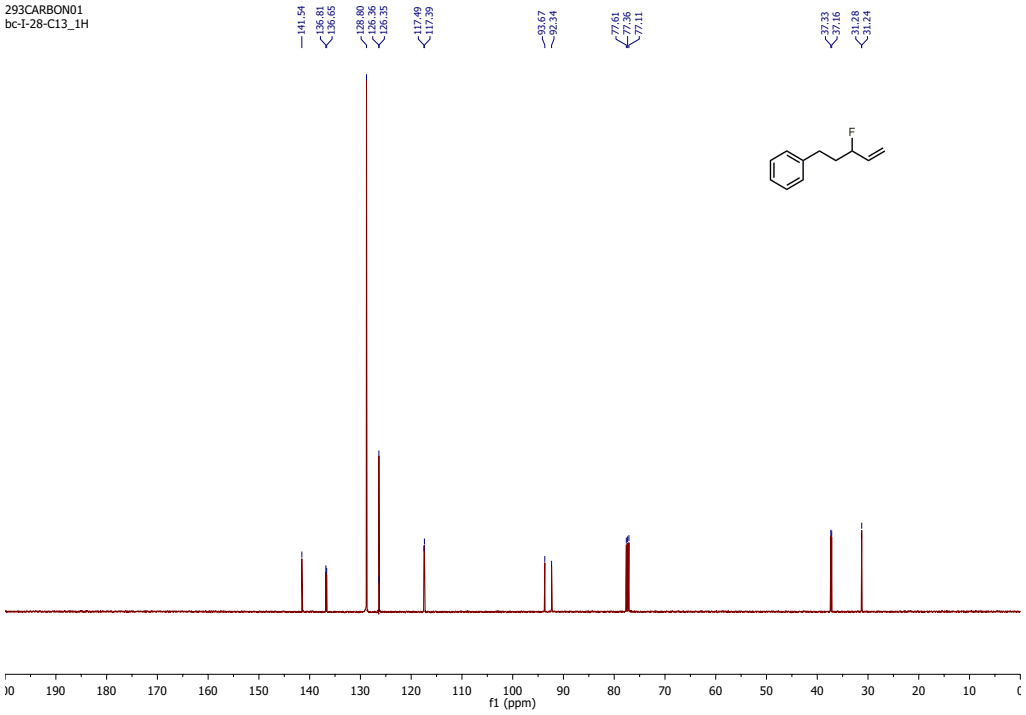

FLUORINE01
CKC0293siena

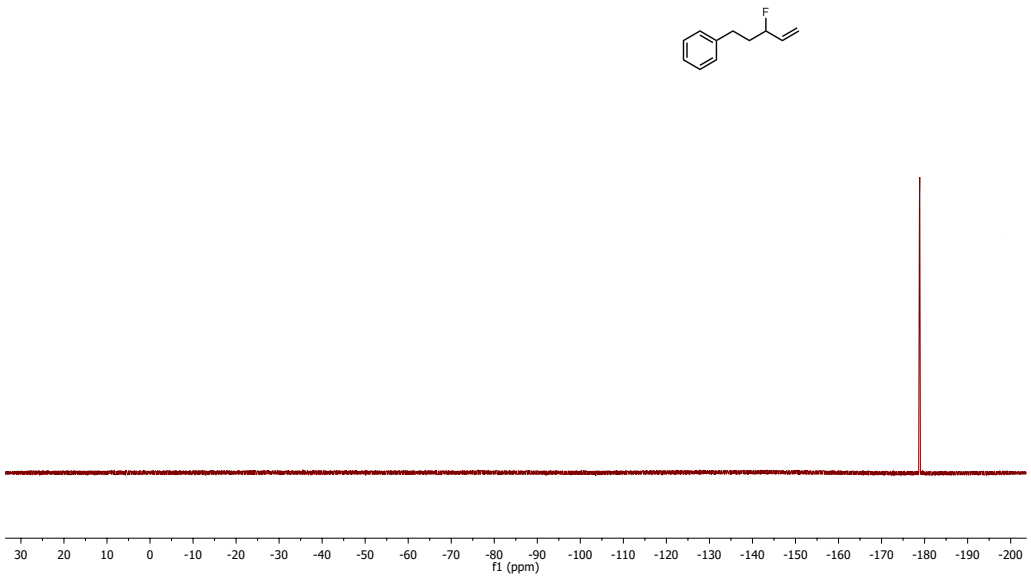

CKC0123SIr
CKC0123SIr

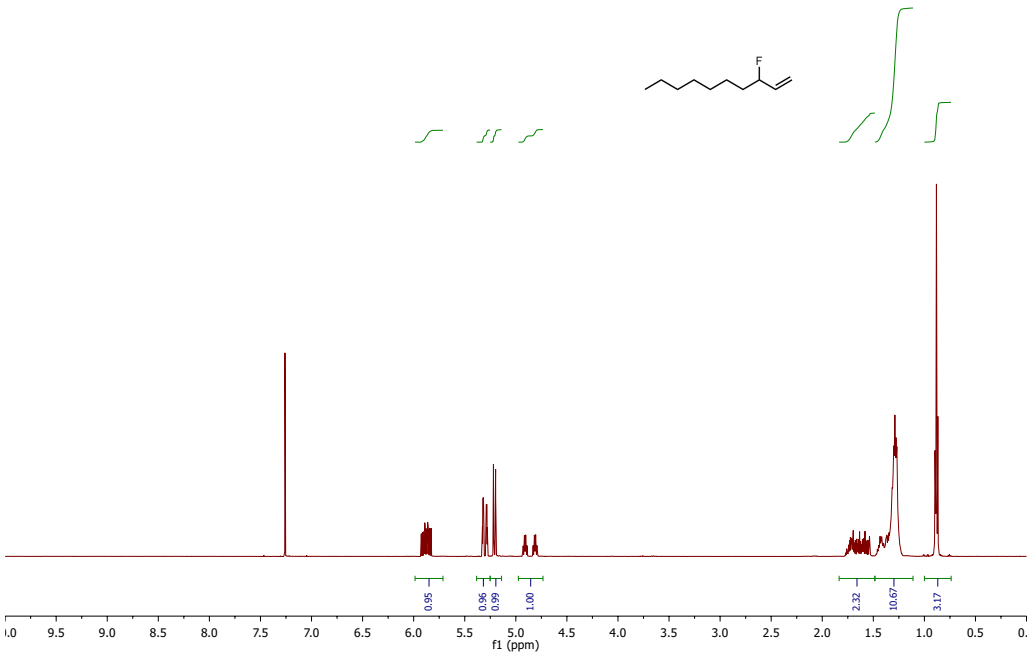

123CARBON01
CKC0123SI

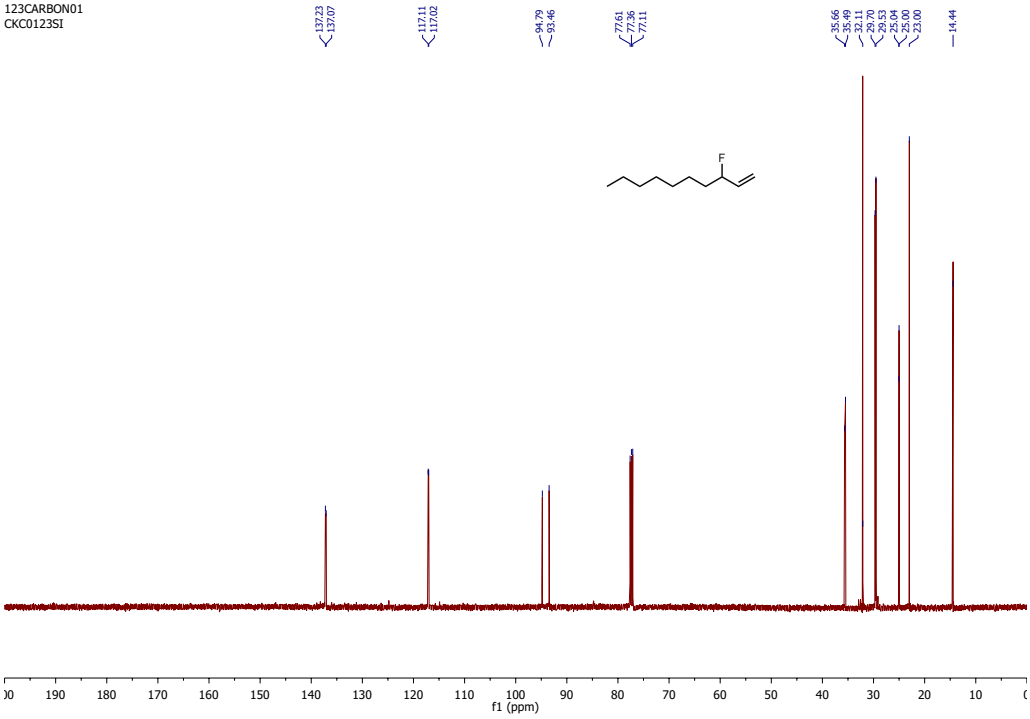

FLUORINE01
CKC0123siena

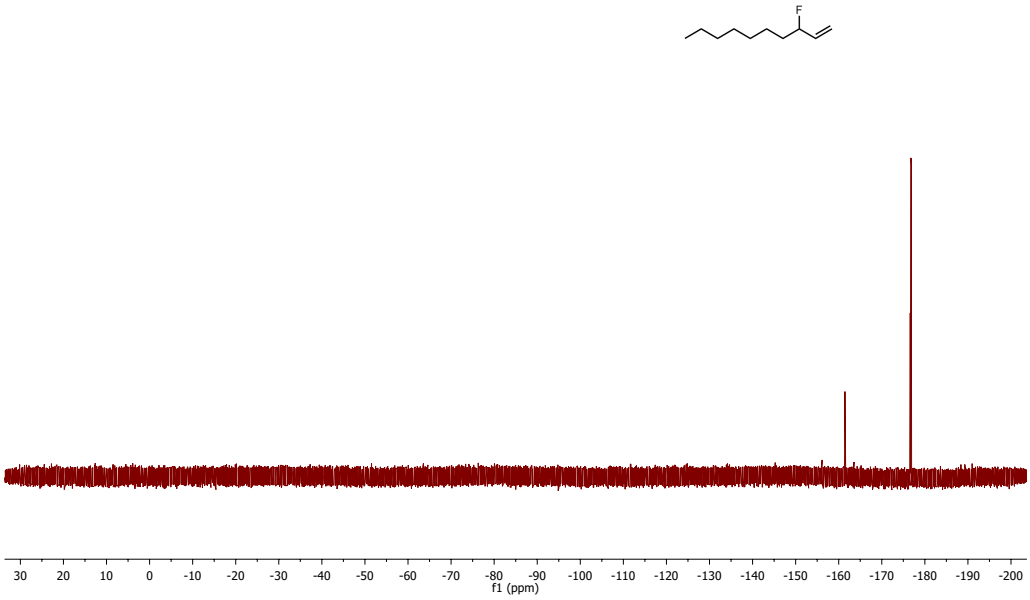

BC-1-47PROTON01
bc-I-47-13C_1H

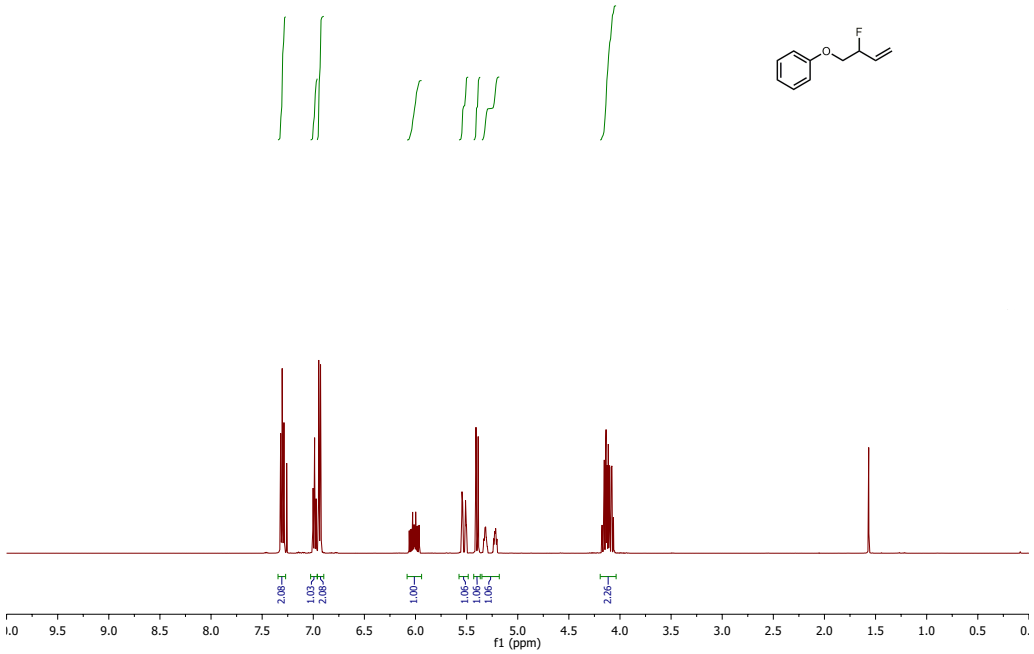

BC-1-47CARBON01
BC-1-47

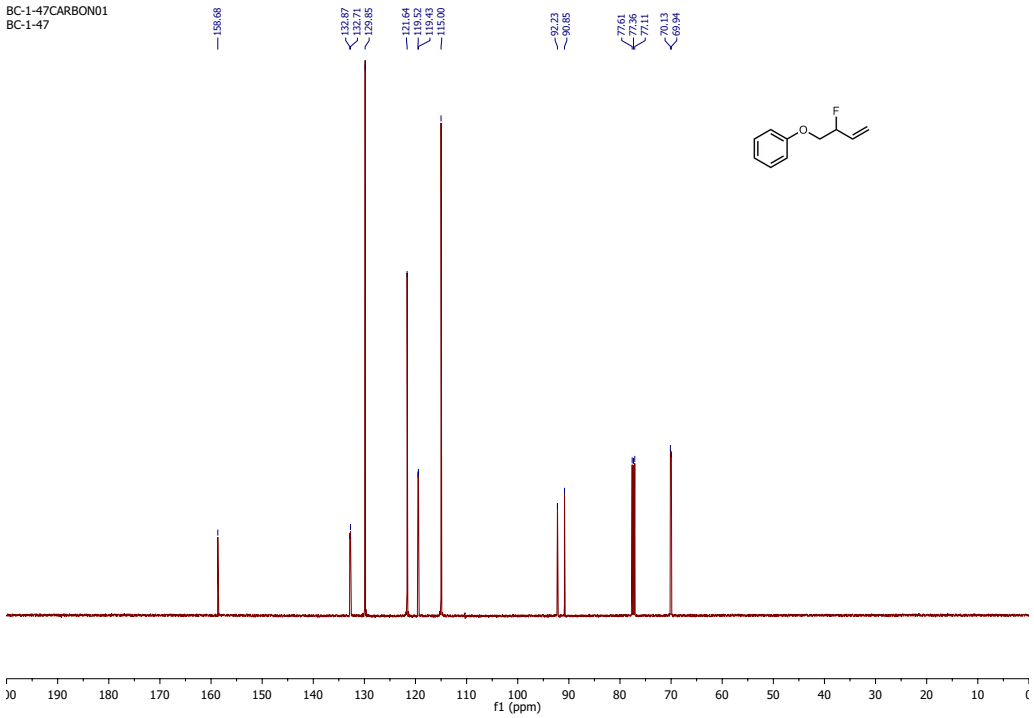

FLUORINE01
BC-1-47siena

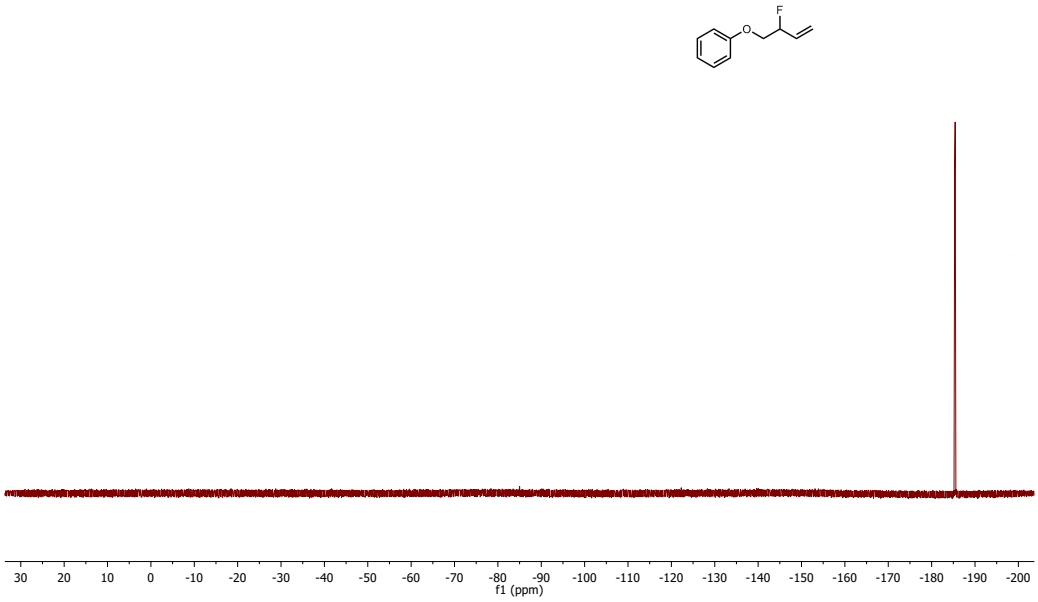

BC-1-46PROTON01
bc-I-46-H1

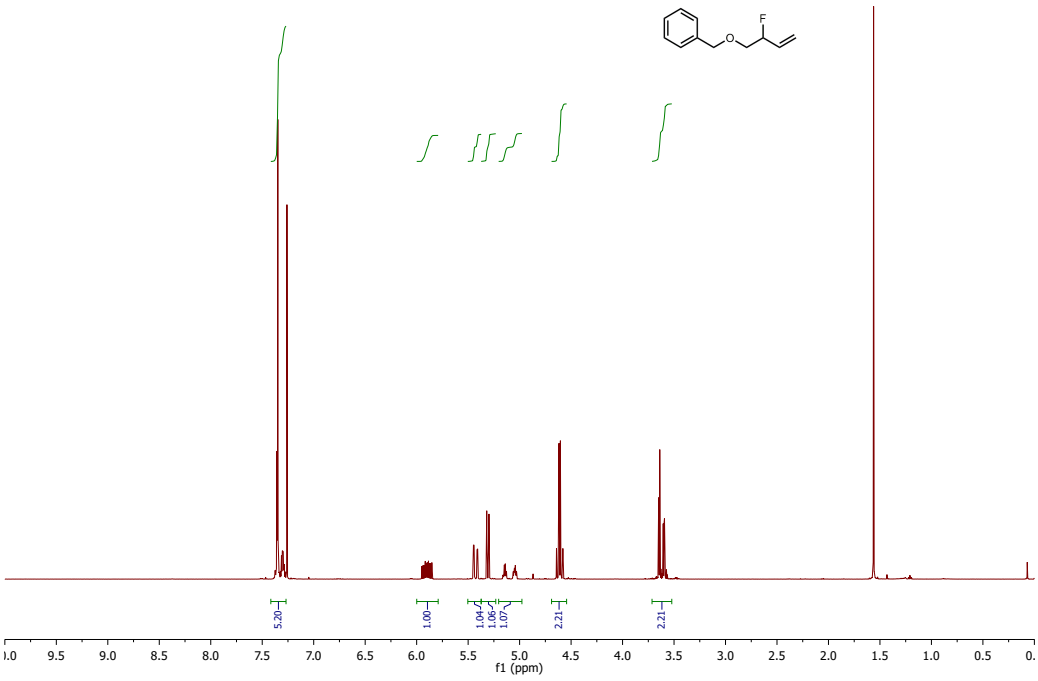

BC-1-46CARBON01
BC-1-46CH

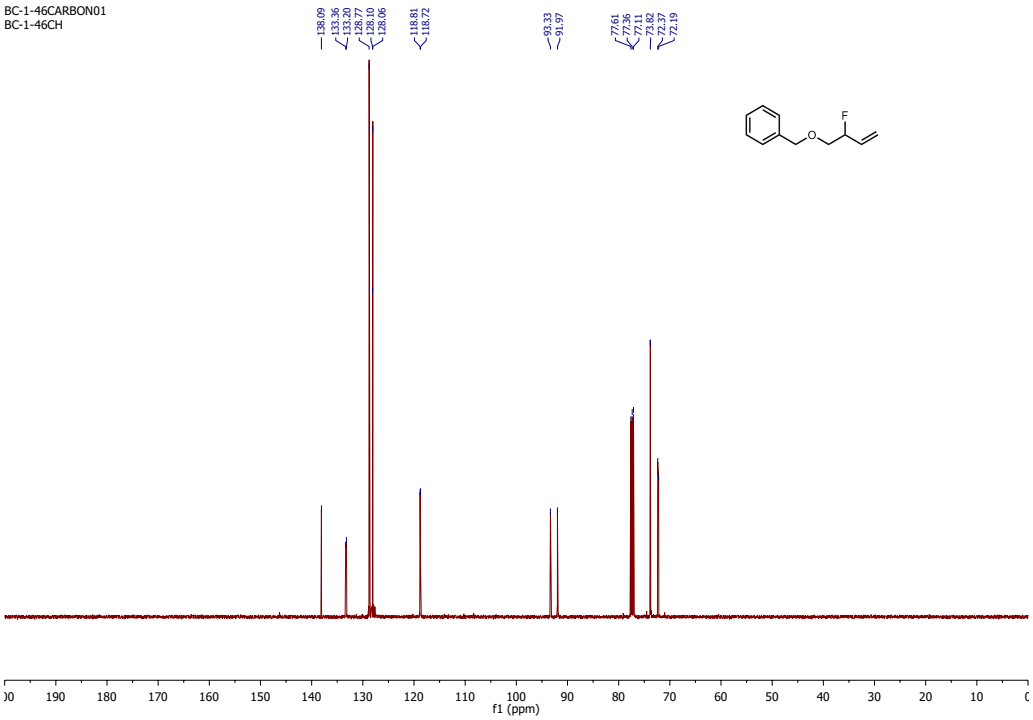

FLUORINE01
BC-1-46siena

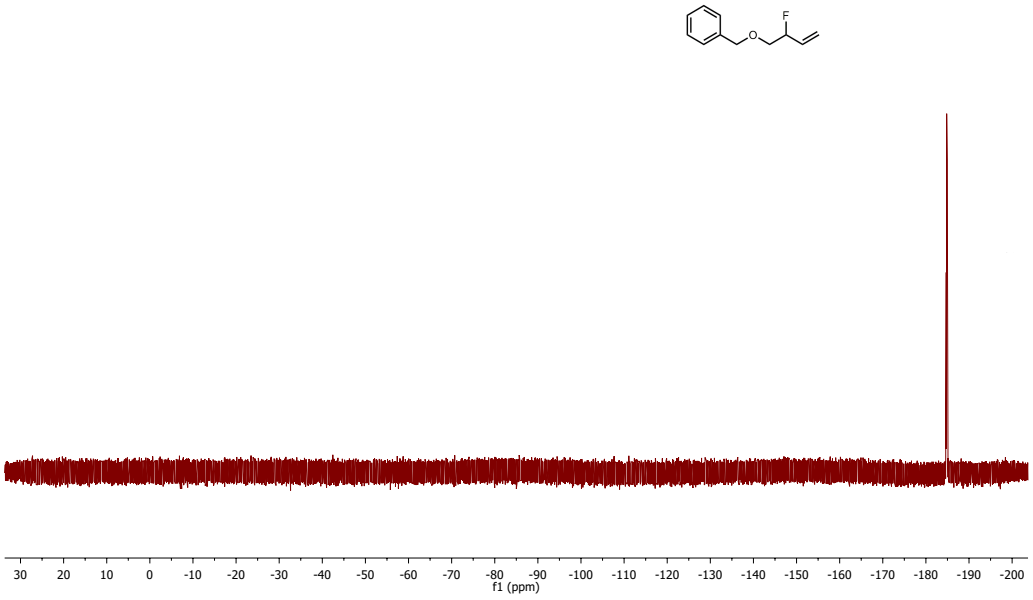

BC-1-29PROTON01
bc-I-29-H1

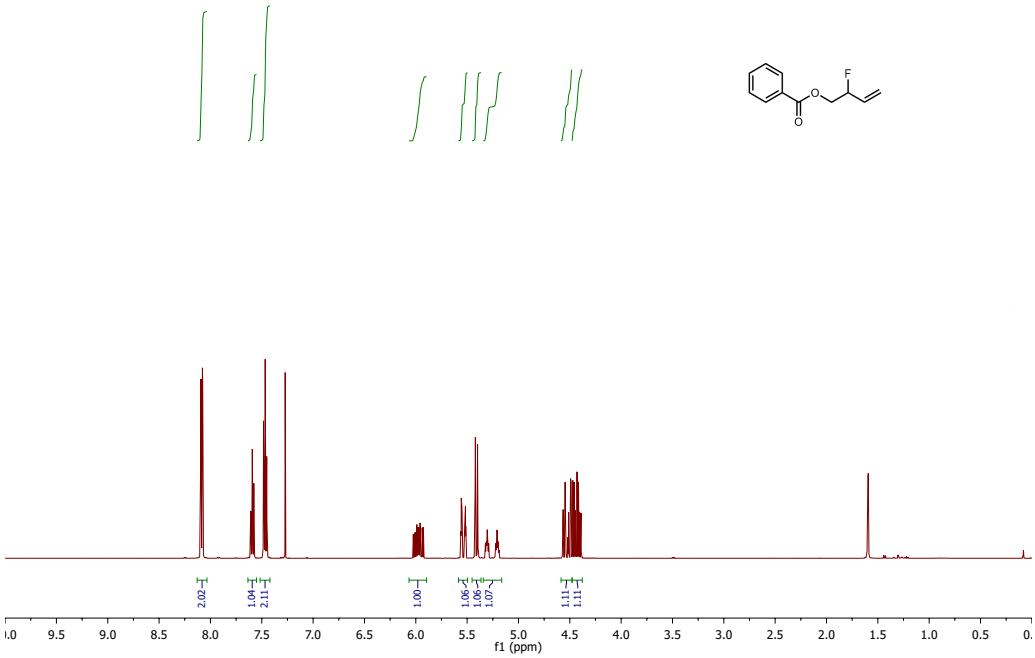

BC-1-29CARBON01
BC-1-29CH

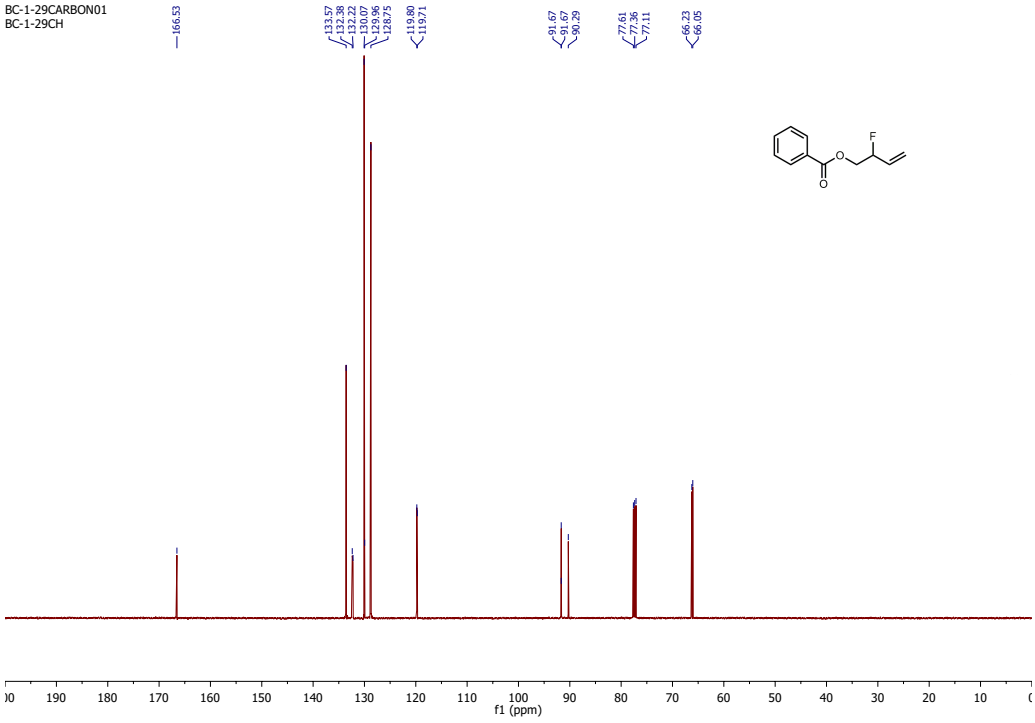

FLUORINE01
BC-1-29siena

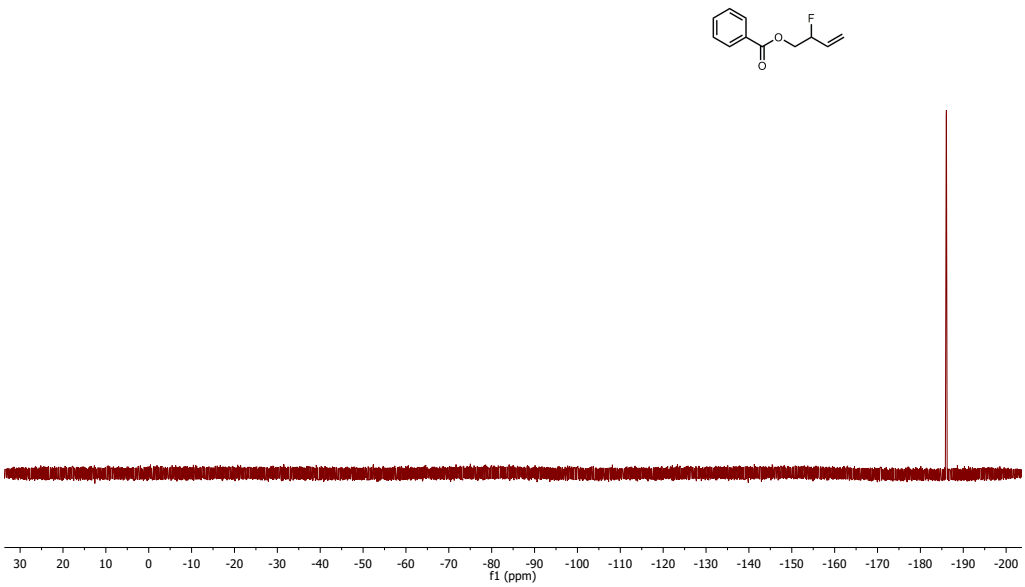

CKC0127-1H-CH.1.fid

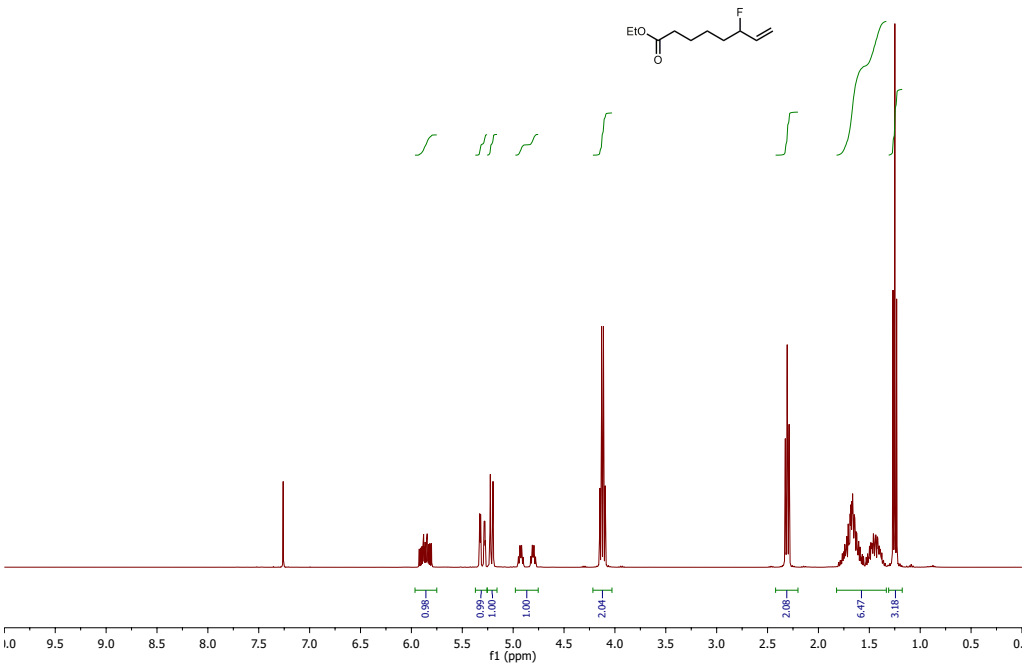

CKC0127-13C-CH.1.fid

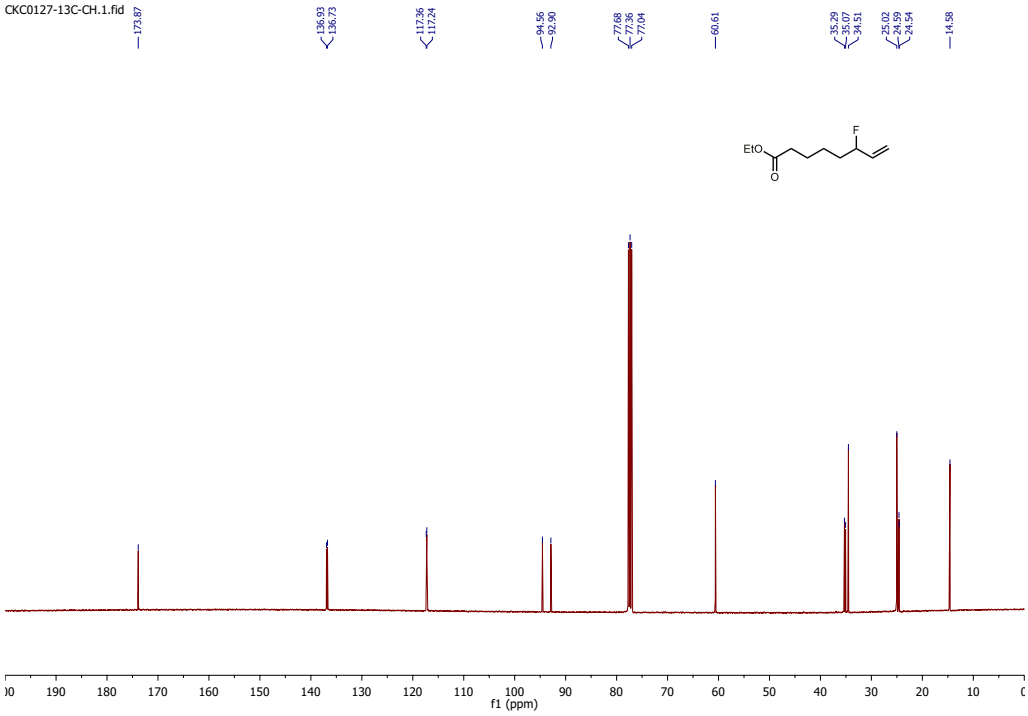

FLUORINE01
BC-1-29siena

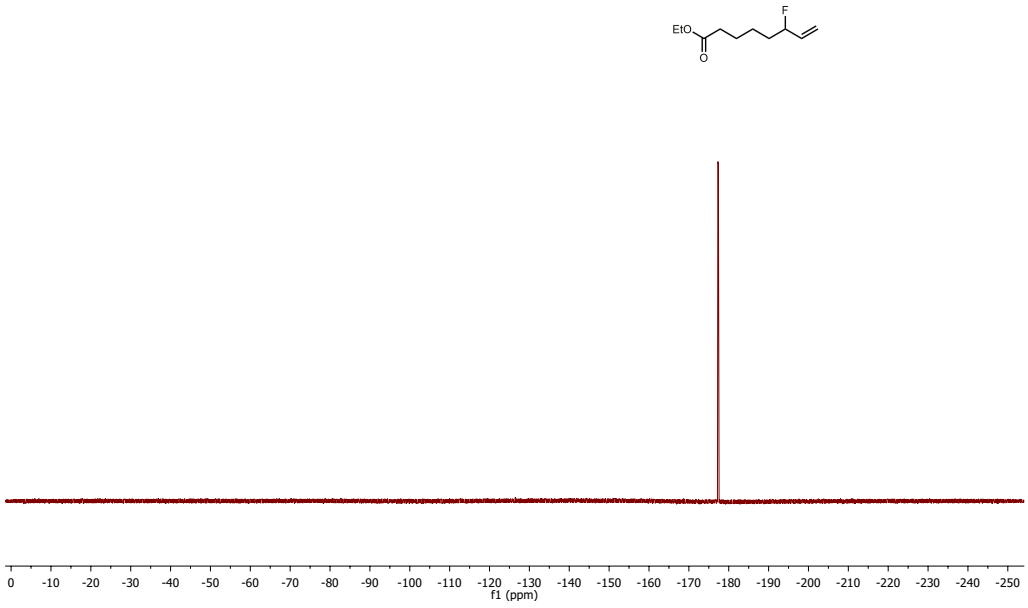

CKC0333PROTON01
CKC0333rota2

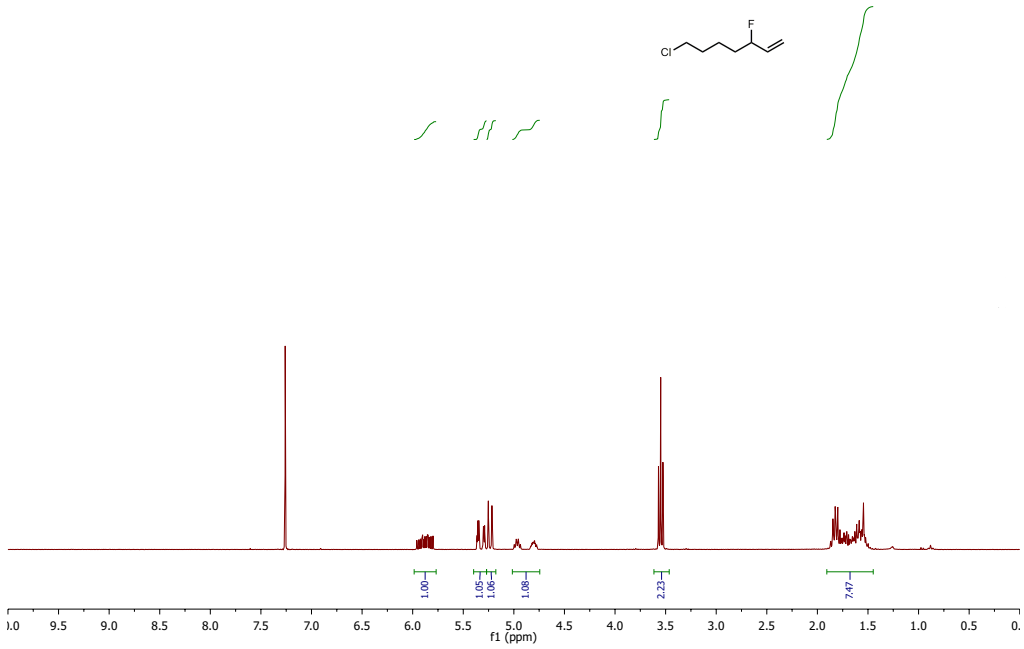

CKC0333CARBON01
CKC0333CH

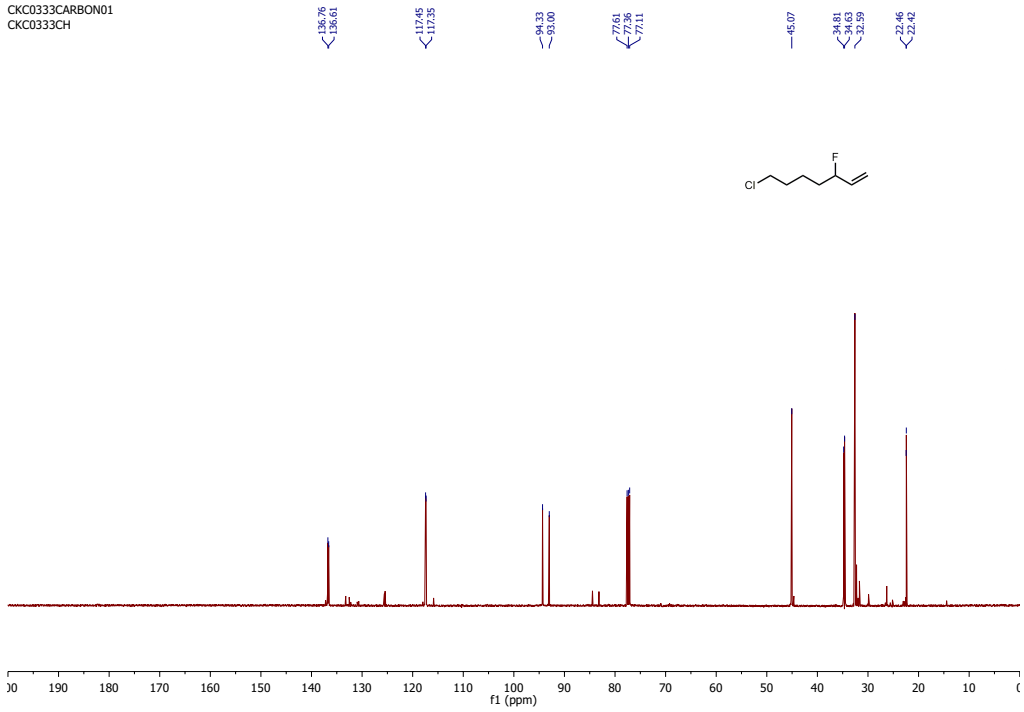

FLUORINE01
CKC0333siena

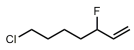

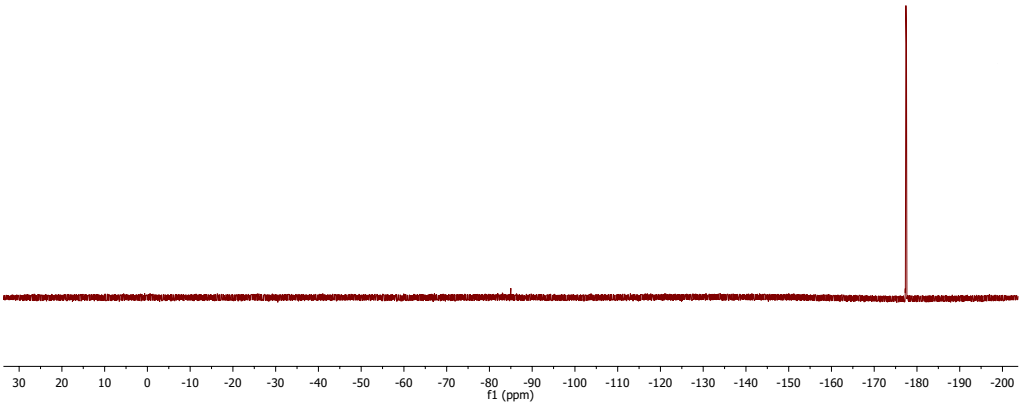

CKC0126PROTON01
CKC0126SIr

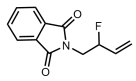

CKC0126CARBON01
CKC0126SI

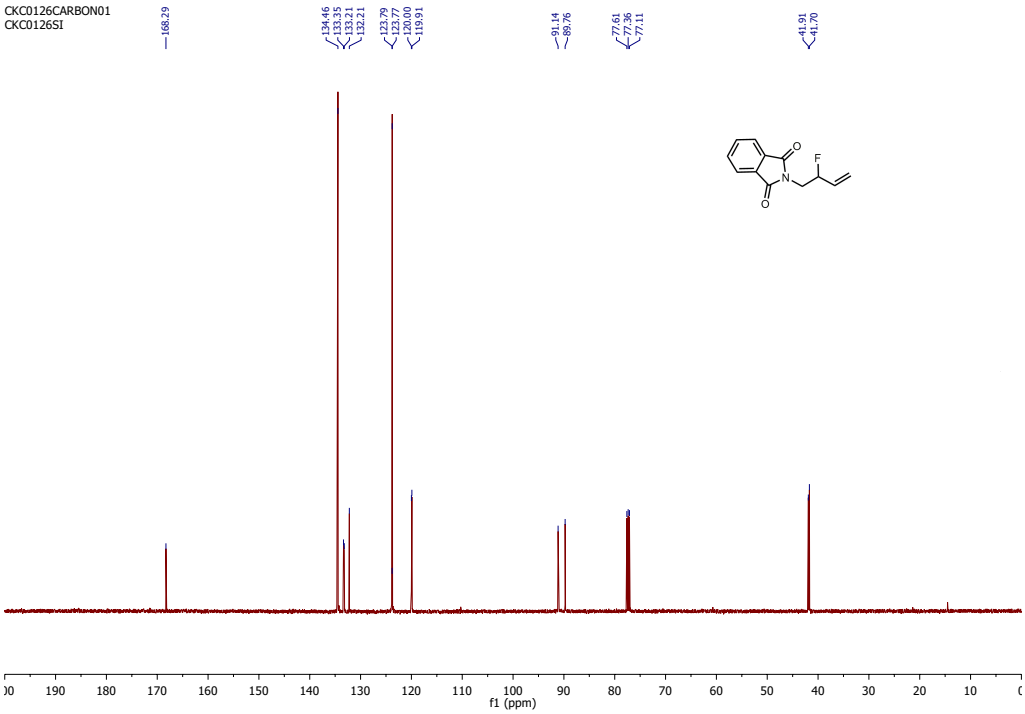

FLUORINE01
CKC0126siena

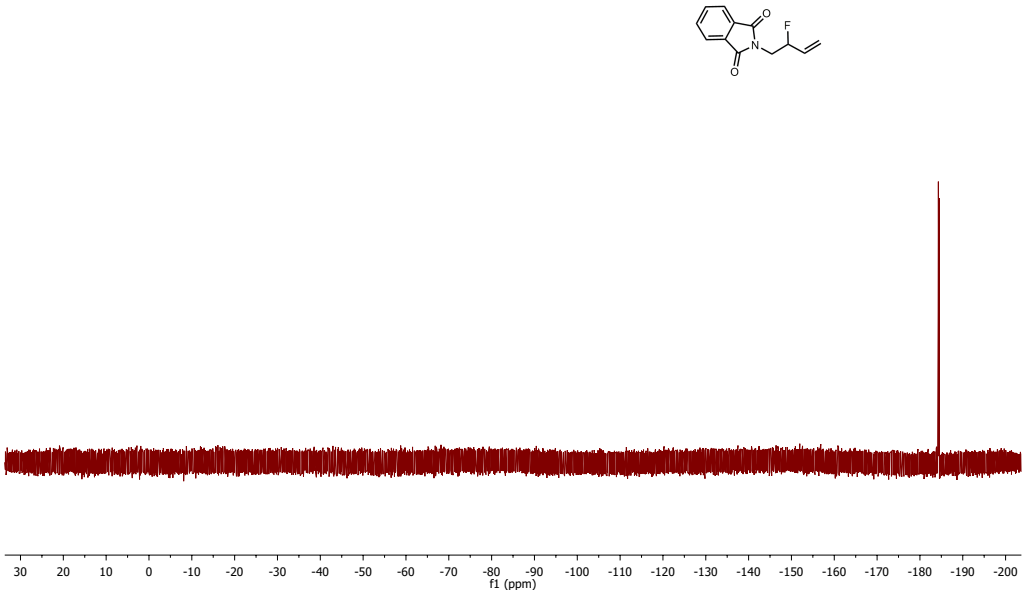

PROTON05
DZ-01-072-2-Purified

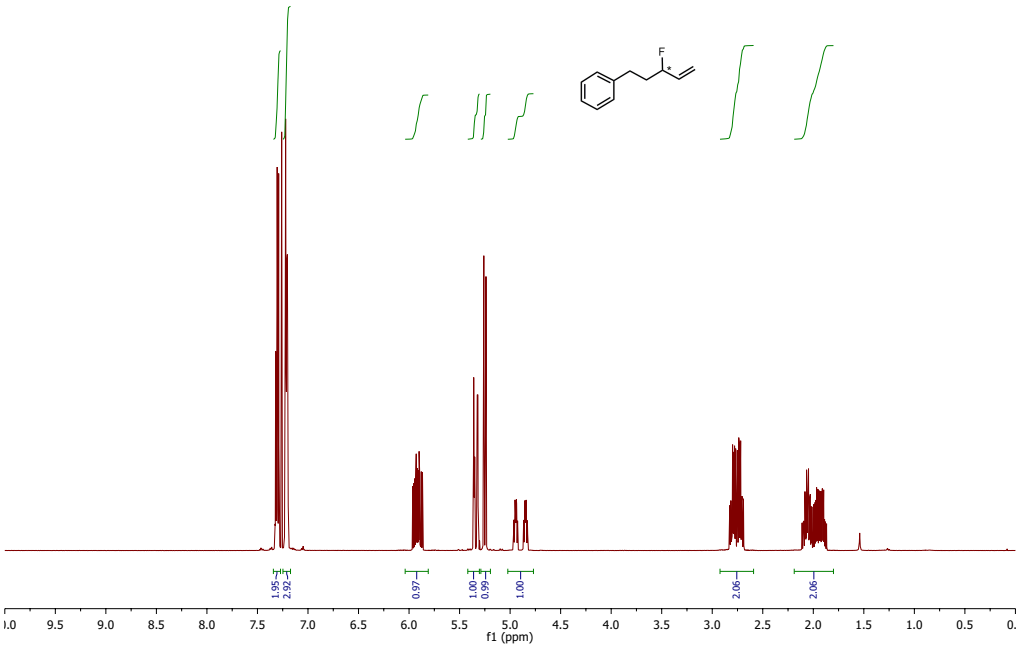

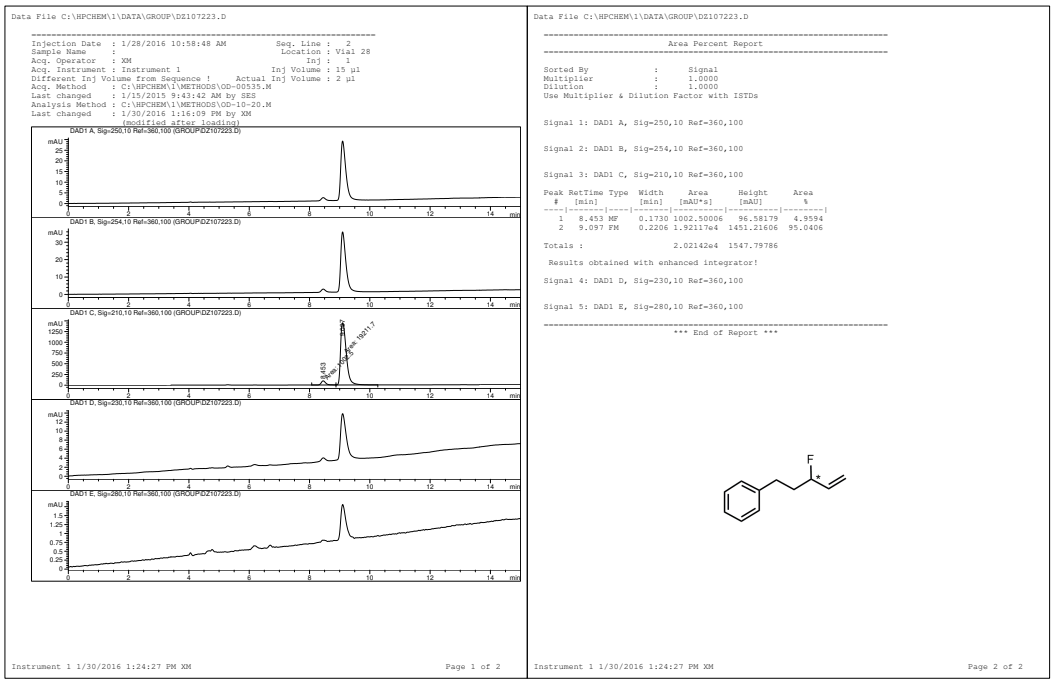

Data File C:\HPCHEM\1\DATA\GROUP\DZ107223.D

Injection Date : 1/28/2016 10:58:48 AM Seq. Line : 2
Sample Name : Location : Vial 28
Acq. Operator : XM Inj : 1
Acq. Instrument : Instrument 1 Inj Volume : 15 µl
Different Inj Volume from Sequence ! Actual Inj Volume : 2 µl
Acq. Method : C:\HPCHEM\1\METHODS\OD-00535.M
Last changed : 1/15/2015 9:43:42 AM by SES
Analysis Method : C:\HPCHEM\1\METHODS\OD-10-20.M
Last changed : 1/30/2016 1:16:09 PM by XM
(modified after loading)

DAD1 A, Sig=250,10 Ref=360,100 (GROUP\DZ107223.D)
DAD1 B, Sig=254,10 Ref=360,100 (GROUP\DZ107223.D)
DAD1 C, Sig=210,10 Ref=360,100 (GROUP\DZ107223.D)
8.453 MF 0.1730 1002.50006
9.097 FM 0.2206 1.92117e4
DAD1 D, Sig=230,10 Ref=360,100 (GROUP\DZ107223.D)
DAD1 E, Sig=280,10 Ref=360,100 (GROUP\DZ107223.D)

Instrument 1 1/30/2016 1:24:27 PM XM Page 1 of 2

Data File C:\HPCHEM\1\DATA\GROUP\DZ107223.D

Area Percent Report

Sorted By : Signal
Multiplier : 1.0000
Dilution : 1.0000
Use Multiplier & Dilution Factor with ISTDs

Signal 1: DAD1 A, Sig=250,10 Ref=360,100

Signal 2: DAD1 B, Sig=254,10 Ref=360,100

Signal 3: DAD1 C, Sig=210,10 Ref=360,100

Peak #	RetTime [min]	Type	Width [min]	Area [mAU*s]	Height [mAU]	Area %
1	8.453	MF	0.1730	1002.50006	96.58179	4.9594
2	9.097	FM	0.2206	1.92117e4	1451.21606	95.0406

Totals : 2.02142e4 1547.79786

Results obtained with enhanced integrator!

Signal 4: DAD1 D, Sig=230,10 Ref=360,100

Signal 5: DAD1 E, Sig=280,10 Ref=360,100

*** End of Report ***

Instrument 1 1/30/2016 1:24:27 PM XM Page 2 of 2

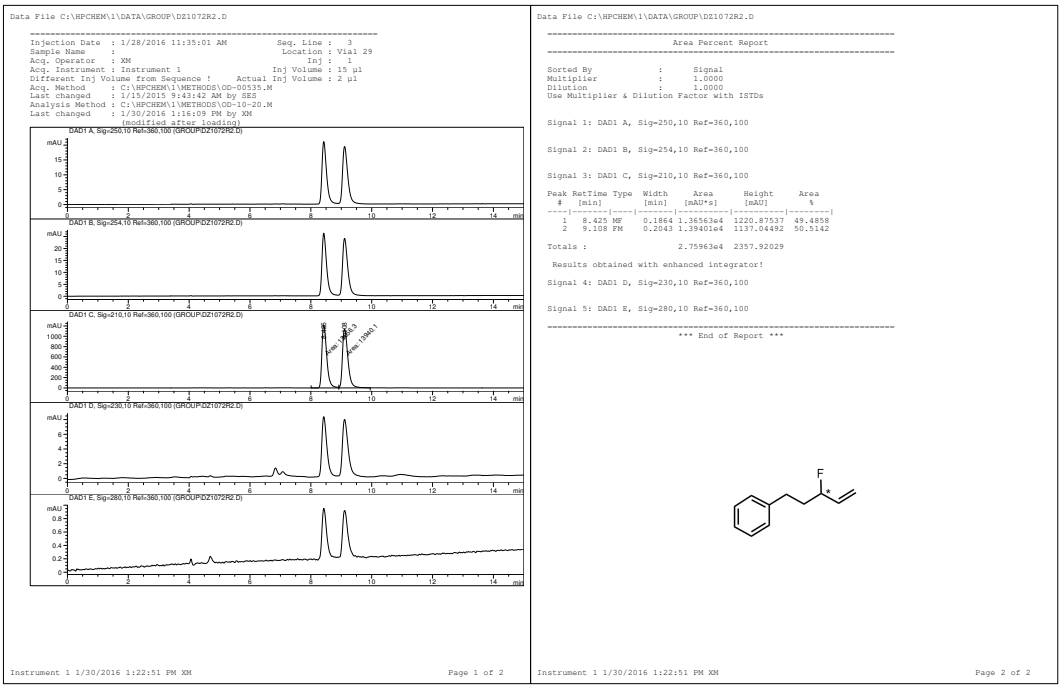

Data File C:\HPCHEM\1\DATA\GROUP\DZ1072R2.D

Injection Date : 1/28/2016 11:35:01 AM Seq. Line : 3
Sample Name : Location : Vial 29
Acq. Operator : XM Inj : 1
Acq. Instrument : Instrument 1 Inj Volume : 15 µl
Different Inj Volume from Sequence ! Actual Inj Volume : 2 µl
Acq. Method : C:\HPCHEM\1\METHODS\OD-00535.M
Last changed : 1/15/2015 9:43:42 AM by SES
Analysis Method : C:\HPCHEM\1\METHODS\OD-10-20.M
Last changed : 1/30/2016 1:16:09 PM by XM
(modified after loading)

DAD1 A, Sig=250,10 Ref=360,100 (GROUP\DZ1072R2.D)
DAD1 B, Sig=254,10 Ref=360,100 (GROUP\DZ1072R2.D)
DAD1 C, Sig=210,10 Ref=360,100 (GROUP\DZ1072R2.D)
Area: 13563.9
Area: 13940.1
DAD1 D, Sig=230,10 Ref=360,100 (GROUP\DZ1072R2.D)
DAD1 E, Sig=280,10 Ref=360,100 (GROUP\DZ1072R2.D)

Instrument 1 1/30/2016 1:22:51 PM XM Page 1 of 2

Data File C:\HPCHEM\1\DATA\GROUP\DZ1072R2.D

Area Percent Report

Sorted By : Signal
Multiplier : 1.0000
Dilution : 1.0000
Use Multiplier & Dilution Factor with ISTDs

Signal 1: DAD1 A, Sig=250,10 Ref=360,100

Signal 2: DAD1 B, Sig=254,10 Ref=360,100

Signal 3: DAD1 C, Sig=210,10 Ref=360,100

Peak #	RetTime [min]	Type	Width [min]	Area [mAU*s]	Height [mAU]	Area %
1	8.425	MF	0.1864	1.36563e4	1220.87537	49.4858
2	9.108	FM	0.2043	1.39401e4	1137.04492	50.5142

Totals : 2.75963e4 2357.92029

Results obtained with enhanced integrator!

Signal 4: DAD1 D, Sig=230,10 Ref=360,100

Signal 5: DAD1 E, Sig=280,10 Ref=360,100

*** End of Report ***

Instrument 1 1/30/2016 1:22:51 PM XM Page 2 of 2

270PROTON01
CKC0270CH-proton

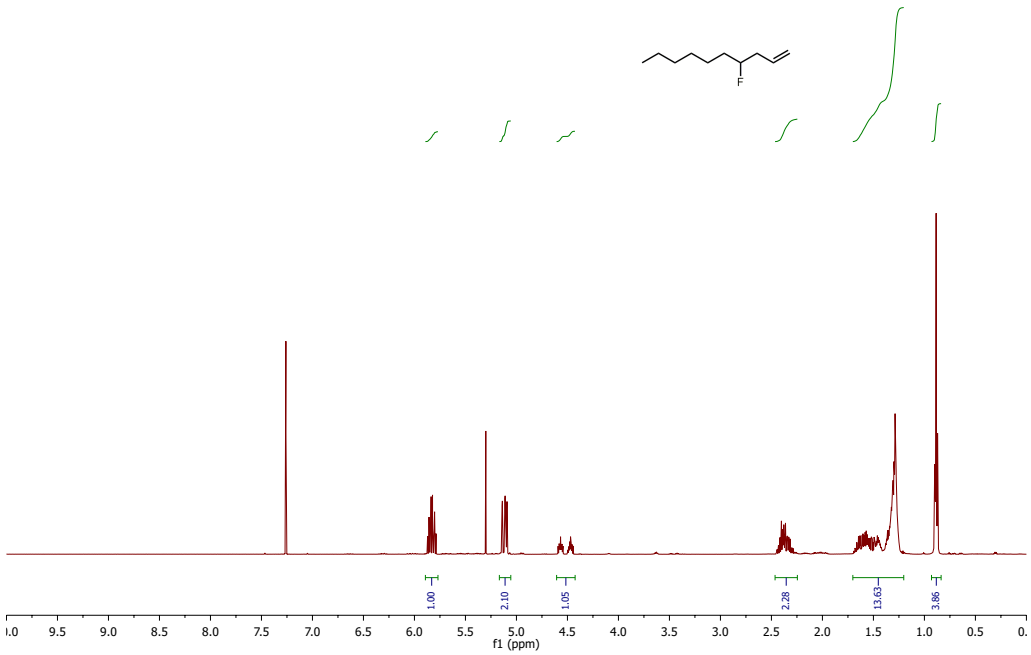

270CARBON01
CKC0270CH-carbon

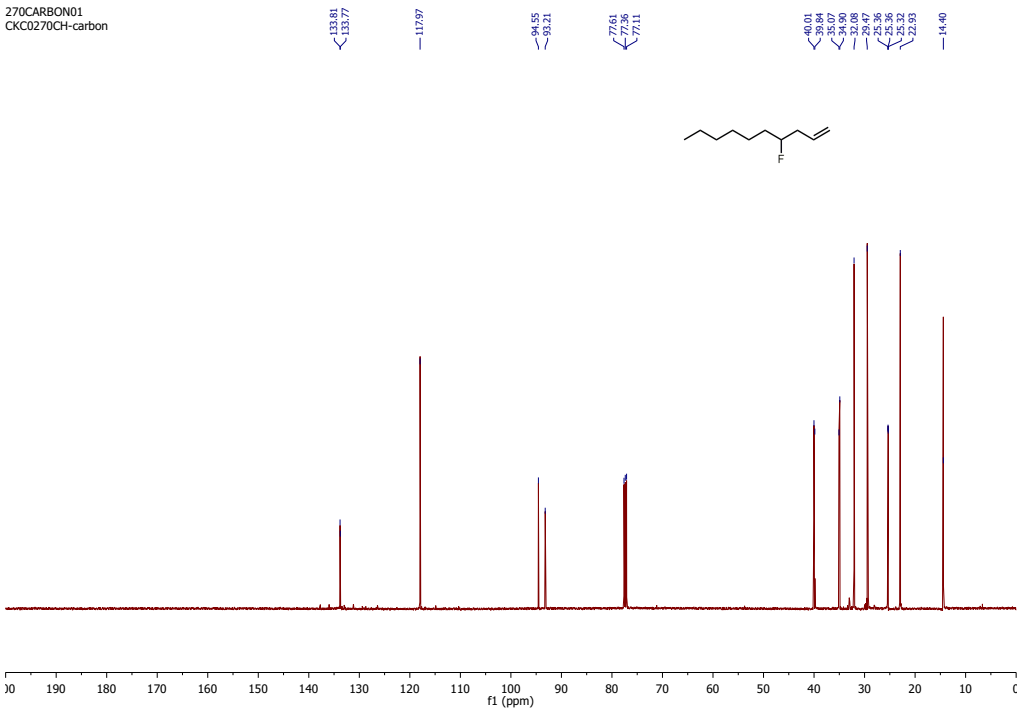

FLUORINE01
CKC0270sienaNo2

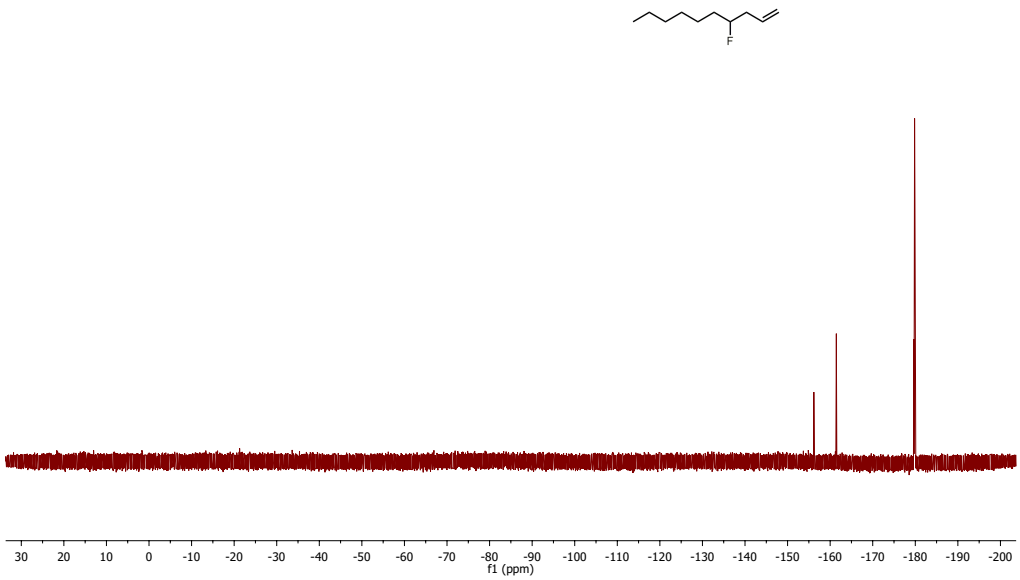

CKC0268nosolvent
CKC0268-7-8-15

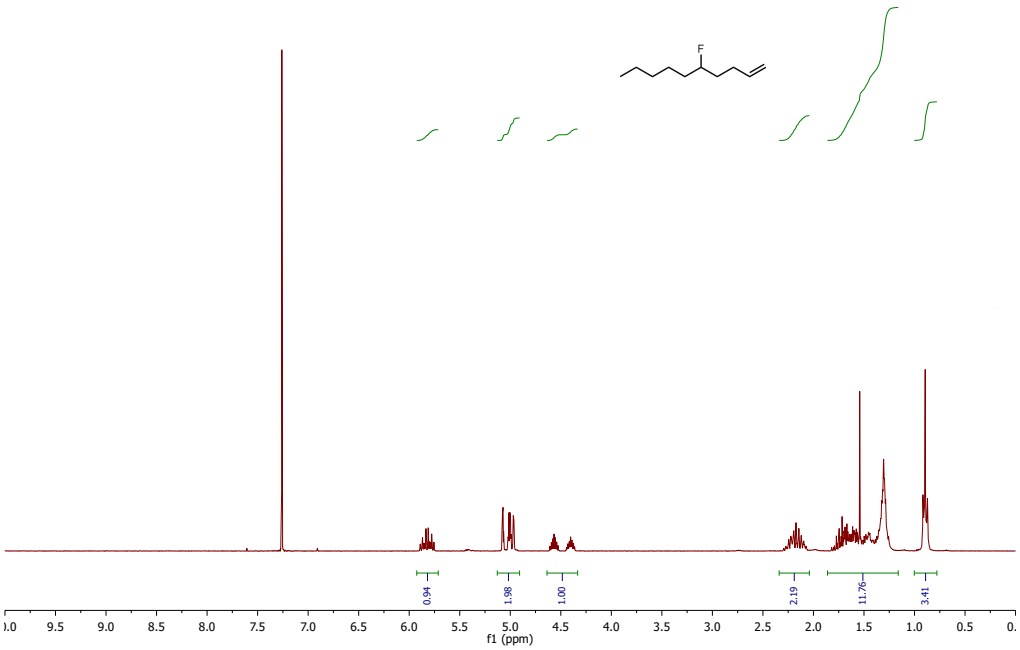

CKC0268CARBON01
CKC0268CH

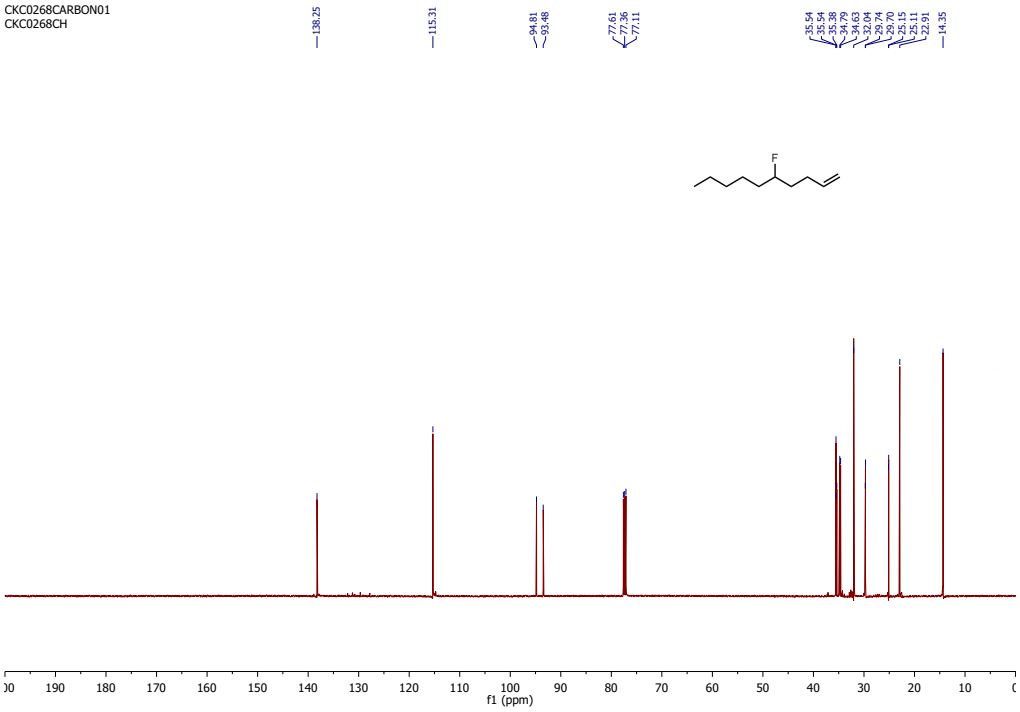

FLUORINE01
CKC0268siena

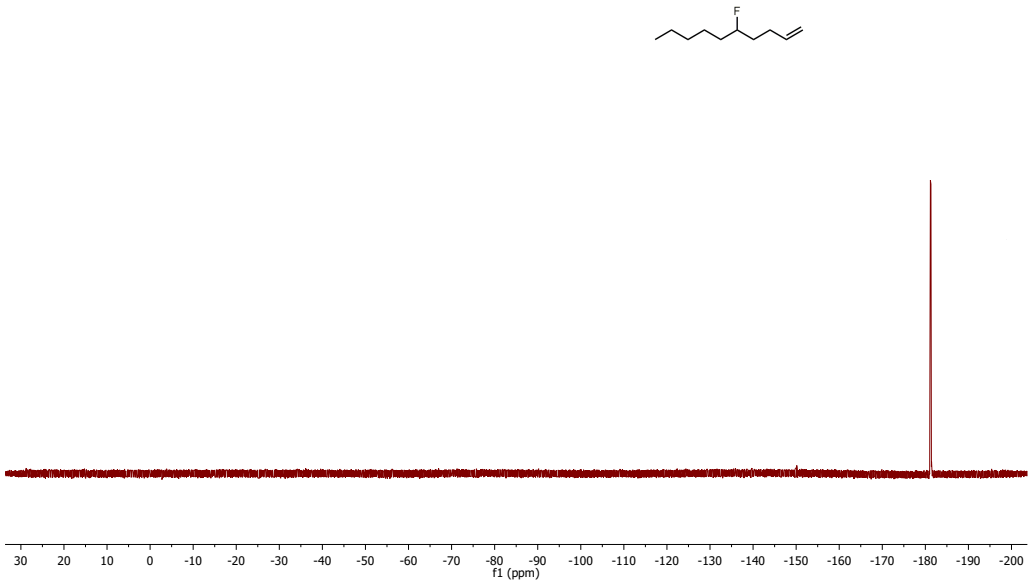

PROTON03
DZ-01-062-1-Purified

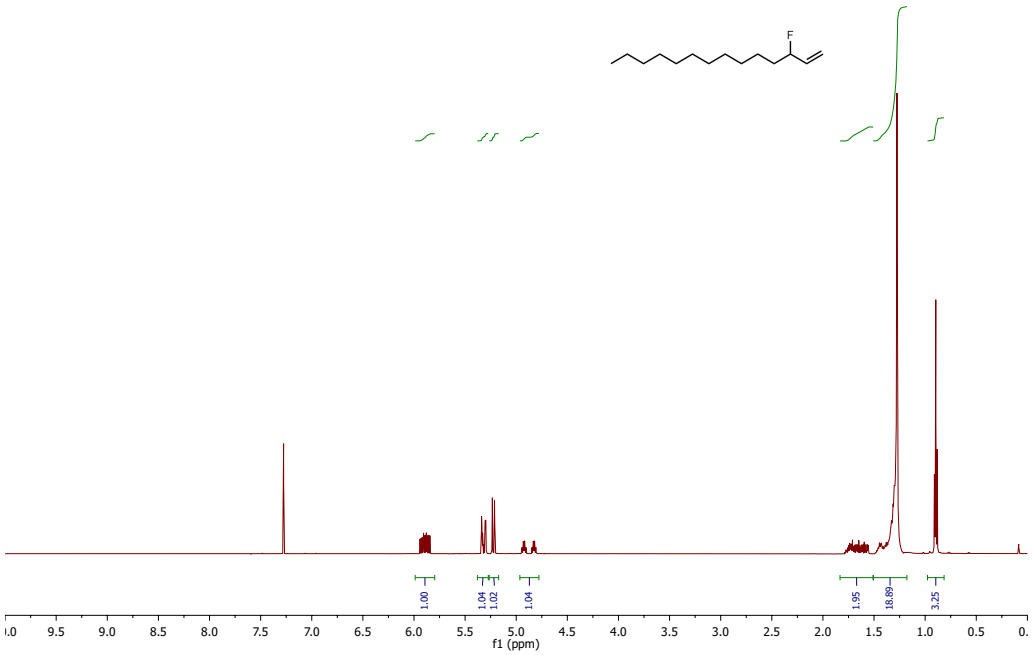

CARBON02
DZ-01-062-1-Purified

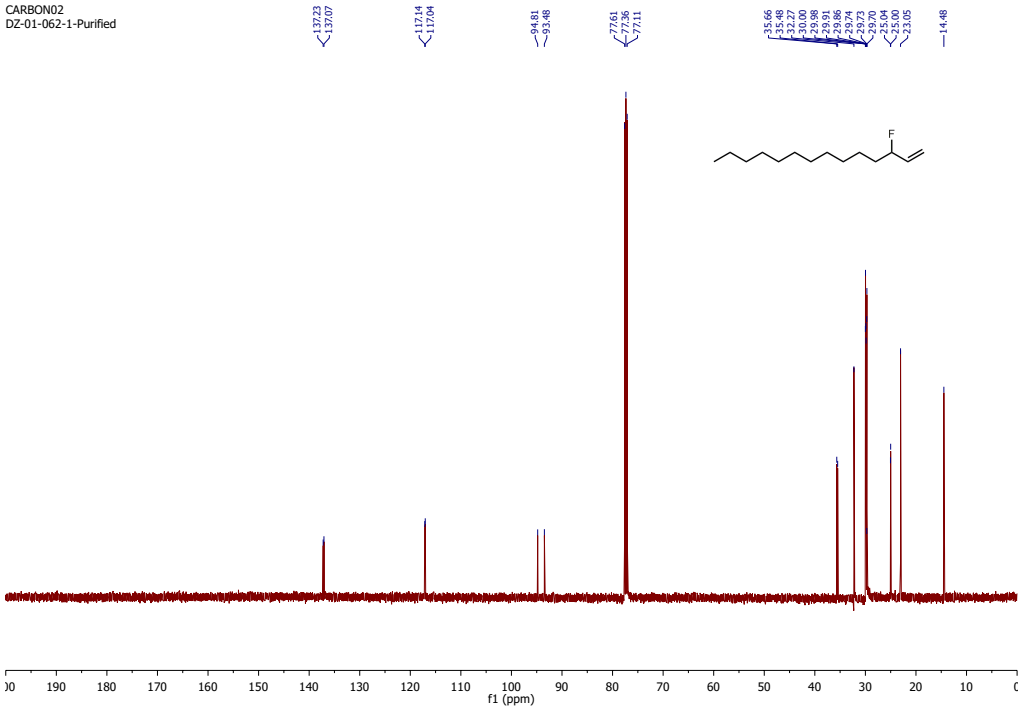

FLUORINE01
BC-1-29siena

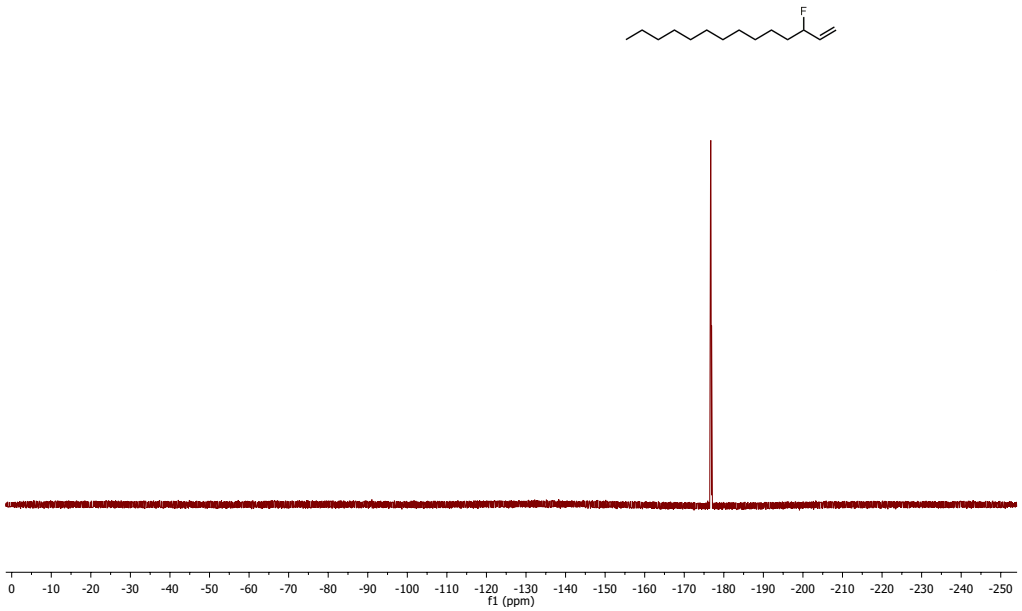

BC-1-60PROTON01
bc-I-60-pure_13C_1H

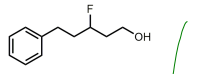

(Table 1, Entry 1)

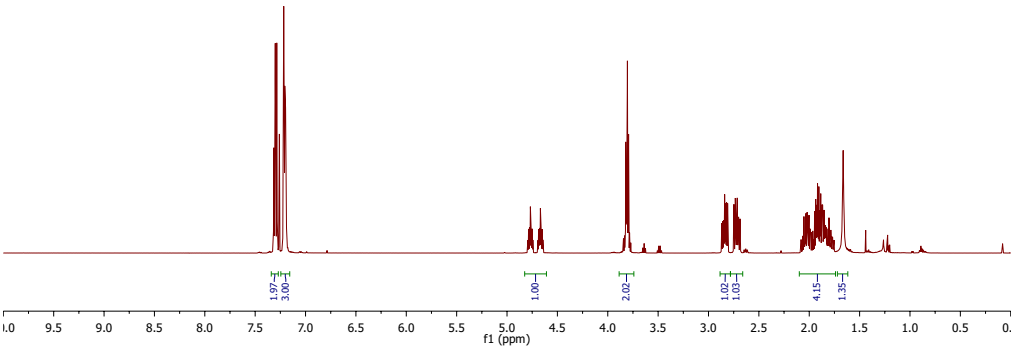

BC-1-60CARBON01
bc-I-60-pure_13C_1H

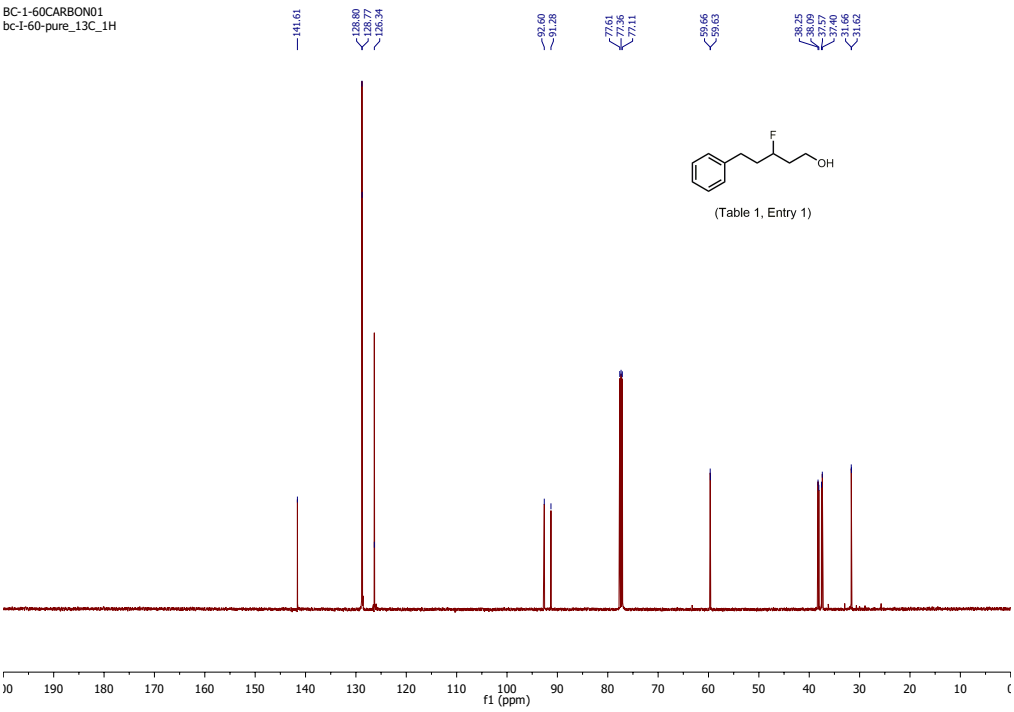

(Table 1, Entry 1)

FLUORINE01
CKC0064siena

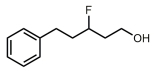

(Table 1, Entry 1)

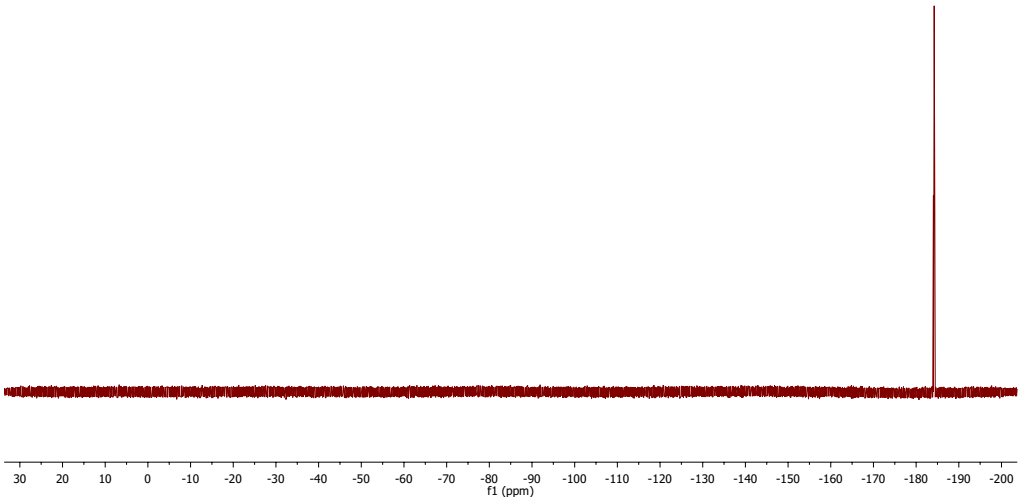

CKC0128PROTON01
CKC0128hivac

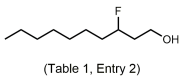

(Table 1, Entry 2)

CKC0128CARBON01
CKC0128CH

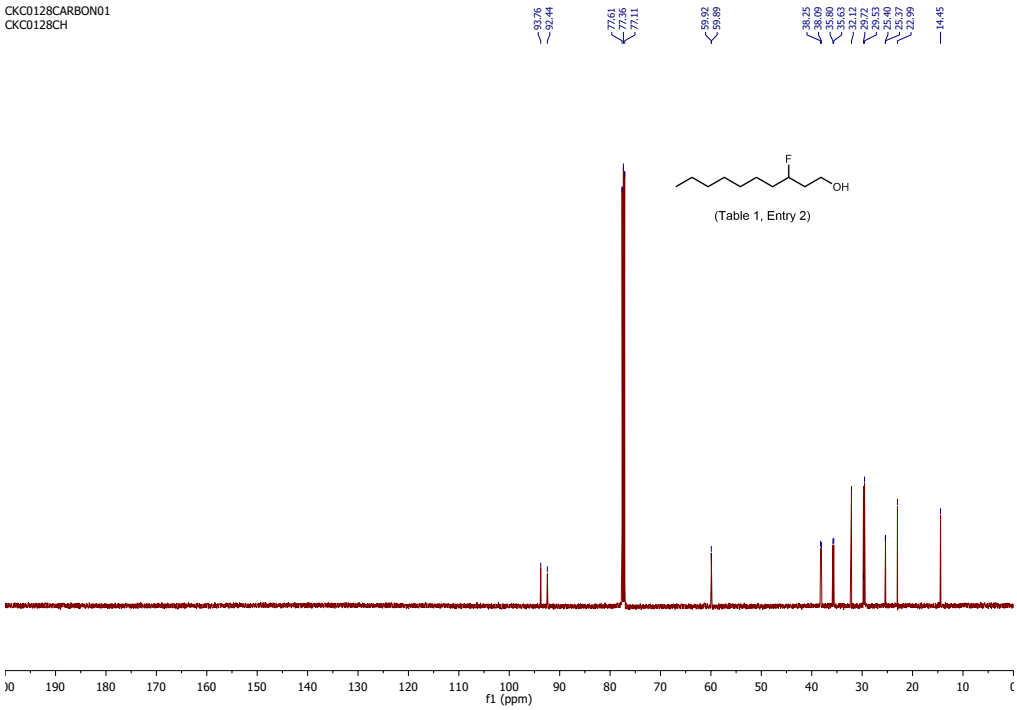

FLUORINE01
CKC0128siena

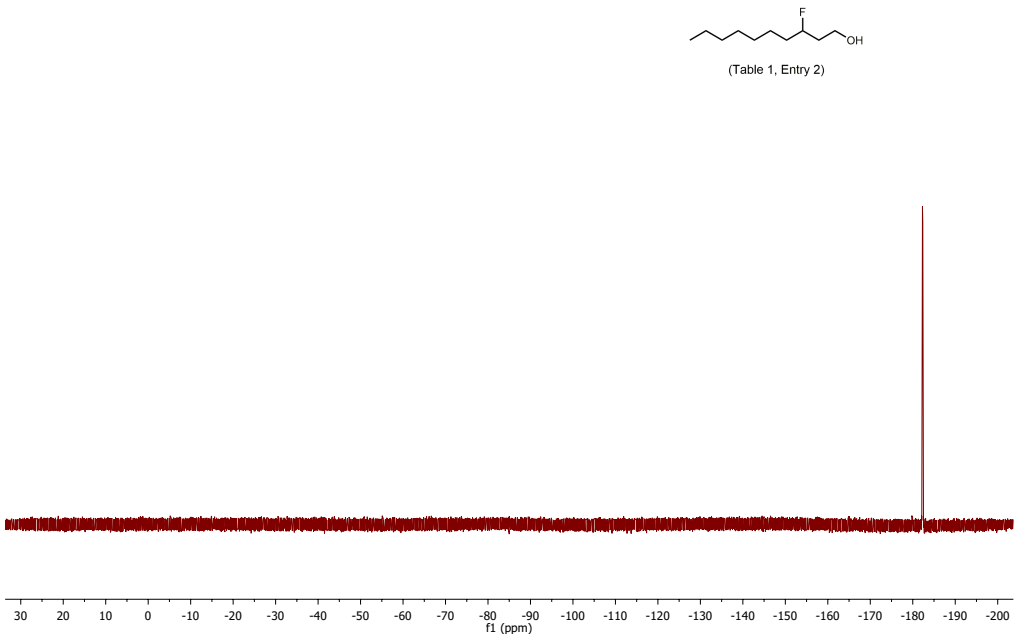

BC-1-61PROTON01
bc-I-61-13C_1H

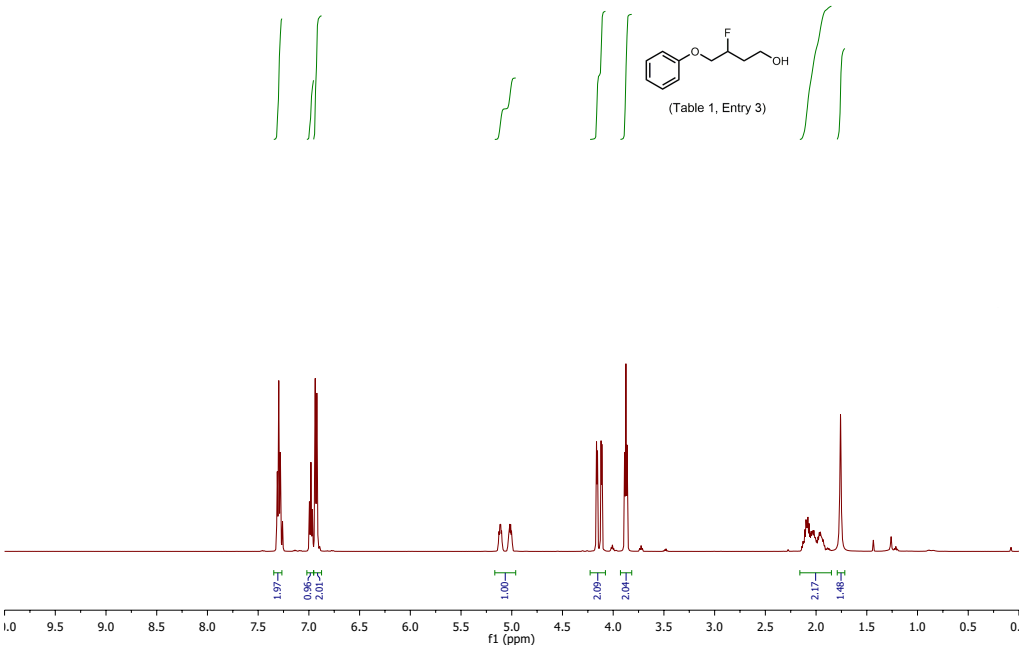

BC-1-61CARBON01
bc-I-61-13C_1H

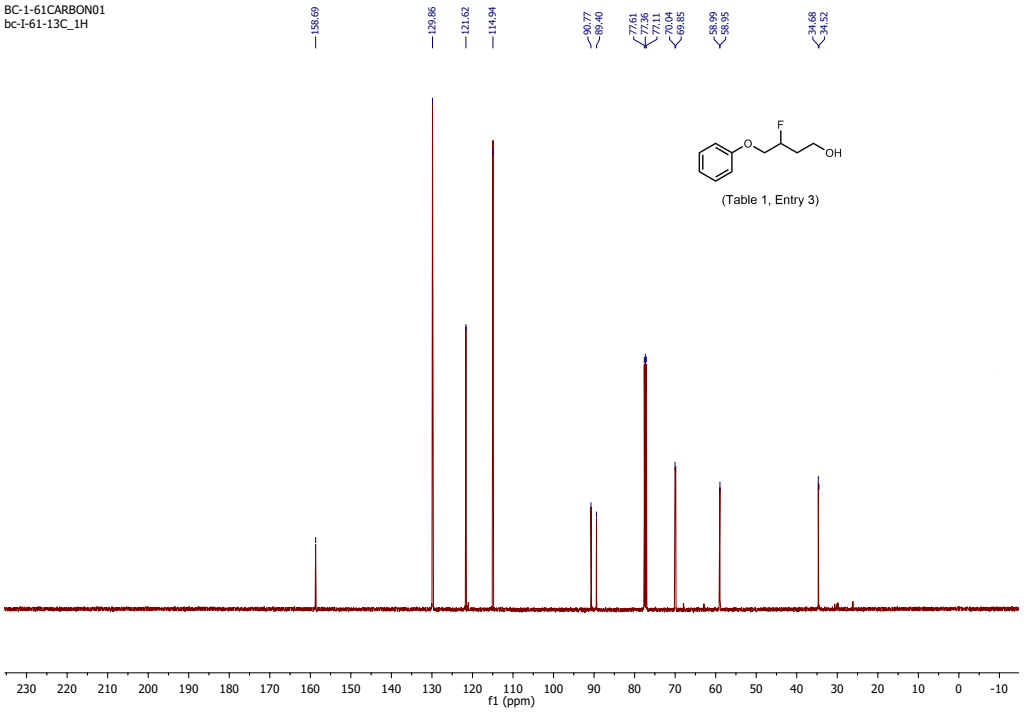

FLUORINE01
CKC0103siena

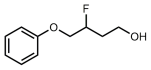

(Table 1, Entry 3)

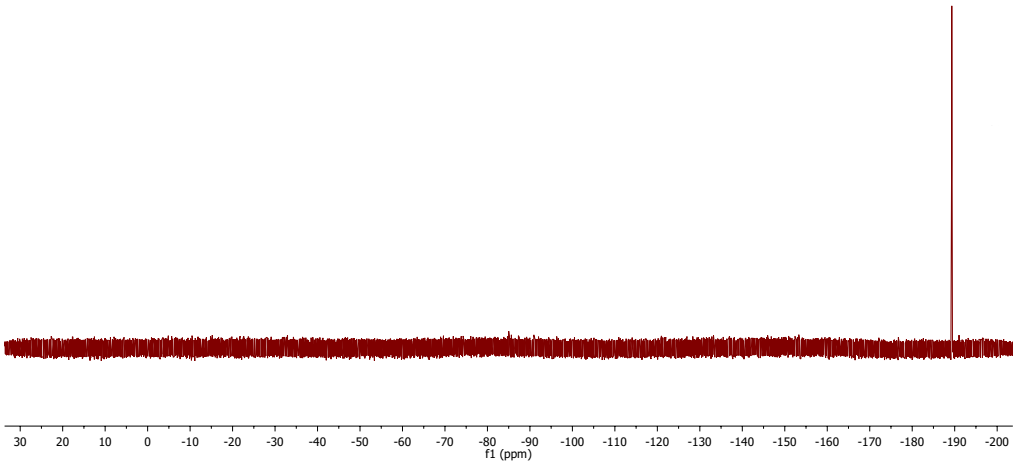

CKC0109CH-protonRE
CKC0109CH-protonRE

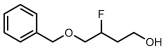

(Table 1, Entry 4)

109CARBON01
CKC0109SI

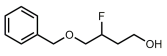

(Table 1, Entry 4)

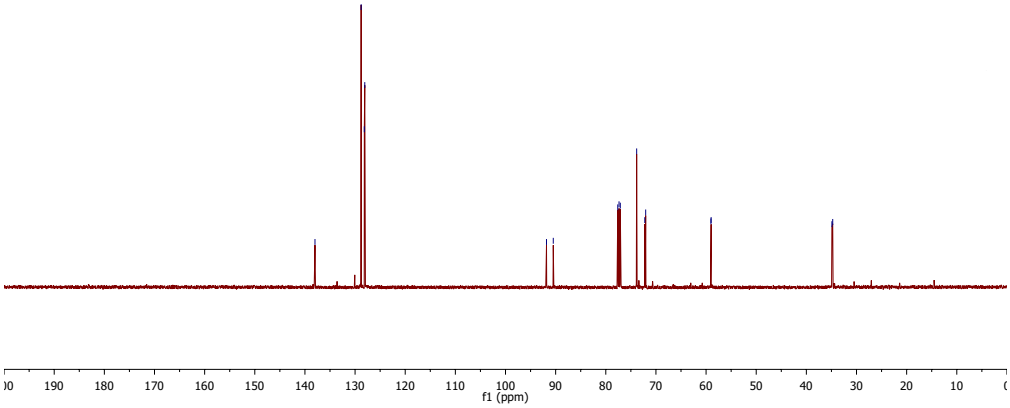

FLUORINE01
CKC0109siena

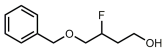

(Table 1, Entry 4)

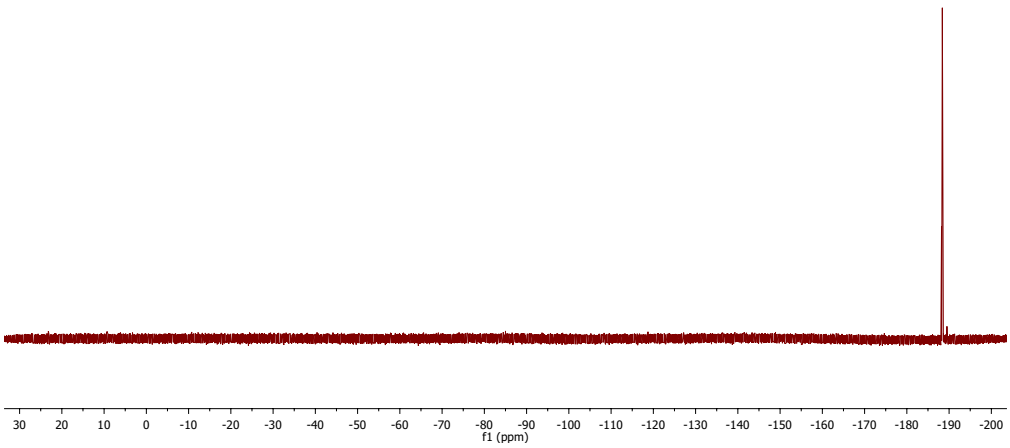

108PROTON01
CKC0108CH-proton

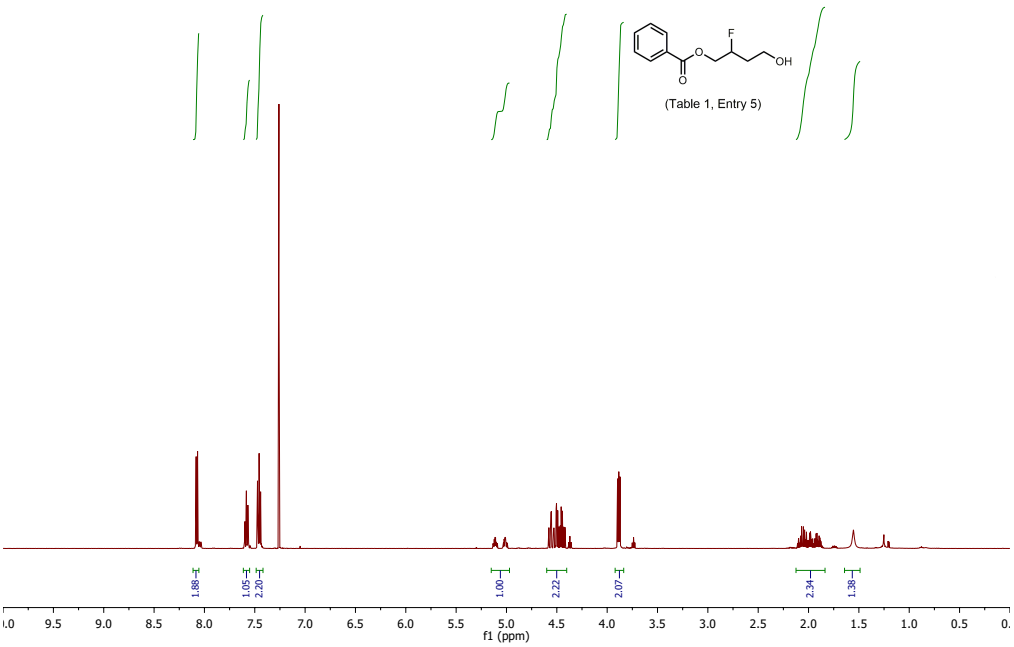

108CARBON01
CKC0108SI

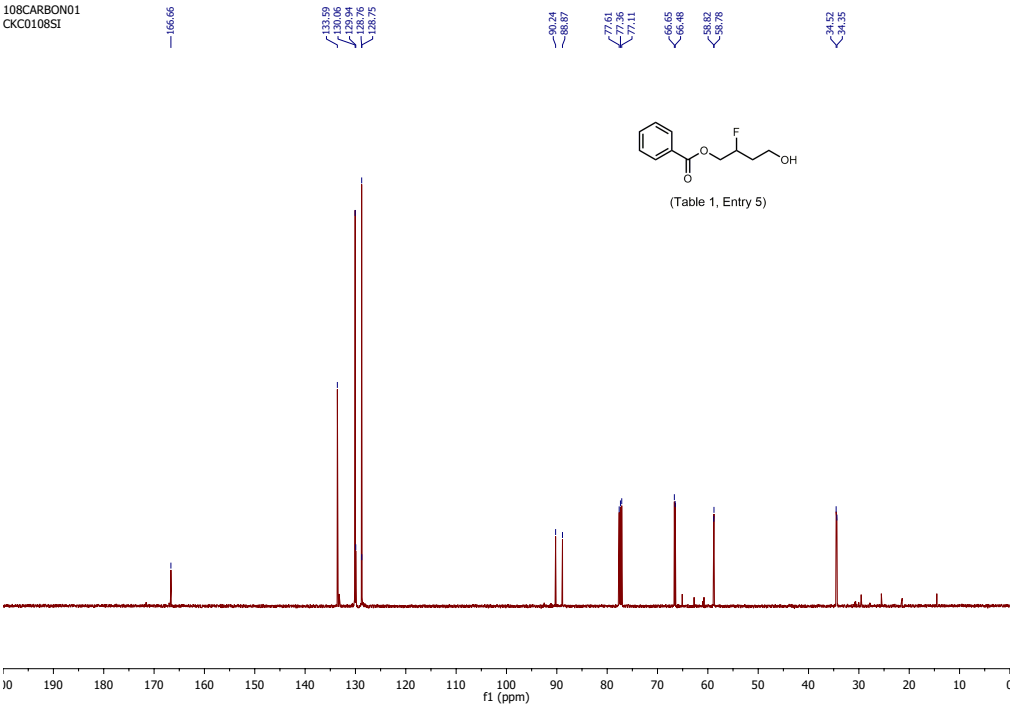

FLUORINE01
CKC0108siena

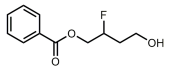

(Table 1, Entry 5)

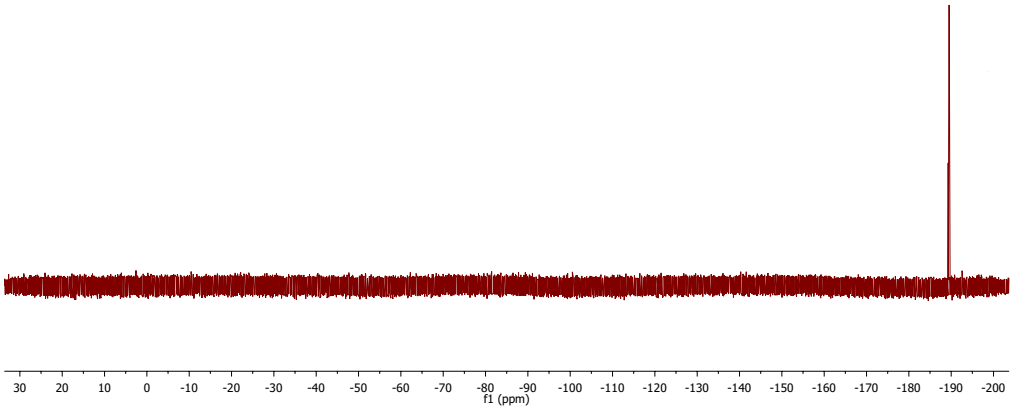

CKC0154PROTON01
CKC0154hivac

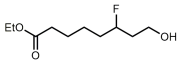

(Table 1, Entry 6)

CKC0154CARBON01
CKC0154hivac

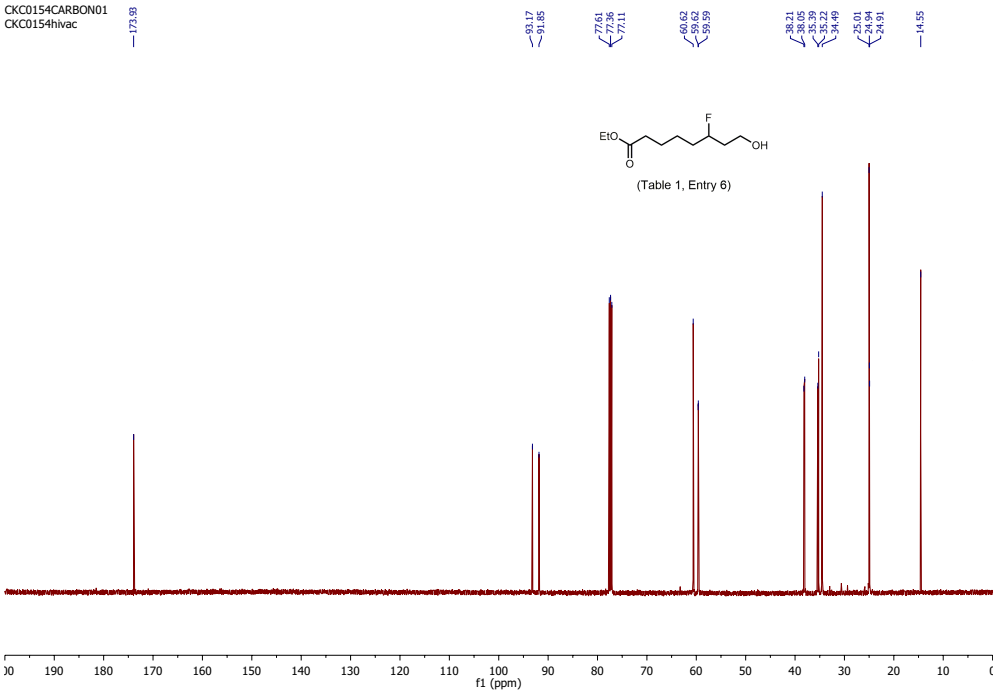

FLUORINE01
BC-1-29siena

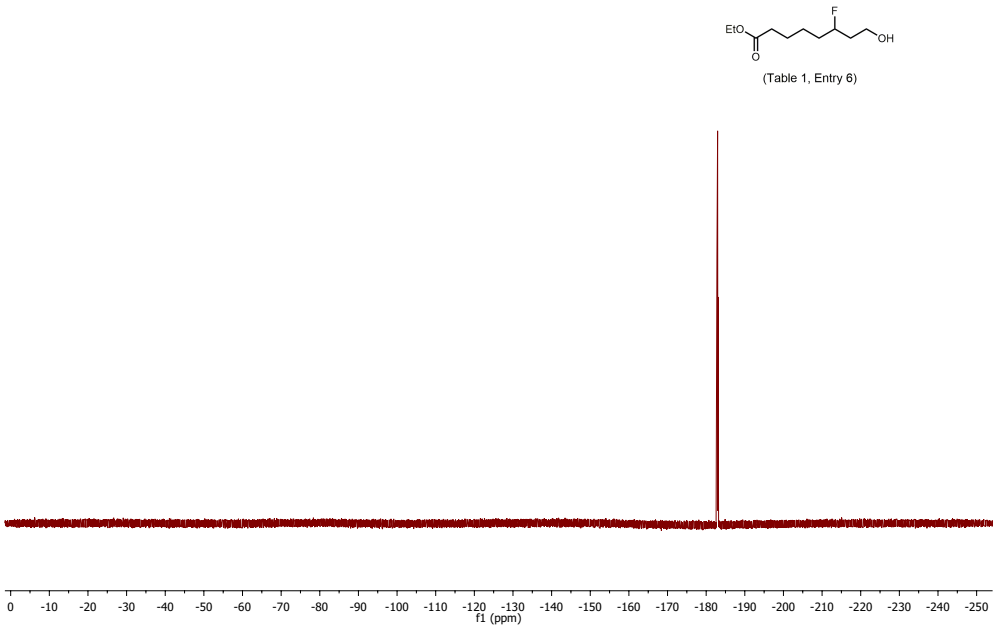

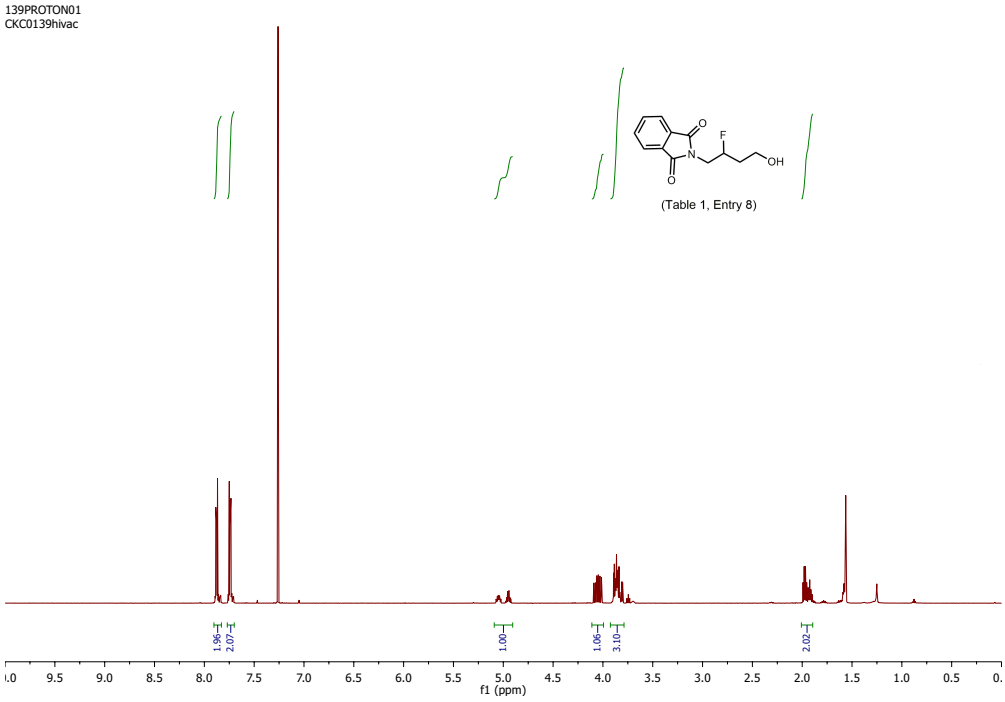
139PROTON01
CKC0139hivac
O
F
N
OH
O
(Table 1, Entry 8)
1.98
2.07
1.00
1.06
3.10
2.02
f1 (ppm)

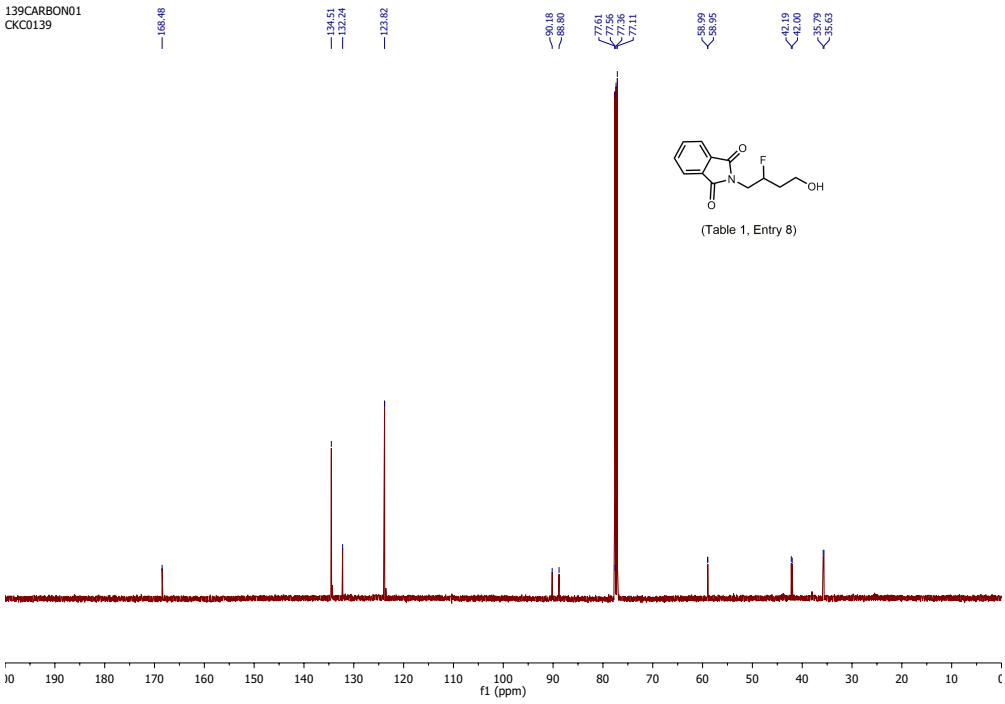
139CARBON01
CKC0139
168.48
134.51
132.24
123.82
90.18
88.80
77.61
77.56
77.36
77.11
58.99
58.95
42.19
42.00
35.79
35.63
O
F
N
OH
O
(Table 1, Entry 8)
f1 (ppm)

FLUORINE01
CKC0139siena

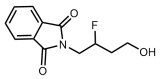

(Table 1, Entry 8)

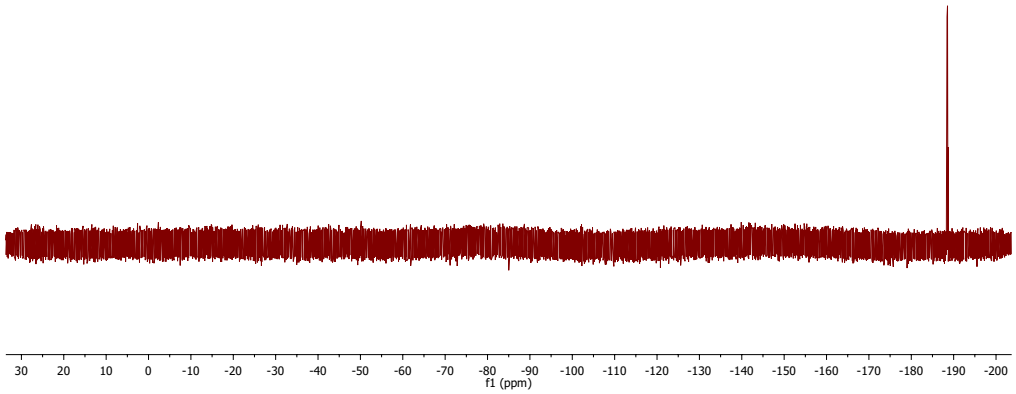

PROTON03
DZ-01-074-1-Purified

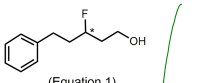

(Equation 1)

Data File C:\HPCHEM\1\DATA\GROUP\DZ107411.D

Injection Date : 1/30/2016 12:27:33 PM Seq. Line : 3
Sample Name : Location : Vial 2
Acq. Operator : XM Inj : 1
Acq. Instrument : Instrument 1 Inj Volume : 15 µl
Different Inj Volume from Sequence ! Actual Inj Volume : 2 µl
Acq. Method : C:\HPCHEM\1\METHODS\OD-15-20.M
Last changed : 5/19/2011 9:25:09 PM by NB
Analysis Method : C:\HPCHEM\1\METHODS\OD-10-20.M
Last changed : 1/30/2016 1:16:09 PM by XM
(modified after loading)

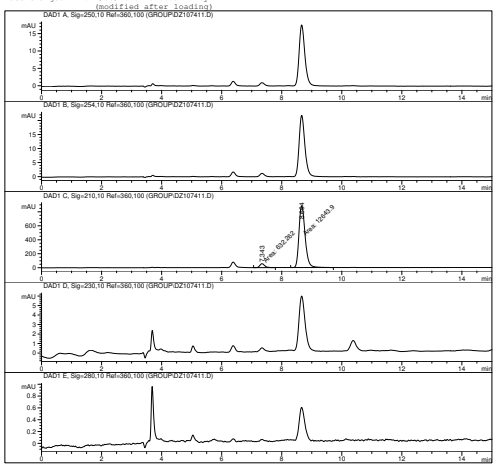

Data File C:\HPCHEM\1\DATA\GROUP\DZ107411.D

Area Percent Report

Sorted By : Signal
Multiplier : 1.0000
Dilution : 1.0000
Use Multiplier & Dilution Factor with ISTDs

Signal 1: DAD1 A, Sig=250,10 Ref=360,100

Signal 2: DAD1 B, Sig=254,10 Ref=360,100

Signal 3: DAD1 C, Sig=210,10 Ref=360,100

Peak #	RetTime [min]	Type	Width [min]	Area [mAU*s]	Height [mAU]	Area %
1	7.343	MM	0.1888	632.26190	55.80346	4.7624
2	8.664	MM	0.2383	1.26439e4	884.45312	95.2376

Totals : 1.32762e4 940.25658

Results obtained with enhanced integrator!

Signal 4: DAD1 D, Sig=230,10 Ref=360,100

Signal 5: DAD1 E, Sig=280,10 Ref=360,100

*** End of Report ***

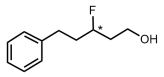

(Equation 1)

Data File C:\HPCHEM\1\DATA\GROUP\DZ10741R.D

Injection Date : 1/30/2016 12:06:19 PM Seq. Line : 2
Sample Name : Location : Vial 1
Acq. Operator : XM Inj : 1
Acq. Instrument : Instrument 1 Inj Volume : 15 µl
Different Inj Volume from Sequence ! Actual Inj Volume : 2 µl
Acq. Method : C:\HPCHEM\1\METHODS\OD-15-20.M
Last changed : 5/19/2011 9:25:09 PM by NB
Analysis Method : C:\HPCHEM\1\METHODS\OD-10-20.M
Last changed : 1/30/2016 1:16:09 PM by XM
(modified after loading)

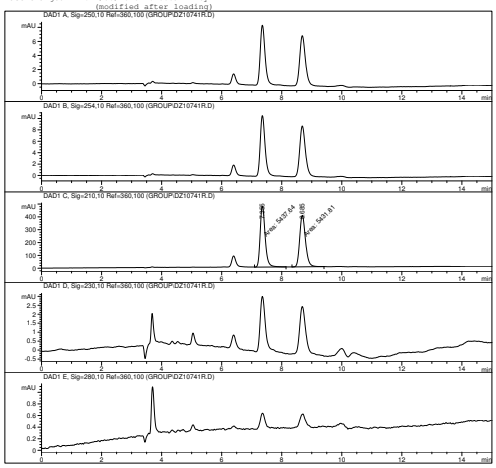

Data File C:\HPCHEM\1\DATA\GROUP\DZ10741R.D

Area Percent Report

Sorted By : Signal
Multiplier : 1.0000
Dilution : 1.0000
Use Multiplier & Dilution Factor with ISTDs

Signal 1: DAD1 A, Sig=250,10 Ref=360,100

Signal 2: DAD1 B, Sig=254,10 Ref=360,100

Signal 3: DAD1 C, Sig=210,10 Ref=360,100

Peak #	RetTime [min]	Type	Width [min]	Area [mAU*s]	Height [mAU]	Area %
1	7.355	MM	0.1907	5437.64014	475.33261	50.0268
2	8.685	MM	0.2258	5431.81152	400.93201	49.9732

Totals : 1.08695e4 876.26462

Results obtained with enhanced integrator!

Signal 4: DAD1 D, Sig=230,10 Ref=360,100

Signal 5: DAD1 E, Sig=280,10 Ref=360,100

*** End of Report ***

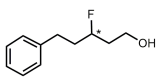

(Equation 1)

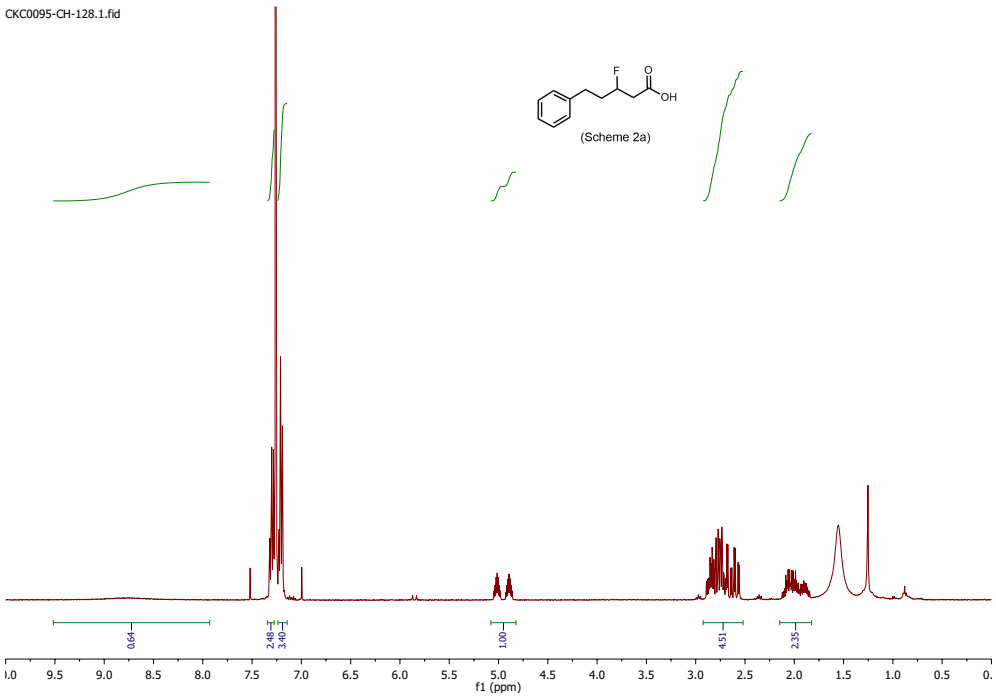
CKC0095-CH-128.1.fid
F
O
OH
(Scheme 2a)
0.64
2.48
3.40
1.00
4.51
2.35
f1 (ppm)

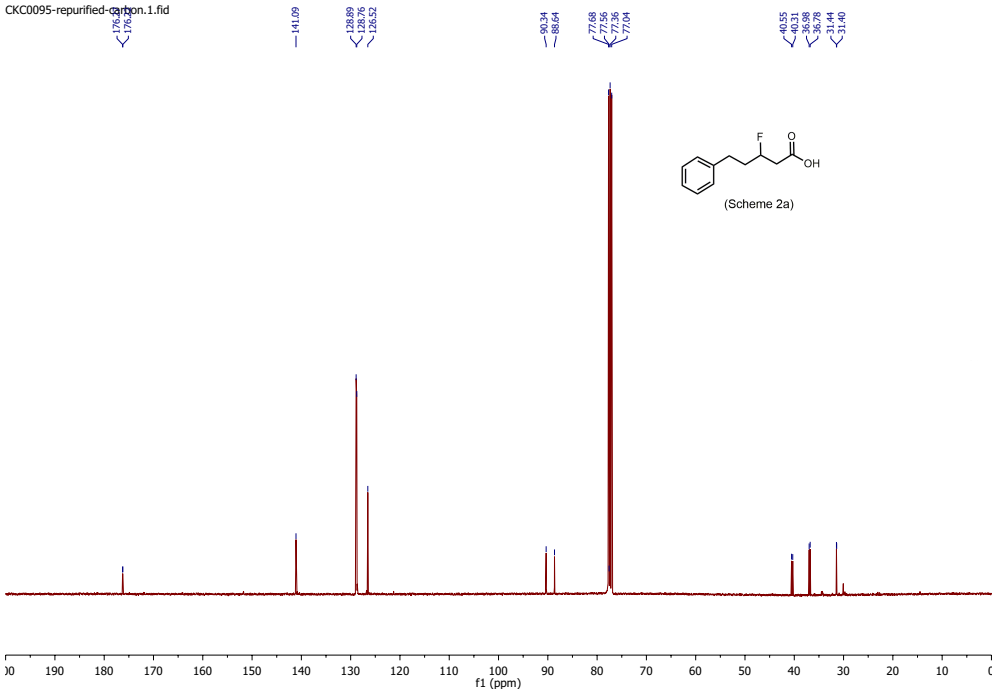
CKC0095-repurified-carbon.1.fid
176.29
176.52
141.09
128.89
128.76
126.52
90.34
88.64
77.68
77.56
77.36
77.04
40.55
40.31
36.98
36.78
31.44
31.40
F
O
OH
(Scheme 2a)
f1 (ppm)

CKC0095FLUORINE
BC-1-29siena

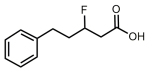

(Scheme 2a)

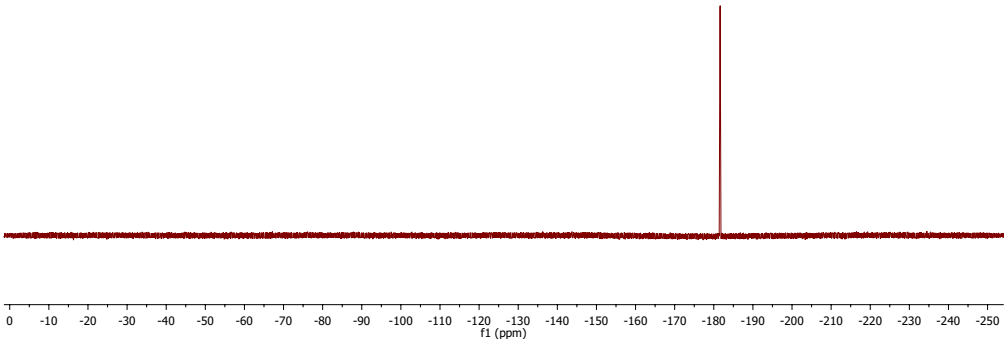

CKC0310cleanPROTON01
CKC0310prep

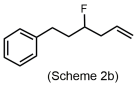

(Scheme 2b)

CKC0110CARBON01
CKC0110CH

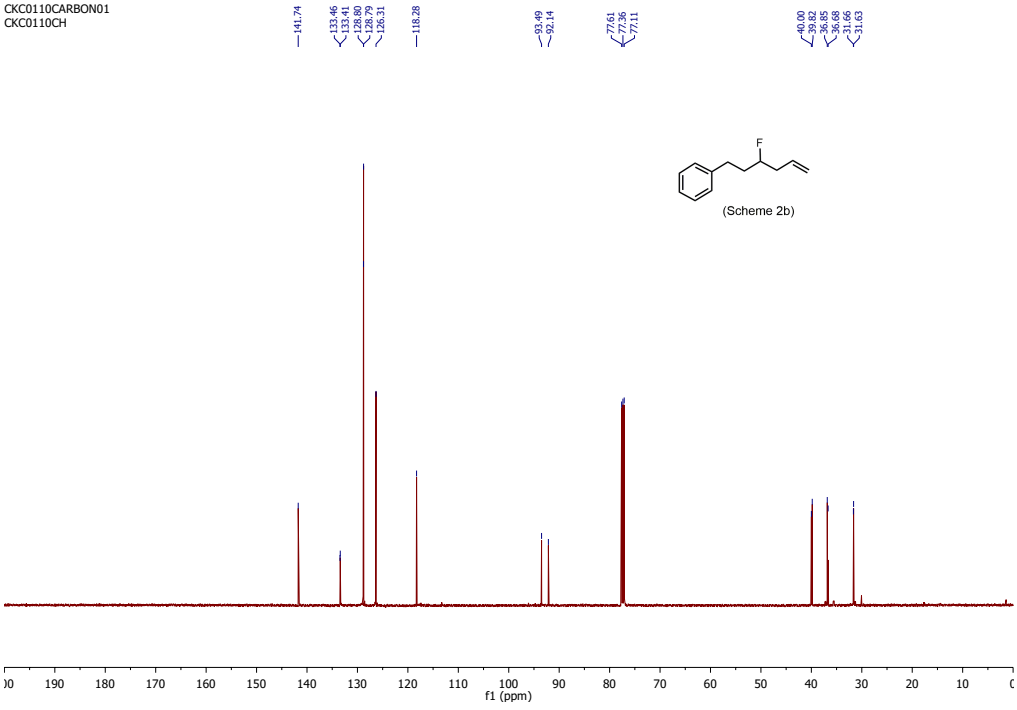

CKC0110FLUORINE01
BC-1-29siena

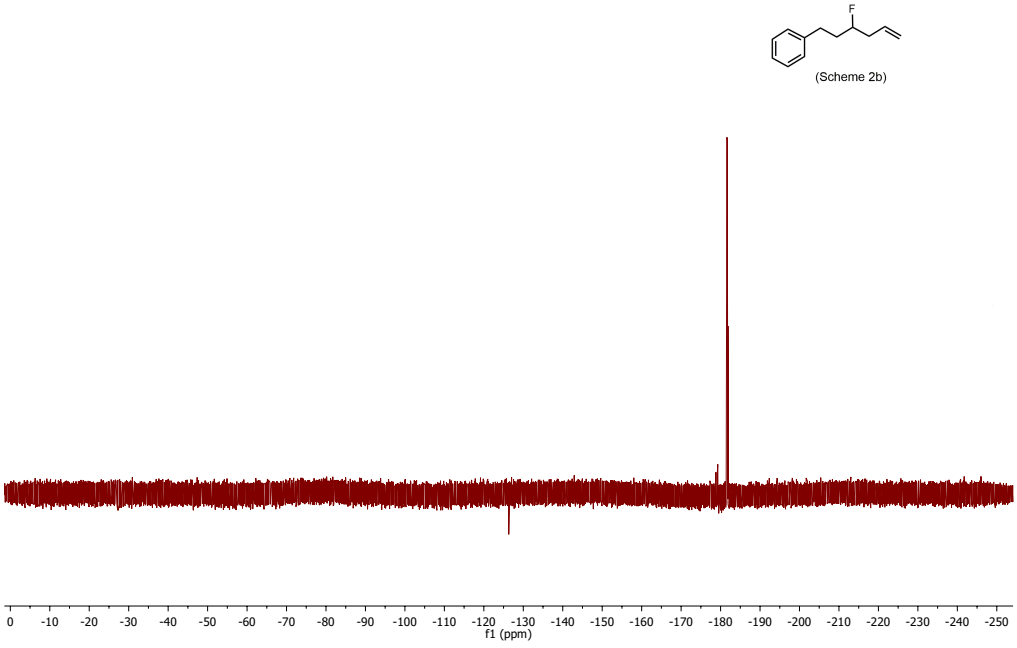

336PROTON01
CKC0336hivac

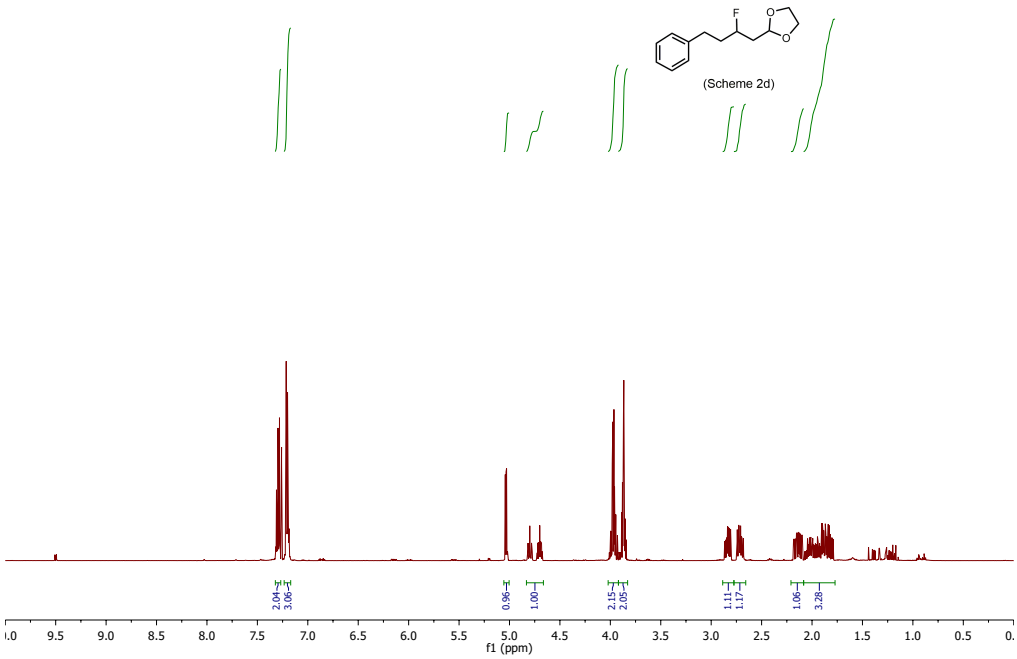

336CARBON01
CKC0336hivac

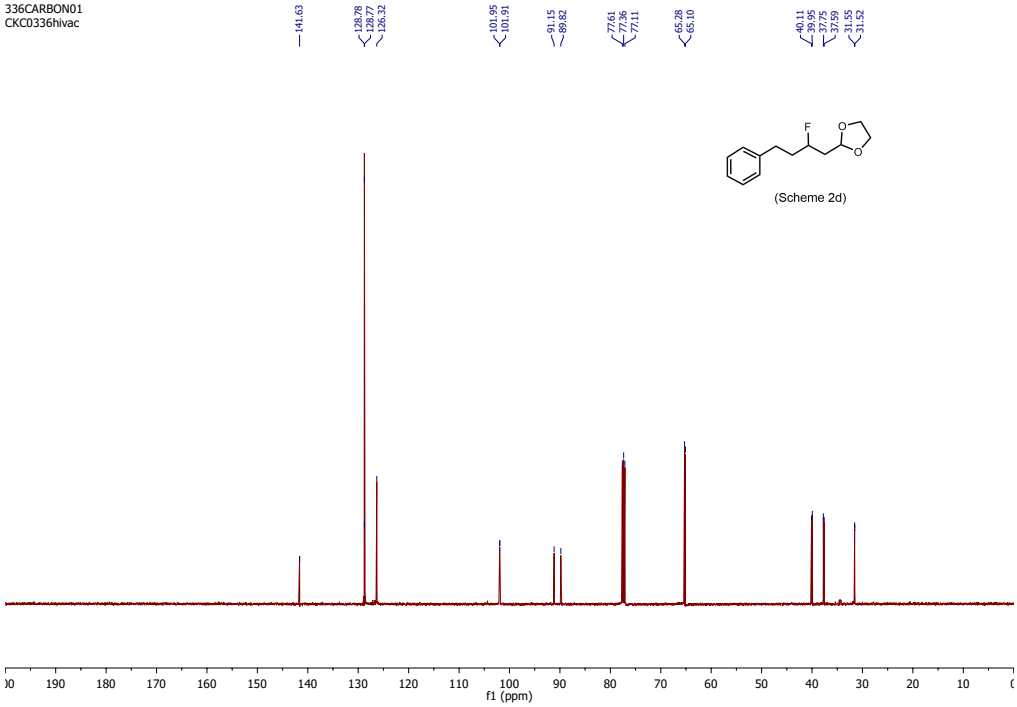

FLUORINE01
BC-1-29siena

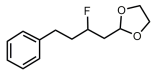

(Scheme 2d)

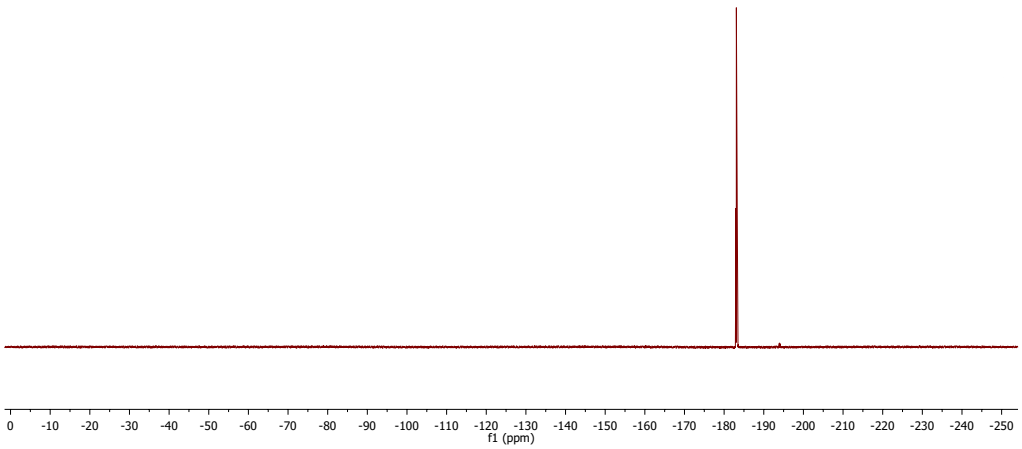

CKC0094pure2
CKC0094pure2

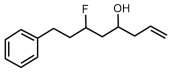

(Scheme 2e)

CKC0094CARBON01
CKC0094SI

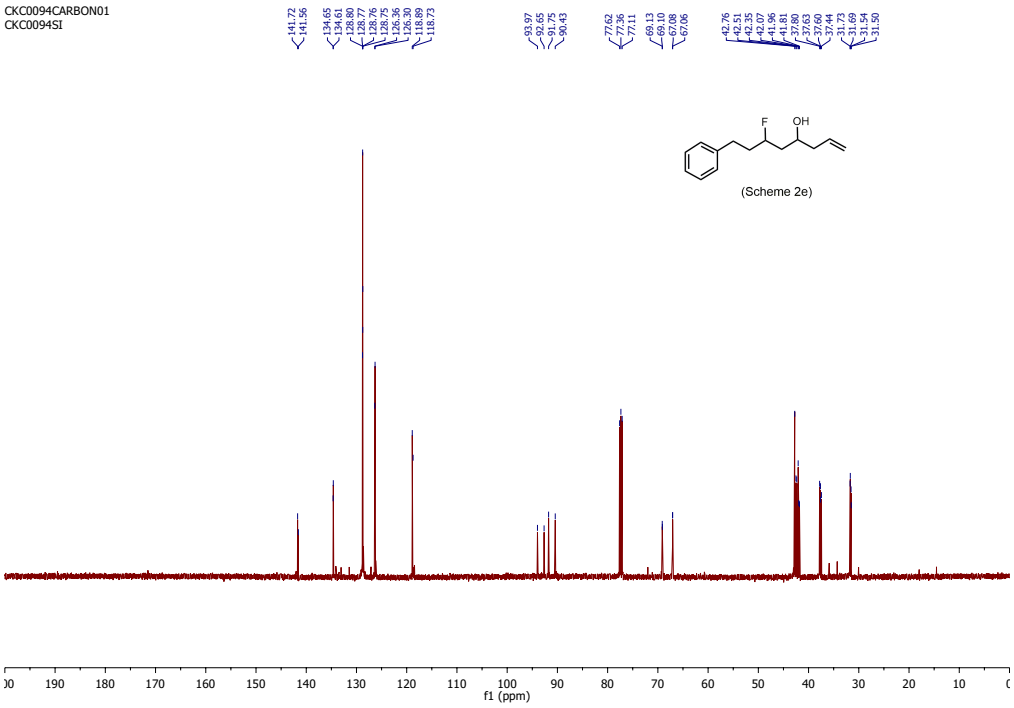

FLUORINE01
CKC0094siena

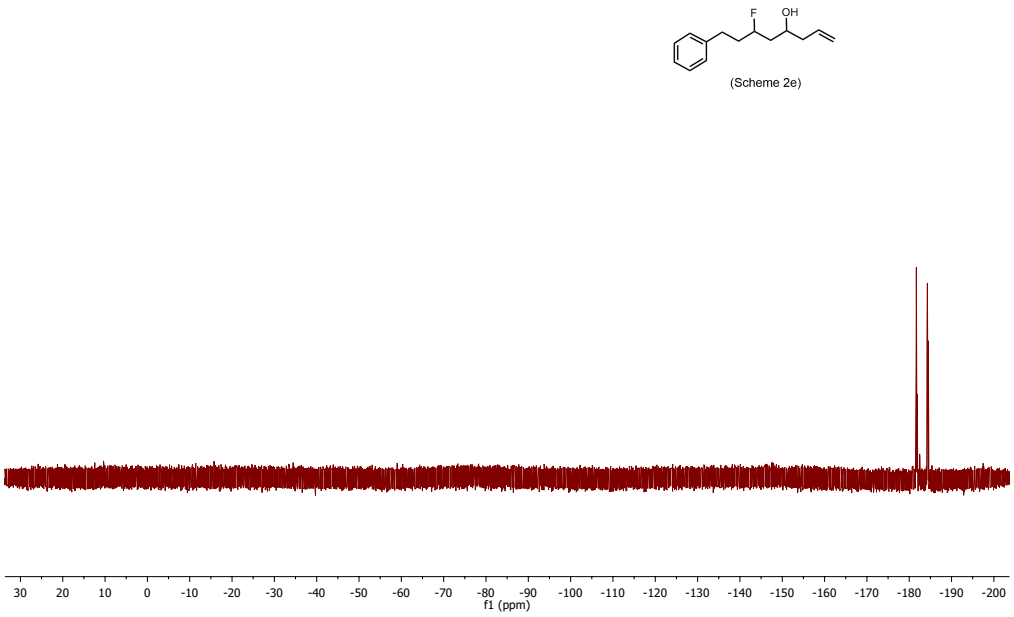

References

(1) For reviews of fluorine in the pharmaceutical industry and the biological properties of fluorine-containing compounds, see: (a) Müller, K.; Faeh, C.; Diederich, F. *Science* **2007,** *317*, 1881-1886. (b) Purser, S.; Moore, P. R.; Swallow, S.; Gouverneur, V. *Chem. Soc. Rev.* **2008,** *37*, 320-330. (c) Kirk, K. L. *Org. Process Res. Dev.* **2008,** *12*, 305-321. (d) O'Hagan, D. *J. Fluorine Chem.* **2010,** *131*, 1071-1081. (e) Wang, J.; Sánchez-Roselló, M.; Aceña, J. L.; del Pozo, C.; Sorochinsky, A. E.; Fustero, S.; Soloshonok, V. A.; Liu, H. *Chem. Rev.* **2014,** *114*, 2432-2506.

(2) For an introduction to fluorine in agrochemicals, see: (a) Jeschke, P. *ChemBioChem* **2004,** *5*, 570-589. (b) P. Jeschke in *Modern Methods in Crop Protection Research*, Wiley-VCH, Weinheim, **2012**, pp. 73-128. (c) Fujiwara, T.; O'Hagan, D. *J. Fluorine Chem.* **2014,** *167*, 16-29.

(3) For an introduction to fluorinated compounds in materials chemistry, see: Berger, R.; Resnati, G.; Metrangolo, P.; Weber, E.; Hulliger, J. *Chem. Soc. Rev.* **2011,** *40*, 3496-3508.

(4) For a review on the sustainability of organofluorine chemistry, see: Harsanyi, A.; Sandford, G. *Green Chem.* **2015,** *17*, 2081-2086.

(5) For reviews of modern methods in organofluorine chemistry, see: (a) Shimizu, M.; Hiyama, T. *Angew. Chem. Int. Ed.* **2005,** *44*, 214-231. (b) Furuya, T.; Kamlet, A. S.; Ritter, T. *Nature* **2011,** *473*, 470-477. (c) Liang, T.; Neumann, C. N.; Ritter, T. *Angew. Chem. Int. Ed.* **2013,** *52*, 8214-8264. (d) Campbell, M. G.; Ritter, T. *Chem. Rev.* **2015,** *115*, 612-633. (e) Yang, X.; Wu, T.; Phipps, R. J.; Toste, F. D. *Chem. Rev.* **2015,** *115*, 826-870.

(6) Singh, R. P.; Shreeve, J. M. *Synthesis* **2002,** *17*, 2561-2578.

(7) For selected examples of benzylic and allylic fluorination, see: (a) Thibaudeau, S.; Gouverneur, V. *Org. Lett.* **2003,** *5*, 4891-4893. (b) Ishimaru, T.; Shibata, N.; Horikawa, T.; Yasuda, N.; Nakamura, S.; Toru, T.; Shiro, M. *Angew. Chem. Int. Ed.* **2008,** *47*, 4157-4161. (c) Katcher, M. H.; Sha, A.; Doyle, A. G. *J. Am. Chem. Soc.* **2011,** *133*, 15902-15905. (d) Topczewski, J. J.; Tewson, T. J.; Nguyen, H. M. *J. Am. Chem. Soc.* **2011,** *133*, 19318-19321. (e) McMurtrey, K. B.; Racowski, J. M.; Sanford, M. S. *Org.*

Lett. **2012,** *14*, 4094-4097. (f) Braun, M.-G.; Doyle, A. G. *J. Am. Chem. Soc.* **2013,** *135*, 12990-12993. (g) Huang, X.; Liu, W.; Ren, H.; Neelamegam, R.; Hooker, J. M.; Groves, J. T. *J. Am. Chem. Soc.* **2014,** *136*, 6842-6845. (h) Zhang, Q.; Stockdale, D. P.; Mixdorf, J. C.; Topczewski, J. J.; Nguyen, H. M. *J. Am. Chem. Soc.* **2015**, *137*, 11912-11915.

(8) For reviews on catalytic α-fluorination of carbonyl compounds, see: (a) Mukherjee, S.; Yang, J. W.; Hoffman, S.; List, B. *Chem. Rev.* **2007**, *107*, 5471-5569. (b) Lectard, S.; Hamashima, Y.; Sodeoka, M. *Adv. Synth. Catal.* **2010**, *352*, 2708-2732.

(9) For a review on distal fluorination of ketones, see: Fan, X.; Zhao, H.; Zhu, C. *Acta Chim. Sinica* **2015,** *73*, 979-983.

(10) For examples, see: (a) Zhao, H.; Fan, X.; Yu, J.; Zhu, C. *J. Am. Chem. Soc.* **2015,** *137*, 3490-3493. (b) Bloom, S.; Bume, D. D.; Pitts, C. R.; Lectka, T. *Chem. Eur. J.* **2015**, *21*, 8060-8063. (c) Ren, S.; Feng, C.; Loh, T.-P. *Org. Biomol. Chem.* **2015**, *13*, 5105-5109. (d) Ishida, N.; Okumura, S.; Nakanishi, Y.; Murakami, M. *Chem. Lett.* **2015**, *44*, 821-823.

(11) For selected examples of the synthesis of β-fluorinated carbonyl compounds, see: (a) Bloom, S.; Sharber, S. A.; Holl, M. G.; Knippel, J. L.; Lectka, T. *J. Org. Chem.* **2013,** *78*, 11082-11086. (b) Kee, C. W.; Chin, K. F.; Wong, M. W.; Tan, C.-H. *Chem. Commun.* **2014,** *50*, 8211-8214. (c) Xia, J.-B.; Ma, Y.; Chen, C. *Org. Chem. Front.* **2014,** *1*, 468-472. (d) Pitts, C. R.; Ling, B.; Woltornist, R.; Liu, R.; Lectka, T. *J. Org. Chem.* **2014**, *79*, 8895-8899. (e) Halperin, S. D.; Fan, H.; Chang, S.; Martin, R. E.; Britton, R. *Angew. Chem. Int. Ed.* **2014,** *53*, 4690-4693. (f) Ventre, S.; Petronijevic, F. R.; MacMillan, D. W. C. *J. Am. Chem. Soc.* **2015**, *137*, 5654-5657.

(12) (a) Smidt, J.; Hafner, W.; Sedlmeier, J.; Jira, R.; Rüttinger, R. *Angew. Chem.* **1959**, *71*, 176-182. (b) Jira, R. *Angew. Chem. Int. Ed.* **2009**, *48*, 9034-9037. (c) Michel, B. M.; Steffens, L. D.; Sigman M. S. in *Organic Reactions Volume 84* (Ed.: S. E. Denmark), John Wiley & Sons, **2014**, pp. 75-414.

(13) Tsuji, J. *Synthesis* **1984,** 369-384.

(14) For reviews on selectivity in Wacker oxidations, see: (a) Muzart, J. *Tetrahedron* **2007**, *63*, 7505-7521. (b) McDonald, R. I.; Liu, G.; Stahl, S. S. *Chem. Rev.* **2011**, *111*, 2981-

3019. (c) Sigman, M. S.; Werner, E. W. *Acc. Chem. Res.* **2012**, *45*, 874-884. (d) Dong, J. J.; Browne, W. R.; Feringa, B. L. *Angew. Chem. Int. Ed.* **2015**, *54*, 734-744.

(15) (a) Morandi, B.; Wickens, Z. K.; Grubbs, R. H. *Angew. Chem. Int. Ed.* **2013,** *52*, 2944-2948. (b) Morandi, B.; Wickens, Z. K.; Grubbs, R. H. *Angew. Chem. Int. Ed.* **2013,** *52*, 9751-9754.

(16) Lerch, M. M.; Morandi, B.; Wickens, Z. K.; Grubbs, R. H. *Angew. Chem. Int. Ed.* **2014,** *53*, 8654-8658.

(17) For examples of fluorinated terminal olefins in Wacker oxidations, see: (a) Guidotti, J.; Tordeux, M.; Blazejewski, J.-C.; Wakselman, C. *Lett. Org. Chem.* **2005**, *2*, 148-150. (b) see Reference 7(c).

(18) For a review on NO_x ligands in palladium catalysis, see: Fairlamb, I. J. S. *Angew. Chem. Int. Ed.* **2015**, *54*, 10415-10427.

(19) Weiner, B.; Baeza, A.; Jerphagnon, T.; Feringa, B. L. *J. Am. Chem. Soc.* **2009,** *131*, 9473-9474.

(20) (a) Wickens, Z. K.; Morandi, B.; Grubbs, R. H. *Angew. Chem. Int. Ed.* **2013,** *52*, 11257-11260. (b) Wickens, Z. K.; Skakuj, K.; Morandi, B.; Grubbs, R. H. *J. Am. Chem. Soc.* **2014,** *136*, 890-893.

(21) For a discussion on the role of *t*BuOH in aldehyde-selective Wacker oxidations, see: Dong, J. J.; Harvey, E. C.; Fañanás-Mastral, M.; Browne, W. R.; Feringa, B. L. *J. Am. Chem. Soc.* **2014,** *136*, 17302-17307.

(22) For examples of using *t*BuOH to enhance aldehyde-selectivity in Wacker-type oxidations, see: (a) Feringa, B. L. *J. Chem. Soc., Chem. Commun.* **1986**, 909-910. (b) Wenzel, T. T. *J. Chem. Soc., Chem. Commun.* **1993**, 862-864. (c) Ogura, T.; Kamimura, R.; Shiga, A.; Hosokawa, T. *Bull. Chem. Soc. Jpn.* **2005,** *78*, 1555-1557. (d) Teo, P.; Wickens, Z. K.; Dong, G.; Grubbs, R. H. *Org. Lett.* **2012,** *14*, 3237-3239. (e) Dong, J. J.; Fañanás-Mastral, M.; Alsters, P. L.; Browne, W. R.; Feringa, B. L. *Angew. Chem. Int. Ed.* **2013,** *52*, 5561-5565. (f) Bourne, S. L.; Ley, S. V. *Adv. Synth. Catal.* **2013,** *355*, 1905-1910.

(23) In addition to 9% unsaturated aldehyde detected by ^{1}H NMR, a linear allylic alcohol (S_N2') was formed in 28% yield, confirmed by GC-MS.

(24) Although β-fluorinated aldehydes are not stable to column chromatography, the crude products could be directly reduced to stable alcohol derivatives by treatment with $NaBH_4$.

(25) Studies by Feringa have shown retention of enantiopurity in allylic amides (Reference 21) and racemization in the case of allylic esters (Reference 22(e)).

(26) Under related conditions optimized for the oxidation of unbiased olefins, 1-dodecene was oxidized with 79% aldehyde selectivity (Reference 20(a)).

(27) Travis, B. R.; Sivakumar, M.; Hollist, G. O.; Borhan, B. *Org. Lett.* **2003**, *5*, 1031-1034.

Chapter 4

EFFECTS OF AMINOPHOSPHINE LIGANDS ON RUTHENIUM OLEFIN METATHESIS CATALYST ACTIVITY

This work was performed in collaboration with Dr. Tzu-Pin Lin, who contributed to project design, catalyst synthesis and characterization, and kinetics experiments, and Dr. Allegra Liberman-Martin, who performed ROMP studies. All related computational studies were performed by Huiling Shao and Professor Peng Liu from the University of Pittsburgh.

Abstract

Second-generation ruthenium olefin metathesis catalysts bearing aminophosphine ligands were investigated with systematic variation of the ligand structure. The rates of phosphine dissociation (k_1; initiation rate) and relative phosphine reassociation (k_{-1}) were determined for two series of catalysts bearing cyclohexyl(morpholino)phosphine and cyclohexyl(piperidino)phosphine ligands. In both cases, incorporating P–N bonds into the architecture of the dissociating phosphine accelerates catalyst initiation relative to the parent complex (–PCy_3); however, this effect is muted for the tris(amino)phosphine-ligated complexes, which exhibit higher ligand binding constants in comparison to those with phosphines containing one or two Cy substituents. These results, along with X-ray crystallographic data and DFT calculations, were used to understand the influence of ligand structure on catalyst activity. Especially noteworthy is the application of phosphines containing incongruent substituents ($PR_1R'_2$); detailed analyses of factors affecting ligand dissociation, including steric effects, inductive effects, and ligand conformation, are presented. Computational studies of the reaction coordinate for ligand dissociation reveal that ligand conformational changes in the transition state contribute to rapid dissociation for the fastest initiating catalyst of these series, which bears a cyclohexyl-bis(morpholino)phosphine ligand. Furthermore, the effect of amine incorporation was also examined in the context of ring-opening metathesis polymerization, and reaction rates were found to correlate well with catalyst initiation rates. The combined experimental and

computational studies presented reveal important considerations for promoting phosphine dissociation in ruthenium olefin metathesis catalysts.

Introduction

Since its discovery in the 1950s, olefin metathesis has evolved into a versatile and powerful reaction for organic synthesis.[1] Molybdenum, tungsten, and ruthenium catalysts have been extensively investigated in the synthesis of natural and unnatural products, including the formation of substituted olefins and cyclic organic compounds.[2] Furthermore, significant efforts toward the development of olefin metathesis polymerizations,[3] notably ring-opening metathesis polymerization (ROMP)[4] and acyclic diene metathesis (ADMET),[5] have enabled the synthesis of new functional materials[6] and have led to important industrial applications.[7]

Complexes based on molybdenum and tungsten were the earliest reported well-defined olefin metathesis catalysts, and since their initial discovery, have been widely used for their high reactivity.[8] Extensive research of ruthenium-based complexes has resulted in metathesis catalysts with increased functional group tolerance and stability to air and moisture. Demonstration of ruthenium alkylidene complexes as viable olefin metathesis catalysts[9] led to the development of catalyst **4-1** (Figure 4.1).[10] The lower activity of **4-1** in comparison to molybdenum catalysts was later addressed by our group through the development of second-generation ruthenium olefin metathesis catalysts, notably **4-2**,[11] in which a phosphine is substituted for an *N*-heterocyclic carbene (NHC) ligand.[12,13] The bispyridine complex **4-3** and related complexes have proven to be fast-initiating, enabling cross metathesis of challenging substrates[14] and ROMP to produce polymers with controllable molecular weight and low dispersity;[15] additionally, complex **4-3** can serve as a useful precursor for variants of catalyst **4-2** that bear a variety of organic substituents on the dissociating phosphine.[16]

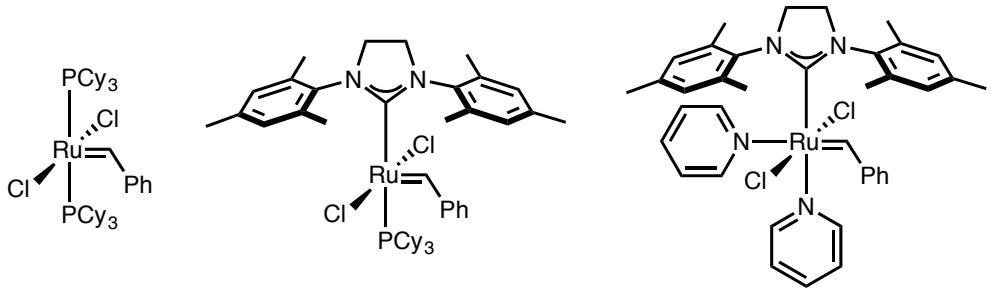

4-1 **4-2** **4-3**

Figure 4.1. Established Ruthenium Olefin Metathesis Catalysts.

Mechanistic studies of olefin metathesis promoted by second-generation ruthenium catalysts have suggested that these reactions occur by a dissociative pathway, in which phosphine dissociation occurs to form a 14-electron intermediate in an initiation step prior to olefin binding (Scheme 4.1).[17] Thus, the activity of these catalysts is affected by the rate of phosphine dissociation (k_1; initiation rate) and the relative rate of phosphine reassociation (k_{-1}). Following formation of the 14-electron intermediate, the likelihood of phosphine reassociation versus productive olefin binding (k_{-1}/k_2) can be experimentally determined; higher selectivity for binding of the olefin over the phosphine, rather than higher initation kinetics, has been shown to be the underlying cause for increased activity of **4-2** compared to **4-1**.[18]

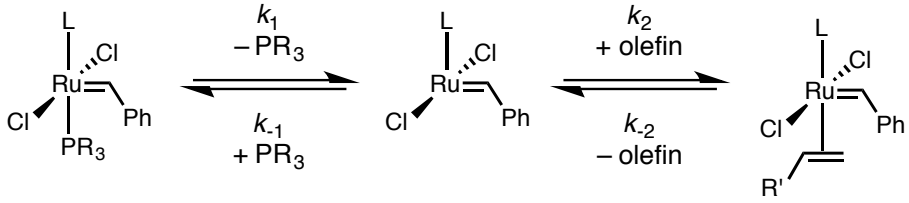

Scheme 4.1. Proposed Dissociative Mechanism for Second-Generation Ruthenium Olefin Metathesis Catalysts.

Rate constants have been reported for a variety of second-generation ruthenium catalysts bearing phosphine ligands with different substituents.[19] While phosphine electronics have been shown previously not to directly correlate with phosphine reassociation, initiation rates are known to increase with decreasing σ-donating ability of the phosphine. With this in mind, we became interested in further exploring phosphines

that are weak σ-donors as ligands for second-generation catalysts. While phosphines containing halogenated arenes have been investigated, the incorporation of P–X bonds, where X is an electron-withdrawing heteroatom, has been much less explored in this context. Such ligands have been broadly applied in organometallic chemistry, spanning a wide range of accessible σ-donating and π-accepting properties.[20] NMR studies of aminophosphines, with structure $P(NR)_3$, have demonstrated decreased σ-basicity of these ligands in comparison to triphenylphosphine.[21] Due to the electronic properties and ease of preparation of aminophosphines, these ligands are particularly well suited to systematically investigate the incorporation of P–X bonds to increase catalyst activity. The kinetics and computational studies described herein demonstrate the importance of several key factors in promoting phosphine dissociation, facilitating the design of new ligands for efficient ruthenium olefin metathesis catalysts.

In this study, nitrogen-containing heterocycles were systematically introduced in place of the cyclohexyl groups in complex **2** to probe the effect of P–N bonds on catalyst activity. NMR spectroscopic and X-ray crystallographic data were obtained to gather structural information, and these data were analyzed in the context of kinetics studies. Initiation rates and the relative phosphine reassociation rates were measured, together providing a metric to compare aminophosphine binding strengths. Trends in ligand binding strengths and initiation rates agree well with DFT calculations, which account for important parameters affecting ligand properties. Furthermore, the use of phosphines bearing incongruent substituents allows for a more comprehensive understanding of ligand structure, providing additional information regarding the effects of sterics and ligand conformation on phosphine dissociation. Simple substitution of nitrogen and oxygen atoms in the ligand composition of complex **2** delivered over an order of magnitude increase in catalyst initiation rates, which directly correlate with rates of conversion in ROMP studies.

Ligand and Catalyst Synthesis and Characterization

Two new series of second-generation ruthenium olefin metathesis catalysts bearing aminophosphine ligands in place of the tricyclohexylphosphine present in catalyst **4-2** were synthesized. Morpholine and piperidine substituents were incorporated to decrease

phosphine donor strength through the introduction of P–N bonds due to their similar size to cyclohexane, and complexation of these aminophosphines led to the formation of six new catalysts **4-4** through **4-9** (Figure 4.2).

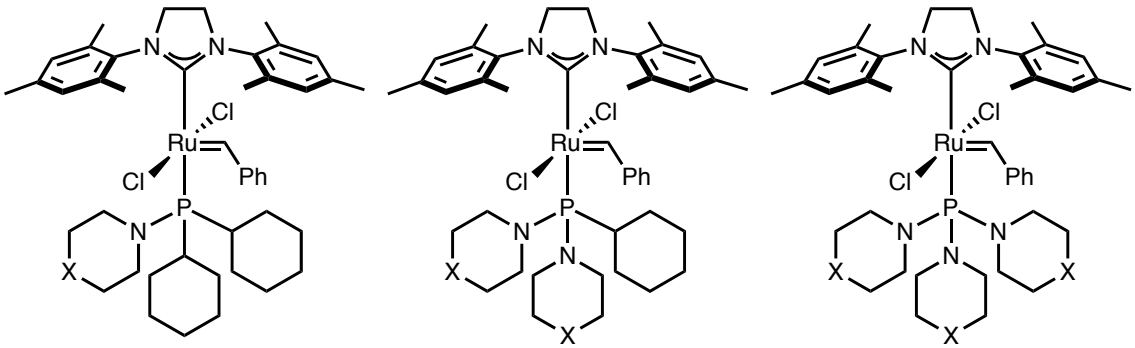

4-4 (X = O)
4-7 (X = CH_2)

4-5 (X = O)
4-8 (X = CH_2)

4-6 (X = O)
4-9 (X = CH_2)

Figure 4.2. New Ruthenium-Based Olefin Metathesis Catalysts Bearing Aminophosphine Ligands Derived from Morpholine and Piperidine.

Treatment of the appropriate chlorocyclohexylphosphine or trichlorophosphine starting materials with excess morpholine or piperidine produced the corresponding aminophosphines **4-10** through **4-15** (Scheme 4.2A). Following successful synthesis of the desired ligands, complexation to form catalysts **4-4** through **4-9** was achieved by reacting the bis(pyridine) catalyst **3** with an excess of aminophosphine in THF (Scheme 4.2B), modified from a previously reported procedure.[16]

Second-generation ruthenium olefin metathesis catalysts with aromatic phosphine ligands are known to be faster initiating than their alkylphosphine counterparts, and the effects of replacing the PCy_3 ligand with PPh_3 in **4-2** and related catalysts have been well-studied for ring-closing metathesis (RCM)[22] and ROMP[19a] reactions. Thus, following the successful synthesis of catalysts **4-4** through **4-9**, we became interested in potentially faster initiating species derived from aromatic amines. A pyrrolylphosphine ligand **4-16** was synthesized by a procedure modified from that shown in Scheme 4.2. Synthesis and characterization for **4-17** can be found in the Experimental Section.

A) Synthesis of Aminophosphine Ligands

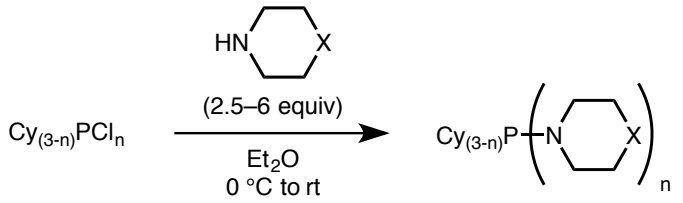

4-10 (n = 1; X = O) **4-13** (n = 1; X = CH_2)
4-11 (n = 2; X = O) **4-14** (n = 2; X = CH_2)
4-12 (n = 3; X = O) **4-15** (n = 3; X = CH_2)

B) Representative Complexation to Generate Catalyst 4-4

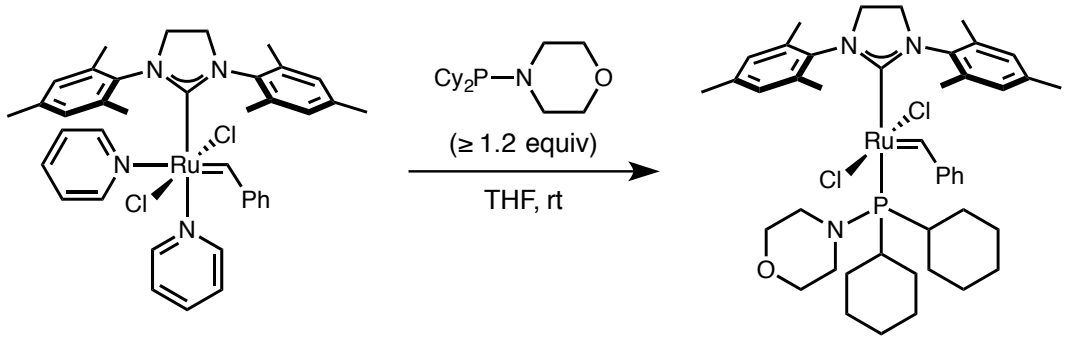

4-3 **4-4**

Scheme 4.2. Synthetic Route to Prepare Complexes **4-4** Through **4-9**.

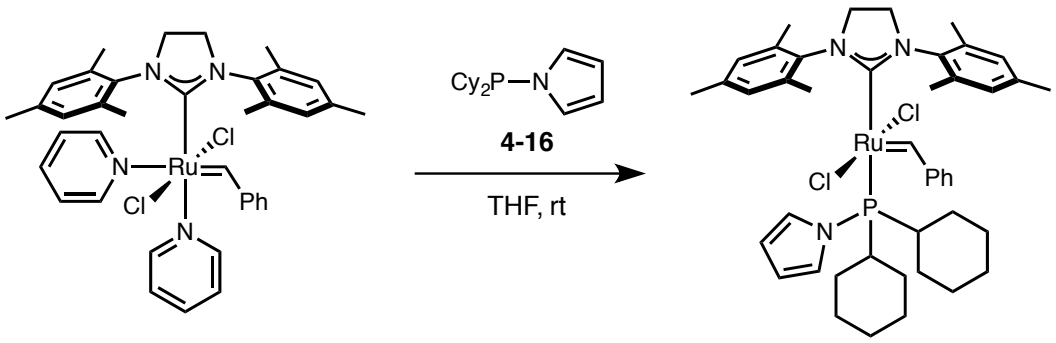

4-3 **4-17**

Scheme 4.3. Synthesis of a Ruthenium-Based Olefin Metathesis Catalyst Bearing a Pyrrolylphosphine Ligand.

All catalysts described in this report were characterized by ^{1}H, ^{13}C, and ^{31}P NMR as well as high-resolution mass spectrometry. Furthermore, X-ray crystallography was performed for certain complexes to compare selected bond lengths and angles within a

series of new catalysts. Trends observed in the characterization of these compounds are discussed below, with further data described in the Experimental Section.

The ^{31}P NMR shifts for catalysts **4-2**, **4-4** through **4-9**, and **4-17** were compared along with those for the corresponding free phosphine ligands (Table 4.1). In both the morpholine- and piperidine-based series, the chemical shift for the free phosphine becomes more downfield as amine substitution increases. However, following complexation, this trend is not observed in the case of ^{31}P NMR shifts for the ruthenium catalysts. While the phosphorus nuclei are significantly deshielded in the mono- and bis(amino)phosphine cases (Δppm > 16 ppm), the phosphorus nuclei of the tris(amino)phosphine-ligated catalysts are far less deshielded following complexation (Δppm ~ 2 ppm).

Table 4.1. Signature ^{31}P NMR Shifts of Free Aminophosphines and Catalysts[a]

catalyst	cat. (^{31}P)	ligand	free ligand (^{31}P)	Δ ppm
4-2	29.4	PCy_3	8.8	20.6
4-4	92.4	**4-10**	75.6	16.8
4-5	131.9	**4-11**	98	33.9
4-6	116.7	**4-12**	114.7	2.0
4-7	92.1	**4-13**	75.9	16.2
4-8	133.0	**4-14**	98.8	34.0
4-9	118.7	**4-15**	116.8	1.9
4-17	92.3	**4-16**	66.1	26.2

[a]All samples prepared in C_6D_6.

Catalysts **4-7** through **4-9**, containing piperidine-substituted phosphine ligands, as well as catalyst **4-17** were selected for further characterization by X-ray crystallography. The structures of **4-7** through **4-9** and **4-17** are shown in Figures 4.3-4.6. The crystal structures confirm the connectivity expected for the phosphine-ligated complexes. Selected bond lengths and bond angles of catalysts **4-2** and **4-7** through **4-9** are displayed in Table 4.2 for comparison within a single series.

In each case, the catalysts in Figures 4.3-4.6 crystallize in such a way that one substituent on the phosphine ligand occupies a pseudo-equatorial position and is oriented

away from the benzylidene. Complexes **4-8** and **4-9** are distinguished in that a piperidine ring occupies this position (Figures 4.4 and 4.5), whereas in cases in which only one amine group is present, one of the two cyclohexyl rings will take this position (Figures 4.3 and 4.6). All catalysts within the piperidine series (**4-7** through **4-9**) have similar Ru–C1 bond lengths when compared to that of the parent catalyst **4-2** (Table 4.2). The length of the Ru–C8 bond increases as piperidine substitution is systematically introduced. Additionally, the Ru–P bond of catalyst **4-7**, with one piperidine substituent, is longer than that of catalyst **4-8**, which contains two piperidine rings; these Ru–P bond lengths show no direct correlation with the rate of phosphine dissociation (*vide infra*).

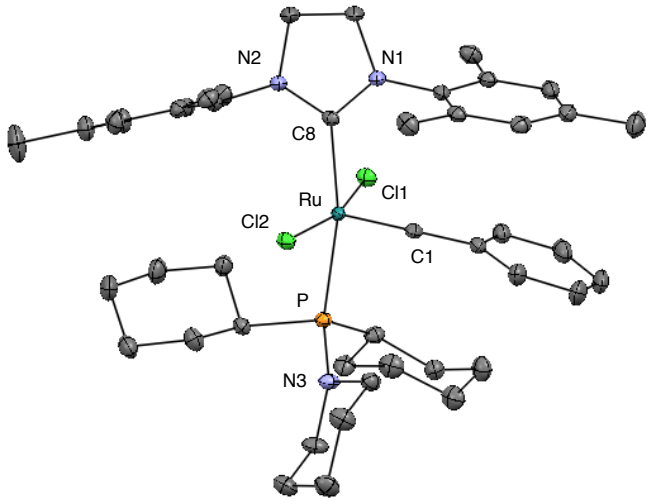

Figure 4.3. X-ray crystal structure of catalyst **4-7** with 50% probability ellipsoids. Hydrogen atoms have been omitted for clarity.

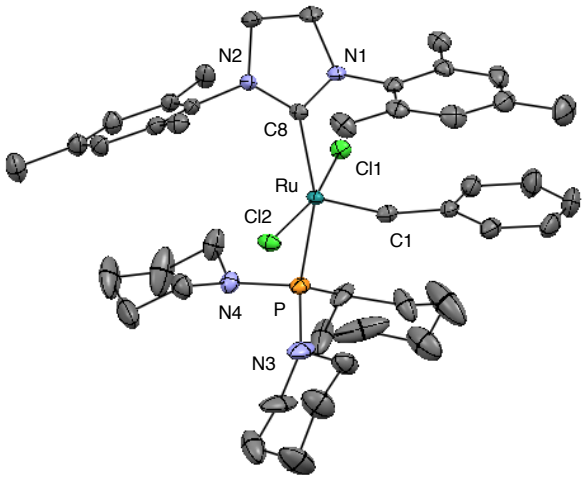

Figure 4.4. X-ray crystal structure of catalyst **4-8** with 50% probability ellipsoids. Hydrogen atoms have been omitted for clarity.

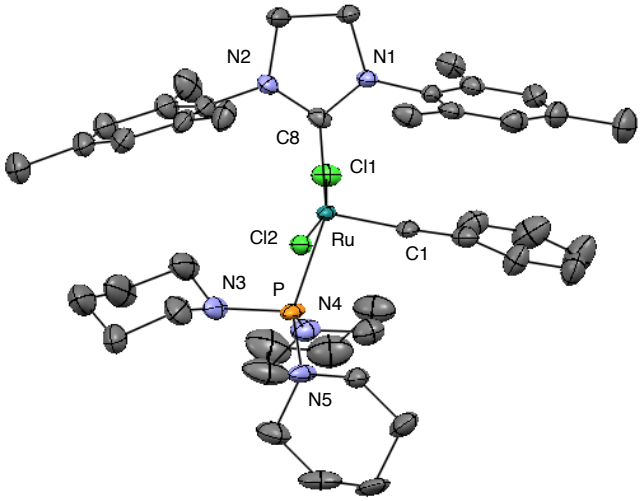

Figure 4.5. X-ray crystal structure of catalyst **4-9** with 50% probability ellipsoids. Hydrogen atoms have been omitted for clarity.

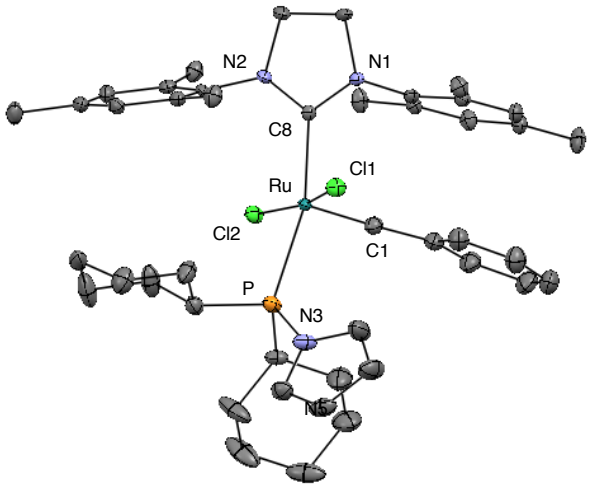

Figure 4.6. X-ray crystal structure of catalyst **4-17** with 50% probability ellipsoids. Hydrogen atoms have been omitted for clarity.

Table 4.2. Selected Bond Lengths and Angles for Complexes 4-2 and 4-7 through 4-9

bond lengths[a]	complex **4-2**	complex **4-7**	complex **4-8**	complex **4-9**
Ru–C1	1.835(2)	1.836(2)	1.839(3)	1.825(5)
Ru–C8	2.085(2)	2.0877(19)	2.097(3)	2.121(4)
Ru–P	2.4245(5)	2.4340(5)	2.3820(10)	2.394(3)
Ru–Cl1	2.3988(5)	2.4032(5)	2.3944(9)	2.374(5)
Ru–Cl2	2.3912(5)	2.3860(5)	2.4005(10)	2.421(3)
bond angles[b]	complex **4-2**	complex **4-7**	complex **4-8**	complex **4-9**
C1–Ru–C8	100.24(8)	99.70(8)	102.32(14)	102.1(2)
C1–Ru–P	95.89(6)	94.79(6)	100.29(11)	100.64(17)
C8–Ru–P	163.73(6)	165.40(6)	157.29(9)	157.17(14)

[a]Bond lengths reported in angstroms (Å). [b]Bond angles reported in degrees (º).

Kinetics Studies

The effect of P–N bonds on catalyst activity was first analyzed by comparing catalyst initiation rates for **4-4** through **4-9**. The rate constants of phosphine dissociation (k_1) for complexes **4-2** and **4-4** through **4-9** were measured at 30 °C in toluene-d_8 by ^{1}H NMR spectroscopy. These experiments allow for the comparison of two complete series

of new morpholinophosphine- (Figure 4.7) and piperidinophosphine-ligated (Figure 4.8) catalysts along with the known parent catalyst **4-2**. Initiation rate constants of the complexes were determined using a previously described method involving quenching with excess ethyl vinyl ether under pseudo-first-order conditions and monitoring the disappearance of the benzylidene resonance by ^{1}H NMR spectroscopy.[19a,23] Furthermore, the dissociation rates shown in Figures 4.7 and 4.8 are consistent with predicted values (within 10%) from kinetics experiments performed to compare the relative k_{-1} constants, or the rate of phosphine reassociation (*vide infra*). Under the same conditions, an experiment to determine the initiation rate of catalyst **4-17** resulted in full consumption of the benzylidene faster than the time scale to obtain a precise rate measurement. As expected, catalyst **4-17** is faster-initiating than all other complexes reported in this study containing morpholine and piperidine substituents; the lower limit of the initiation rate constant for this catalyst is $> 2 \times 10^{-2}$ s^{-1}. While the reaction kinetics of this complex are not included for the systematic study of amine incorporation, **4-17** was later tested in ROMP studies.

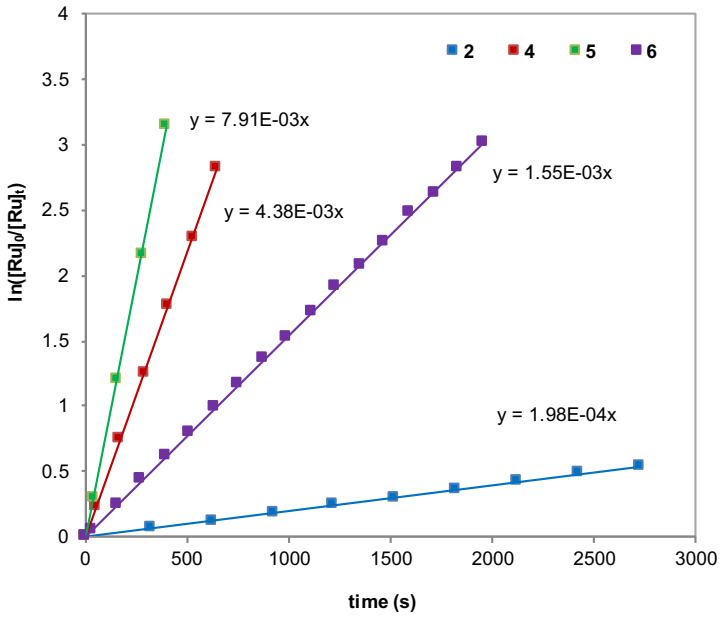

Figure 4.7. Initiation rates of catalyst series bearing morpholinophosphine ligands (catalysts **4-4** through **4-6**) and catalyst **4-2** determined by ^{1}H NMR spectroscopy at 30 °C with [Ru] = 0.017 M in toluene-d_8. The rates of phosphine dissociation are reported as the slopes of the lines fit to pseudo-first-order kinetics; units are (s^{-1}).

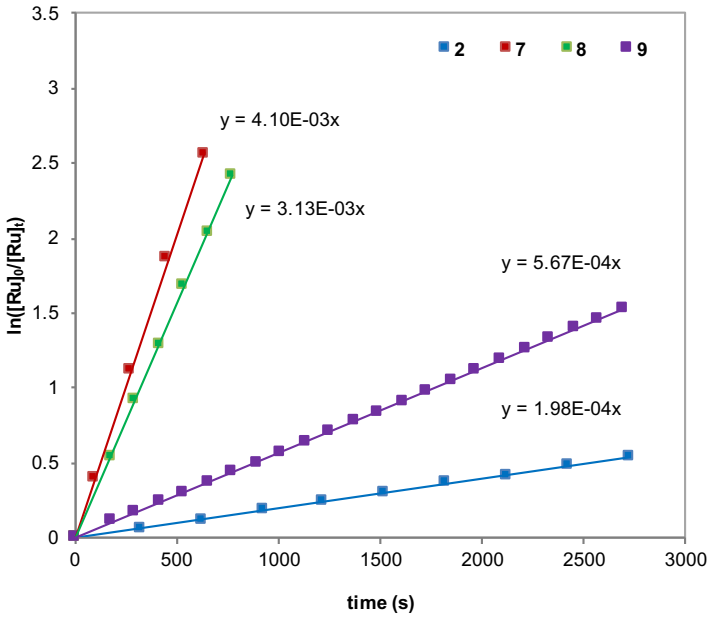

Figure 4.8. Initiation rates of catalyst series bearing morpholinophosphine ligands (catalysts **4-7** through **4-9**) and catalyst **4-2** determined by ^{1}H NMR spectroscopy at 30 °C with [Ru] = 0.017 M in toluene-d_8. The rates of phosphine dissociation are reported as the slopes of the lines fit to pseudo-first-order kinetics; units are (s^{-1}).

In all cases, the aminophosphine ligands dissociate at a faster rate than the PCy_3 ligand of catalyst **4-2**. In fact, complex **4-5,** containing a ligand with two morpholine substituents, initiates ~40 times faster than the parent catalyst and has the highest initiation rate of these two series. Interestingly, the tris(amino)phosphine-ligated complexes in both series appear to have anomalous reactivity. While amine substitution seems to dramatically accelerate phosphine dissociation for both mono-and bis(amino)phosphines relative to the PCy_3 ligand of catalyst **4-2**, this effect is somewhat muted for the tris(amino)phosphine-ligated complexes **4-6** and **4-9**, which are the slowest initiating complexes of each respective series. The initiation rates of catalysts **4-7** through **4-9**, although faster than that of catalyst **4-2**, decrease with increasing piperidine substitution (Figure 4.8). These data suggest that factors other than the anticipated inductive effects associated with amine incorporation significantly contribute to phosphine donor strength and dissociation rates. Further investigations of catalyst activity, including comparison of phosphine reassociation rates and DFT studies, were required to understand the observed trends in initiation rates.

In order to gain a more complete understanding of the effect of amine substitution on the strength of phosphine binding in second-generation ruthenium catalysts, we next performed experiments to compare the phosphine reassociation rate constants (k_{-1}) at 30 °C in toluene-d_8 by ^{1}H NMR spectroscopy. Following phosphine dissociation, the 14-electron intermediate, which is equivalent for all catalysts discussed in this study, can remain in the catalytic cycle and undergo olefin binding (k_2) or the phosphine can rebind to the metal (k_{-1}). Thus, the measurable ratio k_{-1}/k_2, determined from the slope of the line of best fit according to Equation 4.1,[24] represents the relative likelihood of these two events. Because phosphine dissociation leads to the same 14-electron intermediate in each case, the propagation rate k_2 is expected to be equivalent for catalysts **4-2** and **4-4** through **4-9**. For this reason, studies to determine k_{-1}/k_2 also allow for the comparison of phosphine reassociation rates (k_{-1}) across catalysts **4-4** through **4-9**.

$$1/k_{obs} = k_{-1}[\text{free aminophosphine}]/k_1k_2[\text{olefin}] + 1/k_1 \quad (4.1)$$

We applied our previously described procedure[19a] to determine relative phosphine reassociation rates to aminophosphine ligated catalysts, in order to evaluate the effect of P–N bonds on the propensity of these ligands to rebind to the ruthenium center. An example of the results of such an experiment, which incorporates a large excess of ethyl vinyl either and the free phosphine, for catalyst **4-2** is shown in Figure 4.9. The slope of the line of best fit is an estimate for the value of $k_{-1}/(k_1k_2)$, and the reciprocal of the y-intercept provides a predicted value of the initiation rate.

The estimated values of k_{-1}/k_2 for catalysts **4-2**, and **4-4** through **4-9** were determined at 30 ºC (Table 4.3). For the morpholinophophine series (**4-4** through **4-6**), the rate of phosphine reassociation directly correlates with amine substitution. As an increasing number of P–N bonds is systematically introduced into the ligand structure of catalyst **4-2**, a gradual increase in k_{-1} is observed in the case of morpholine substitution. However, this trend is not observed for the piperidinophophine series (**4-7** through **4-9**). Instead, the kinetics of phosphine reassociation are much less varied across this series, and all estimated values of k_{-1} are similar to that of the parent catalyst **4-2**.

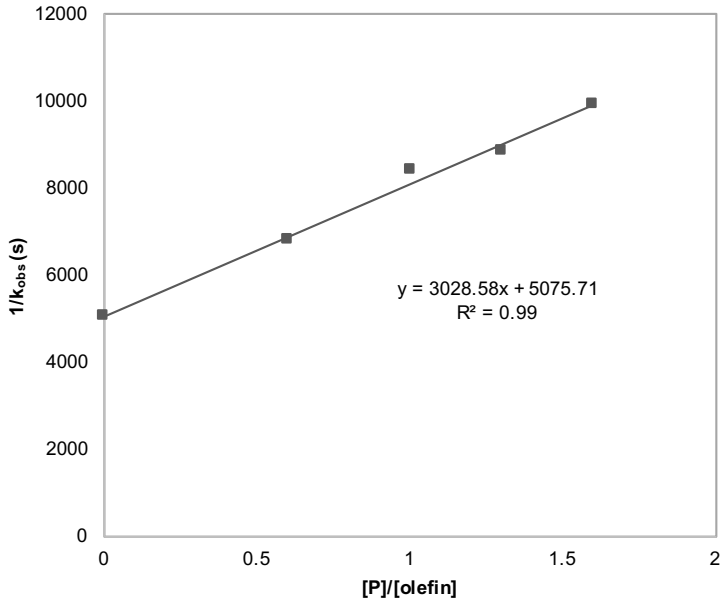

Figure 4.9. Example of $1/k_{obs}$ vs. [P]/[olefin] for catalyst **4-2** determined by ^{1}H NMR spectroscopy at 30 °C with [Ru] = 0.017 M in toluene-d_8.

Table 4.3. Estimated k_{-1}/k_2 Values for Catalysts 4-2 and 4-4 Through 4-9.[a]

catalyst	k_{-1}/k_2
4-2	0.60
4-4	1.44
4-5	1.82
4-6	3.00
4-7	0.70
4-8	0.57
4-9	0.71

[a]Measured using ^{1}H NMR spectroscopy at 30 °C with [Ru] = 0.017 M in toluene-d_8.

Discussion

The combined results from kinetics studies of complexes **4-4** through **4-9** were analyzed in detail to determine the effect of amine substituents on phosphine binding and to identify key factors that correlate to observed trends. The relative ratios of k_{-1} to k_1 were calculated for each complex, and this value k_{-1}/k_1 is used as a metric for ligand binding

strength. Thus, a stronger ligand is expected to have a higher k_{-1}/k_1, and these values provide an approximation of the relative phosphine binding constants. Normalized values for k_1, k_{-1}, and k_{-1}/k_1 are compared across each series **4-4** through **4-6** and **4-7** through **4-9** in Figure 4.10.

Increasing the number of morpholine substituents causes a steady increase in initiation rates when comparing catalysts **4-2**, **4-4**, and **4-5**. However, there is a break in trend for the tris(morpholino)phosphine, which dissociates at a significantly slower rate. In comparison, the incorporation of piperidine rings into the ligand composition of catalyst **4-2** leads to faster-initiating catalysts, but initiation rates decrease as more piperidine substituents are introduced. Despite these differences in trend, for both series, the tris(amino)phosphine ligated complexes **4-6** and **4-9** are clearly the slowest-initiating catalysts. As stated previously, the observed trend in k_{-1} for the morpholine series is not true for the piperidine series. These data suggest that k_{-1} constants do not correlate well with inductive effects related to phosphine composition.

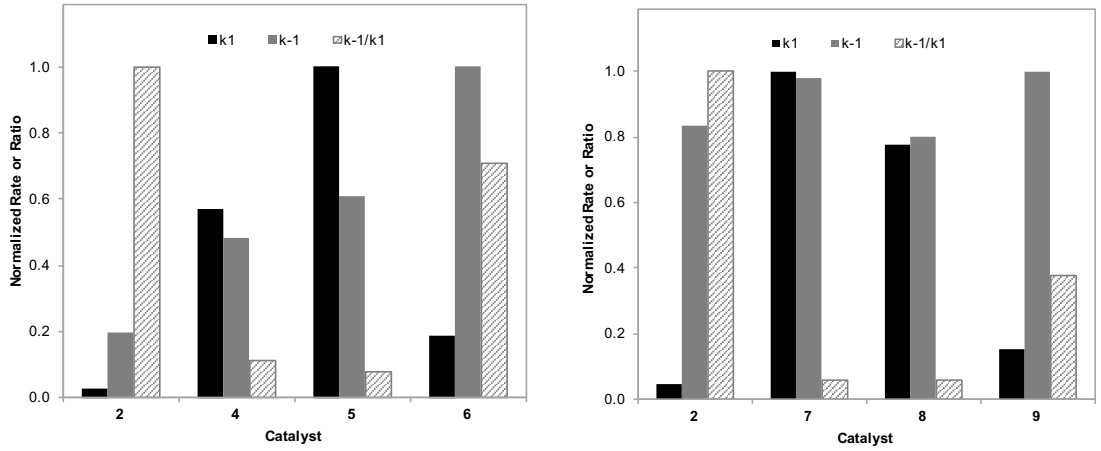

Figure 4.10. Comparisons of k_1, k_{-1}, and k_{-1}/k_1 for catalyst series bearing morpholinophosphine ligands (catalysts **4-4** through **4-6**) and piperidinophosphine ligands (catalysts **4-7** through **4-9**) as well as catalyst **4-2**. All values are normalized with respect to the highest value in each data set (denoted by shading).

The k_{-1}/k_1 ratios were compared and normalized with respect to that of catalyst **4-2**, which has a higher k_{-1}/k_1 and binding constant than catalysts **4-4** through **4-9**. Although the trends in phosphine dissociation and reassociation rates in the morpholine series differ

from those in the piperidine series, the overall trend in k_{-1}/k_1 are the same in both series of aminophosphine ligated catalysts. For both graphs shown in Figure 4.10, a U-shaped trend is observed for the phosphine binding constants as the number of P–N bonds increases from 0 (for catalyst **4-2**) to 3 (for catalysts **4-6** and **4-9**).

Computational studies were performed by collaborators[26] to gain insight into the underlying factors influencing the observed trends shown in Figure 4.10 and are briefly summarized below. These studies have confirmed that two favorable ligand conformations exist for mono- or bis(amino)phosphine ligands; the observed ligand geometry is dependent upon the nature of the substituents on the phosphine and its presence as a free or complexed ligand. In one case, a cyclohexyl ring sits in a pseudo-equatorial position, which is observed in the crystal structure of catalyst **4-7**, confirming the orientation of this cyclohexyl ring away from the benzylidene and under a mesityl group of the NHC (Figure 4.3). In the other case, an amine group is in the pseudo-equatorial position, and this ligand conformation is confirmed in the crystal structure of catalyst **4-8**, which shows a piperidine ring in this position oriented away from the benzylidene (Figure 4.4). The DFT-optimized geometries suggest that trends in phosphine dissociation energy are the result of a combination of steric effects (notably those involving the pseudo-equatorial phosphine substituent and the NHC mesityl), inductive effects (derived from the increased electronegativity of nitrogen compared to carbon), orbital overlap of the nitrogen (amine) lone pair with the Ru–P σ^* orbital, and ligand distortion energy. Computed pKa and Tolman Electronic Parameter values are in agreement with observed trends in phosphine binding constants. Furthermore, modeling of the phosphine dissociation reaction coordinate suggests that differences in ligand conformation of the catalyst ground state and transition state can have a significant influence in accelerating initiation rates.

Applications to Ring-Opening Metathesis Polymerization

The catalysts were next evaluated in ROMP, and the reaction kinetics as well as dispersities of the resulting polymers were compared. The substituted norbornene **4-18** was selected as a model monomer[25] to distinguish the catalytic activities of piperidinophosphine-ligated complexes **4-7** through **4-9** from those of catalysts **4-2** and **4-**

3, and to identify potential correlations with the previously determined rate constants (Figure 4.11). Catalyst **4-3** is known to be an efficient and effective ROMP catalyst, while use of the parent catalyst **4-2** can lead to uncontrolled molecular weights and broad molecular weight distributions.[15] Furthermore, the activity of the fast-initiating catalyst **4-17** containing a pyrrole was evaluated.

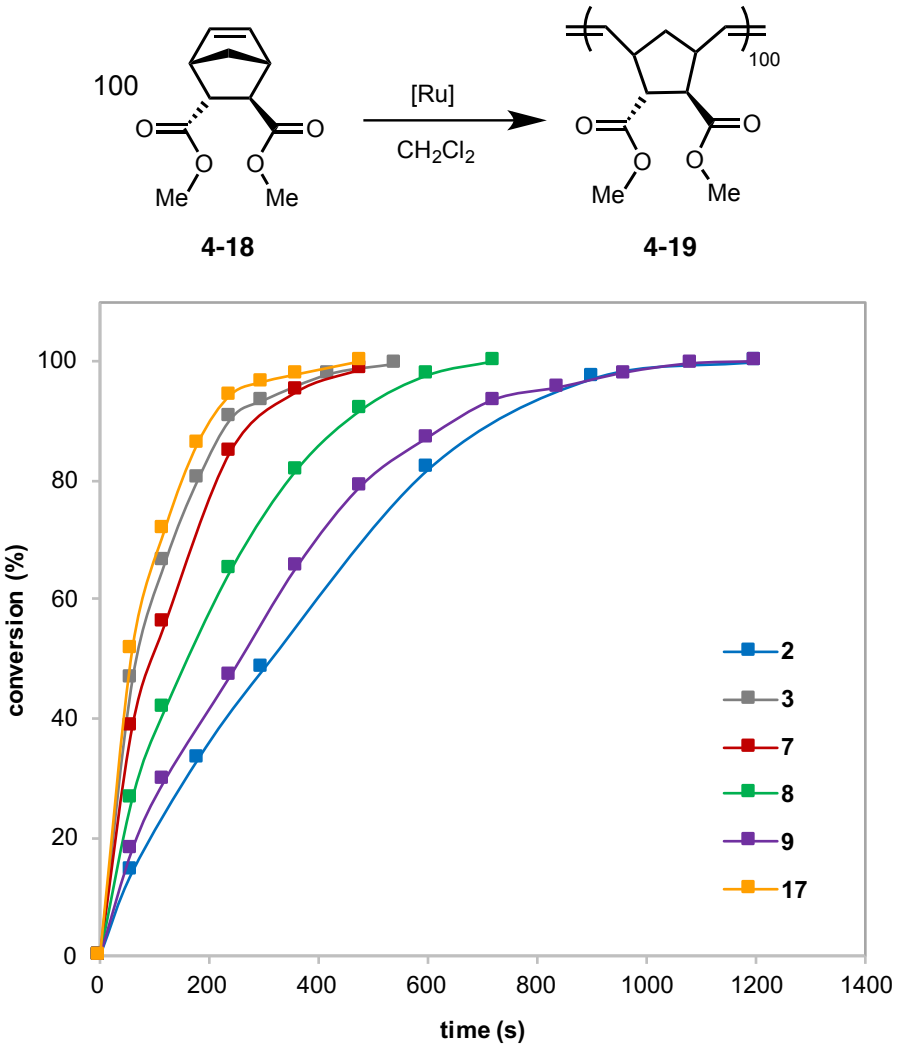

Figure 4.11. Reaction profiles of aminophosphine-ligated complexes **4-7** through **4-9** and **4-17** compared to known catalysts **4-2** and **4-3**.

The ROMP of **4-18** was performed in DCM at 30 ºC and monomer conversion was monitored by size-exclusion chromatography (SEC) and ^{1}H NMR spectroscopy. All tested aminophosphine-ligated complexes had higher rates of polymerization than the parent catalyst **4-2**, which showed the lowest rate of conversion and broadest molecular weight

distribution. For the piperidine catalyst series **4-7** through **4-9**, the rates of polymerization directly correlate with the initiation rates; while amine substitution causes an increase in the rate relative to **4-2**, the rate of polymerization increases as the number of P–N bonds (*n*) decreases, provided $n > 0$. The dispersities of the resulting polymers follow a similar trend, with catalyst **4-7** leading to narrower molecular weight distribution in comparison to **4-9**. Furthermore, although none of the catalysts in this series prove to be as efficient as **4-3** in the ROMP of **4-18**, polymerization with the fast-initiating pyrrolylphosphine-ligated catalyst **4-17** proceeded with a rate of conversion slightly higher than that of **4-3**, with similarly low polydispersity (1.03). Through the application of aminophosphine ligands, a simple change to a substituent in the phosphine in **4-2** results in the formation of much more efficient ROMP catalysts with reaction kinetics comparable to **4-3**. Studies of phosphines containing P–X bonds can aide in the design of new catalysts to broaden the scope of suitable monomer classes.

Conclusion

A new class of olefin metathesis catalysts, based on the incorporation of P–N bonds in the phosphine ligand of second-generation ruthenium complex **4-2**, was synthesized. Following facile synthesis of the aminophosphine ligands from morpholine and piperidine, the catalysts were formed in one step from complex **4-3**. The initiation rate and relative phosphine reassociation rate constants were determined, allowing for the comparison of aminophosphine ligand binding strengths. The results of kinetics studies and computational studies reveal that a combination of steric, inductive, and ligand conformational effects contribute to the observed trends in phosphine binding. Furthermore, DFT calculations suggest that ligand conformational changes in the transition state of the phosphine dissociation reaction coordinate are responsible for accelerated catalyst initiation rates. Finally, the application of the aminophosphine-ligated catalysts to ROMP demonstrates that simple changes to the substituents on the phosphine ligand can lead to a dramatic enhancement in catalyst reactivity. Investigations of novel phosphine classes, notably those containing incongruent substituents and P–X bonds, will facilitate catalyst modification and expand applications of metathesis to new olefin substrates.

Experimental Section

General Information

Solvents were dried by passing through an activated alumina column (*n*-pentane, benzene, toluene, Et_2O, and THF). Deuterated solvents were purchased from Cambridge Isotopes Laboratories, Inc. and were degassed and stored over activated 3 Å molecular sieves prior to use. C_6D_6 was purified by passage through a solvent purification column. Ethyl vinyl ether was degassed with argon or nitrogen gas prior to use. Catalyst **4-2** was obtained from Materia, Inc. The bispyridine complex **4-3** was synthesized according to literature procedure.[16] All reactions were carried out in dry glassware under an N_2 atmosphere unless otherwise indicated.

NMR spectra were measured with Varian 500 MHz, Varian 400 MHz, and Bruker 400 MHz spectrometers. High-resolution mass spectra (HRMS) were provided by the California Institute of Technology Mass Spectrometry Facility using a JEOL JMS-600H High Resolution Mass Spectrometer.

SEC data were collected using two Agilent PLgel MIXED-B 300 × 7.5 mm columns with 10 μm beads, connected to an Agilent 1260 Series pump, a Wyatt 18-angle DAWN HELEOS light scattering detector, and Optilab rEX differential refractive index detector. The mobile phase was THF.

The crystallographic measurements were performed at 100(2) K using a Bruker APEX–II CCD area detector diffractometer (Mo-K_α radiation, λ = 0.71073 Å). In each case, a specimen of suitable size and quality was selected and mounted onto a nylon loop. The structures were solved by direct methods, which successfully located most of the non-hydrogen atoms. Semi-empirical absorption corrections were applied. Subsequent refinement on F^2 using the SHELXTL/PC package (version 6.1) allowed location of the remaining non-hydrogen atoms.

Synthesis and Characterization of Aminophosphine-Ligated Complexes

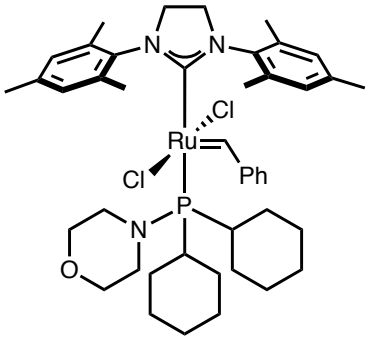

Catalyst 4-4. To a THF solution (2 mL) of the bispyridine complex **4-3** (150 mg, 0.206 mmol), was added 2.5 equivalent (146 mg, 0.516 mmol) of the appropriate phosphine ligand, 4-(dicyclohexylphosphanyl)morpholine in THF (1 mL). The resulting mixture was stirred at room temperature for 20 min. All volatiles were then removed under reduced pressure. Addition of pentane led to the formation of a pink precipitate of the desired complex, **4-4,** which was isolated by filtration through celite and dried under vacuum (129 mg, 73%). Dark brown crystals were obtained by slow Et_2O vapor diffusion into a THF solution of the title complex.

^{1}H NMR (500 MHz; C_7D_8): δ 19.51 (s, 1H), 9.14 (bs, 1H), 7.18 – 7.10 (m, 2H), 6.98 – 6.83 (m, 4H), 6.23 (bs, 2H), 3.61 – 3.17 (m, 9H), 2.76 (s, 6H), 2.65 – 2.25 (m, 10H), 2.21 (s, 3H), 1.79 (s, 3H), 1.70 – 1.39 (m, 11H), 1.23 – 0.98 (m, 8H), 0.76 (d, J = 12.5 Hz, 2H).

^{13}C NMR (101 MHz; C_6D_6): δ 296.25, 220.71 (d, $^2J_{C\text{-}P}$ = 84.8 Hz), 151.99, 139.39, 138.61, 137.63, 137.23, 135.59, 130.31, 129.39, 68.02, 52.11, 51.08, 49.37, 35.39 (d, $J_{C\text{-}P}$ = 19.6 Hz), 29.18, 28.74, 28.02, 27.93, 27.84, 27.72, 26.59, 21.23, 21.03, 20.57, 19.00.

^{31}P{^{1}H} NMR (162 MHz; C_6D_6): δ 92.4 (s).

MS (FAB) *m/z* (M^++H) calcd for $C_{44}H_{63}ON_3RuPCl_2$: 852.3130, found: 852.3153.

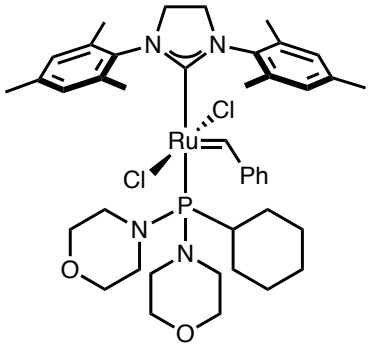

Catalyst 4-5. To a THF solution (2 mL) of the bispyridine complex **4-3** (100 mg, 0.138 mmol), was added 1.2 equivalent (47 mg, 0.165 mmol) of the appropriate phosphine ligand, 4,4'-(cyclohexylphosphanediyl)dimorpholine in THF (1 mL). The resulting mixture was stirred at room temperature for 20 min. All volatiles were then removed under reduced pressure. Addition of pentane led to the formation of a pink precipitate of the desired complex, **4-5,** which was isolated by filtration through celite and dried under vacuum (79 mg, 67%).

^{1}H NMR (400 MHz; C_6D_6): δ 19.40 (s, 1H), 8.17 (bs, 2H), 7.12 (t, J = 7.6 Hz, 1H), 7.06 (s, 2H), 6.93 (t, J = 7.6 Hz, 2H), 6.21 (bs, 2H), 3.50 – 3.21 (m, 12H), 3.09 (t, J = 12.3 Hz, 1H), 2.86 (bs, 9H), 2.66 – 2.40 (m, 13H), 1.79 (s, 3H), 1.67 – 1.51 (m, 6H), 1.17 – 1.10 (m, 2H), 0.99 (tt, J = 12.6 Hz, J = 3.5 Hz, 1H), 0.77 (q, J = 12.4 Hz, 2H).

^{13}C NMR (101 MHz; C_6D_6): δ 293.55, 221.10 (d, $^{2}J_{C\text{-}P}$ = 89.0 Hz), 151.59, 139.44, 139.26, 137.69, 137.49, 136.93, 135.03, 131.06, 130.55, 129.37, 67.64, 52.14, 50.97, 47.16, 37.38 (d, $J_{C\text{-}P}$ = 23.7 Hz), 27.66, 27.48, 27.36, 27.25, 21.23, 21.00, 20.63, 18.92.

^{31}P{^{1}H} NMR (161.8 MHz; C_6D_6): δ 131.9 (s).

MS (FAB) *m/z* (M^+) calcd for $C_{42}H_{59}O_2N_4RuPCl_2$: 854.2797, found: 854.2834.

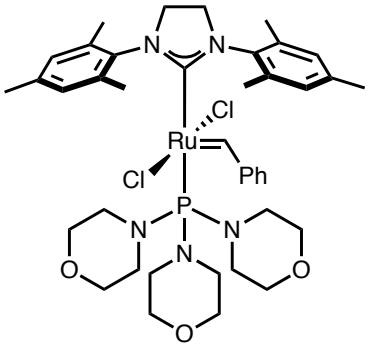

Catalyst 4-6. To a THF solution (2 mL) of the bispyridine complex **4-3** (173 mg, 0.238 mmol), was added 1.2 equivalent (82 mg, 0.286 mmol) of the appropriate phosphine ligand, trimorpholinophosphane in THF (1 mL). The resulting mixture was stirred at room temperature for 20 min. All volatiles were then removed under reduced pressure. Addition of pentane led to the formation of a pink precipitate of the desired complex, **4-6,** which was isolated by filtration through celite and dried under vacuum (157 mg, 77%).

^{1}H NMR (500 MHz; C_7D_8): δ 19.44 (s, 1H), 8.03 (s, 2H), 7.12 (s, 1H), 6.93 – 6.85 (m, 4H), 6.16 (s, 2H), 3.46 – 3.37 (m, 2H), 3.33 – 3.21 (m, 14H), 2.75 (s, 6H), 2.68 (q, J = 4.7 Hz, 12H), 2.35 (s, 6H), 2.28 (s, 3H), 1.77 (s, 3H).

^{13}C NMR (101 MHz; C_6D_6): δ 298.46, 219.58 (d, $^{2}J_{C\text{-}P}$ = 107.3 Hz), 151.81, 139.51, 139.07, 137.61, 137.52, 137.09, 135.33, 130.95, 130.24, 129.40, 128.80, 128.59, 67.60 (d, $J_{C\text{-}P}$ = 5.8 Hz), 51.90 (d, $J_{C\text{-}P}$ = 4.7 Hz), 50.91 (d, $J_{C\text{-}P}$ = 2.9 Hz), 46.86 (d, $J_{C\text{-}P}$ = 3.0 Hz), 21.14, 20.97, 20.65, 18.92.

^{31}P{^{1}H} NMR (162 MHz; C_6D_6): δ 116.7 (s).

MS (FAB) *m/z* (M^+) calcd for $C_{40}H_{56}O_3N_5RuPCl_2$: 857.2542, found: 857.2517.

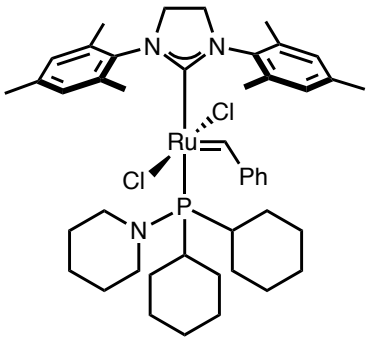

Catalyst 4-7. To a THF solution (2 mL) of the bispyridine complex **4-3** (100 mg, 0.138 mmol), was added 1.2 equivalent (46.5 mg, 0.165 mmol) of the appropriate phosphine ligand,

1-(dicyclohexylphosphanyl)piperidine in THF (1 mL). The resulting mixture was stirred at room temperature for 20 min. All volatiles were then removed under reduced pressure. Addition of pentane led to the formation of a pink precipitate of the desired complex, **4-7,** which was isolated by filtration through celite and dried under vacuum (93 mg, 80%). Dark brown crystals were obtained by slow Et_2O vapor diffusion into a benzene solution of the title complex.

^{1}H NMR (400 MHz; C_6D_6): δ 19.70 (s, 1H), 9.37 (bs, 1H), 7.19 – 7.12 (m, 2H), 7.06 – 6.89 (m, 4H), 6.80 – 5.56 (m, 2H), 3.50 – 3.14 (m, 5H), 3.08 – 2.75 (m, 7H), 2.73 – 2.55 (m, 7H), 2.21 (s, 3H), 1.82 (s, 3H), 1.79 – 1.04 (m, 26H), 0.95 – 0.77 (m, 2H).

^{13}C NMR (101 MHz; C_6D_6): δ 296.05, 221.10 (d, $^2J_{C\text{-}P}$ = 83.5 Hz), 152.07, 139.43, 138.29, 137.75, 137.54, 137.27, 135.87, 130.29, 129.39, 128.30, 128.06, 127.82, 52.19, 51.10, 50.31, 35.88 (d, $J_{C\text{-}P}$ = 19.9 Hz), 29.31, 28.86, 28.12, 28.03, 27.94, 27.81, 27.45, 27.40, 26.68, 25.18, 21.14 (d, $J_{C\text{-}P}$ = 18.0 Hz), 20.60, 19.07.

^{31}P{^{1}H} NMR (161.8 MHz; C_6D_6): δ 92.1 (s).

MS (FAB) *m/z* (M^+) calcd for $C_{45}H_{64}N_3RuPCl_2$: 849.3259, found: 849.3267.

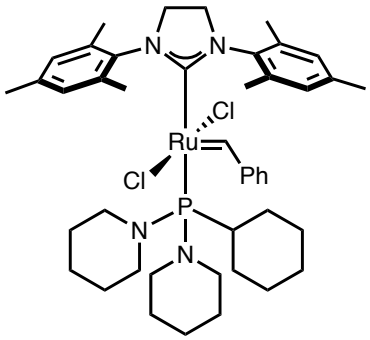

Catalyst 4-8. To a THF solution (2 mL) of the bispyridine complex **4-3** (130 mg, 0.179 mmol), was added 1.2 equivalent (210 mg, 0.744 mmol) of the appropriate phosphine ligand, 1,1'-(cyclohexylphosphanediyl)dipiperidine in THF (1 mL). The resulting mixture was stirred at room temperature for 20 min. All volatiles were then removed under reduced pressure. Addition of pentane led to the formation of a pink precipitate of the desired complex, **4-8,** which was isolated by filtration through celite and dried under vacuum (82 mg, 54%). Dark brown crystals were obtained by slow Et_2O vapor diffusion into a THF solution of the title complex.

^{1}H NMR (400 MHz; C_6D_6): δ 19.47 (s, 1H), 8.46 (bs, 1H), 7.19 – 7.13 (m, 2H), 7.01 (t, J = 7.7 Hz, 2H), 6.94 (s, 2H), 6.77 – 5.44 (m, 2H), 3.44 – 3.17 (m, 4H), 3.04 – 2.75 (m, 11H), 2.75 – 2.56 (s, 6H), 2.22 (s, 3H), 1.82 (s, 3H), 1.69 – 1.50 (m, 5H), 1.41 (s, 11H), 1.28 (s, 7H), 1.08 – 0.75 (m, 3H).

^{13}C NMR (101 MHz; C_6D_6): δ 291.90, 222.33 (d, $^{2}J_{C\text{-}P}$ = 87.8 Hz), 151.79, 139.65, 138.08, 137.96, 137.35, 136.97, 135.91, 131.17, 130.35, 129.36, 128.30, 128.06, 127.82, 52.34, 52.30, 50.97, 47.68, 38.15 (d, $J_{C\text{-}P}$ = 23.9 Hz), 27.80, 27.63, 27.50, 27.16, 27.11, 25.77, 25.22, 21.12 (d, $J_{C\text{-}P}$ = 12.9 Hz), 20.64, 19.07.

^{31}P{^{1}H} NMR (161.8 MHz; C_6D_6): δ 133.0 (s).

MS (FAB) *m/z* (M^+) calcd for $C_{44}H_{63}N_4RuPCl_2$: 850.3211, found: 850.3212.

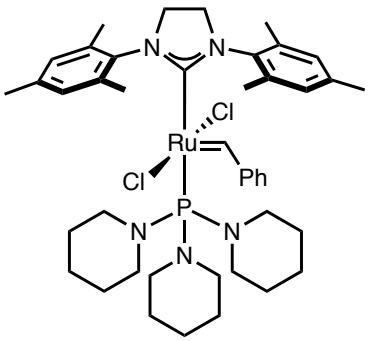

Catalyst 4-9. To a THF solution (2 mL) of the bispyridine complex **4-3** (100 mg, 0.138 mmol), was added 1.5 equivalent (58.7 mg, 0.207 mmol) of the appropriate phosphine ligand, tri(piperidin-1-yl)phosphane in THF (1 mL). The resulting mixture was stirred at room temperature for 20 min. All volatiles were then removed under reduced pressure. Addition of pentane led to the formation of a pink precipitate of the desired complex, **4-9,** which was isolated by filtration through celite and dried under vacuum (92 mg, 78%). Dark brown crystals were obtained by slow pentane vapor diffusion into a THF solution of the title complex.

^{1}H NMR (400 MHz; C_6D_6): δ 19.70 (s, 1H), 8.30 (bs, 2H), 7.21 – 7.17 (m, 1H), 7.04 – 6.98 (m, 2H), 6.93 (s, 2H), 6.25 (s, 2H), 3.43 – 3.16 (m, 4H), 2.86 (s, 6H), 2.85 – 2.77 (m, 12H), 2.48 (s, 6H), 2.22 (s, 3H), 1.82 (s, 3H), 1.48 – 1.34 (m, 6H), 1.29 (m, 12H).

^{13}C NMR (101 MHz; C_6D_6): δ 296.09, 221.30 (d, $^{2}J_{C\text{-}P}$ = 105.2 Hz), 152.12, 139.67, 138.04, 137.89, 137.38, 137.17, 136.04, 131.22, 130.18, 129.37, 52.07 (d, $J_{C\text{-}P}$ = 4.9 Hz),

50.94, 47.19 (d, $J_{C\text{-}P}$ = 4.4 Hz), 27.08 (d, $J_{C\text{-}P}$ = 4.6 Hz), 25.70, 21.09 (d, $J_{C\text{-}P}$ = 10.4 Hz), 20.72, 19.10.

$^{31}P\{^{1}H\}$ NMR (161.8 MHz; C_6D_6): δ 118.7 (s).

MS (FAB) *m/z* (M^+) calcd for $C_{43}H_{62}N_5RuPCl_2$: 851.3164, found: 851.3178.

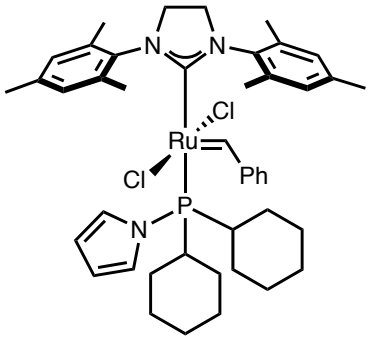

Catalyst 4-17. To a THF solution (2 mL) of the bispyridine complex **4-3** (100 mg, 0.138 mmol), was added 2.0 equivalent (73 mg, 0.275 mmol) of the appropriate phosphine ligand, 1-(dicyclohexylphosphanyl)-1*H*-pyrrole in THF (1 mL). The resulting mixture was stirred at room temperature for 20 min. All volatiles were then removed under reduced pressure. Addition of pentane led to the formation of a pink precipitate of the desired complex, **4-17,** which was isolated by filtration through celite and dried under vacuum (110 mg, 96%). Dark brown crystals were obtained by slow pentane vapor diffusion into a THF solution of the title complex.

^{1}H NMR (400 MHz; C_6D_6): δ 19.82 (s, 1H), 8.24 (bs, 2H), 7.10 (t, *J* = 7.2 Hz, 1H), 6.94 – 6.90 (m, 4H), 6.74 (q, *J* = 2.2 Hz, 2H), 6.21 (s, 4H), 3.36 (dt, *J* = 2.3 Hz, *J* = 10.6 Hz, 2H), 3.23 (dt, *J* = 2.3 Hz, *J* = 10.6 Hz, 2H), 2.81 (s, 6H), 2.44 (s, 6H), 2.19 (s, 3H), 1.80 (s, 3H), 1.63 (d, *J* = 10.8 Hz, 2H), 1.54 (d, *J* = 11.0 Hz, 2H), 1.46 – 1.35 (m, 6H), 1.27 (qt, *J* = 12.7 Hz, *J* = 3.4 Hz, 2H), 1.12 – 0.91 (m, 6H), 0.52 (qt, *J* = 12.7 Hz, *J* = 3.4 Hz, 2H).

^{13}C NMR (101 MHz; C_6D_6): δ 301.30, 219.39 (d, $^{2}J_{C\text{-}P}$ = 89.9 Hz), 151.99, 139.40, 138.57, 137.86, 137.37, 137.25, 135.47, 131.50, 130.28, 129.44, 128.97, 128.59, 125.32 (d, $J_{C\text{-}P}$ = 2.8 Hz), 110.26 (d, $J_{C\text{-}P}$ = 4.6 Hz), 52.09 (d, $J_{C\text{-}P}$ = 4.1 Hz), 51.11 (d, $J_{C\text{-}P}$ = 2.1 Hz), 35.81 (d, $J_{C\text{-}P}$ = 18.6 Hz), 28.30 (d, $J_{C\text{-}P}$ = 4.3 Hz), 27.85 (d, $J_{C\text{-}P}$ = 2.8 Hz), 27.53, 27.44, 27.40, 27.27, 25.99, 21.25, 21.01, 20.58, 18.95.

$^{31}P\{^{1}H\}$ NMR (162 MHz; C_6D_6): δ 92.3 (s).

MS (FAB) *m/z* (M^+) calcd for $C_{44}H_{58}N_3RuPCl_2$: 831.2789, found: 831.2761.

Initiation Rate Studies

The ruthenium benzylidene complex was dissolved in toluene-d_8 (600 μL, 0.017 M) in an NMR tube fitted with a septum cap sealed under an N_2 atmosphere. To this NMR tube was injected neat ethyl vinyl ether (30 equiv.) using a micro-syringe under inert atmosphere. The tube was inverted and immediately loaded into a 500 MHz ^{1}H NMR spectrometer pre-warmed to 30 °C, at which point the first-order depletion of the benzylidene Ru=C*H*Ph signal was monitored.

Estimation of k_{-1}/k_2

A solution of toluene-d_8 (600 μL) containing the ruthenium benzylidene complex (0.017 M) and free aminophosphine ([P]/[ethyl vinyl ether] = 0.6, 1.0, 1.6) was added to an NMR tube fitted with a septum cap and sealed under an N_2 atmosphere. To this NMR tube was injected neat ethyl vinyl ether (15 μL) using a micro-syringe under inert atmosphere. The tube was inverted and immediately loaded into a 500 MHz ^{1}H NMR spectrometer pre-warmed to 30 °C, at which point the first-order depletion of the benzylidene Ru=C*H*Ph signal was monitored. The values of $1/k_{obs}$ were plotted vs. [P]/[ethyl vinyl ether], including the data from initiation rate studies where [P]/[olefin] = 0. The graph for each catalyst is shown below. The ratio of k_{-1}/k_2 was calculated by dividing the slope of the line of best fit by the y-intercept.

Catalyst 4-4

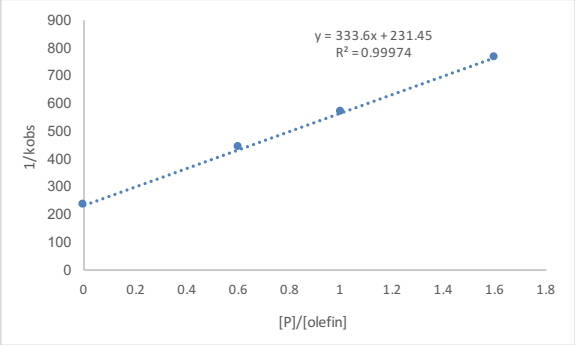

Catalyst 4-5

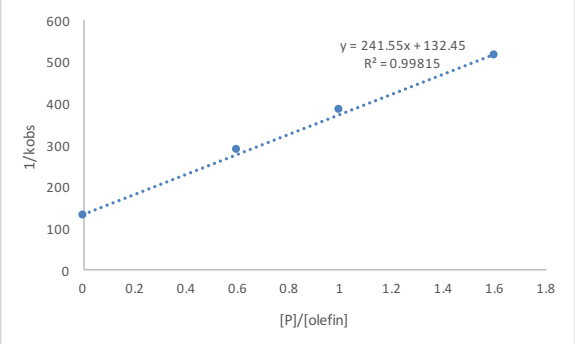

Catalyst 4-6

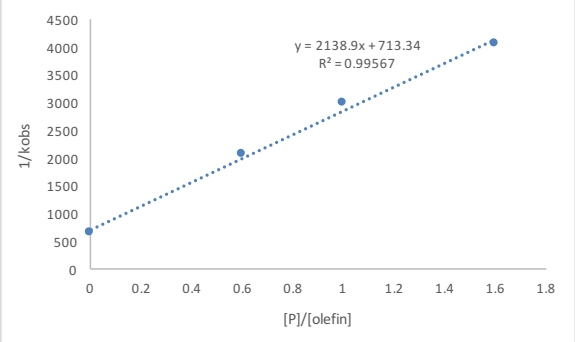

Catalyst 4-7

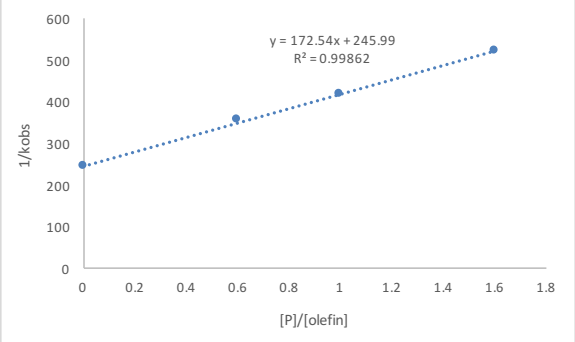

Catalyst 4-8

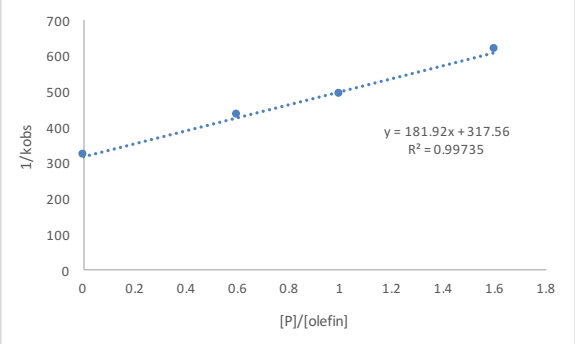

Catalyst 4-9

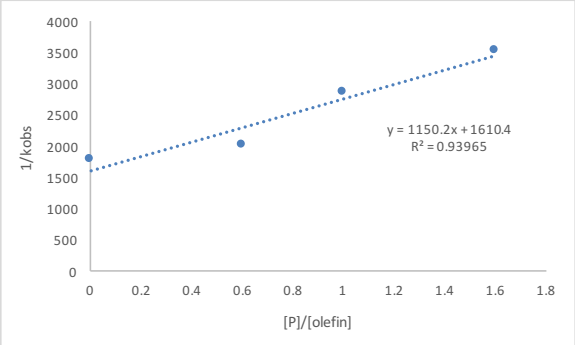

Evaluation of Selected Catalysts in ROMP

A solution of **4-18** (21.0 mg, 0.100 mmol) was prepared in 2 mL of dichloromethane at 298 K. While stirring, the polymerization was initiated by addition of a CH_2Cl_2 solution of catalyst (0.0500 M, 20.0 µL, 0.100 µmol). During the course of the reaction, aliquots (~50 µL) were extracted and quenched in separate vials containing a large excess of ethyl vinyl ether (0.1 mL) in THF (0.9 mL). The quenched reaction mixtures were analyzed by SEC and ^{1}H NMR spectroscopy to determine norbornene conversion, molecular weight (M_n), and dispersity ($Đ$).

Table 4.4. Molecular Weights and Dispersities of Polymers 4-19.

Catalyst	M_n (kDa)	*Đ*
4-3	23.1	1.02
4-2	96.1	1.50
4-7	46.3	1.17
4-8	55.2	1.22
4-9	70.1	1.41
4-17	25.9	1.03

Crystallographic Data

Table 4.5. Crystal Data and Structure Analysis Details for Catalyst 4-7.
(Structure shown in Figure 4.3)

Empirical formula	C100 H144 Cl4 N6 O P2 Ru2	
Formula weight	1852.08	
Crystal shape	block	
Crystal color	brown	
Crystal size	0.050 x 0.080 x 0.100 mm^3	
Data Collection		
Preliminary photograph(s)	rotation	
Type of diffractometer	CCD area detector	
Wavelength	0.71073 Å	
Data collection temperature	100(2) K	
Theta range for 9838 reflections used		
in lattice determination	4.655 to 65.411º	
Unit cell dimensions	a = 12.5478(5) Å	α= 90º
	b = 14.1495(6) Å	β= 92.828(2)º
	c = 26.7547(11) Å	γ = 90º
Volume	4744.4(3) $Å^3$	
Z	2	
Crystal system	monoclinic	

Space group	P $2_1/c$
Density (calculated)	1.296 g/cm^3
F(000)	1960
Theta range for data collection	1.6 to 37.7º
Completeness to theta = 25.242º	100.0%
Index ranges	$-21 \leq h \leq 21$, $-24 \leq k \leq 23$, $-45 \leq l \leq 45$
Reflections collected	180275
Independent reflections	24676 [R_{int}= 0.0782]
Reflections > 2s(I)	17555
Average s(I)/(net I)	0.0619
Absorption coefficient	0.51 mm^{-1}
Absorption correction	Semi-empirical from equivalents
Max. and min. transmission	0.6876 and 0.6876
Structure Solution and Refinement	
Hydrogen placement	geom
Refinement method	Full-matrix least-squares on F^2
Data / restraints / parameters	24676 / 17 / 520
Treatment of hydrogen atoms	constr
Goodness-of-fit on F^2	1.07
Final R indices [I>2s(I), 17555 reflections]	R1 = 0.0561, *w*R2 = 0.1214
R indices (all data)	R1 = 0.0959, *w*R2 = 0.1363
Type of weighting scheme used	calc
Max shift/error	0.001
Average shift/error	0.000
Extinction coefficient	n/a
Largest diff. peak and hole	2.49 and -1.63 e/Å^{-3}
Programs Used	
Structure refinement	SHELXL-2013 (Sheldrick, 2013)

Table 4.6. Crystal Data and Structure Analysis Details for Catalyst 4-8.
(Structure shown in Figure 4.4)

Empirical formula	C100 H152 Cl4 N8 O3 P2 Ru2 Si0	
Formula weight	1920.17	
Crystal shape	block	
Crystal color	brown	
Crystal size	0.020 x 0.150 x 0.150 mm^3	
Data Collection		
Preliminary photograph(s)	rotation	
Type of diffractometer	CCD area detector	
Wavelength	0.71073 Å	
Data collection temperature	100(2) K	
Theta range for 9872 reflections used		
in lattice determination	4.877 to 60.270º	
Unit cell dimensions	a = 12.582(4) Å	α= 90º
	b = 14.694(4) Å	β= 102.711(9)º
	c = 26.929(9) Å	γ = 90º
Volume	4856(3) $Å^3$	
Z	2	
Crystal system	monoclinic	
Space group	P $2_1/n$	
Density (calculated)	1.313 g/cm^3	
F(000)	2036	
Theta range for data collection	2.1 to 31.3º	
Completeness to theta = 25.242º	99.9%	
Index ranges	$-18 \le h \le 17$, $-21 \le k \le 21$, $-39 \le l \le 39$	
Reflections collected	109331	
Independent reflections	14689 [R_{int}= 0.0561]	
Reflections > 2s(I)	10910	
Average s(I)/(net I)	0.0580	

Absorption coefficient	0.51 mm^{-1}
Absorption correction	Semi-empirical from equivalents
Max. and min. transmission	1.0000 and 0.9533
Structure Solution and Refinement	
Hydrogen placement	geom
Refinement method	Full-matrix least-squares on F^2
Data / restraints / parameters	14689 / 2 / 538
Treatment of hydrogen atoms	constr
Goodness-of-fit on F^2	1.04
Final R indices [I>2s(I), 10910 reflections]	R1 = 0.0645, *w*R2 = 0.1465
R indices (all data)	R1 = 0.1013, *w*R2 = 0.1643
Type of weighting scheme used	calc
Max shift/error	0.001
Average shift/error	0.000
Extinction coefficient	n/a
Largest diff. peak and hole	2.26 and -1.25 e/$Å^{-3}$
Programs Used	
Structure refinement	SHELXL-2013 (Sheldrick, 2013)

Table 4.7. Crystal Data and Structure Analysis Details for Catalyst 4-9.
(Structure shown in Figure 4.5)

Empirical formula	C43 H62 Cl2 N5 P Ru
Formula weight	851.91
Crystal shape	block
Crystal color	brown
Crystal size	0.030 x 0.120 x 0.140 mm^3
Data Collection	
Preliminary photograph(s)	rotation
Type of diffractometer	CCD area detector
Wavelength	0.71073 Å

Data collection temperature	100(2) K	
Theta range for 9656 reflections used		
in lattice determination	5.207 to 62.321º	
Unit cell dimensions	a = 12.685(4) Å	α= 90º
	b = 14.502(4) Å	β= 99.043(12)º
	c = 22.983(7) Å	γ = 90º
Volume	4176(2) $Å^3$	
Z	4	
Crystal system	monoclinic	
Space group	P $2_1/c$	
Density (calculated)	1.355 g/cm^3	
F(000)	1792	
Theta range for data collection	2.3 to 33.6º	
Completeness to theta = 25.000º	99.9%	
Index ranges	$-18 \le h \le 19$, $-22 \le k \le 22$, $-34 \le l \le 30$	
Reflections collected	100488	
Independent reflections	15279 [R_{int}= 0.0733]	
Reflections > 2s(I)	10188	
Average s(I)/(net I)	0.0882	
Absorption coefficient	0.58 mm^{-1}	
Absorption correction	Semi-empirical from equivalents	
Max. and min. transmission	0.9954 and 0.9389	
Structure Solution and Refinement		
Hydrogen placement	geom	
Refinement method	Full-matrix least-squares on F^2	
Data / restraints / parameters	15279 / 138 / 704	
Treatment of hydrogen atoms	constr	
Goodness-of-fit on F^2	1.16	
Final R indices [I>2s(I), 10188 reflections]	R1 = 0.0820, *w*R2 = 0.1464	
R indices (all data)	R1 = 0.1400, *w*R2 = 0.1609	
Type of weighting scheme used	calc	

Max shift/error	0.001
Average shift/error	0.000
Extinction coefficient	n/a
Largest diff. peak and hole	1.13 and -1.50 e/Å^{-3}
Programs Used	
Structure refinement	SHELXL-2013 (Sheldrick, 2013)

Table 4.8. Crystal Data and Structure Analysis Details for Catalyst 4-17.
(Structure shown in Figure 4.6)

Empirical formula	C44 H58 Cl2 N3 P Ru	
Formula weight	831.87	
Crystal shape	block	
Crystal color	brown	
Crystal size	0.050 x 0.090 x 0.100 mm^3	
Data Collection		
Preliminary photograph(s)	rotation	
Type of diffractometer	CCD area detector	
Wavelength	0.71073 Å	
Data collection temperature	100(2) K	
Theta range for 9838 reflections used in lattice determination	4.655 to 65.411º	
Unit cell dimensions	a = 12.1351(9) Å	α= 90º
	b = 14.8021(10) Å	β= 98.642(3)º
	c = 22.944(2) Å	γ = 90º
Volume	4074.6(6) Å^3	
Z	4	
Crystal system	monoclinic	
Space group	P $2_1/c$	
Density (calculated)	1.356 g/cm^3	
F(000)	1744	

Theta range for data collection	2.2 to 33.2º
Completeness to theta = 25.242º	99.9%
Index ranges	$-17 \leq h \leq 18$, $-21 \leq k \leq 22$, $-34 \leq l \leq 34$
Reflections collected	125473
Independent reflections	14290 [R_{int}= 0.1065]
Reflections > 2s(I)	9560
Average s(I)/(net I)	0.1029
Absorption coefficient	0.59 mm^{-1}
Absorption correction	Semi-empirical from equivalents
Max. and min. transmission	0.7466 and 0.7034
Structure Solution and Refinement	
Hydrogen placement	geom
Refinement method	Full-matrix least-squares on F^2
Data / restraints / parameters	14290 / 0 / 460
Treatment of hydrogen atoms	constr
Goodness-of-fit on F^2	1.08
Final R indices [I>2s(I), 9560 reflections]	R1 = 0.0641, *w*R2 = 0.1225
R indices (all data)	R1 = 0.1239, *w*R2 = 0.1426
Type of weighting scheme used	calc
Max shift/error	0.001
Average shift/error	0.000
Extinction coefficient	n/a
Largest diff. peak and hole	2.73 and -0.90 e/$Å^{-3}$
Programs Used	
Structure refinement	SHELXL-2013 (Sheldrick, 2013)

^{1}H and ^{13}C NMR Spectra

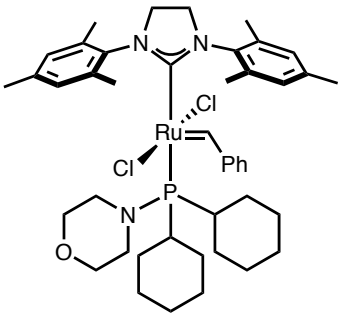
N
N
Cl
Ru
Cl
Ph
P
N
O

4-4

1.00
0.83
2.02
4.67
1.82
9.02
5.99
10.27
3.81
3.16
10.70
8.16
1.98
24
22
20
18
16
14
12
10
8
6
4
2
0

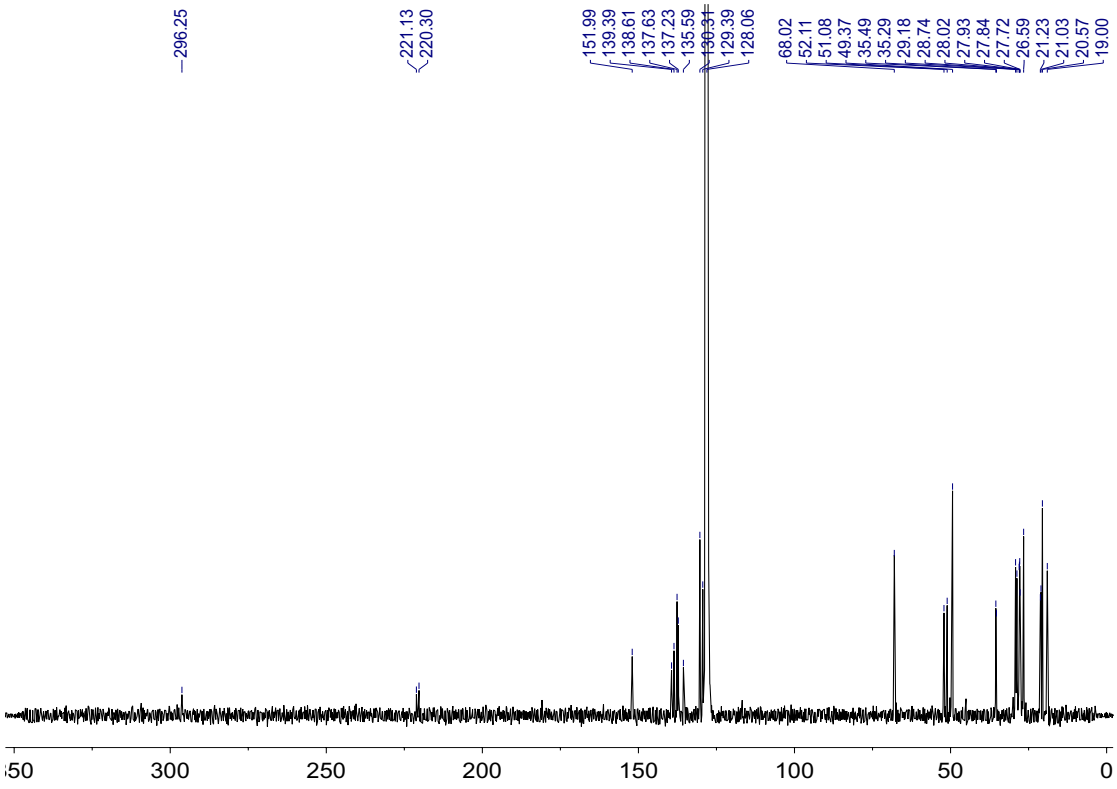
296.25
221.13
220.30
151.99
139.39
138.61
137.63
137.23
135.59
130.31
129.39
128.06
68.02
52.11
51.08
49.37
35.49
35.29
29.18
28.74
28.02
27.93
27.84
27.72
26.59
21.23
21.03
20.57
19.00
300
250
200
150
100
50
0

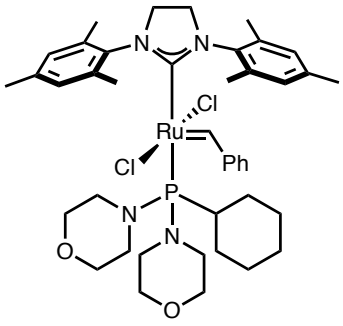
N
N
Cl
Ru
Cl
Ph
P
N
N
O
O

4-5

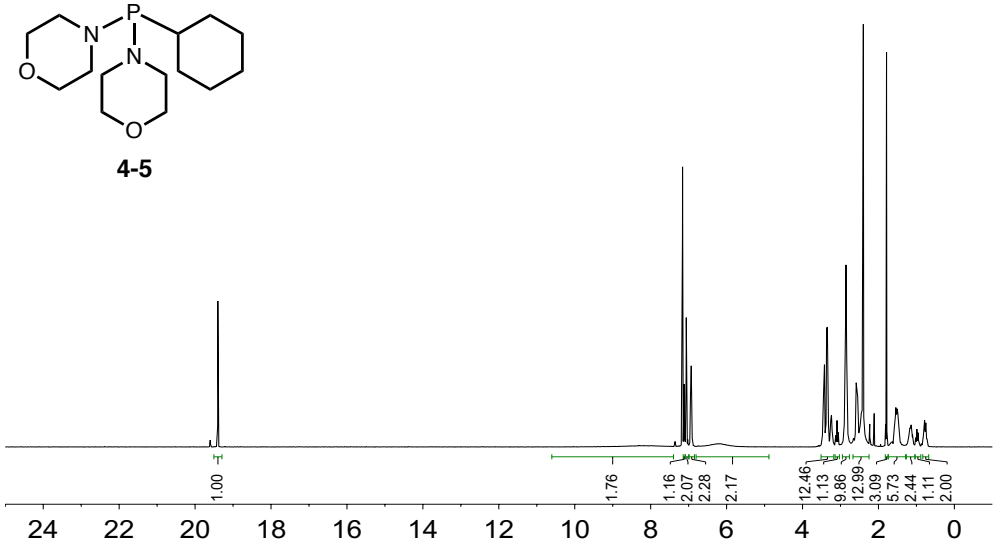
1.00
1.76
1.16
2.07
2.28
2.17
12.46
1.13
9.86
12.99
3.09
5.73
2.44
1.11
2.00
24
22
20
18
16
14
12
10
8
6
4
2
0

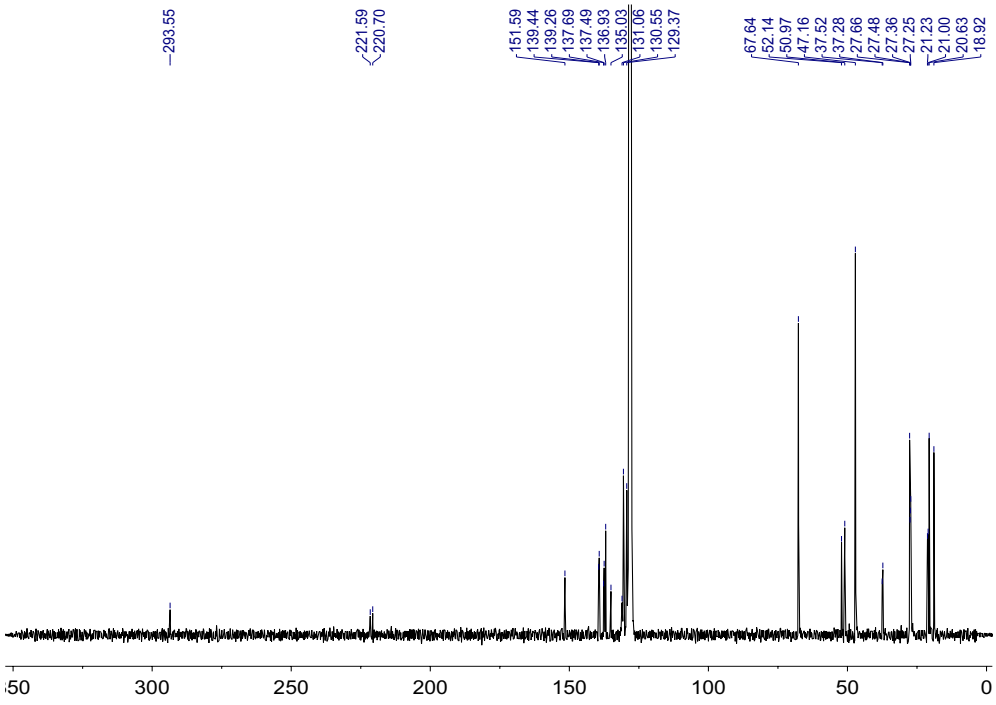
293.55
221.59
220.70
151.59
139.44
139.26
137.69
137.49
136.93
135.03
131.06
130.55
129.37
67.64
52.14
50.97
47.16
37.52
37.28
27.66
27.48
27.36
27.25
21.23
21.00
20.63
18.92
300
250
200
150
100
50
0

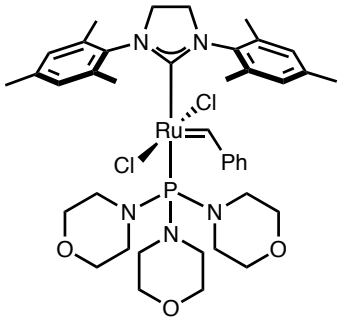
N
N
Cl
Ru
Cl
Ph
P
N
N
N
O
O
O

4-6

1.00
1.64
1.73
4.11
1.72
2.47
15.37
6.50
13.15
6.27
3.18
3.06
24
22
20
18
16
14
12
10
8
6
4
2
0

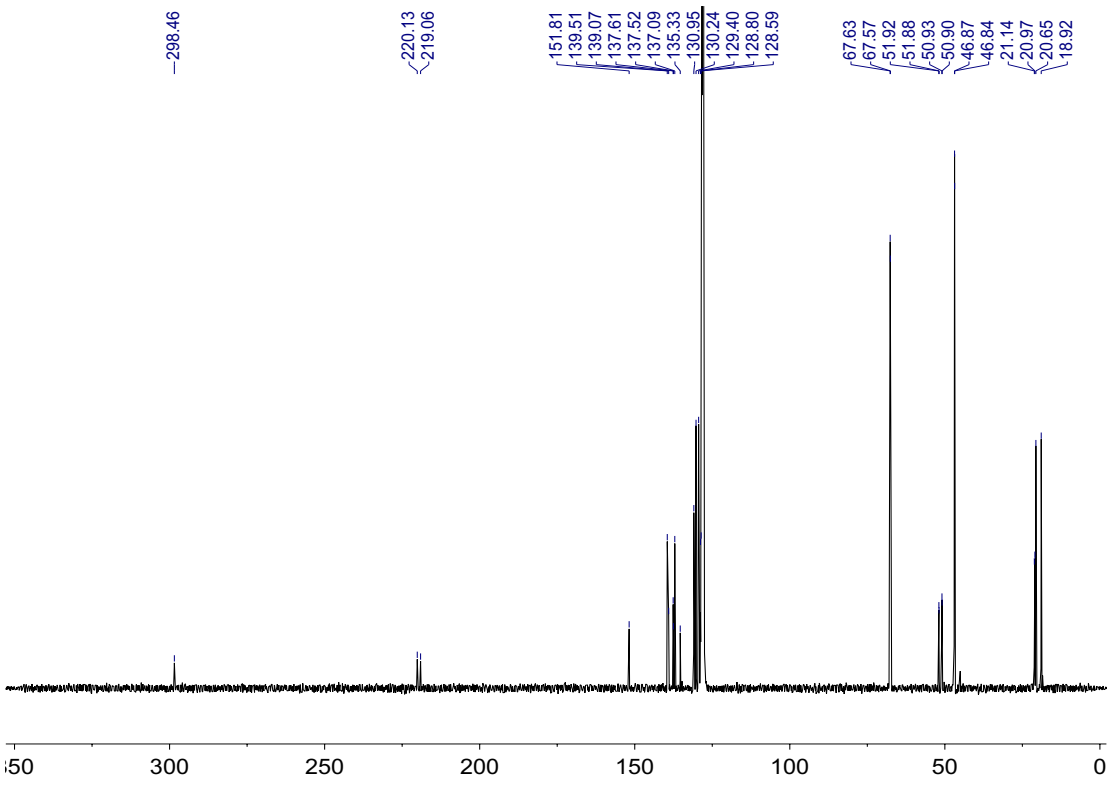
298.46
220.13
219.06
151.81
139.51
139.07
137.61
137.52
137.09
135.33
130.95
130.24
129.40
128.80
128.59
67.63
67.57
51.92
51.88
50.93
50.90
46.87
46.84
21.14
20.97
20.65
18.92
300
250
200
150
100
50
0

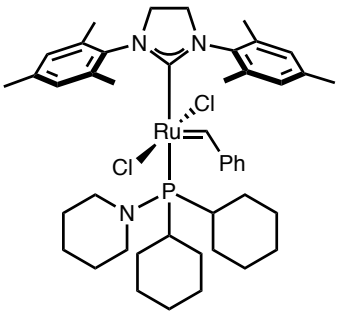
N
N
Cl
Ru
Cl
Ph
P
N

4-7

1.00
0.48
1.29
0.31
4.20
1.65
4.99
7.83
6.97
3.83
3.89
26.64
1.95
5 24 23 22 21 20 19 18 17 16 15 14 13 12 11 10 9 8 7 6 5 4 3 2 1
f1 (ppm)

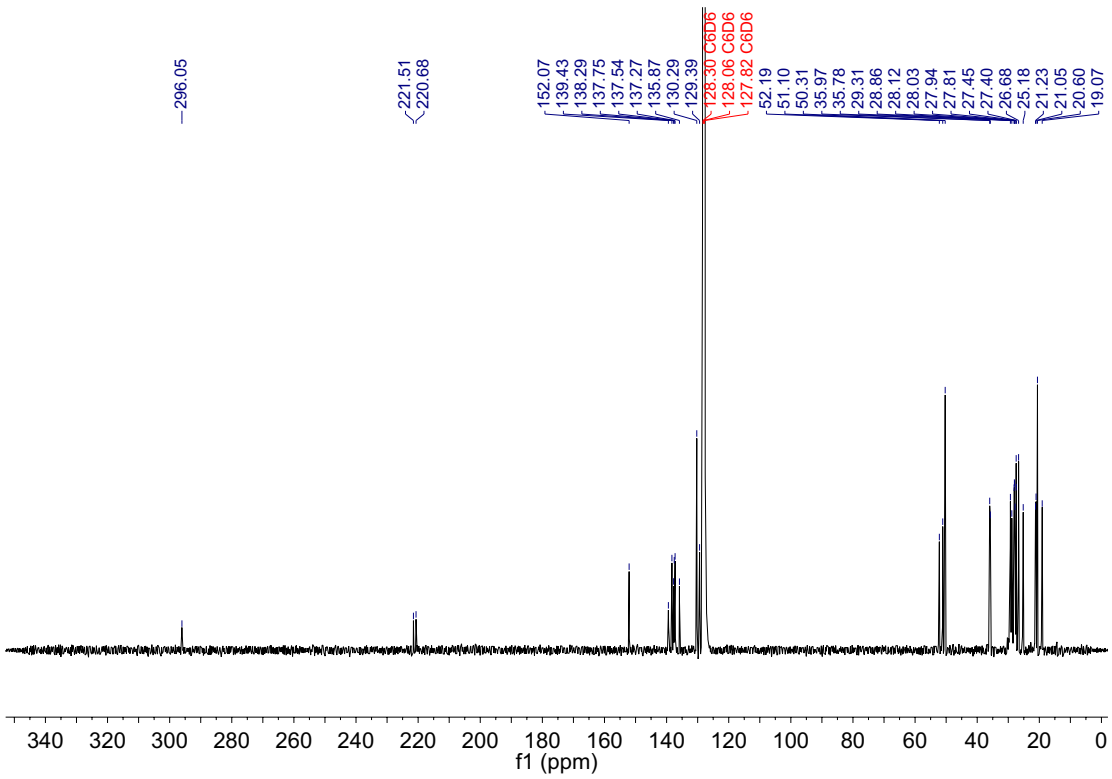
296.05
221.51
220.68
152.07
139.43
138.29
137.75
137.54
137.27
135.87
130.29
129.39
128.30 C6D6
128.06 C6D6
127.82 C6D6
52.19
51.10
50.31
35.97
35.78
29.31
28.86
28.12
28.03
27.94
27.81
27.45
27.40
26.68
25.18
21.23
21.05
20.60
19.07
340 320 300 280 260 240 220 200 180 160 140 120 100 80 60 40 20 0
f1 (ppm)

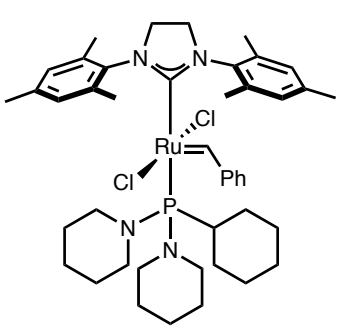
N
N
Cl
Ru
Cl
Ph
P
N
N

4-8

1.00
0.50
1.99
1.94
1.65
4.97
11.29
5.55
3.31
3.68
4.99
10.59
6.61
3.47
5 24 23 22 21 20 19 18 17 16 15 14 13 12 11 10 9 8 7 6 5 4 3 2 1 0
f1 (ppm)

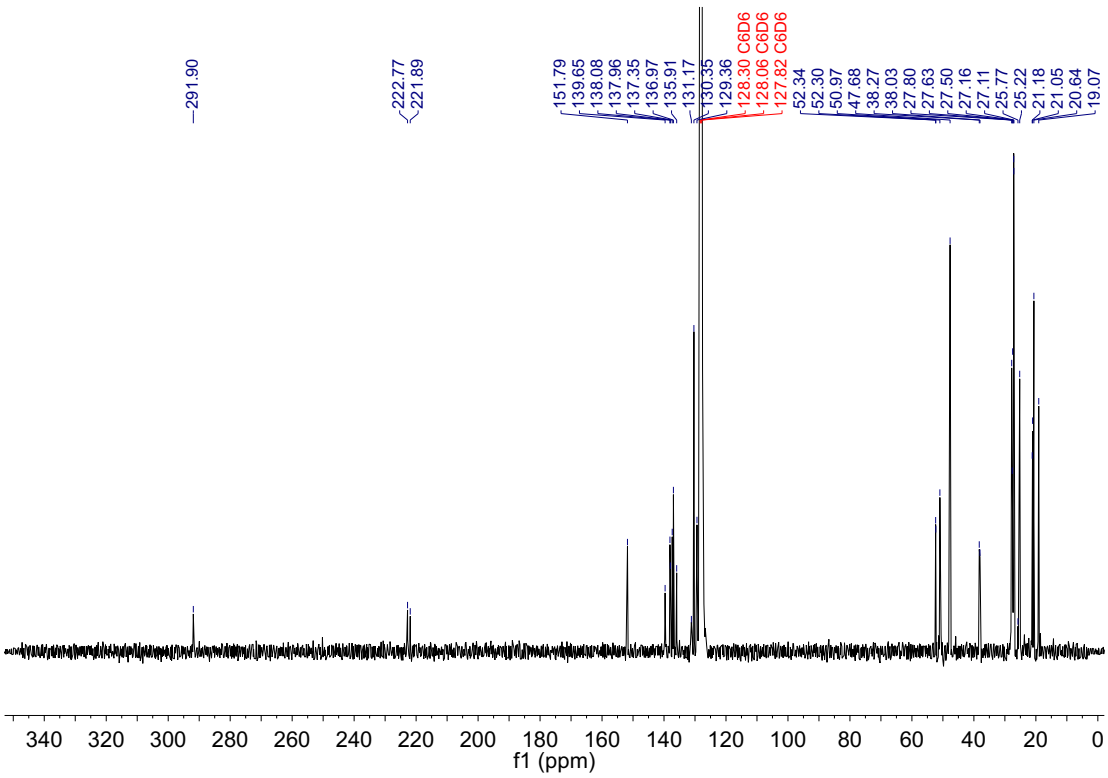
291.90
222.77
221.89
151.79
139.65
138.08
137.96
137.35
136.97
135.91
131.17
130.35
129.36
128.30 C6D6
128.06 C6D6
127.82 C6D6
52.34
52.30
50.97
47.68
38.27
38.03
27.80
27.63
27.50
27.16
27.11
25.77
25.22
21.18
21.05
20.64
19.07
340 320 300 280 260 240 220 200 180 160 140 120 100 80 60 40 20 0
f1 (ppm)

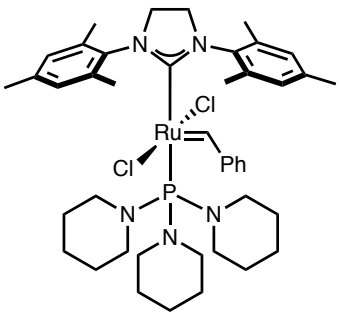
N
N
Cl
Ru
Cl
Ph
P
N
N
N

4-9

1.00
1.69
0.92
1.97
1.95
1.80
4.21
6.10
11.53
5.81
3.00
2.99
6.86
12.31
5 24 23 22 21 20 19 18 17 16 15 14 13 12 11 10 9 8 7 6 5 4 3 2 1 0
f1 (ppm)

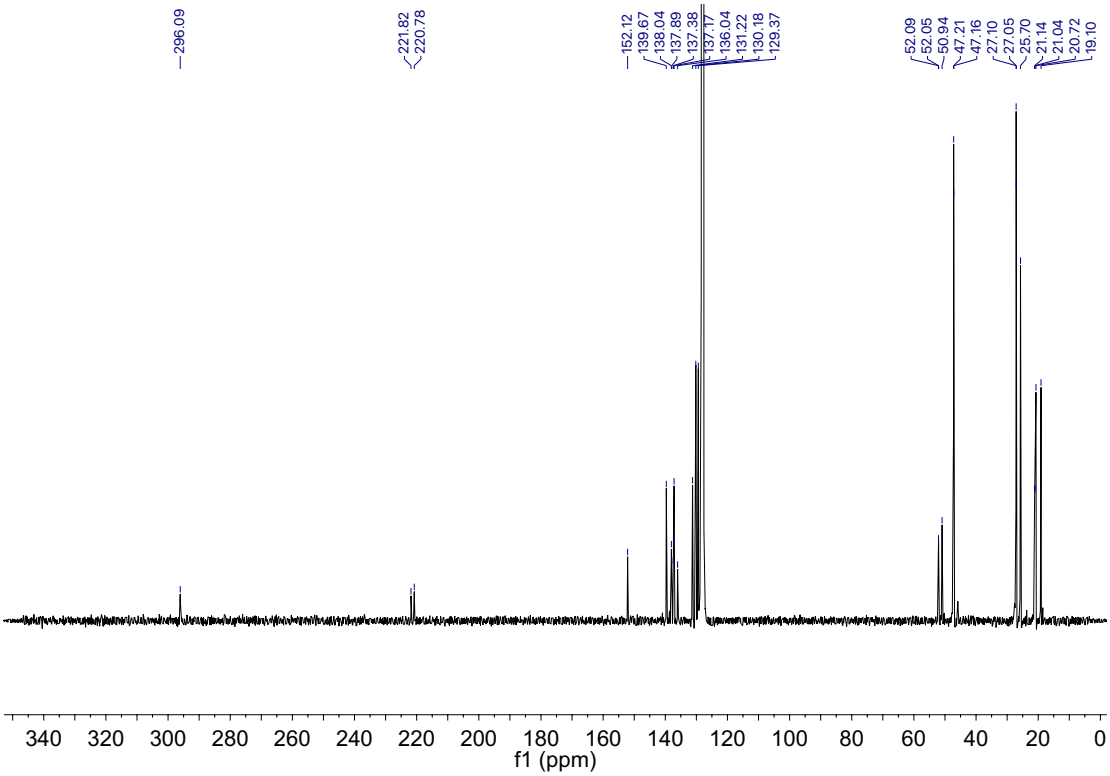
296.09
221.82
220.78
152.12
139.67
138.04
137.89
137.38
137.17
136.04
131.22
130.18
129.37
52.09
52.05
50.94
47.21
47.16
27.10
27.05
25.70
21.14
21.04
20.72
19.10
340 320 300 280 260 240 220 200 180 160 140 120 100 80 60 40 20 0
f1 (ppm)

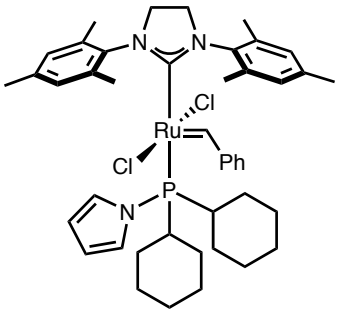
N
N
Cl
Ru
Cl
Ph
P
N

4-17

1.00
1.95
1.12
4.17
2.11
3.83
2.04
2.09
5.98
6.04
3.20
3.10
2.23
2.36
6.53
2.11
6.61
2.00
24
22
20
18
16
14
12
10
8
6
4
2
0

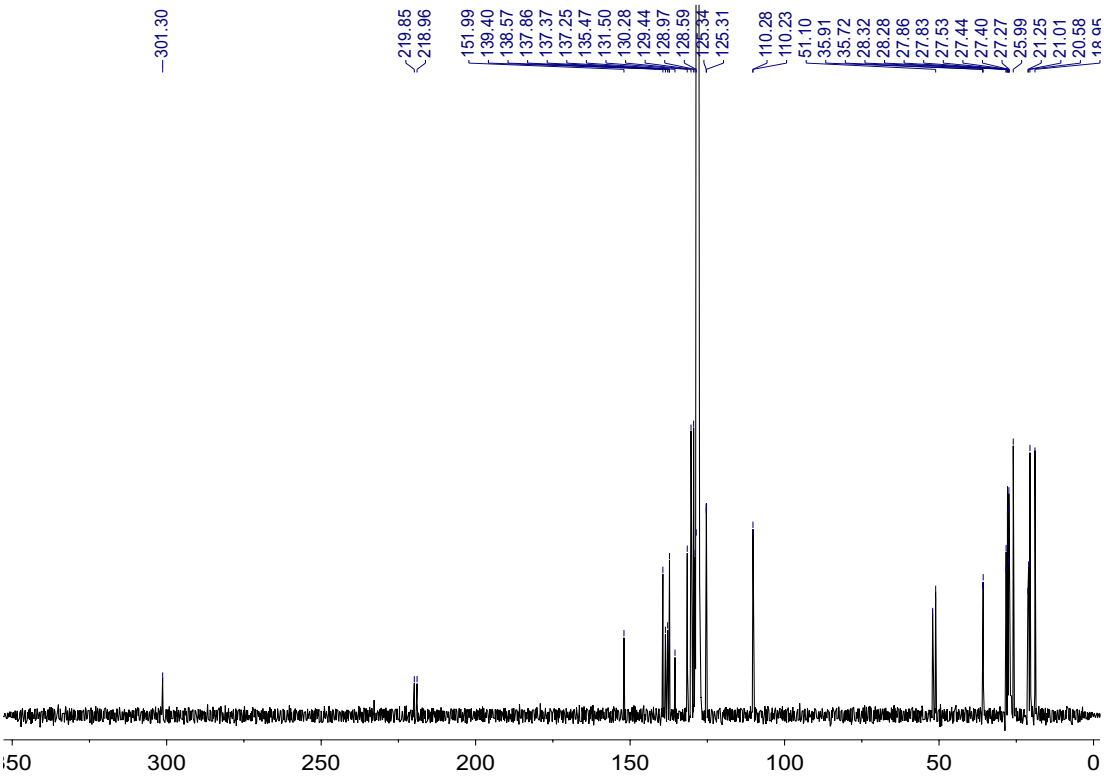
301.30
219.85
218.96
151.99
139.40
138.57
137.86
137.37
137.25
135.47
131.50
130.28
129.44
128.97
128.59
126.34
125.31
110.28
110.23
51.10
35.91
35.72
28.32
28.28
27.86
27.83
27.53
27.44
27.40
27.27
25.99
21.25
21.01
20.58
300
250
200
150
100
50
0

References

(1) For reviews, see: (a) Trnka, T. M.; Grubbs, R. H. *Acc. Chem. Res.* **2001,** *34*, 18-29. (b) Connon, S. J.; Blechert, S. *Angew. Chem., Int. Ed.* **2003,** *42*, 1900-1923. (c) Schrock, R. R.; Hoveyda, A. H. *Angew. Chem., Int. Ed.* **2003,** *42*, 4592-4633. (d) Grubbs, R. H. *Tetrahedron* **2004,** *60*, 7117-7140. (e) Hoveyda, A. H.; Zhugralin, A. R. *Nature* **2007,** *450*, 243-251. (f) Hoveyda, A. H. *J. Org. Chem.* **2014,** *79*, 4763-4792.

(2) For reviews on applications of metathesis in synthesis, see: (a) Fürstner, A. *Angew. Chem., Int. Ed.* **2000,** *39*, 3012-3043. (b) Monfette, S.; Fogg, D. E. *Chem. Rev.* **2009,** *109*, 3783-3816.

(3) For reviews on olefin metathesis polymerizations, see: (a) Buchmeiser, M. R. *Chem. Rev.* **2000,** *100*, 1565-1604. (b) Knall, A.-C.; Slugovc, C., Olefin Metathesis Polymerization. In *Olefin Metathesis*, John Wiley & Sons, Inc.: 2014; pp 269-284.

(4) For reviews related to ROMP, see: (a) Bielawski, C. W.; Grubbs, R. H. *Prog. Polym. Sci.* **2007,** *32*, 1-29. (b) Leitgeb, A.; Wappel, J.; Slugovc, C. *Polymer* **2010,** *51*, 2927-2946. (c) Schrock, R. R. *Acc. Chem. Res.* **2014,** *47*, 2457-2466.

(5) Atallah, P.; Wagener, K. B.; Schulz, M. D. *Macromolecules* **2013,** *46*, 4735-4741.

(6) Sutthasupa, S.; Shiotsuki, M.; Sanda, F. *Polym. J.* **2010,** *42*, 905-915.

(7) For examples of industrial applications of olefin metathesis, see: (a) Mol, J. C. *J. Mol. Catal. A: Chem.* **2004,** *213*, 39-45. (b) Slugovc, C., Industrial Applications of Olefin Metathesis Polymerization. In *Olefin Metathesis*, John Wiley & Sons, Inc.: 2014; pp 329-333.

(8) For early reports of olefin metathesis catalyzed by molybdenum and tungsten, see: (a) Schrock, R. R.; Feldman, J.; Cannizzo, L. F.; Grubbs, R. H. *Macromolecules* **1987,** *20*, 1169-1172. (b) Bazan, G. C.; Khosravi, E.; Schrock, R. R.; Feast, W. J.; Gibson, V. C.; O'Regan, M. B.; Thomas, J. K.; Davis, W. M. *J. Am. Chem. Soc.* **1990,** *112*, 8378.

(9) (a) Nguyen, S. T.; Johnson, L. K.; Grubbs, R. H.; Ziller, J. W. *J. Am. Chem. Soc.* **1992,** *114*, 3974-3975. (b) Nguyen, S. T.; Grubbs, R. H.; Ziller, J. W. *J. Am. Chem. Soc.* **1993,** *115*, 9858-9859.

(10) (a) Schwab, P.; France, M. B.; Ziller, J. W.; Grubbs, R. H. *Angew. Chem., Int. Ed. Engl.* **1995**, *34*, 2039-2041. (b) Schwab, P.; Grubbs, R. H.; Ziller, J. W. *J. Am. Chem. Soc.* **1996,** *118*, 100-110.

(11) Scholl, M.; Ding, S.; Lee, C. W.; Grubbs, R. H. *Org. Lett.* **1999,** *1*, 953-956.

(12) For reviews on ruthenium catalysts with NHC ligands, see: (a) Samojłowicz, C.; Bieniek, M.; Grela, K. *Chem. Rev.* **2009,** *109*, 3708-3742. (b) Vougioukalakis, G. C.; Grubbs, R. H. *Chem. Rev.* **2010,** *110*, 1746-1787.

(13) Getty, K.; Delgado-Jaime, M. U.; Kennepohl, P. *J. Am. Chem. Soc.* **2007,** *129*, 15774-15776.

(14) Love, J. A.; Morgan, J. P.; Trnka, T. M.; Grubbs, R. H. *Angew. Chem., Int. Ed.* **2002,** *41*, 4035-4037.

(15) Choi, T.-L.; Grubbs, R. H. *Angew. Chem., Int. Ed.* **2003,** *42*, 1743-1746.

(16) Sanford, M. S.; Love, J. A.; Grubbs, R. H. *Organometallics* **2001,** *20*, 5314-5318.

(17) (a) van der EideEdwin, F.; Piers, W. E. *Nat. Chem.* **2010,** *2*, 571-576. (b) Nelson, D. J.; Manzini, S.; Urbina-Blanco, C. A.; Nolan, S. P. *Chem. Commun.* **2014,** *50*, 10355-10375.

(18) Sanford, M. S.; Ulman, M.; Grubbs, R. H. *J. Am. Chem. Soc.* **2001,** *123*, 749-750.

(19) (a) Sanford, M. S.; Love, J. A.; Grubbs, R. H. *J. Am. Chem. Soc.* **2001,** *123*, 6543-6554. (b) Love, J. A.; Sanford, M. S.; Day, M. W.; Grubbs, R. H. *J. Am. Chem. Soc.* **2003,** *125*, 10103-10109.

(20) Moloy, K. G.; Petersen, J. L. *J. Am. Chem. Soc.* **1995,** *117*, 7696-7710.

(21) For studies related to the electronic properties of aminophosphines, see: (a) Kroshefsky, R. D.; Weiss, R.; Verkade, J. G. *Inorg. Chem.* **1979,** *18*, 469-472. (b) Barnard, T. S.; Mason, M. R. *Inorg. Chem.* **2001,** *40*, 5001-5009.

(22) Huang, J.; Stevens, E. D.; Nolan, S. P.; Petersen, J. L. *J. Am. Chem. Soc.* **1999,** *121*, 2674-2678.

(23) Maynard, H. D.; Okada, S. Y.; Grubbs, R. H. *Macromolecules* **2000,** *33*, 6239-6248.

(24) Equation 4.1 can be derived by applying the steady-state approximation to the 14-electron intermediate shown in Scheme 4.1. See ref. 19a.

(25) Lin, T.-P.; Chang, A. B.; Chen, H.-Y.; Liberman-Martin, A. L.; Bates, C. M.; Voegtle, M. J.; Bauer, C. A.; Grubbs, R. H. *J. Am. Chem. Soc.* **2017,** *139*, 3896-3903.

(26) Computational studies were performed by graduate student Huiling Shao and Professor Peng Liu of the University of Pittsburgh.